THE CNOT COMPLEX CONTRIBUTES TO THE MAINTENANCE OF GENOME STABILITY

By

NAFISEH CHALABI HAGKARIM

A thesis presented to the College of Medical and Dental Sciences, the University of Birmingham, for the degree of Doctor of Philosophy

Institute of Cancer & Genomic Sciences
College of Medical and Dental Sciences
University of Birmingham
December 2019

Abstract

The yeast CCR4-NOT (CNOT in mammals) complex is a large (1.0-MDa) and highly conserved multifunctional set of proteins. It is involved in many different aspects of mRNA metabolism, including repression and activation of mRNA initiation, control of mRNA elongation, and deadenylation-dependent mRNA turnover; it also has a role in ubiquitin-protein transferase activity and histone methylation. Some studies have suggested that the yeast complex may be involved in the recognition and repair of DNA damage. To investigate whether similar properties are attributable to the mammalian complex we have examined the effects of inactivation of the complex on various aspects of the DNA damage response. Inactivation was achieved by depletion of CNOT1, the largest of the CNOT proteins, which forms a scaffold to the complex. Ablation of CNOT1 expression disrupts cell cycle progression through S and G2/M phases, which subsequently arrests the cell cycle in G1, with markedly elevated levels of cyclin E, p27 and p21. At later times, the cells appear to senesce and /or undergo autophagy. As expected, depletion of CNOT1 affects global transcription and can lead to transcription-dependent replication stress and R-loop formation. CNOT1 depletion can also affect DNA replication by reducing dNTP synthesis. Activity of the RNase H2 complex decreases following loss of CNOT1, which increases the sensitivity of genomic DNA to alkaline lysis due to an increase in embedded ribonucleotides. In addition, depletion of CNOT1 results in DNA damage as seen by comet assay, and formation of micronuclei. This is accompanied by activation of Chk2 in the absence of extraneous DNA damage. In this study, we have demonstrated that the CNOT complex contributes to the maintenance of genome stability and to the response to DNA damage.

To my parents

Acknowledgments

I would like to thank many people for their help and support during my PhD, without them I might have given up a long time ago. I would like to begin with my wonderful supervisor Dr Roger Grand, who never stopped believing in me when the other people did! His encouraging support allowed me to grow as a research scientist. His advice on both research as well as on my career have been invaluable. He has also been a great friend to me, especially during the tough time in my PhD. I have experienced a very peaceful time with him. I cannot be more thankful. Many thanks to Grant Stewart for his help and encouragement.

I cannot think of becoming a doctor without my best friend, my other half, my husband Ali. Frankly, I cannot express in words my massive appreciation of him who supported me in the worst and the best moments of my PhD. I took full advantage of his previous experience of doing a PhD by constant questioning (sometimes very stupid ones) and demanding requests; however, his never-ending patience and encouragement made me feel that I am still welcome to ask more.

I would also like to acknowledge my parents to whom my life itself! I am not sure I would have made my life through without you. You were always there for me without hesitation and I apologise if I was not there for you when you needed me. My brother also deserves a line in here for his great help with my RNA-Seq bioinformatics data analysis, childhood partners in crime are now partners in science!

My special thanks goes to Grant Stewart' group members Martin, John, Rob, Sati and Danxu, Tanja's group Angelo, Phil, Edward and Nick; Liza from Eva's group, Marco and also Panagiotis whom were always on hand to offer scientific advice and to lend reagents and materials. **"No gain no pain"** this is what I have learned during my PhD, hats off to all doctors out there!

PUBLICATIONS AND CONFERENCES

- **Chalabi Hagkarim, N.,** Ryan, E.L., Byrd, P.J., Hollingworth, R., Shimwell, N.J., Agathanggelou, A., Vavasseur, M., Kolbe, V., Speiseder, T., Dobner, T. and Stewart, G.S., (2018). Degradation of a novel DNA damage response protein, tankyrase 1 binding protein 1, following adenovirus infection. *Journal of virology*, 92 (12), pp. e02034-17.

- **Chalabi Hagkarim, N.,** Eskandarian S., Stewart, G., Grand, R.J (2018). The Role of the Human CNOT1 Protein in the DNA Damage Response. Poster session presented at the BCGB symposium 2018. Birmingham-UK.

- **Chalabi Hagkarim, N.,** Eskandarian S., Stewart, G., Grand, R.J (2019). The CNOT complex contributes to the maintenance of genome stability. Poster session presented at the BCGB symposium 2018. Birmingham-UK.

- Gerrard, G., **Chalabi Hagkarim, N.,** Szydlo, R., Alikian, M., Alonso-Dominguez, J.M., Grinfeld, J., Hedgley, C., O'Brien, S., Clark, R.E., Apperley, J., Foroni, L. et al., 2014, Transcript Levels of the Hedgehog Pathway Members PTCH1 and SMO are predictive of Imatinib Failure in pre-treatment Chronic Myeloid Leukaemia, 19th Congress of the European-Hematology-Association, Publisher: Ferrata Storti Foundation , pp. 510-510, ISSN: 0390-6078.

- **Chalabi Hagkarim, N.,** Eskandarian S., Stewart, G., Grand, R.J (2017). The Role of the Human CNOT1 Protein in the DNA Damage Response. Poster session presented at the 1st Cancer symposium Bath. Bath-UK.

- **Chalabi Hagkarim, N.,** Ryan, E.L Stewart, G., Grand, R.J (2017). Degradation of a novel DNA damage response protein, tankyrase 1 binding protein 1 (Tab182), following adenovirus infection. Poster session presented at the DNA Tumour Virus 2017. Birmingham-UK.

- **Chalabi Hagkarim, N.,** Eskandarian S., Stewart, G., Grand, R.J (2017). The Role of the Human CNOT1 Protein in the DNA Damage Response. Oral presentation at the Midlands Cell Cycle & Cytoskeleton workshop 2017. Nottingham-UK.

- **Chalabi Hagkarim, N.,** Eskandarian S., Stewart, G., Grand, R.J (2017). The Role of the Human CNOT1 Protein in the DNA Damage Response. Poster session presented at EMBO DDR symposium 2017. Greece-Athene.

TABLE OF CONTENTS

1 INTRODUCTION 20
1.1 The CCR4-NOT complex 20
1.1.1 CNOT1 26
1.1.2 Deadenylation of mRNAs and the CNOT complex 29
1.1.3 Transcription initiation and the CNOT complex 32
1.1.4 Transcription elongation and the CNOT complex 35
1.2 Cell cycle 38
1.2.1 The Cell Cycle Checkpoints 41
1.3 DNA Replication 51
1.3.1 DNA origin licencing and activation 51
1.3.2 DNA replication stress response 55
1.3.3 Activation of the ATR/Chk1 pathway and fork stabilization 55
1.3.4 Replication forks reversal 58
1.3.5 Oncogene-induced replication stress 65
1.4 Transcription-induced stress response 75
1.4.1 Repair of Intra-strand crosslinks (ICLs) and DNA bulky adducts 75
1.4.2 Imbalanced rNTP / dNTP pool ratio and DNA polymerase-mediated incorporation errors 80
1.4.3 Repair of mis-inserted rNMPs in genomic DNA by ribonucleotide excision repair (RER) 83
1.4.4 Repair of TOP1-dependent single-stranded DNA (ssDNA) nicks 84
1.4.5 Repair of R-Loop-dependent genome instability 87
1.5 Double-strand break repair 90
1.5.1 Homologous recombination (HR) pathway 92
1.5.2 Non-Homologous End Joining 95
1.5.3 Fanconi anaemia pathway and interstrand cross-links 97
1.6 Hypothesis and aims 98
2 MATERIALS AND METHODS 100
2.1 CELL CULTURE TECHNIQUES 100
2.1.1 Human Cell Lines 100
2.1.2 Tissue Culture Media 100
2.1.3 Maintenance of Human Cell Lines 100
2.1.4 Cryopreservation of human cell Lines 101
2.2 CELL BIOLOGY TECHNIQUES 101

2.2.1 siRNA transfection of cell lines 101
2.2.2 Transient transfection of DNA 103
2.2.3 Cytotoxic Agents 104
2.2.4 Buffers Recipes 105
2.2.5 Colony Survival Assays 106
2.2.6 Natural Comet Assay 106
2.2.7 DNA Fibre Assay 107
2.2.8 Homologous Recombination Assay 108
2.2.9 Cell Growth Assay 109
2.2.10 Cell Cycle Analysis 110
2.3 PROTEIN BIOCHEMISTRY TECHNIQUES 111
2.3.1 Protein Extraction 111
2.3.2 Protein Determination (Bradford Assay) 113
2.3.3 SDS-Polyacrylamide Gel Electrophoresis (SDS-PAGE) 113
2.3.4 Electrophoretic Transfer of Protein 114
2.3.5 Visualisation of Protein Bands on Nitrocellulose Membranes 114
2.4 IMMUNOCHEMISTRY TECHNIQUES 115
2.4.1 Antibodies 115
2.4.2 Immunodetection of proteins 115
2.4.3 Co-Immunoprecipitation 118
2.4.4 Subcellular Chromatin Fractionation (SCF) assay 119
2.4.5 Immunofluorescence 119
2.4.6 Immunostaining of DNA Fibres 120
2.4.7 Transcription Assay 121
2.4.8 Deadenylase Assay 122
2.5 MOLECULAR BIOLOGY TECHNIQUES 122
2.5.1 Total Nucleic Acid Isolation 122
2.5.2 DNA Concentration Quantification 123
2.5.3 Densitometric quantification of DNA 123
2.5.4 Alkaline Hydrolysis of Genomic DNA 124
2.5.5 Slot Blots 124
2.5.6 Isolation of Total RNA 125
2.5.7 RNA Quality Control 126
2.5.8 Total RNA-Sequencing 126
2.5.9 Bioinformatics data analysis 127

3 CNOT1 AND CELL CYCLE PROGRESSION 129
3.1 INTRODUCTION 129
3.2 RESULTS 130
3.2.1 Depletion of CNOT1 leads to reduction in level of the other CNOT subunits 130
3.2.2 Depletion of CNOT1 disrupts the cell cycle progression in HeLa cells 132
3.2.3 Depletion of CNOT1 reduces the S-phase indices in HeLa cells 135
3.2.4 Depletion of CNOT1 remarkably reduced the G2/M cell cycle transition 137
3.2.5 Depletion of CNOT1 disrupts the cell cycle progression beyond the G1/S boundary 140
3.2.6 p53-independent upregulation of p21 and p27 promote the G1-cell cycle upregulation in CNOT1-depleted HeLa and U2OS cells 143
3.2.7 Depletion of CNOT1 decreased the expression of genes involved in cell cycle progression 145
3.2.8 Autophagy, Senescence or Apoptosis? 151
3.3 DISCUSSION 163
4 CNOT1 AND DNA REPLICATION STRESS 168
4.1 INTRODUCTION 168
4.2 RESULTS 171
4.2.1 CNOT1-depleted cells show increased transcription activity 171
4.2.2 Depletion of CNOT1 induces replication stress through ongoing transcription . 174
4.2.3 Depletion of CNOT1 causes replication stress through R-loop formation in HeLa cells 178
4.2.4 Depletion of CNOT1 causes replication stress by an increase in embedded rNTP into genomic DNA following dNTP pool reduction 183
4.2.5 The CNOT complex may function in origin firing 186
4.2.6 CNOT1-depleted cells show reduced deadenylase activity 189
4.3 DISCUSSION 194
5 CNOT1 AND DNA DAMAGE RESPONSE 199
5.1 INTRODUCTION 199
5.2 RESULTS 200
5.2.1 Increased spontaneous genome instability in CNOT1-depleted cells 200
5.2.2 Downregulation of ATR signalling in CNOT1-depleted cells 204
5.2.3 Reduced homologous recombination (HR) repair in CNOT1-depleted HeLa cells 208
5.2.4 CNOT1-depleted HeLa cells show resistance to MMC treatment 212
5.3 DISCUSSION 215
6 CONCLUSIONS 218

6.1 Proposed Model 218
6.2 Unanswered questions and future work 221

LIST OF FIGURES

Figure 1.1 Architecture of the yeast Ccr4-Not complex structure. 24
Figure 1.2 Architecture of the mammalian CCR4-NOT complex structure. 24
Figure 1.3 CNOT1 interaction regions with the other CNOT subunits. 27
Figure 1.4 The mRNA decay pathway. 31
Figure 1.5 The Ccer4-Not complex interacts with transcription machinery in yeast. 34
Figure 1.6 Cartoon explaining the role of the CNOT complex in transcription elongation. 37
Figure 1.7 The diagram shows the different cyclin concentrations across the cell cycle. 40
Figure 1.8 The cell cycle and its checkpoints. 41
Figure 1.9 A schematic diagram showing maturation of Okazaki fragment in two pathways. 54
Figure 1.10 A schematic diagram showing ATR-mediated fork stabilization. 57
Figure 1.11 The repair of a stalled fork. 63
Figure 1.12 Transcription-dependent replication stress. 69
Figure 1.13 The molecular mechanisms of oncogene action in nucleotide metabolism and aberrant DNA replication. 73
Figure 1.14 The molecular mechanisms of GG-NER and TC-NER in mammals. 78
Figure 1.15 Repair of TOP1-PARP trapping lesions. 86
Figure 1.16 R-loop resolution 89
Figure 1.17 The choice between HR and NHEJ at DSBs. 91
Figure 1.18 The mechanism of HR repair pathway. 94
Figure 1.19 The mechanism of NHEJ repair pathway. 96
Figure 3.1 Depletion of CNOT1 leads to reduction in the other CNOT subunits 131
Figure 3.2 Ablation of CNOT1 expression leads to G1-cell cycle arrest. 134
Figure 3.3 Ablation of CNOT1 expression reduces the S-phase indices in HeLa cells 136
Figure 3.4 Ablation of CNOT1 expression remarkably reduced the G2/M cell cycle transition 139
Figure 3.5 Depletion of CNOT1 disrupts cell cycle progression beyond the G1/S boundary 142
Figure 3.6 p53-independent upregulation of p21 and p27 promote the G1-cell cycle upregulation in CNOT1-depleted HeLa and U2OS cells. 144
Figure 3.7 Depletion of CNOT1 decreased the expression of genes involved in cell cycle progression through S phase and G2/M phase transition. 149

Figure 3.8 Induction of autophagy in CNOT1-depleted HeLa, U2OS and H1299 cells. 155
Figure 3.9 Induction of senescence in CNOT1-depleted HeLa cells. 159
Figure 3.10 Reduced cell proliferation and viability in CNOT1-depleted HeLa cells in the absence of activated apoptosis via procaspase-3 activation or PARP1 degradation. 162
Figure 4.1 CNOT1 depletion increases transcription 173
Figure 4.2 CNOT1-induced replication stress is promoted by ongoing transcription 177
Figure 4.3 CNOT1-depleted HeLa cells have increased R-loop accumulation 182
Figure 4.4 CNOT1-depleted HeLa cells show increased embedded ribonucleotide in genomic DNA 185
Figure 4.5 The CNOT complex regulates replication initiation in Hela cells 188
Figure 4.6 Deadenylase activity is suppressed in CNOT1-depleted HeLa cells, but not in CNOT7 and Tab182 -depleted HeLa cells 193
Figure 5.1 Increased genome instability in CNOT1-depleted cells 203
Figure 5.2 Downregulation of ATR signalling in CNOT1-depleted cells 206
Figure 5.3 Reduced homologous recombination (HR) repair in CNOT1-depleted HeLa cells 211
Figure 5.4 CNOT1-depleted HeLa cells show resistance to MMC treatment 214
Figure 6.1 Model for the action of CNOT1 in mammalian cells 220

LIST OF TABLES

Table 1.1 Classification of human-yeast orthologues of CNOT complex subunits.....21
Table 2.1 List of cell lines used in this study.....100
Table 2.2 List of siRNAs used in the study.....102
Table 2.3 A List of DNA plasmids used during this study.....103
Table 2.4 A List of all cytotoxic components used during this study.....104
Table 2.5 A List of all buffers used during this study.....105
Table 2.6 Polyacrylamide Gel Recipe.....114
Table 2.7 Table demonstrates the primary antibodies used in this study including species, application, dilution and supplier.....117
Table 2.8 Table demonstrates the secondary antibodies in used this study including species, application, dilution and supplier.....118
Table 2.9 RNA concentration and purity measured by Qubit 2.0 and TapeStation system..126

LIST OF ABBREVIATIONS

53BP1	p53-binding protein 1
9-1-1	Rad9-Rad1-Hus1
AP	Apurinic-apyrimidinic
ATM	Ataxia telangiectasia mutated
ATR	Ataxia telangiectasia and Rad3-related protein
ATRIP	ATR-interacting protein
BER	base excision repair
BLM	Bloom syndrome protein
BRCA1	breast cancer type 1 susceptibility protein
BRCA2	breast cancer type 2 susceptibility protein
BSA	bovine serum albumin
Caf1	chromatin assembly factor-1
CCR4-NOT	the carbon catabolite repression-negative on TATA-less
CCR4	chemokine (C-C motif) receptor 4 -NOT
CDC25	cell division cycle 25
CDC45	cell division cycle 45
Cdc6	cell division cycle 6
Cdc7	cell division cycle 7
CDK	cyclin dependent kinase
Cdt1	cell division cycle 10-dependent transcript 1
CFS	common fragile site
CldU	5-chloro-2'-deoxyuridine
CNOT	CCR4-NOT transcription complex
CPD	cyclobutane pyridine dimer

CtIP	CtBP interacting protein
Cul	cullin
D-loop	displacement loop
DAPI	4', 6-diamidino-2-phenylindole
DBP	DNA binding protein
dCMP	deoxycitidine monophosphate
DDK	dbf4-dependent kinase (Cdc7-Dbf4)
DDR	DNA damage response
DMEM	Dulbecco's modified Eagle's medium
DMSO	dimethyl sulphoxide
DNA	deoxyribonucleic acid
DNA-PK	DNA---dependent protein kinase
DNA2	DNA replication helicase/nuclease 2
dNTPs	deoxyribonucleotides
DSB	double-strand break
dsDNA	double-stranded DNA
DUF3819	domain of unknown function
EME1	essential meiotic endonuclease 1 homologue 1
ERCC1	excision repair cross---complementation group 1
EXO1	exonuclease 1
FANCA	Fanconi anaemia complementation group A
FANCD2	Fanconi anaemia complementation group D2
FANCM	Fanconi anaemia complementation group M
FCS	foetal calf serum
FEN1	flap endonuclease 1
G1	gap phase 1

G2	gap phase 2
GADD45α	growth arrest and DNA damage inducible 45 alpha
GST	gluthathione S-transferase
HAT	histone acetyltransferase
HCl	hydrochloric acid
HR	homologous recombination
HRP	horseradish-peroxidase
HU	hydroxyurea
IDL	insertion/deletion loop
IdU	5-iodo-2'deoxyuridine
iPOND	isolation of proteins on nascent DNA
IR	ionising radiation
M	mitosis
MCM	mini chromosome maintenance
MDC1	mediator of damage checkpoint 1
MDM2	mouse double minute 2
MIF4G	middle domain of eukaryotic initiation factor 4G
MMR	mismatch repair
MRN	Mre11-Rad50-NBS1
mRNA	messenger RNA
MUS81	mus81 endonuclease homologue
MutLα	MLH1/PMS2
MutSα	MSH2-MSH6
MutSβ	MSH2-MSH3
NER	nucleotide excision repair

NF-κB	nuclear factor-kappa B
NHEJ	non-homologous end-joining
ORC	origin recognition complex
ORF	open reading frame
PABPC	poly A binding protein complex
PAR	poly (ADP-ribose)
PARP1	poly (ADP-ribose) polymerase 1
PBS	phosphate buffered saline
PCNA	proliferating cell nuclear antigen
PCR	polymerase chain reaction
PFA	paraformaldehyde
PFGE	pulse-field gel electrophoresis
PI	propidium iodide
Plk3	polo-like kinase 3
pRB	retinoblastoma protein
pre-RC	pre-replicative complex
PRMT3	protein arginine N-methyltransferase 3
RBP	RNA-binding proteins
RFC	replication factor C
RFC2	Rad17---replication factor C
RNA	ribonucleic acid
RNAPII	elongating polymerase II
RNF8/168	RING finger protein 8/168
RNR	ribonucleotide reductase
rNTP	ribonucleotide
ROS	reactive oxidative species

RPA	replication protein A
SDSA	synthesis-dependent strand annealing
SMARCAL1	SWI/SNF-related matrix-associated actin-dependent regulator of chromatin subfamily A-like protein 1
SSB	single-strand break
ssDNA	single-stranded DNA
SUMO	small ubiquitin-like modifier
TAB182	tankyrase 1 binding protein 1 of 182kDa
TAF	TBP-binding protein
TBP	TATA-binding protein
TCR	transcription-coupled repair
TFIID	transcription factor IID
TLS	translesion synthesis
TOPBP1	topoisomerase II binding protein 1
TOPI	topoisomerase I
TOPII	topoisomerase II
Ub	ubiquitin
UTB	urea-Tris HCl-β-mercaptoethanol
UV-C	ultra violet C
WRN	Werner syndrome protein
XPB	xeroderma pigmentosum complementation group B
XPC	XPC-Rad23B-Centrin2
XPD	xeroderma pigmentosum complementation group D
XPF	xeroderma pigmentosum complementation group F
XPG	xeroderma pigmentosum complementation group G
XRCC1	X-ray repair cross-complementing protein 1

XRCC3	X-ray repair cross-complementing protein 3
XRCC4	X-ray repair cross-complementing protein

CHAPTER ONE

INTRODUCTION

1 INTRODUCTION

1.1 The CCR4-NOT complex

The yeast Ccr4-Not, carbon catabolite repression 4 (Ccr4)–negative on TATA-less (Not) complex is a large (1.0-MDa) and highly conserved multifunctional set of proteins (Kumagai and Dunphy 1999, Nasertorabi, Batisse et al. 2011). It is involved in different aspects of mRNA metabolism, including repression and activation of mRNA initiation, control of mRNA elongation, deadenylation-dependent mRNA turnover, and in ubiquitin-protein transferase activity and histone methylation (Kruk, Dutta et al. 2011). Most studies have investigated the Ccr4-Not complex in *S. cerevisiae*, thus much of our understanding of the complex function is a yeast-based model (Denis and Chen 2003, Morita, Suzuki et al. 2007). In *S. cerevisiae* the multi-subunit CCR4-NOT complex comprises nine core subunits, including the *Ccr4* (Carbon Catabolite Repression), Caf proteins (Ccr4 associated factor) (Caf1, Caf40, Caf130) and Not proteins (Not1, Not2, Not3, Not4, and Not5) as well as several less well characterised components (Collart 2003). The Ccr4-Caf1 mRNA deadenylase complex contains a 3' exoribonuclease motif which is involved in removing poly (A) tails from mRNA (Tucker, Valencia-Sanchez et al. 2001). More evidence in support of the Ccr4-Not complex's role in co-transcriptional RNA processing has been already reported (Lee, Wyrick et al. 1998). Genetic approaches in yeast have identified four Not genes (Not1-4) that can globally repress RNA polymerase II activity. Mutation of these genes increase basal expression of many genes in yeast (Collart and Struhl 1994).

Complexes of a similar size, containing the human orthologues CNOT1–CNOT9 with three extra subunits of CNOT10, Tab182 (Tankyrase 1-binding protein1, TNKS1BP1) and C2ORF29 (CNOT11), have been identified in mammals (Table 1.1).

Yeast Protein	Human Orthologue	Function
NOT1/CDC39	CNOT1	Scaffold
NOT2/CDC36	CNOT2	Unknown
NOT3/NOT5	CNOT3	Unknown
NOT4/MOT2/SIG1	CNOT4	E3ligase activity
CCR4α	CNOT6	Deadenylase
CCR4β	CNOT6L	Deadenylase
CAF1α	CNOT7	Deadenylase
CAF1β/P0P2	CNOT8	Deadenylase
RCD1/CAF40	CNOT9 (RQCD1)	Transcriptional cofactor
Not present	CNOT10	Unknown
Not present	CNOT11 (C2orf29)	Unknown
CAF130	Unknown	Unknown
Not present	TNKS1BP1 (Tab182)	Multifunctional

Table 1.1 Classification of human-yeast orthologues of CNOT complex subunits

The yeast Ccr4-Not complex subunits and their human orthologues are listed, together with their function if known.

Four deadenylase subunits CNOT7/CNOT6, CNOT7/CNOT6L, CNOT8/CNOT6 and CNOT8/CNOT6L are expressed in mammalian cells; however, deadenylation is mediated by only one complex (Ccr4/Caf1 subunits) in yeast. In mammalian cells, that the complex contains either CNOT7 or CNOT8 (not both as in yeast), suggesting they compete for binding to CNOT1 (Lau, Kolkman et al. 2009). While the E3 ubiquitin ligase Not4 is consistently present in the yeast complex, CNOT4 is not stably associated with the other subunits in mammalian cells (Lau, Kolkman et al. 2009). No orthologues of CNOT10, CNOT11 or Tab182 have been identified in yeast (Mauxion, Prève et al. 2013). The CNOT3 subunit which is not reported to have an enzymatic activity is orthologous to two yeast subunits, Not3 and Not5. Every individual subunit appears to have a unique role with a slight overlap between some proteins (Panepinto, Heinz et al. 2013). The evidence in support of this includes the observation that mutations and deletions of the different subunits are responsible for different phenotypes in yeast (Azzouz, Panasenko et al. 2009). Mammalian CNOT1 is the largest component of the CCR4-NOT complex with a molecular weight of 267 kDa. It is a scaffold protein and its depletion destabilises the whole complex's integrity, leading to a reduction in the level of other subunits (Bawankar, Loh et al. 2013). In addition, CNOT1 has no enzymatic function; however, it guarantees the enzymatic activities of the complex. It has been shown that in CNOT1-depleted HeLa cells the level of CHOP mRNA increased and the cells undergo caspase-4 activation causing ER stress-mediated apoptosis, suggesting CNOT1 is essential for viability and cell proliferation (Ito, Takahashi et al. 2011). CNOT1 is the focal point of the complex and interacts with CNOT11 and CNOT10 at its N-terminal region although the function of this is not evident at present (Bawankar, Loh et al. 2013). CNOT7 or CNOT8 bind to MIF4G, the middle domain of CNOT1, forming a bridge between CNOT1 and CNOT6 or CNOT6 (Petit, Wohlbold et al. 2012). CNOT9 binds in close proximity to a domain of uncharacterised

function DUF3819, the remaining residues of the middle part of CNOT1. At the C-terminus of CNOT1, it interacts with the heterodimer CNOT2/CNOT3. Although the function of these latter two CNOT proteins is still not clear they appear to regulate the stability of the complex (Bawankar, Loh et al. 2013) (Figure 1.1) and (Figure 1.2). The location of Tankyrase1 binding protein 1 (TNKS1BP1, also known as Tab182), which is a novel subunit we have studied previously, in the complex, is still undetermined (Hagkarim, Ryan et al. 2018).

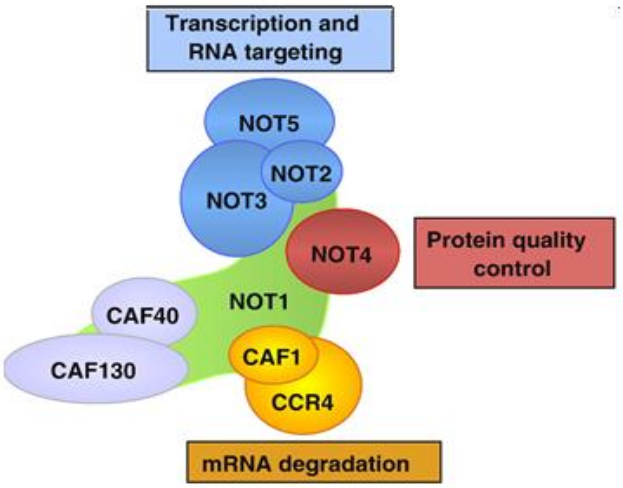

Figure 1.1 Architecture of the yeast Ccr4-Not complex structure.

An L-shape configuration of the CNOT complex was confirmed using electron microscopy. The complex is composed of a pair of arms of 180Å and 190Å. NOT1 is described as the scaffold protein, to which all the other subunits bind , obtained from (Collart, Panasenko et al. 2013). Permission is obtained from publisher (Elsevier) through RightLinks under the licence number 4691371252345 on October 17, 2019.

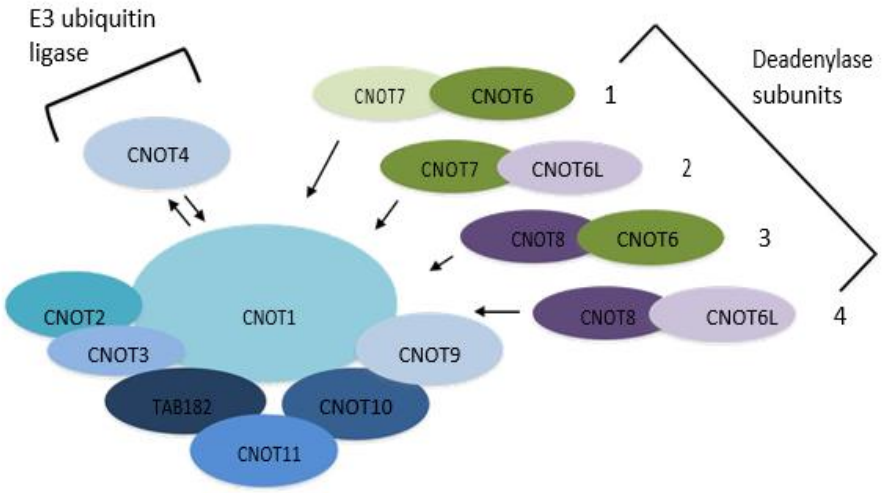

Figure 1.2 Architecture of the mammalian CCR4-NOT complex structure.

Electron microscopy analysis has established that the multi-subunit CCR4-NOT complex consists of a scaffold protein CNOT1 and deadenylase subunits CNO6/CNOT6L and

CNOT7/CNOT8. The E3 ubiquitin ligase component CNOT4 is not stably associated with the CNOT complex. TAB182 is a novel integral component of the CCR4-NOT complex. Adapted from (Ryan 2016).

1.1.1 CNOT1

CNOT1 is the largest subunit (an amino acid length of 2376 and a mass of 266.9 kDa in *Homo sapiens*) and the scaffolding component of the complex (Shirai, Suzuki et al. 2014). Three domains have been delineated for CNOT1, *N*-terminal, MIF4G (middle domain of eukaryotic initiation factor 4G) and *C*-terminal domains. CNOT1 interacts with CNOT11, which is required for the association of CNOT10 with the NOT complex, through its N-terminal domain (Bawankar, Loh et al. 2013, Mauxion, Prève et al. 2013). CNOT1 directly associates with the deadenylase module through its middle region MIF4G region (Petit, Wohlbold et al. 2012, Bawankar, Loh et al. 2013). CNOT7 / CNOT8 function as an adaptor between CNOT1 and CNOT6 / CNOT6L. The remaining residues of the middle domain of CNOT1, named domain of unknown function (DUF3819) associates with CNOT9 (Bawankar, Loh et al. 2013, Chen, Boland et al. 2014). CNOT3 via CNOT2 binds to the C-terminal region of CNOT1 (Bawankar, Loh et al. 2013, Boland, Chen et al. 2013) (Figure 1.3).

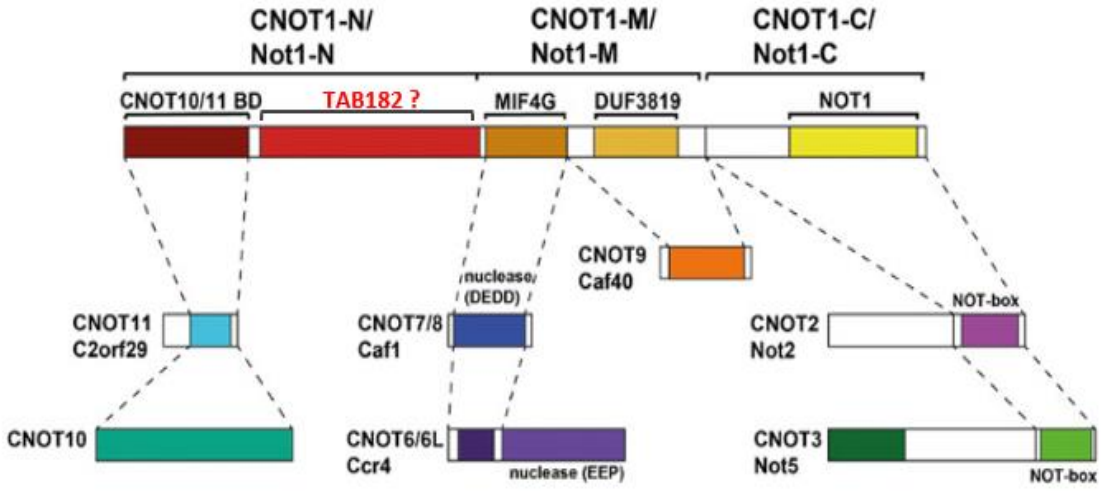

Figure 1.3 CNOT1 interaction regions with the other CNOT subunits.

Interaction map obtained from negative-stain electron microscopy showing the interaction sites between CNOT1 as a scaffolding platform and the other CNOT subunits, adapted from (Nasertorabi, Batisse et al. 2011). Different colours represent the different regions as shown above. The TAB182 interacting site has not been mapped. This article published by Frontiers in Genetics is under an open access license (published material can be re-used without obtaining permission as long as a correct citation to the original publication is given).

CNOT1 scaffolding function, through these interactions, provides a platform for complex formation. Therefore, depletion of CNOT1 would result in the destabilization of the whole complex and degradation of the other subunits such as CNOT2, CNOT6L, CNOT7, and CNOT9, but not CNOT3, in HeLa cells (Ito, Takahashi et al. 2011). Although, CNOT1 has no enzymatic activity, as far as is known, the importance of its scaffolding function for the deadenylase activities of the CNOT complex cannot be overstated.

The specificity of deadenylase activity to the selected mRNA 3'UTRs has been determined by RNA-binding proteins (RBP) through their interaction with CNOT1. For example, Tristetraprolin (TTP; zinc-finger protein ZFP36) has an effect on tumour necrosis factor-α (TNF-α) mRNA turnover (Sandler, Kreth et al. 2011). It has been reported that Nanos2, which is a sequence-specific RNA-binding protein, degrades specific mRNAs, such as Stra8 and plays a key role in murine male germ cell development (Suzuki, Saba et al. 2012). CNOT1 also plays an important role in miRNA-mediated gene silencing. Human GW182 (TNRC6), which is a core component of the miRNA-repression complex provides a platform for CCR4–NOT and PAN2–PAN3 to promote degradation of miRNA–target mRNAs (Braun, Huntzinger et al. 2011). CNOT1, through its MIF4G domain, binds to the C-terminal RecA domain of the DEAD-box protein DDX6, a central component of translational repression, and stimulates the DDX6 RNA helicase ATPase and its recruitment to miRNA-targeted mRNAs (Chen, Boland et al. 2014). The failure of cell differentiation in *planaria* can occur due to elevated stem cell specific-mRNAs with elongated poly (A) tails following depletion of CNOT1 (Solana, Gamberi et al. 2013). Similarly, lethality in *Saccharomyces cerevisiae* can be promoted following a single deletion of only the NOT1 gene. Double deletion of the CCR4 and CAF1 genes, however, does not lead to lethality, suggesting that CNOT1 is essential not only for integrity of the CNOT

complex but is also involved in other functions that are crucial for homeostasis (Maillet, Tu et al. 2000).

Several studies have implicated CNOT1 in transcription regulation. (Lee, Wyrick et al. 1998) have reported Not1p to be a negative TBP-associated regulator of RNA polymerase II in yeast. CNOT1 supresses the ligand-dependent transcriptional activation of oestrogen receptor α (ERα). This is achieved by a conserved LXXXLL motif on CNOT1 which mediates interaction with ERα in MCF-7 human breast cancer cells (Winkler, Mulder et al. 2006). The other nuclear receptor that CNOT1 is able to interact with retinoid X receptor α (RXRα); this association suppresses RXR-mediated transcription in a ligand-dependent manner (Winkler, Mulder et al. 2006). Among those proteins involved in controlling major histocompatibility complex class II (MHC-II) transcription and transport, CNOT1 and CNOT2 were identified using a genome-wide RNAi screen (Paul, van den Hoorn et al. 2011). Single nucleotide polymorphisms (SNPs) within the CNOT1 and CNOT6 genes are associated with B-cell paediatric lymphoblastic leukaemia (B-ALL) (Gutierrez-Camino, Lopez-Lopez et al. 2014). (Cheng, Li et al. 2017) have proposed a role for CNOT1 as an oncogene in osteosarcoma progression; depletion of CNOT1 inhibits osteosarcoma cell proliferation through inhibition of the Hedgehog signalling pathway.

1.1.2 Deadenylation of mRNAs and the CNOT complex

In response to different cellular conditions, transcription patterns of messenger RNA (mRNA) are rapidly adjusted through, among other factors, polyadenylation and deadenylation. Poly (A) tail length determines mRNA fate. Poly (A) tails of species-specific length (~70 nucleotide in yeast and ~250 nucleotides in mammals) are added to the 3' end of newly synthesised mRNA in the nucleus to help with mRNA translation and stability (Brown and Sachs 1998). The poly(A) tail is bound by poly(A)-binding protein (PABP) which increases the stability of the

mRNA and stimulates its translation in the cytoplasm (Svitkin and Sonenberg 2006). The protein level produced during mRNA translation is controlled by deadenylation which is determined by the rates of mRNA synthesis (Wada and Becskei 2017). The rate of deadenylation varies between different mRNAs and determines their half-lives. Deadenylation-dependent mRNA decay plays an important role in eukaryotic fine-tuning of gene expression and this is achieved by monitoring mRNA translation and initiating degradation under appropriate circumstances (Chen, Ezzeddine et al. 2008). Pan2-Pan3 deadenylation complex initiates the mRNA turnover by removing long poly (A) tails of above 150 nt. A subsequent step is carried out by CCR4–NOT which can remove the PABPC-bound A tails. Following deadenylation, the removal of the 5' 7-methylguanosine cap is performed by the decapping complex DCP1/2 following the binding of the Lsm1–7 complex to the oligoadenylated 3' end. Finally, 5' to 3' exonucleolytic degradation is carried out by XRN1 (Du, Liu et al. 2018) (Figure 1.4). In an alternate pathway after poly (A) tail removal, the cytoplasmic exosome complex is entirely responsible for degradation of mRNA in the 3' > 5'direction (Siwaszek, Ukleja et al. 2014) (Figure 1.4). Several studies have reported deadenylase involvement in different cellular processes, including the DDR (Morita, Suzuki et al. 2007) (Traven, Hammet et al. 2005) , cell cycle regulation (Morel, Sentis et al. 2003) and cell proliferation (Ito, Takahashi et al. 2011). In particular, the balance between polyadenylation and deadenylation is thought to underlie this involvement, but the exact mechanism is unknown.

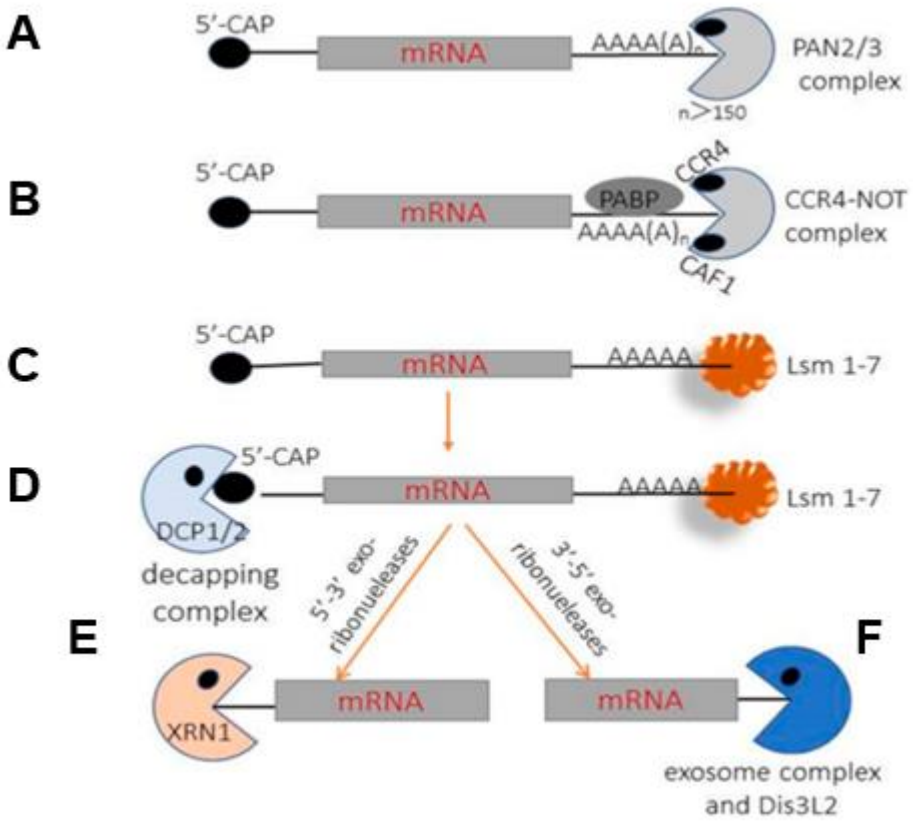

Figure 1.4 The mRNA decay pathway.

*Initial Poly (A) degradation is carried out by the **A)** Pan2-Pan3 (n> 150 nt) followed by a further degradation by **B)** CCR4-NOT complex. Subsequent to this, two general pathways of mRNA decay have been identified. **C & D)** The first involves the decapping of the mRNA 5' cap by the DCP1-DCP2 enzymatic complex following the binding of the Lsm1–7 complex. **E)** This allows XRN1 to act on the mRNA body and complete the degradation process. **F)** In the other pathway, 3' to 5' degradation is entirely performed by the cytoplasmic exosome, obtained from (Du, Liu et al. 2018). This article published by MDPI is under an open access license (published material can be re-used without obtaining permission as long as a correct citation to the original publication is given).*

1.1.3 Transcription initiation and the CNOT complex

The CNOT complex appears to be crucial for regulation of gene expression homeostasis in eukaryotes (Collart 2016). The Not proteins were previously reported in yeast to be a part of a transcription pre-initiation complex. Using co-immunoprecipitation (Kruk, Dutta et al. 2011) showed that the CCR4-NOT complex assembles at promoters, in yeast, through an interaction with RNA polymerase II (RNA Pol II) and binds to nascent RNA transcripts during elongation. The five Not 1-5 subunits were originally described as negative regulators of transcription initiation by impeding the access of TBP (TFIID) to TATA-less genes which are mostly involved in energy metabolism and the inflammatory response (Lee, Wyrick et al. 1998). It was also suggested that they could act by inhibiting the interaction between TBP and DNA, possibly through interactions of Not5 and Not2 with TFIID (Badarinarayana, Chiang et al. 2000). The Not-Box domain, present in Not2 and hCNOT3 orthologues, has been found to be an active repressor of transcription upon promoter targeting. This Not-Box-mediated suppression is sensitive to the histone deacetylase inhibitor TSA, suggesting the involvement of histone deacetylases in the process (Zwartjes, Jayne et al. 2004). Significantly, CNOT3 was identified among those genes whose function contribute to the formation of a unique module in the transcriptional network required for self-renewal in mouse ES cells (Hu, Kim et al. 2009). More evidence in support of the Ccr4-Not complex's role in transcription initiation has been presented by (Lee, Wyrick et al. 1998). These authors showed that Not1 has the ability to bind to TBP in the TFIID and SAGA transcription factors at promoters, which is essential for the presence of RNA polymerase II at transcription start sites. TFIID is typically found on promoters of constitutive housekeeping genes that are required for the maintenance of basic cellular functions, while SAGA is mainly present at highly inducible gene promoters (Figure 1.5). Ccr4-Not subunit crosslinking is enriched at SAGA-dependent genes and genome-wide

gene expression analyses of Ccr4-Not mutants have confirmed that SAGA-responsive genes are largely affected (Cui, Ramnarain et al. 2008). The other regulators that are biased towards the SAGA-pathway are Spt6, a replication-independent histone chaperone, and COMPASS, a histone H3 lysine 4 (H3K4) methylase (Venters, Wachi et al. 2011). Interaction between Spt6 and RNA Pol II promotes the recruitment of deadenylation activity, by the Ccr4-Not complex, at the site of transcription in order to facilitate the degradation of mRNAs required for cell-cycle progression (Dronamraju, Hepperla et al. 2018). *Saccharomyces cerevisiae* H3K4 methylation is catalysed by Set1/COMPASS and removed by Jhd2 demethylase. The yeast E3 ligase Not44 regulates the level of H3K4me3 through proteasomal degradation of Jhd2 demethylase (Mersman, Du et al. 2009) and Not4Δ cells show a significant reduction in the level of H3K4me3 (Mulder, Brenkman et al. 2007). ATP-dependent chromatin remodelling factors such as histone methylase (HMT) and histone acetyltransferase (HAT) increase the accessibility of DNA to RNA Pol II. Yeast cells lacking Not4 or Not5, histones H3 and H4 are mostly hypoacetylated (Peng, Togawa et al. 2008).

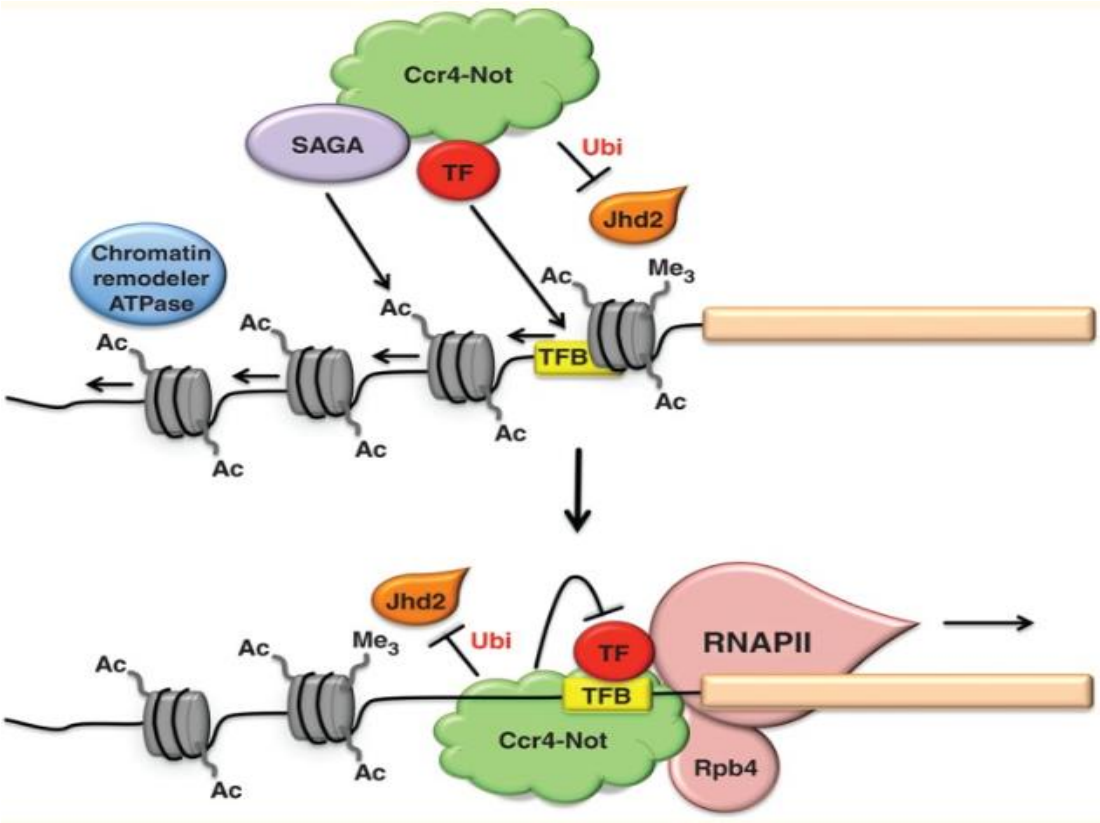

Figure 1.5 The Ccer4-Not complex interacts with transcription machinery in yeast.

A schematic diagram showing the contribution of the CNOT complex to the transcription machinery, Top panel presents the interactions of CNOT complex with components required for transcription initiation. Bottom panel shows the interactions of CNOT complex with components likely to recruit the complex to the transcription machinery. TF (transcription factor); TFB (transcription factor binding site); Ubi, (ubiquitination); Ac (acetylation); Me3, (trimethylation); SAGA (Spt–Ada–Gcn5 acetyltransferase). Obtained from (Collart 2016). This article published by Wiley Interdiscip Rev RNA is under an open access license (published material can be re-used without obtaining permission as long as a correct citation to the original publication is given).

1.1.4 Transcription elongation and the CNOT complex

A number of sites on DNA, for example those containing A/T-rich regions (hairpin structures), DNA binding proteins and DNA lesions, as well as a low concentration of ribonucleotides all cause disruption of mRNA-DNA-RNA polymerase ternary elongation complexes (TECs); this results in a situation generally referred to as transcription stress (Fish and Kane 2002). Stalled transcribing RNA Poll can also be problematic for replisomes, causing a conflict between the replisome and the transcription machinery leading to an interruption of DNA replication and loss of genome stability (Hawkins, Dimude et al. 2019). Therefore, efficient RNA polymerase II transcription elongation through template-encoded pausing sites is necessary for normal cell viability. Although the CNOT complex appears to have no effect on the transcription rate of an active elongating RNA polymerase II, it contributes to transcription elongation by regulation of histone H3 K4 methylation through Jhd2. This, in turn, will result in forward translocation of a stalled RNA Pol II (Reese 2013); this requires the association between the Rpb4/7 module of the polymerase RNA Pol II and both Not3 and Not5 in *Saccharomyces cerevisiae* (Babbarwal, Fu et al. 2014) (Figure 1.6). It seems that the length of the transcript is an important determinant in this rescue operation by the CNOT complex, suggesting that an association of the complex with nascent RNA also contributes to the promotion of transcription elongation (Collart 2016). Transcription factor S-II (TFIIS) is another factor that directly induces resumption of elongation and helps RNA Pol II to pass through trapping sites by increasing the intrinsic nuclease activity of RNA Pol II and displacing transcripts. The ribonuclease activity of the CNOT complex does not appear to contribute to this mechanism; however, the CNOT complex improves the recruitment of TFIIS to elongation complexes and this is mediated by an interaction between the complex and the N terminus of TFIIS (Wind and Reines 2000) (Figure 1.6). Following nascent mRNA removal an increased time is spent

stalled at that site by RNA Pol II; there is also a decreased stability of the transcription machinery which targets the destruction of RNA Pol II, returning the DNA template to its initial state (von Hippel 1998).

Similar to the DNA trapping sites, increased global transcription activity can also lead to elevated transcription stress and genome instability (Saponaro, Kantidakis et al. 2014, Kotsantis, Silva et al. 2016). Although RNA Pol II transcript elongation rate is fast, the transcribing RNA Pol II is not fully functional or effective, which leads to increased incidents during which polymerase is arrested or stalled in the transcribed genes (Saponaro, Kantidakis et al. 2014).

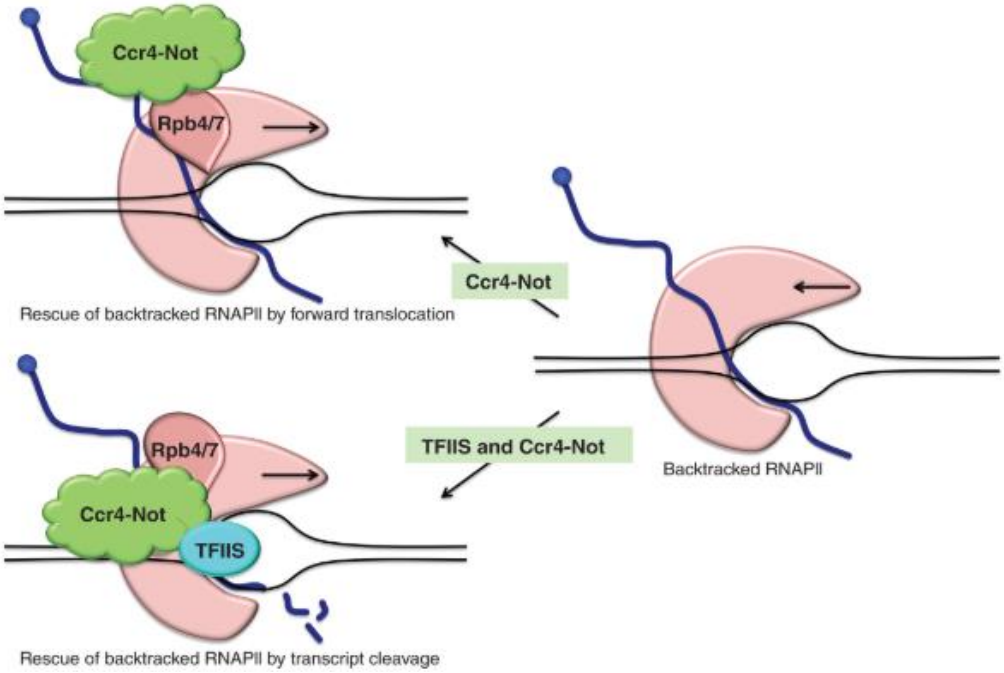

Figure 1.6 Cartoon explaining the role of the CNOT complex in transcription elongation.

Top Panel left; Forward translocation of a stalled RNA Pol II by increasing histone H3 K4 methylation through polyubiquitylation of Jhd2 by NOT4 and its proteasomal degradation. Bottom panel left; Cleavage of the displaced transcript in backtracked RNA Pol II by TFIIS. CNOT complex improves the recruitment of TFIIS to transcription unit. Obtained from (Collart 2016). This article published by Wiley Interdiscip Rev RNA is under an open access license (published material can be re-used without obtaining permission as long as a correct citation to the original publication is given).

1.2 Cell cycle

The cell cycle consists of four phases: gap-phase 1 (G1), synthesis of DNA (S), gap-phase 2 (G2) and mitosis (M). The mammalian cell cycle progression is controlled by a family of cyclin-dependent kinases (CDKs), in conjunction with several activators (cyclins) and inhibitors (CKIs) that form the regulatory subunits of CDKs. CDK activators belong to three different classes: G1 cyclins (D-type cyclins D1, D2 and D3), G1/S cyclins (E-type cyclins E1 and E2), S cyclins (A-type cyclins A1 and A2), and G2/M cyclins (A-type cyclins and B-type cyclins B1 and B2). D-type cyclins can interact with CDKs 2, 4, 5 and 6, while cyclins E, A and B interact with CDK1 and CDK2 only. CDK inhibitors have been divided into three families; INK4a proteins ($p16^{INK4a}$, $p15^{INK4b}$, $p18^{INK4c}$, $p19^{INK4d}$) are inhibitors of CDK4 and of CDK6. The other family of CKIs, comprising CIP ($p21^{cip1/waf1}$) and KIP ($P27^{kip1}$, $p57^{kip2}$) proteins can inhibit all CDKs. The expression of cyclins is cell cycle-dependent and their concentration varies in a cyclical fashion, promoting the cell cycle progression through different phases (Figure 1.7). Unlike the other cyclins, the level of cyclin D gradually increases with no oscillation, through the stages of the cell cycle based on cell growth regulatory signals. For example, a mitogen-stimulating signal in G0/G1 cells promotes the expression of cyclin D proteins which interact with CDK4 and CDK6, stimulating their kinase activities. The increase in concentration of E-type cyclins begins in G1 and peaks dramatically at the G1/S boundary, promoting G1/S transition; the level of expression then drops in early S phase. Cyclin E complexed to CDK2 begins to induce the initial processes of DNA replication. The active cyclin D-CDK4/6 complexes mono-phosphorylate the tumour suppressor RB and its homologues p107 and p130. Hypo-phosphorylation of RB promotes the G0/G1 transition and activation of cyclin E which in return hyper-phosphorylates RB and removes the negative inhibitory effect of RB, leading dissociation from E2F. Free E2F is then able to

promote expression of genes, including cyclin E, which drive G1/S transition and DNA synthesis. The cyclin E-CDK2 complex also triggers hyper-phosphorylation of pRB leading to further dissociation of pRB from E2F family members. Increased level of cyclin E parallels an increase in cyclin A. Expression of cyclin A1 is limited to germ cells while cyclin A2 is expressed in dividing somatic cells. The cyclin A2-CDK2 complex is implicated in DNA replication in S phase; however, the cyclin A2-CDK1 complex is involved in the G2/M transition, followed by cyclin B1-CDK1 activation. Wee1 and Myt1 kinases phosphorylate CDK1 on Tyr15 and Tyr14 respectively, causing inactivation of cyclin B1-CDK1 complexes during G2. The G2/M transition is promoted by dephosphorylation of CDK1 by CDC25C. Mitotic entry is triggered by a positive feedback loop at the end of G2 when active cyclin B1-CDK1 complexes phosphorylate CDC25A/B/C, which, in turn, activate further cyclin B1-CDK1 complexes. As G2 cells begin to enter mitosis cyclin B1 concentration increases with the maximum concentrations at metaphase. The cyclin B1-CDK1 complex promotes the assembly of mitotic spindles and alignment of sister-chromatids at the metaphase plate of the mitotic spindle and is degraded when cells begin to enter anaphase.

Deregulated activity of certain cyclin-CDK complexes, such as cyclin E-CDK2, has been reported to play a role in carcinogenesis. The overexpression of cyclin E decreases the duration of G1 and accelerates premature entry into S-phase. Unscheduled S-phase entry does not allow cells enough time to gather all the necessary materials required for DNA replication, resulting in aberrant DNA replication but continued proliferation (Bester, Roniger et al. 2011).

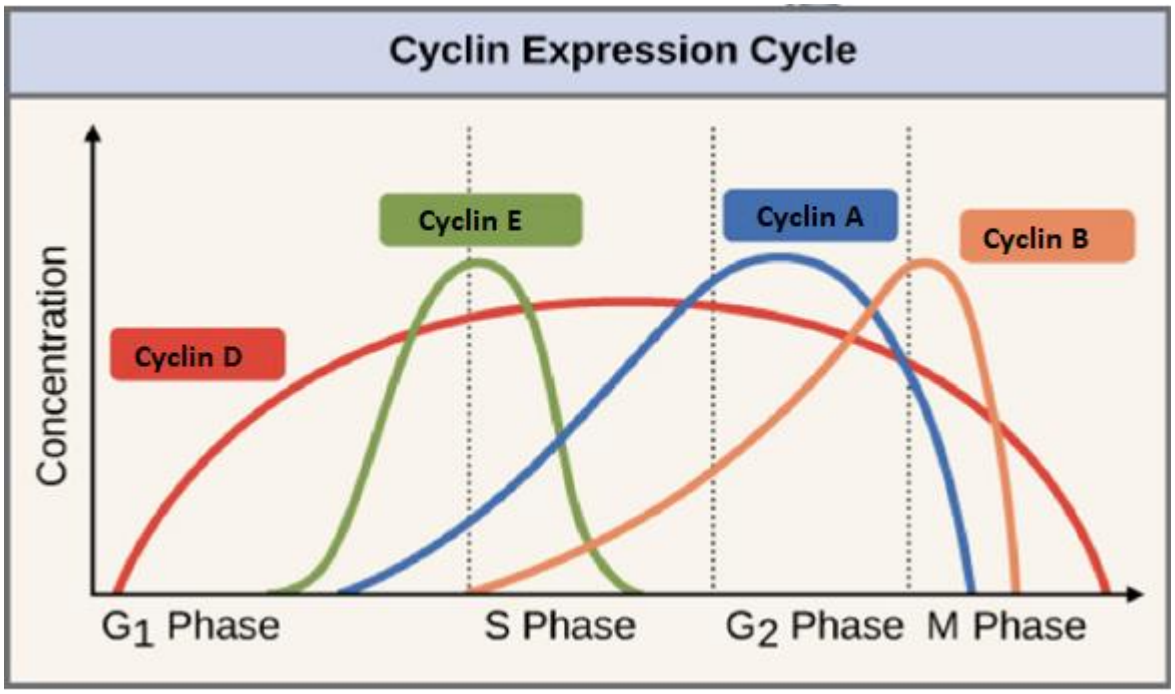

Figure 1.7 The diagram shows the different cyclin concentrations across the cell cycle. *Cyclin D is present for most stages of the cell cycle* and gradually increases *with no oscillation during G1 and S phases. The increased concentration of cyclin E begins in G1 and peaks at the G1/S boundary, promoting G1/S transition; it then and drops in early S phase. The concentration of cyclin A begins to increase in late G1 and remains high during S and G2. Cyclin B peaks at the transition from G2 to M followed by a rapid reduction in the middle of M* phase. *Adapted from Wikimedia Commons, the free media repository.*

1.2.1 The Cell Cycle Checkpoints

G0/G1, G1/S, S and G2/M checkpoints are the mechanisms that monitor correct replication, segregation or repair of damaged DNA throughout the cell cycle.

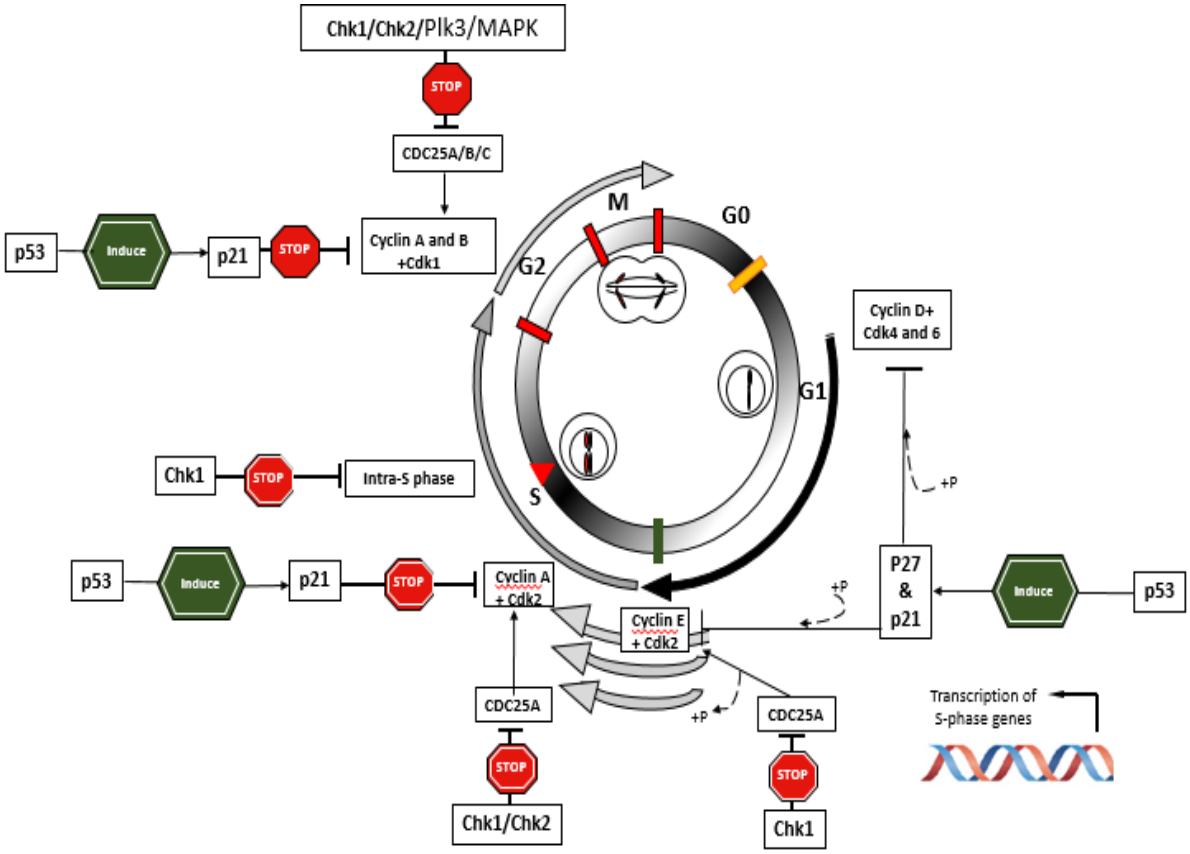

Figure 1.8 The cell cycle and its checkpoints.

Transition through each cell cycle phase (G1, S, G2 and M) is regulated by Cyclin-CDK complexes. Cyclin D-CDK4/6 and Cyclin E-CDK2 complexes are responsible for progression through G1. Progression through S phase is mediated by cyclin A-CDK2. The G2/M transition is promoted following formation of cyclin A-CDK1 complex and completed by formation of the cyclin B-CDK1 complex. This activation of CDKs occurs once their N-terminal inhibitory phosphates are removed by CDC25 phosphatases. The cell cycle checkpoint arrest is performed by different mechanisms; 1) CDK inhibitors such as p21 and p27. 2) CDC25 phosphorylation, inhibition and sequestering by the Chk1/Chk2/Plk/MAPK kinases.

1.2.1.1 The G0/G1 Checkpoint

Somatic cells can enter a reversible (quiescent) or irreversible (senescent and differentiated) G0 state. Quiescent cells are able to re-enter the cycle, whereas senescent cells are permanently arrested in G0 (Figure 1.8). The G0/G1 checkpoint regulates the entry of quiescent cells, where the cells are neither dividing nor preparing to divide, back into the cycle. However, the difference between the G0 and G1 phase has remained obscure. In G0 cells, RB promotes the recruitment of the nucleosome remodelling complex SWI/SNF and the histone deacetylases (HDACs) to E2F binding sites, leading to repression of E2F target genes such as cyclin E (Swanton and Jones 2001). Exiting from G0 to G1 is initiated by exogenous mitogens that induce expression of cyclin D that, in a complex with CDK4 or CDK 6, removes the inhibition of cyclin E expression through the phosphorylation of Rb and release of HDACs (Swanton and Jones 2001). It is noteworthy that most p27 is in a complex with cyclin D-CDK4 and less with cyclin E-CDK2 (Quintanilla-Martinez, Davies-Hill et al. 2003). The levels of p27 have been reported to be higher in quiescent cells in G0, while p21 levels are lower; however, they readily increase in response to mitogenic stimulation and entry into G1 (Ladha, Lee et al. 1998).

1.2.1.2 The G1/S Checkpoint

The G1 checkpoint is in place to prevent initiation of replication in cells with DNA damage, before S phase entry. G1 checkpoint arrest is achieved through two mechanisms; firstly, Chk1-mediated phosphorylation of CDC25A at multiple sites. Chk1, downstream of ATR, mediates phosphorylation and degradation of CDC25A preventing aberrant or excessive replication firing during unperturbed S phase. This is achieved through the downregulation of CDK2, in association with cyclin E (Sørensen, Syljuåsen et al. 2004). In the absence of CDC25A, de-

phosphorylation of cyclin E–CDK2 complexes is inhibited, which in turn, blocks the loading of Cdc45 onto the pre-RC complex. Secondly, p53-dependent phosphorylation of p21 and p27 can occur. Stabilization and activation of p53 is achieved through phosphorylation of p53 directly by ATM on Ser15 (Banin, Moyal et al. 1998) and by Chk1 on Ser20/Thr18 (Canman, Lim et al. 1998) (Shieh, Ahn et al. 2000). Phosphorylation of these amino acids disrupts the binding between p53 and MDM2, which prevents MDM2-mediated nuclear export and degradation of p53 (Dumaz and Meek 1999). Increased stabilisation of p53 leads to induction of the transcriptional activation of its targets such as p21 and p27 and subsequently impairing of the progression of the cell cycle from the G1 to S phase (Figure 1.8). The E3 ubiquitin ligase SCF^{Skp} is thought to be responsible for ubiquitin-mediated proteasomal degradation of both p27 and cyclin E in response to G1/S arrest or G1/S transition, respectively. Several groups have reported dual regulatory behaviour between Cyclin E and p27. For example; p27 accumulation leads to the inactivation of cyclin E–CDK2 kinase activity followed by phosphorylation of cyclin E on Thr380, securing it from cyclin E-specific F-box degradation (Mazumder, DuPree et al. 2004). In contrast, the data from *Bornstein, Bloom et al* showed that cyclin E–CDK2 can facilitate its own activation by phosphorylating p27 on Thr187 to trigger its degradation by the SCF SCF^{Skp} ubiquitin ligase (Bornstein, Bloom et al. 2003). p27 can inhibit origin firing independent of CDK inhibition by interacting with, and blocking, MCM7 (Nallamshetty, Crook et al. 2005).

1.2.1.3 The S phase checkpoint

The S-phase checkpoint is a surveillance mechanism to ensure that faulty DNA is not replicated, in order to preserve genome integrity. Three canonical S-phase checkpoint pathways exist: the intra-S phase checkpoint, the replication checkpoint and the S/M

checkpoint (Bartek, Lukas et al. 2004). The replication checkpoint contributes to salvaging of stalled forks by increasing dNTP replenishment and this is achieved via integrating signals from RPA, ATRIP, and RAD17 as we will discuss in more detail in section 1.4.2. The S/M checkpoint blocks the transition into M phase to ensure that replication has been accurately completed before cells divide. The S/M checkpoint is a Chk1-dependent pathway, since treatment of mammalian cells, lacking ATR expression, with replication inhibitors still prevents M phase entry (Brown and Baltimore 2000, Brown 2003). S/M checkpoint arrest is achieved by inhibiting the cyclin B-CDK1 complex, which progressively increases throughout the cell cycle to promote entry into mitosis. Unlike the latter two checkpoints, the intra-S phase checkpoint does not require replicating DNA and is triggered by DSB structures. Both ATM and ATR kinases stall cell cycle progression through S phase by phosphorylation of CDC25A, leading to the consequent inhibition of cyclin A-CDK2 activity and CDC7-Dbf4 (Sørensen, Syljuåsen et al. 2004) (Figure 1.8).

1.2.1.4 The G2/M Checkpoint

The G2/M DNA checkpoint prevents cells from entering mitosis until unrepaired/damaged DNA or incompletely replicated DNA is sufficiently repaired. CDC25 phosphatases (CDC25A, CDC25B, CDC25C) are predominantly phosphorylated and inhibited by Chk1 and Chk2, leading to the inactivation of the Cyclin B1-CDK1 complex which is necessary for the progression into M phase. Phosphorylation of CDC25B/C facilitates the binding of 14-3-3 proteins to this phosphatase which sequesters it in the cytoplasm (Abraham 2001). Further phosphorylation and sequestering of CDC25B/C protein to the cytoplasm is mediated by polo-like kinase 3 (Plk3) and the p38 mitogen-activated protein kinase (MAPK) pathway; these activities are ATR and ATM dependent (Bahassi, Hennigan et al. 2004) and (Bulavin, Higashimoto et al. 2001).

In parallel, p53-dependent inhibition of CDK1 also regulates the G2/M checkpoint arrest through the transcriptional activation of cell cycle inhibitors such as p21, 14-3-3σ and GADD45α. p21 inhibits CDK1 directly, 14-3-3σ relocates CDK1 to the cytoplasm, and GADD45α prevents the association between CDK1 and Cyclin B1 (Hermeking, Lengauer et al. 1997, Wang, Zhan et al. 1999) (Figure 1.8).

1.2.1.5 The M phase checkpoint

The M phase checkpoint, that is also known as the spindle assembly checkpoint (SAC), functions at the point in metaphase where all the chromosomes align at the mitotic equator under bipolar tension and attach from their centromeres to kinetochore microtubules extended from the poles at either end of the cell (Lara-Gonzalez, Westhorpe et al. 2012). The inaccurate attachment leads to generation of daughter cells with aneuploidy. Daughter cells with fewer or a greater number of chromosomes may result in cell death, or the generation of severe genetic disorders (Kops, Weaver et al. 2005). When chromosomes are incorrectly attached to the spindle apparatus, the SAC is activated and maintained in an active state until they properly attach. The SAC prevents cells from entry into anaphase by inhibiting the anaphase promoting complex/cyclosome (APC/C), RING finger E3 ubiquitin ligase that targets several anaphase inhibitors for proteolysis, including securin and cyclin B1 (Joazeiro and Weissman 2000, Thornton and Toczyski 2003). The mechanism by which APC/C is inhibited is poorly understood; however, it is thought that the mitotic checkpoint complex (MCC) indirectly inhibits the activity of the APC/C complex by binding to the APC/C activator CDC20 and this precludes passage into anaphase (Manchado, Eguren et al. 2010). In addition, the centromere protein CENP-E actives BubR1 which hinders metaphase-anaphase transition (Chan, Jablonski et al. 1999). When chromosomes are correctly attached to the spindles, the

MCC complex is disassembled in order to liberate CDC20 so that it can activate the APC/C. The APC/C is now free to degrade proteins containing D-box degrons, such as cyclin B1 and securin. Securin binds to, and inhibits, a Separase which catalyses the degradation of the cohesin rings that keep the two sister chromatids together; thus by ubiquitylation-mediated degradation of securin the sister chromatids can be separated and anaphase onset promoted (Yu 2002) (Figure 1.8).

1.2.1.6 Senescence

One of the most significant findings in modern cell biology was the observation that primary mammalian cells have a limited, very reproducible lifespan in culture under defined conditions (Hayflick and Moorhead 1961, Hayflick 1965). It was shown that after a certain number of population doublings (slightly more than 50 in the case of human foetal fibroblasts) the cells became quiescent and went into what was termed 'replicative senescence'. The number of population doublings could vary depending on the culture conditions and the age of the donor. In senescence, as it is generally known, the cells are still viable and metabolically active but fail to go through the cell cycle or divide. Since the original observations, it has been demonstrated that the limitations on cell growth are due to telomere erosion (Allsopp, Vaziri et al. 1992). The telomeres shorten because DNA polymerase fails to duplicate the lagging strands totally. The telomere erosion acts as a 'molecular clock' determined by the number of cell divisions until the cells reach their 'Hayflick limit'. When the telomeres reach a minimal length, the DDR is activated and DDR foci can be seen, staining positive for γH2AX, 53BP1 and MDC1 (di Fagagna, Reaper et al. 2003). In addition, the p53, CDC25 and the $p16^{INK4A}$-Rb pathways are also activated, leading to cell cycle arrest. Telomeres are maintained by the telomerase enzyme, which is present in stem cells but is absent for human somatic cells;

however, primary cells can be immortalised *in vitro* by the expression of the telomerase holoenzyme, hTert (Bodnar, Ouellette et al. 1998, Vaziri and Benchimol 1998).

Importantly, senescence can also occur before telomere shortening occurs and this has been termed 'premature senescence'. A number of different events can trigger premature senescence, such as cellular stress induced *in vitro* by changes in cell culture conditions (Sherr and DePinho 2000) or oncogene activation (Serrano, Lin et al. 1997). It was originally shown that activated RAS, when expressed in primary human cells, induces cell cycle arrest and produces a state very similar to replicative senescence. This is in contrast to what happens when it is introduced into already immortalised cells or with a second co-operating oncogene (such as adenovirus E1A) when it gives rise to a permanently transformed cell line (Land, Parada et al. 1983), (Franza Jr, Maruyama et al. 1986, Serrano, Lin et al. 1997). Although the triggers for replicative and premature senescence are not the same, similar pathways appear to be affected; for example, p53 and $p16^{INK4A}$ –Rb are involved in both cases, at least in human cells.

Senescence is always accompanied by cell cycle arrest although inactivation of the p53 pathway is able to put cells back into cycle (Beauséjour, Krtolica et al. 2003, Dirac and Bernards 2003). In addition, changes in cellular morphology are very common although these can vary depending on the cause of senescence and the original cell type. In some cases, cells become larger, flatter, and multi-nucleate whereas others may become spindle- shaped (Kuilman, Michaloglou et al. 2010). For example, it has been reported that expression of mutant HRAS in melanocytes leads to premature senescence, which is accompanied by extensive vacuole formation (Denoyelle, Abou-Rjaily et al. 2006). This may be explained by an increase in the endoplasmic reticulum-mediated unfolded protein response (UPR) leading to increased size of the ER. This is a specific response, determined by the cell type and the

oncogene as it was not observed with NRAS (Denoyelle, Abou-Rjaily et al. 2006). In this case, premature senescence did not involve the p53 or $p16^{INK4A}$ pathways. Senescence is also accompanied by an increase in lysosomal β-galactosidase activity in the lysosomes leading to an increase in SA-β-GAL; this is often used as a diagnostic marker for senescent cells *in vitro*. Others features of oncogene-induced senescence include DNA damage foci, increased level of reactive oxygens, DNA damage, ER stress as mentioned above and activation of the senescence associated secretory phenotype.

However, as mentioned above, the p53 and p16INK4A-Rb pathways are considered the main mediators of senescence, although other pathways may sometimes be involved. In many cases hypophosphorylated Rb accumulates, as does an increased level of transcriptionally active p53. Activation of Rb is probably due to accumulation of $p16^{INK4A}$ and/or $p15^{INK4B}$. Links have been established between senescence and autophagy (see section 1.2.1.7) although the relationship is not clear-cut (Aguilera, Delgui et al. 2018). Some studies have suggested that autophagy decreases in senescent cells (Cuervo and Dice 1998, Patschan, Chen et al. 2008). However, more recent reports have shown that autophagy is activated during senescence and, similarly, inhibition of autophagy delays the onset of markers of senescence (Narita, Young et al. 2011). As well as undergoing cell cycle arrest, there are extensive changes in gene expression in senescent cells. This includes changes in the secretion of cytokines, chemokines and growth factors, giving rise to the senescence-associated secretory phenotype (SASP) (Kuilman and Peeper 2009, Coppé, Desprez et al. 2010). It has been shown that SASP factors can favour growth arrest or transmit the senescent phenotype to adjacent cells. SASP is not dependent on p53 or the $p16^{INK4A}$- Rb pathway (Campisi 2013). Significantly, autophagy is involved in SASP through the TOR autophagy spatial coupling compartment (TASCC) (Narita, Young et al. 2011). It has been shown that the transcription factor GATA4 is stabilised during

senescence, regulating it and SASP (Kang, Xu et al. 2015). Normally GATA4 is degraded during autophagy but this degradation is inhibited during senescence leading to increased levels of GATA4, which can go on to activate NFκ-B, initiating SASP and senescence (Kang, Xu et al. 2015). GATA4 activity is not dependent on p53 or p16-Rb but is regulated by the DDR (Kang, Xu et al. 2015). The senescence-associated secretory phenotype can also contribute to tumourigenesis as well as being anti-tumourigenic. A large number of studies have shown that ligands and proteins secreted by senescent cells can encourage tumour development in vivo and proliferation *in vitro* (Coppé, Desprez et al. 2010). The specific factors involved vary from tissue to tissue and cell type to cell type. Furthermore, senescent cells will secrete factors which lead to cell migration and invasion angiogenesis and metastasis *in vivo* (Coppe et al. 2010; Sun et al. 2018). The majority of studies of senescence have used primary cells; therefore, how much of this description applies to tumour cell lines, which are commonly used for laboratory-based cell biology studies, is not clear. However, it seems likely that many of relationships still apply although this has not been confirmed in some cases.

1.2.1.7 Autophagy

The phenomenon of autophagy has been recognised for well over half a century. Its most obvious phenotype in mammalian cells is the presence of large vacuoles present in the cytoplasm of autophagic cells (De Duve and Wattiaux 1966, Ericsson 1969). The mechanism by which this occurs was unclear until a detailed analysis of autophagy in yeast was published throughout the 1990s (Klionsky and Ohsumi 1999). It was shown that autophagy was dependent on a complex pathway comprising a set of Apg proteins (later termed ATG proteins), of which approximately 35 have been confirmed in yeast (Nakatogawa, Suzuki et al. 2009). Orthologues were later shown to be present in mammalian cells (Hammond, Brunet

et al. 1998, Mizushima, Yoshimori et al. 2011). It is now clear that autophagy is a process ubiquitous in eukaryotes.

During macroautophagy (usually just termed autophagy) small areas of the cytoplasm are isolated with a membrane, resulting in the formation of the autophagosome. The autophagosome matures and fuses with the endosomes and then with lysosomes. Lysosomal enzymes hydrolyse the enclosed macromolecules to produce smaller building blocks, such as amino acids. Autophagy may also be involved in the breakdown of organelles such as mitochondria. In general, autophagy can be seen as a response to cellular stress and adverse conditions. Following starvation, it is used to generate amino acids from degraded proteins; it is also used to control the levels of various substrates, to degrade pathogens and in the monitoring of organelles and proteins.

Autophagosomes form transiently, often with a half-life of a few minutes before they fuse with lysosomes. The autophagosome membrane appears to originate in the pre-autophagosomal structure/phagophore assembly site (PAS) which is located in a particular site in the ER. The formation of the membrane structures involves a number of pathways, some of which are still unclear. However, it is known that several autophagic protein complexes are required for formation of the PAS. These include the ULK protein kinase complex (FIP200/ULK1/ATG13/ATG101), the Class III PI3K complex (ATG14/Beclin-1/P150/VPS34), the ATG12 ubiquitin ligase-like complex (ATG12, ATG7, ATG10, ATG16, ATG5) and the ATG8/LC3 conjugation system (ATG8/LC3/ATG3ATG4/ATG7) (Mizushima, Yoshimori et al. 2011, Rubinsztein, Shpilka et al. 2012). After maturation, the autophagosome fuses with the endolysosome. Proteins required for this include syntaxin-17, SNAP29 and VAMPS, which are SNARE proteins and the HOPS complex (Itakura, Kishi-Itakura et al. 2012).

During selective autophagy, the ATG8 family complex interacts with a variety of proteins such as ATG19, ATG32 and p62/SQSTM1 (the neighbour of the BRCA1 gene) and incorporate them into autophagosomes (Lamark, Svenning et al. 2017). It has been suggested that that this is part of the targeting mechanism for the PAS or autophagosome formation site (Mizushima, Yoshimori et al. 2011). Thus, p62/SQSTM1 is an autophagy receptor that connects selected cargo to ATG8 adaptors on the inside of the growing phagophore. Several other autophagy receptors, such as NBR1, BNIP3 and TAX1BP1, have been characterised (Lamark, Svenning et al. 2017). Under normal circumstances, levels of autophagy receptors remain low due to rapid degradation. In response to stress, particularly that due to oxidation, p62 is up regulated by NRF2 via an ARE in its promoter. p62 also contributes to the stabilisation of NRF2, forming a positive feedback loop (Komatsu, Kurokawa et al. 2010).

1.3 DNA Replication

Preparation, initiation, progression and completion of DNA replication is controlled by the cell cycle. Correct DNA replication is essential in order to preserve genome integrity.

1.3.1 DNA origin licencing and activation

The generation of DNA replication components, such as the synthesis of histones, dNTPs and the pre-replication complex (pre- RC) occurs exclusively in G1. DNA replication is licenced during the late phase of mitosis and continues through to the G1 phase (Fragkos, Ganier et al. 2015). The pre-RC consists of the hexameric origin recognition complex proteins 1-6 (ORC1-6), cell division cycle 6 (Cdc6), cell division cycle 10-dependent transcript 1 (Cdt1) and the inactive mini chromosome maintenance (MCM) helicase complex (a hexamer consisting of the six subunits MCM2-7) (Fragkos, Ganier et al. 2015). To ensure DNA re-replication is

suppressed during S phase, cells employ two non-overlapping mechanisms. Prior to S phase, origins are licensed by recruitment of the pre-RC to chromatin. During S phase, these are activated by the subsequent association of Cdc45 and MCM10 with the pre-RC complex, which then binds to GINS to form the active CMG (Cdc45-MCM-GINS) replicative helicase (Moyer, Lewis et al. 2006). In addition, downregulation or inhibition of licensing proteins prior to early S phase would mean that no more origin sites can be licensed (Li and Blow 2005). For example, the recruitment of the MCM complex to chromatin by Cdt1 during S and G2 phases is disrupted once the replication inhibitor geminin (GMNN) binds to Cdt1 (Wohlschlegel, Dwyer et al. 2000). Moreover, in response to replication stress during S phase two kinases, ATR and Chk1, also inhibit DNA origin re-licencing. ATR phosphorylates MLL at Ser-516, which disrupts its association with, and thereby its degradation by, the SCF (Skp2) E3 ligase, leading to its accumulation and stabilization on chromatin. Stabilised MLL methylates histone H3K4 and hinders CDC45 binding to origins during checkpoint activation, blocking origin firing (Liu, Takeda et al. 2010). In addition, the ATR-Chk1 pathway limits origin firing by restricting CDK2 activity in cyclin E/CDK2 and cyclin A/CDK2 complexes; this normally marks the G1/S phase transition where origin firing is initiated (Buisson, Boisvert et al. 2015). Formation of the pre-RC and CMG replicative helicase promotes separation of the inactive MCM2–7 double hexamer into two active single MCM hexamers and the phosphorylation-dependent binding of multiple replication proteins, such as TOPBP1, RECQL4 and MTBP onto origins (Fragkos, Ganier et al. 2015).

The active MCM helicase unwinds the helix at DNA origins to form a replication fork. The recruitment of the rest of the replication machinery, such as RFC, PCNA, RPA, TIPIN-TIMELESS-CLAPSIN, and the DNA polymerases α, ε and δ behind the active helicase leads to the formation of the replisome that moves bi-directionally from the activated origin (Masai,

Matsumoto et al. 2010). DNA replication initiates with synthesis of a short RNA segment by the primase subunit of Pol α and this is elongated by Pol ε and δ. Due to the 5’ to 3’ polarity of DNA synthesis, DNA replication occurs only in one direction as the CMG helicase moves in a 3’->5’ direction. This continuously synthesised strand is the leading strand. The other strand, named the lagging strand, is made as short discontinuous fragments of nascent strands of DNA, and these are termed Okazaki fragments. The lagging strand DNA polymerase begins the replication of Okazaki fragments in the opposite direction to the helicase. The synthesis of the lagging strand is slower as it needs to wait for the leading strand to expose the template strand that is used for the Okazaki fragment synthesis (Alberts, Johnson et al. 2002). During maturation of Okazaki fragment, Pol δ displaces the RNA primer associated with the preceding Okazaki fragment into a 5’ flap. Structure-specific nucleases, DNA2 (the long flaps) or FEN1 (the short flaps), identify the displaced flap, bind to the flap and resolve it. Association of Pol δ with the 5’–3’ helicase Pif1 increases flap formation in the downstream Okazaki fragment, generating a longer 5’ flap. The long flaps (>22 nt in length) are coated by RPA and become resistant to FEN1 endonuclease activity. Therefore, the action of DNA2 nuclease is required for proper cleavage of RPA-bound flaps. DNA2 removes RPA and cuts the flap at different sites leaving a shorter product of ∼ 5–6 nt in length, which is removed by FEN1 to create a nick, before being ligated by DNA ligase I (LIG1) (Balakrishnan and Bambara 2013) (Figure 1.9). Once DNA replication is complete, the replisomes disassemble from the DNA to allow the genome to be replicated once per cell cycle, thus avoiding interference with other chromatin-based processes such as transcription, DNA repair or the next round of replication.

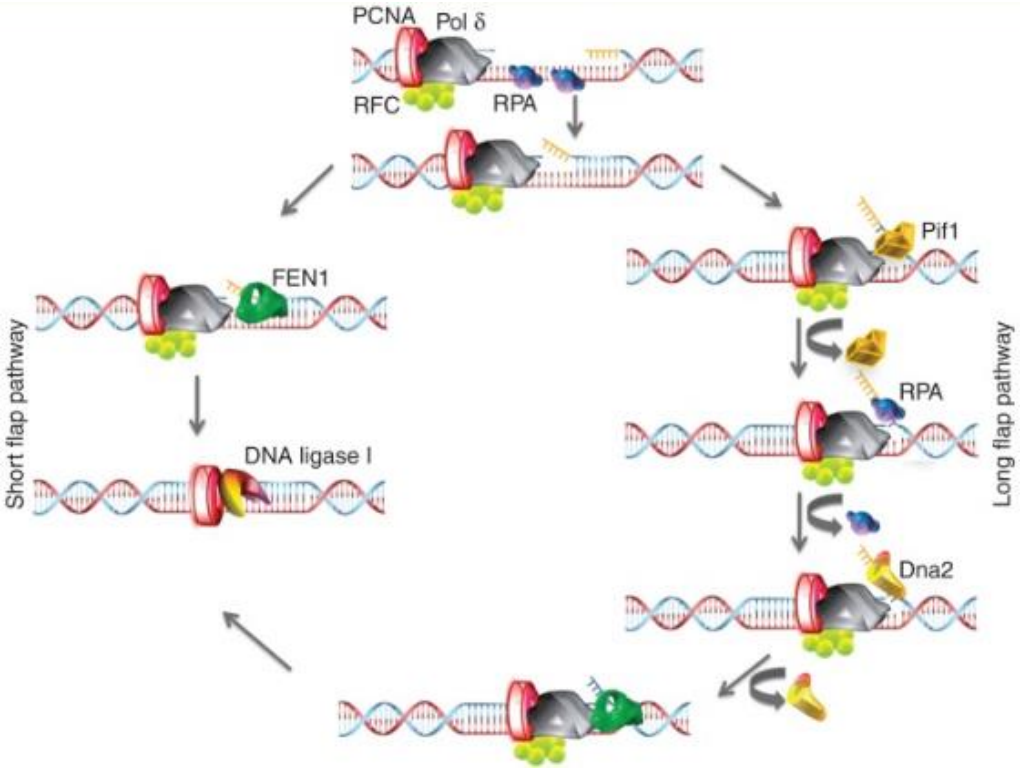

Figure 1.9 A schematic diagram showing maturation of Okazaki fragment in two pathways. *Right panel shows the mechanism of long flap removal; Pif1 contributes to generation of a longer 5' flap in the downstream Okazaki fragment. DNA2 cleaves the RPA-bound flaps and leaves a shorter flap of ~ 5–6 nt length, which is removed by FEN1. Left panel shows the mechanism of short flap removal by FEN1. A terminal nick generated by FEN1 is ligated by DNA ligase I (LIG1). Obtained from (Balakrishnan and Bambara 2013). This article is published under an open access license (published material can be re-used without obtaining permission as long as a correct citation to the original publication is given).*

1.3.2 DNA replication stress response

Replication stress (RS) can refer to any deviation in the process, coordination and timing of DNA synthesis. To avoid genome instability, several surveillance pathways have evolved to deal with RS. Central to these genome surveillance pathways is the ATR/Chk1 axis. In response to a wide range of DNA damage, such as SSBs and bulky lesions, ATR is activated and, together with its primary substrate kinase Chk1, it controls different signalling cascades, including cell cycle checkpoint activation, DNA damage repair induction, and regulation of origin firing and stabilization of replication forks. Although ATR and Chk1 have long been considered to function in the same kinase cascade *Buisson, Boisvert et al* showed that DNA-PK can also phosphorylate Chk1 to provide a backup pathway inhibiting origin firing in ATRi-treated cells.

1.3.3 Activation of the ATR/Chk1 pathway and fork stabilization

The uncoupling of DNA replication from the replicative CMG helicase during fork stalling can lead to increased RPA-coated ssDNA formation, which, in turn, activates the ATR recruitment via its binding partner ATRIP (Cortez, Guntuku et al. 2001). RAD17-RFC clamp loader interacts with RPA and recruits a RAD9-RAD1-HUS1 (9-1-1) clamp complex onto 5’ ends adjacent to the region of RPA-coated ssDNA. The 9-1-1 complex is required for loading of TOPBP1 which induces a large increase in ATR-ATRIP kinase activity, enabling it to phosphorylate numerous downstream targets including its effector kinase Chk1 (Saldivar, Cortez et al. 2017). ETAA1 has recently been recognised as a novel RPA-binding protein that activates ATR in line with TOBP1/RAD17/9-1-1 and functions at stalled replication forks (Bass, Luzwick et al. 2016). The other protein complexes at replication forks that regulate the activation of Chk1 by ATR are Clapsin and TIPIN-TIMELESS (Yang and Zou 2009). Recently, a replication factor, DONSON, has

been shown to contribute to the efficient functioning of the ATR / Chk1 pathway (Reynolds, Bicknell et al. 2017) (Figure 1.10).

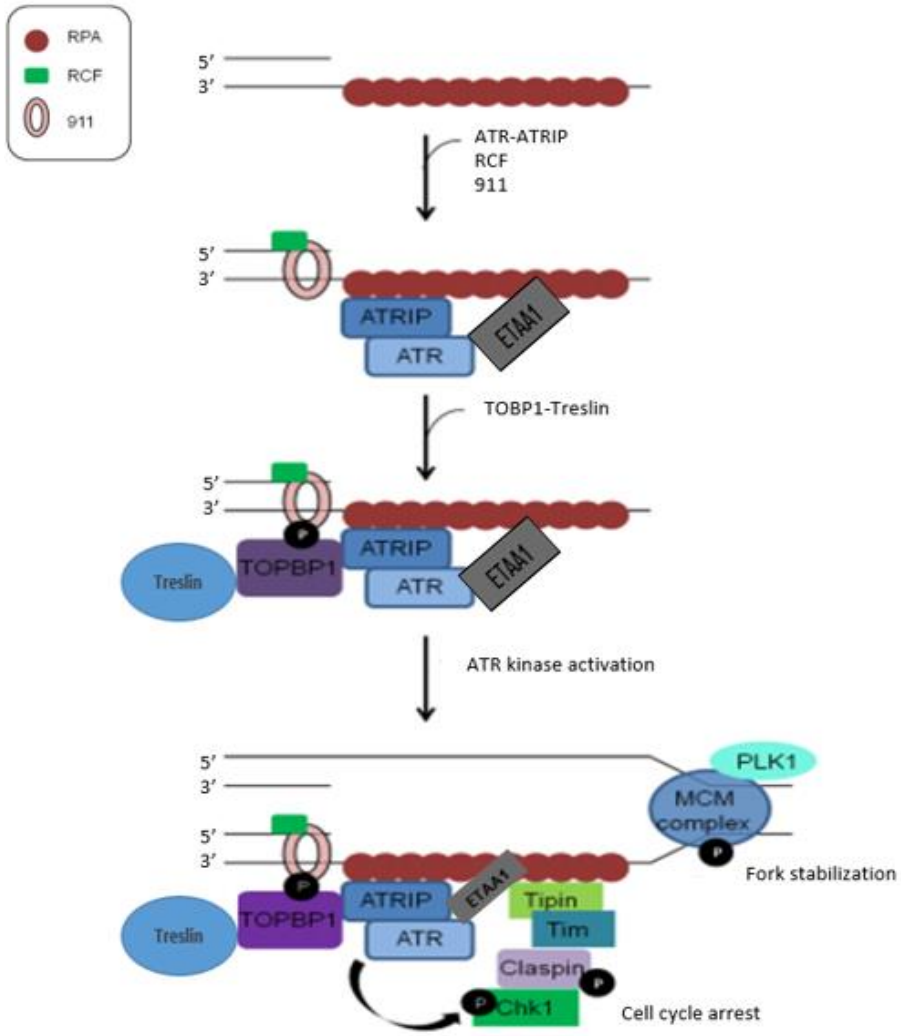

Figure 1.10 A schematic diagram showing ATR-mediated fork stabilization.

Replication stress induces RPA-coated ssDNA, which is identified and captured by the ATR-ATRIP complex. This is followed by recruitment of the 9-1-1 complex in an RCF–dependent manner. ETAA1 is recruited directly to RPA-coated ssDNA. Activation of ATR kinase activity depends on the recruitment of the other mediators, such as ETAA1 and TOBP1. ATR phosphorylates Clapsin, which together with another replication factor Tipin-Timeless mediates the phosphorylation of Chk1 by ATR. Chk1, downstream of ATR, phosphorylates key targets preventing aberrant or excessive replication firing and cell cycle arrest. Modified from (Thomas 2013). This article is published under an open access license (published material can be re-used without obtaining permission as long as a correct citation to the original publication is given).

Chk1, downstream of ATR, mediates phosphorylation of the CDC25A preventing aberrant or excessive replication firing during unperturbed S phase. This is achieved through the downregulation of CDK2, in association with cyclin E or A, and Cdc7 in a complex with Dbf4 (Sørensen, Syljuåsen et al. 2004). Chk1 prevents firing of dormant origins by blocking the interaction between Treslin and TOBP1 which inhibits the assembly of the CMG (Cdc45-MCM-GINS) replicative helicase (Boos, Sanchez-Pulido et al. 2011). Future research will be needed to identify the exact mechanisms by which the ATR/Chk1 pathway can supress new origin firing during replication. Chk1 also phosphorylates CDC25B and CDC25C, preventing entry into mitosis (Schmitt, Boutros et al. 2006). In addition to Chk1, phosphorylation of many more checkpoints proteins such as H2AX, BRCA1, RAD17, RPA2, SMC1, Clapsin, FAND2 and p53 are ATR-dependent (Petermann and Caldecott 2006). In response to replication blocks, ATR also mediates Rad51 recruitment (Zellweger, Dalcher et al. 2015) and FANCD2 monoubiquitination (Andreassen, D'Andrea et al. 2004).

1.3.4 Replication forks reversal

Two steps can be envisaged for the replication fork reversal (RFR) model: firstly, remodelling of the fork to form a four-stranded DNA structure, reminiscent of Holliday junction-like (HJL) structures. This can occur through the separation of two newly synthesised leading and lagging strands from their parental strands and their annealing to each other, simultaneously with the two template strands also re-annealing; secondly, restart of the reversed fork structure, also referred to as regressed forks or 'chicken foot' structures (Postow, Ullsperger et al. 2001). The template switching involved in regression may facilitate excision repair of unrepaired DNA lesions that exist on the template strand by relocation of the DNA damage

into the double-stranded region of the DNA; this allows the conventional excision repair mechanism enough time to repair the damage correctly. This process may also provide an error-free alternative to translesion synthesis, using newly synthesised strands as a template for DNA replication through template switching in order to bypass a DNA lesion on the parental strand (Higgins, Kato et al. 1976). Finally, unwinding and pairing of newly synthesised strands limits the extent of exposed ssDNA, ensuring fork stabilisation. The first fork reversal model in higher eukaryotes *in vivo* was suggested by (Chaudhuri, Hashimoto et al. 2012). They have shown that TOP1 poisoning by CPT causes an immediate induction of replication-fork slowing and PARP1-mediated fork reversal, which can be independent from DSB formation, at sub-lethal inhibitor doses. Further work from this group showed that PARP1 stabilises regressed forks following CPT-mediated TOP1 inhibition by limiting restart activity of the RECQ1 helicase (Berti, Chaudhuri et al. 2013). Another piece of supporting evidence showed that DNA2 in collaboration with WRN promotes replication fork restart by degradation of the 'fourth arm' of the reversed fork (Thangavel, Berti et al. 2015). In addition, Rad51 has been shown to be pivotal in the conversion of single stranded DNA into reversed forks in response to TOP inhibitors, nucleotide depletion or inter-strand crosslinks (Zellweger, Dalcher et al. 2015). Fork reversal mechanisms assist DNA replication, not only when faced with topological stress, induced by TOP1 inhibitors but they also limit the damage associated with DNA synthesis inhibitors, inter-strand cross-linking inducers and alkylating agents (Zellweger, Dalcher et al. 2015). A wide range of proteins with fork remodelling activities has been implicated in fork restart. DNA helicases BLM and WRN, which are both substrates of ATM, contribute to resolution of replication intermediates (Ralf, Hickson et al. 2006) (Bétous, Glick et al. 2013). The Fanconi Anaemia DNA helicase FANCM and its working partners FANCJ and FANCD2 (in corporation with CtIP) generate an effective fork recovery mechanism in response to replication

stress (Gari, Décaillet et al. 2008). This occurs in conjunction with three members of the SWI/SNF-related family helicases (SMARCAL1, ZRANB3 and RAD54) (Bétous, Mason et al. 2012), (Bugreev, Rossi et al. 2010, Vujanovic, Krietsch et al. 2017), and FBH1 (Fugger, Mistrik et al. 2015). In particular, SMARCAL1, which is regulated by the activity of PARP1, through its replication protein A (RPA)-binding motif, binds to RPA-coated ssDNA and catalyses the processing and remodelling of perturbed replication forks (Bansbach, Bétous et al. 2009). DNA translocase ZRANB3 participates in the fork reversal process, this requires an interaction with polyubiquitinated PCNA (Vujanovic, Krietsch et al. 2017). The human RecQ homologue, RECQ1, has also been shown *in vivo* to be involved in restoration of TOP1 inhibitors-associated reversed forks to their original three-armed configuration (Gari, Décaillet et al. 2008).

Various restart pathways, such as re-priming, homologous recombination (HR), template switching, TLS and DSB-mediated restart mechanisms may function at stalled forks to allow restart of DNA replication (Figure 1.11).

1.3.4.1 Fork restart via re-priming

The DNA replication machinery may bypass DNA damage, leaving an un-replicated gap to be repaired by post replication repair (PRR). PrimPol, a recently characterised human primase, and TLS polymerase mediate post-replicative gap repair. PrimPol synthesises short RNA/DNA primers on leading and lagging strands downstream of the lesion, which are extended later by replicative DNA polymerases ϵ and δ. In fact, repriming activity of PrimPol is critical for DNA replication restart (Kobayashi, Guilliam et al. 2016). Unlike the other TLS polymerases, such as Rev 1 and Pol η the recruitment of PrimPol to DNA is not suppressed in the presence of ATR and Chk1 inhibitors (Mourón, Rodriguez-Acebes et al. 2013)(Figure 1.11).

1.3.4.2 Fork restart via homologous recombination

HR-mediated fork restart functionally differs from HR-mediated DSB repair. HR-mediated fork restart promotes the repair of post-replicative ssDNA gaps through DNA-end resection machinery. An initial short-range resection (in the region of∼100–150 bp) is catalysed by the Mre11/Rad50/Nbs1 (MRN) complex and CtIP followed by a long-range resection of DSBs mediated by the DNA nucleases EXO1 or DNA2, generating larger ssDNA regions of up to 1KB which facilitates loading of the HR factor Rad51. Rad51 promotes the 3' overhang invasion into the homologous sister chromatids, priming DNA synthesis followed by restoration of replication forks through endonucleolytic resolution of the recombination D-loop intermediates. HR proteins, such as RAD51, BRCA2/PALB2, BRAC1, and the RAD51 paralogue XRCC3, have been reported to be crucial for maintaining replication fork stability and restart (Petermann, Orta et al. 2010, Zellweger, Dalcher et al. 2015). BRCA2 protects nascent DNA from Mre11-dependent DNA resection at stalled forks and also promotes Rad51 loading and filament formation during replication restart (Hashimoto, Chaudhuri et al. 2010) (Figure 1.11).

1.3.4.3 Fork restart via double-strand break formation

Prolonged fork stalling can lead to the collapse of forks into DSBs, predominately formed by structure-specific nucleases MUS81-EME1, XPF-ERCC1, SLX4 or EXO1 in particular regions of the genome called common fragile sites (CFSs) which are difficult-to-replicate loci. The stalled fork is cleaved by MUS81–EME1 during the G2-phase of the cycle (Forment, Blasius et al. 2011). The entry of cells with un-replicated CFSs into mitotic prophase promotes the recruitment of Rad52 and POLD3-dependent DNA synthesis at the sites and, with the help of SLX4-MUS81, facilitates mitotic DNA synthesis (MiDAS) (Minocherhomji, Ying et al. 2015, Sotiriou, Kamileri et al. 2016). In addition, recruitment of the RECQ5 helicase by MUS81

promotes Rad51 filament removal from stalled forks to allow DSB formation by MUS81-EME1 and MiDAS formation (Di Marco, Hasanova et al. 2017). MiDAS protects CFSs from an extended mis-segregation and non-disjunction during anaphase. In fact, these studies have shown that the lack of MiDAS promotes the appearance of 53BP1 bodies, anaphase bridges and chromosomal rearrangements, acceleration of tumour growth and increased vulnerability to aphidicolin (Figure 1.11).

The details of Translesion synthesis (TLS) and template switching (fork reversal) mechanisms are described elsewhere in this chapter in sections 1.4.1 and 1.3.4, respectively.

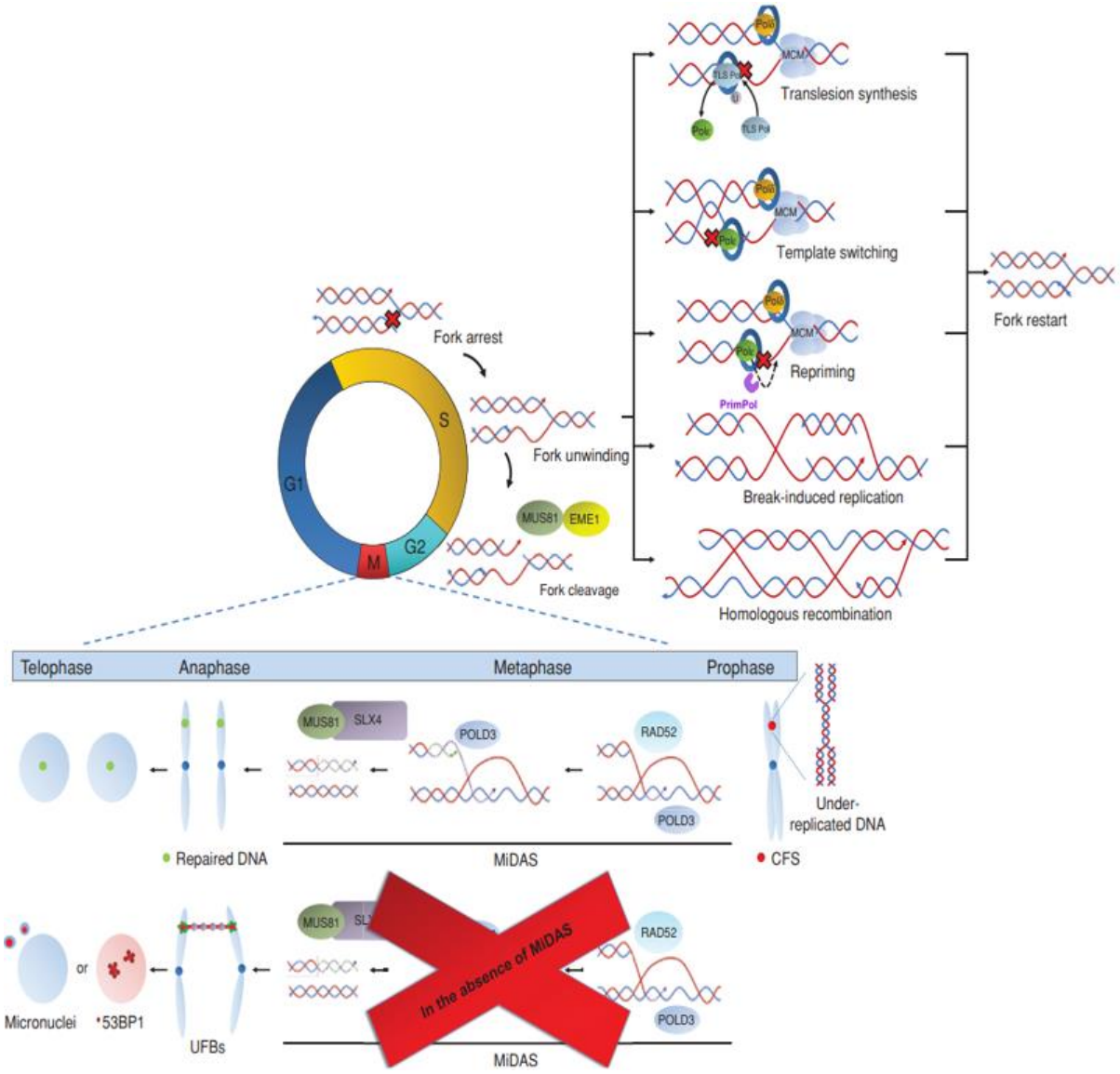

Figure 1.11 The repair of a stalled fork.

When DNA polymerase collides with an obstacle in its path, the replisome is backtracked and the CMG complex unwinds DNA ahead of the stalled fork leaving ssDNA behind. Stalled replication forks can restart DNA replication *by different mechanisms such as translesion synthesis, template switching, repriming, break-induced replication, or homologous recombination. If this fails, MUS81- EME1 dependent cleavage of stalled forks is required during G2-phase before entry into metaphase. In metaphase, Rad52, POLD3, and MUS81–SLX4 collaborate to perform mitotic DNA synthesis (MiDAS). In anaphase, lack of MiDAS during chromosomal separation can lead to formation of ultra-fine anaphase bridges* (*UFBs*) *at the CFSs, which will be manifested as micronuclei or 53BP1 bodies in the daughter cells. Obtained from (Kotsantis, Petermann et al. 2018). This article is published under an open*

access license (published material can be re-used without obtaining permission as long as a correct citation to the original publication is given).

1.3.5 Oncogene-induced replication stress

As aforementioned, DNA replication stress can refer to any deviation in the process, coordination and timing of DNA synthesis. Oncogene-induced replication stress (OIS) is generally attributed to aberrant origin firing, replication–transcription conflicts (TRC), reactive oxygen species (ROS), or defective nucleotide metabolism (Kotsantis, Petermann et al. 2018).

Oncogenes impede replication fork progression through dysregulation of origin firing by promoting either increase or decrease or re-firing of the same origin. Therefore, cells will enter mitosis with incompletely replicated or over-replicated regions that may cause genome instability (GIN). Interestingly, the level of origin firing is inversely correlated to the number of active forks which, in turn, alters the availability of essential replication factors such as the replication machinery itself, nucleotide supply, histones and histone deposition machinery (Zhong, Nellimoottil et al. 2013). Oncogenes may hinder the timing of origin firing by causing unscheduled S-phase entry with limited replication factors or by allowing insufficient time for loading of the replication origins (Bester, Roniger et al. 2011). For example, a hyper-proliferative phase has been shown to occur immediately after induction of activated RAS and this is accompanied by increased origin firing, leading to replication stress (Di Micco, Fumagalli et al. 2006). It seems that the overexpression of cyclin E has a dual influence on pre-replication complex (pre-RC) formation. In one report it has been shown that cyclin E induction inhibits MCM2, 4 and 7 recruitment onto chromatin during telophase and early G1, which contributes to a reduced number of active origins in early S-phase (Ekholm-Reed, Méndez et al. 2004). On the other hand, other groups have shown that overexpression of cyclin E elevates origin firing in S-phase (Bester, Roniger et al. 2011, Jones, Mortusewicz et al. 2013). This inconsistency

could be as a result of different properties of the cell lines used in the studies although it is possible that both explanations are valid.

A growing body of evidence suggests that OIS is also linked to deregulated transcriptional activity, although the molecular mechanism by which oncogenes contribute to replication stress and genome instability has not been completely elucidated. It has been frequently reported that replication stress is induced *in vitro* following overexpression of oncogenes such as MOS, c-MYC, RAS, HPV-16 E6/E7, CDC25A and Cyclin E (Bartkova, Rezaei et al. 2006, Di Micco, Fumagalli et al. 2006, Dominguez-Sola, Ying et al. 2007, Bester, Roniger et al. 2011, Jones, Mortusewicz et al. 2013, Kotsantis, Silva et al. 2016).

The general transcription factor, TATA-box binding protein (TBP), is upregulated following increased global RNA synthesis in response to overexpression of $\mathrm{HRAS}^{\mathrm{V12}}$-induced replication stress (Kotsantis, Silva et al. 2016). (Jones, Mortusewicz et al. 2013) showed that cyclin E-induced replication stress is due to increased levels of transcription, which, together with R-loop accumulation, gives rise to replication fork slowing and genome instability. These authors have shown that treatment with the CDC7/CDK9 dual inhibitor PHA-767491, which inhibits both origin firing and transcription elongation through effects on CDC7 and CDK9 respectively, could rescue cyclin E-induced replication stress. Similarly, an increase in co-transcriptional R-loop formation in estrogen (E2) receptor-positive breast epithelial cells has been identified as a source of E2-induced DSBs (Stork, Bocek et al. 2016). Induction of RAS-associated transcription activity also occurs following activation of mitogen-activated protein kinase extracellular single-regulated kinase (ERK), which activates several transcription factors, such as TIFIA (RRN3), UBTF, TIFIIIB (BRF1) and TBP (Johnson, Mandavia et al. 2000, Zhao, Yuan et al. 2003). Similarly, overexpression of c-MYC stimulates the universal

amplification of gene expression by all three RNA polymerases (Lin, Lovén et al. 2012, Nie, Hu et al. 2012).

These data indicate that deregulated transcription could be a source of tumorigenesis in pre-cancerous lesions, as mentioned above, by compromising the stability of the genome. This hypothesis is supported by a report from (Hatchi, Skourti-Stathaki et al. 2015) showing that SETX is recruited at termination regions (TRs) of actively transcribed genes, in a BRCA1-dependent manner, to inhibit formation of R-loop-driven DNA damage. RNA export factor TREX2 regulates recruitment of BRCA2 to the ssDNA generated at the RNA Pol II pausing sites to avoid formation of R-loops (Bhatia, Barroso et al. 2014). The Fanconi Anaemia pathway has also been reported to be involved in the repair of R-loops generated by transcription replication collisions and this action requires the branch migration activity of FANCM (Schwab, Nieminuszczy et al. 2015).

Replication fork progression can be disrupted as a result of transcription–replication conflicts (TRC). Conflicts include head-on or co-directional collisions between two machines or between replisomes and R-loops (Lin and Pasero 2012) (Figure 1.12). In head-on conflicts, R-loop formation is elevated leading to activation of the ATR/Chk1 pathway. In contrast, co-directional collisions promote R-loop resolution and activation of the ATM/Chk2 pathway following DSB formation (Hamperl, Bocek et al. 2017). In fact, co-directional collisions have little effect on replication fork progression compared to the head-on collisions with respect to fork slowing (Prado and Aguilera 2005). Head-on movement of both replication and transcription machineries can increase the development of positive torsional stress in front of them, which needs to be relaxed by topoisomerases. While the two events progress towards each other the newly produced transcripts may be trapped in the nuclear pore complex (NPC) producing obstacles to fork progression (Kotsantis, Petermann et al. 2018).

Interestingly, the CCR4-NOT complex participates in mRNA export and nuclear quality control by interactions with Mlp1, present in the inner basket of the NPC (Libri, Dower et al. 2002). R-loops can either increase chromatin compaction, marked by H3 phosphorylation at Ser-10, or can modulate formation of G-quadruplexes (G4) which, in turn, can facilitate R-loop stabilization (Abraham, Chan et al. 2016). Formation of G4 structures within promoters of highly transcribed genes such as c-MYC (Siddiqui-Jain, Grand et al. 2002) or KRAS (Cogoi and Xodo 2006) plays an important role in regulation of gene expression. Taken together, these data indicate that oncogene-dependent transcription-replication encounters contribute to replication stress.

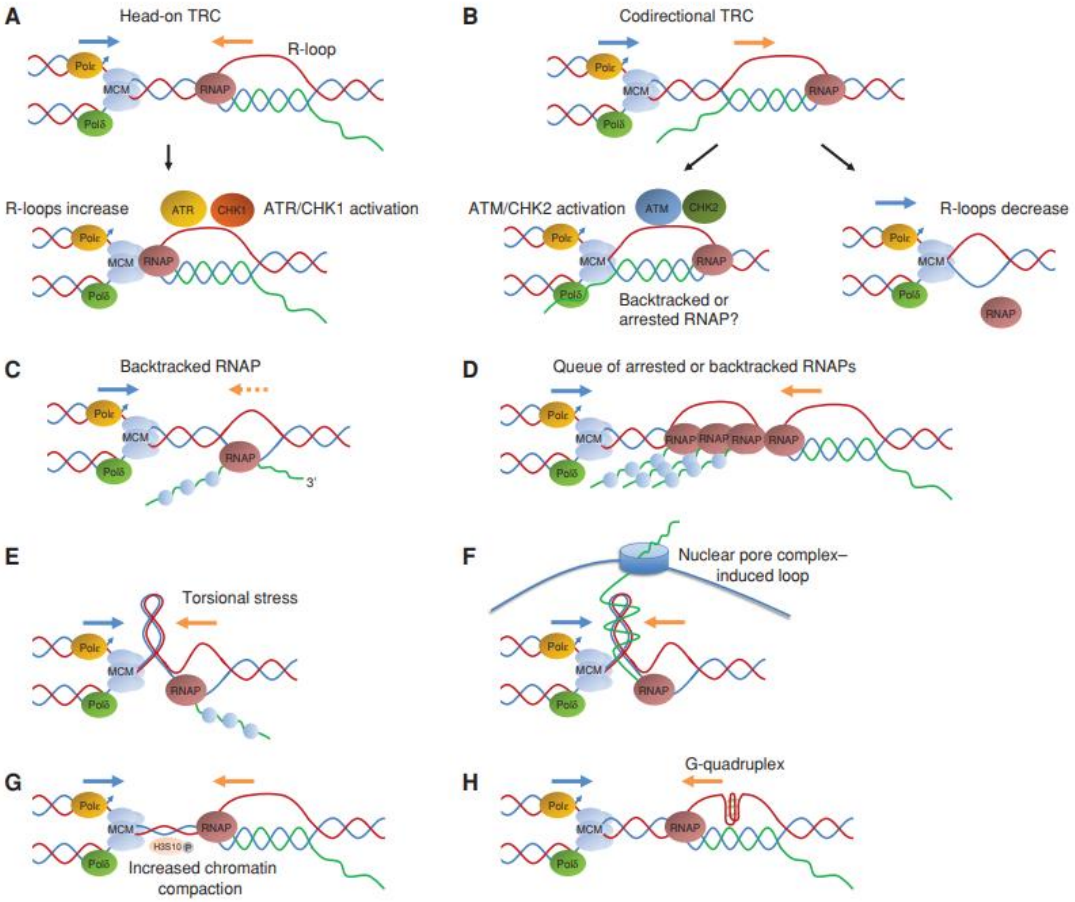

Figure 1.12 Transcription-dependent replication stress.

A) *Upon head-on encounters between transcription and replication machineries, R-loop formation is elevated leading to activation of the ATR / Chk1 pathway.* ***B)*** *Co-directional TRC decreases R-loop structures, which leads to activation of the ATM / Chk2 pathway following DSB formation.* ***C)*** *RNA Poll can be stalled or backtracked once it encounters an obstacle during elongation.* ***D)*** *RNA Poll can also pause or backtrack when confronted with an R-loop. In both cases, this will cause a queue of stalled or backtracked RNA Poll that impedes fork progression.* ***E)*** *Head-on collision of both replication and transcription machineries can also increase the development of positive torsional stress in front of them, which hinders progression of both events.* ***F)*** *While two events progress towards one another, the long nascent RNA may be trapped in the nuclear pore complex (NPC) producing obstacles to fork progression.* ***G)*** *and* ***H)*** *R-loops can either increase chromatin compaction, marked by H3 phosphorylation at Ser-10, or modulate formation of G-quadruplexes (G4); both of these inhibit fork progression Obtained from (Kotsantis, Petermann et al. 2018). This article is published under an open access license*

(published material can be re-used without obtaining permission as long as a correct citation to the original publication is given).

The building blocks of DNA are nucleotides and a ready supply is critical for the maintenance of genome stability; therefore, any changes in their structure or level has an immediate effect on fork progression (Figure 1.13). The metabolism of nucleotides can be altered during oncogenesis; for example, the binding of Bcl2 to RRM2 disrupts the activity of the RNR complex leading to depletion of the dNTP pool and retardation of DNA replication (Xie, Yen et al. 2014). In addition, induction of RAS downregulates RRM2 through binding of the transcription repressor E2F7 to the start site of RRM2, causing exhaustion of the dNTP pool and eventually RAS-induced senescence (Aird, Zhang et al. 2013). Inhibition of ATR or Chk1 induces replication stress and synthetic lethality in conjunction with the action of the oncogenes cyclin E (Toledo, Murga et al. 2011), c-MYC (Schoppy, Ragland et al. 2012) and H/KRAS (Gilad, Nabet et al. 2010). Suppression of Chk1 increases CDK-dependent origin firing, reducing dNTP supply. This causes fork slowing and induction of excess ssDNA that is coated by RPA in an ATR-dependent manner. Therefore, following inhibition of ATR this protective signal is disrupted, leading to senescence as a response to oncogenic stress (Gilad, Nabet et al. 2010). In contrast, c-MYC upregulates genes involved in nucleotide biosynthesis, increasing dNTP pools and enabling/enhancing cell proliferation (Mannava, Grachtchouk et al. 2008). Reduction in dNTP supply increases the level of rNTP mis-incorporation by DNA polymerases. Since rNTP are more susceptible to hydrolysis than dNTPs, their incorporation into DNA will affect fork progression and may cause GIN. It is likely that oncogene-associated rNTP mis-incorporation occurs during hyperproliferation, following induction of oncogene expression (Kotsantis, Petermann et al. 2018). Oncogene-induced reactive oxygen species (ROS) appear to oxidise nucleotides that, when used by DNA polymerases, can initiate fork slowing, breaks and mutations in the DNA and senescence (Rai, Onder et al. 2009). 8-oxoG, which is a major oxidative DNA lesion, is found at elevated levels in senescent cells as a result of RAS induction

(Homma, Tsunoda et al. 1994, Rai, Onder et al. 2009). In addition, (Rai, Onder et al. 2009) showed that overexpression of MTH1, which hydrolyses oxidised dNTPs, can prevent the onset of markers of senescence, such as elevated levels of $p21^{(Cip1)}$, p53, and $p16^{(INK4A)}$, thus preserving genomic integrity. It seems that 8-oxo-dGTP-associated delayed DNA synthesis is due to a decreased rate of chain elongation. This delay is offset following treatment with Staurosporine, a protein kinase C inhibitor (Kai, Matsunaga et al. 2002).

Different oncogenes utilise different mechanisms for induction of replication stress. For instance: the oncogenes RAS and cyclin E create a unique 'fragility landscape' that varies from the fragile sites induced by the replication inhibitor aphidicolin (Miron, Golan-Lev et al. 2015).Furthermore, dysregulation of cyclin E causes chromosomal instability (CIN) in human cells, which is not seen after induction of cyclins A or D1 (Spruck, Won et al. 1999).

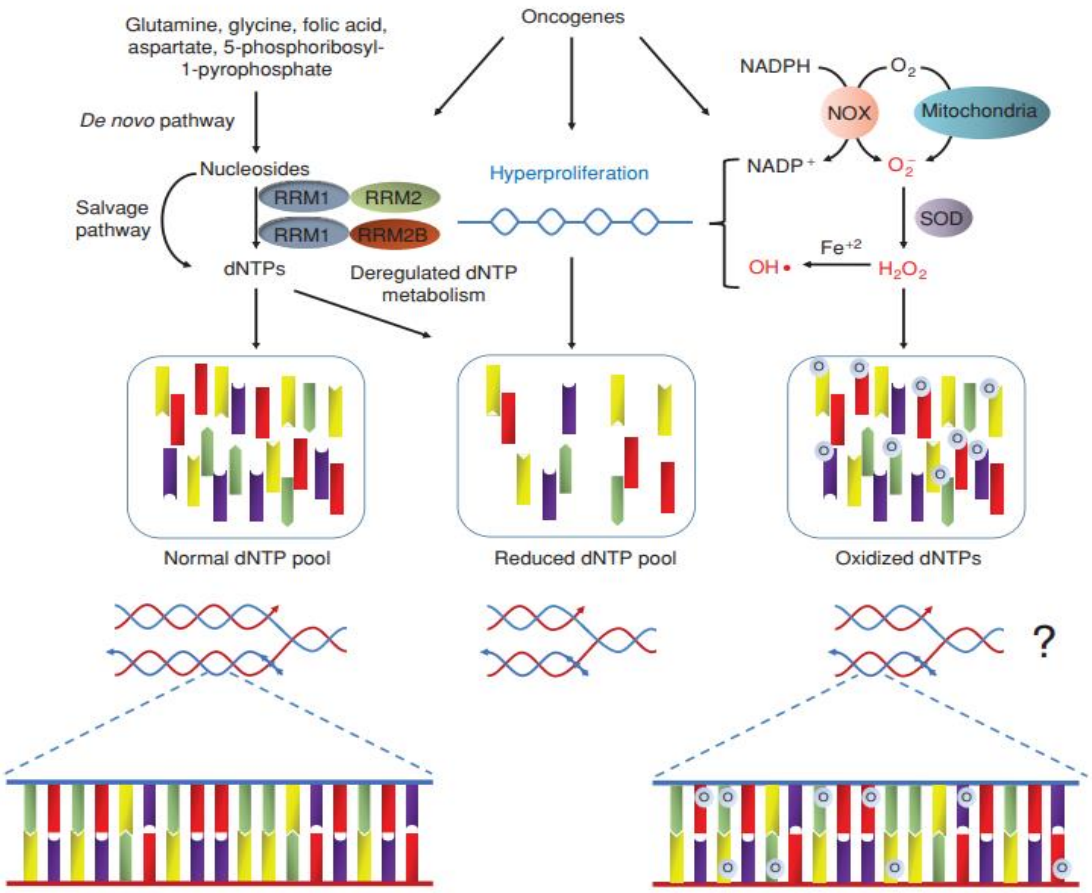

Figure 1.13 The molecular mechanisms of oncogene action in nucleotide metabolism and aberrant DNA replication.

Formation of dNTPs is performed either through the de novo *pathway from glutamine, glycine, folic acid, aspartate, 5-phosphoribosyl-1-pyrophosphate or through the salvage route by turnover of nucleotides (recycling pathway). The RNR reductase complex catalyses the conversion of NTPs to dNTPs. Oncogenes may affect fork progression by inhibiting the activity of the RNR complex or by causing aberrant cell proliferation that will reduce the dNTP supply. Moreover, oncogene overexpression contributes to ROS induction, including the production of* O_2^-, H_2O_2 *and OH radicals.* O_2^- *is generated either by oxidation of NADPH by NOX enzymes or through mitochondrial respiration. Superoxide dismutase (SOD) catalyses the conversion of* O_2^- *to* H_2O_2*. In the presence of* Fe^{2+}*, OH radicals can be formed from* H_2O_2*. Obtained from (Kotsantis, Petermann et al. 2018). This article is published under an open access license*

(published material can be re-used without obtaining permission as long as a correct citation to the original publication is given).

1.4 Transcription-induced stress response

1.4.1 Repair of Intra-strand crosslinks (ICLs) and DNA bulky adducts

RNA Pol II senses DNA lesions or epigenetic modifications: in particular, intra-strand crosslinks (ICLs) such as UV-induced pyrimidine dimers (CPDs) and DNA bulky adducts, such as those produced by cisplatin and MMC (Shin, Xu et al. 2017). The ways in which RNA Pol II stalls at these different DNA lesions varies. For example, cisplatin-induced DNA bulky adducts prevent the lesion from entering the RNA Pol II active site whereas UV-induced CPDs can enter the active site; subsequent stalling is then dependent on which ribonucleotide is incorporated into the nascent RNA complementary to the damaged DNA template. RNA Pol II preferentially incorporates adenine across from these sites, which is error-free and will not arrest RNA Pol II. However, the CPD 5'-thymine leads to uridine mis-incorporation into mRNA, which blocks RNA Pol II progression (Brueckner, Hennecke et al. 2007). These DNA lesions not only shut down transcript production but can also arrest DNA replication fork progression; both of these carry the threat to genome stability (Muniandy, Thapa et al. 2009).

Nucleotide excision repair (NER) is predominantly invoked in response to UV-induced DNA damage (Rastogi, Kumar et al. 2010). The NER pathway may be divided into two subtypes; global genomic NER (GG-NER), and transcription coupled NER (TC-NER). The GG-NER pathway is involved in repair of lesions in the entire genome, including un-transcribed regions and silent DNA strands; while transcription coupled NER (TC-NER) triggers a transcription-dependent genome repair pathway (Sugitani, Sivley et al. 2016). Various forms of DNA damage are recognised by two different sets of proteins, appropriate for each pathway. However, after damage recognition, the two subtypes have the same steps of dual incision, repair, and ligation. The lesion site on the non-transcribed strand is detected by

the global GG-NER structure-specific recognition complex of XPC, RAD23B and CENTN2 (Marteijn, Lans et al. 2014). In addition, the DDB1-DDB2 (XPE) complex binds to DNA lesions to stabilise XPC association to the lesion site. After initial lesion- recognition, the remaining NER cascade triggers DNA double helix unwinding by the two helicase subunits of the transcription factor TFIIH, XPB and XPD, around the damaged site. TFIIH recruits XPA and RPA, which subsequently activate XPF-ERCC1 and XPG (a 5' endonuclease and 3' endonuclease, respectively) to incise a 22-30 nucleotide long DNA strand containing the damage site (Figure 1.14).

In contrast, on the transcribed strand during elongation, the lesion site is recognised by RNA polymerase II itself, which becomes arrested at the site. Stalled RNA Pol II directly recruits CSB at the site of damage and forms a complex with UVSSA and USP7 followed by recruitment of CSA (Nakazawa, Sasaki et al. 2012). Indeed, TC-NER has been involved in two activities: firstly, backtrack of the arrested RNA Pol II in order to provide accessibility for the downstream NER repair components to the DNA lesion and, secondly, removal of a strong signal for apoptosis (Ljungman and Zhang 1996), (Fousteri and Mullenders 2008, Stubbert, Smith et al. 2010).

Following unhooking of the DNA lesion, the gap is filled by DNA polymerases and ligases (Deans and West 2011). A bypass platform is supported by binding of ubiquitinated PCNA to translesion DNA synthesis (TLS) polymerases such as Rev 1, Pol ζ, Pol κ and Pol ε (Godon, Mourgues et al. 2012) (Figure 1.13). (Zafar, Ketkar et al. 2014) have also reported PrimPol-mediated re-priming and elongation of nascent DNA accurately downstream of the DNA lesion. Repair of ICLs or DNA adducts in the G1 and S phases of the cell cycle may use different mechanisms. In G1, bypass repair is carried out by TC-NER repair and translesion DNA synthesis. However, in S phase the Fanconi Anemia (FA) pathway, homologous

recombination (HR) and TLS are responsible for ICL removal during DNA replication (Deans and West 2011). Repair of ICLs in the G1 phase of the cell cycle has received appreciably less attention as ICL tolerance in G1 is much greater than in S-phase, where induction of stalled replication forks can be highly toxic (Guainazzi and Schärer 2010, Muniandy, Liu et al. 2010). The ligase III-XRCC1 complex facilitates the ligation step (Moser, Kool et al. 2007). It has been reported in yeast that deficiency in TC-NER is associated with mutations in the CNOT complex, possibly suggesting functions for the CNOT complex in DNA repair during transcription elongation (Gaillard, Tous et al. 2009)

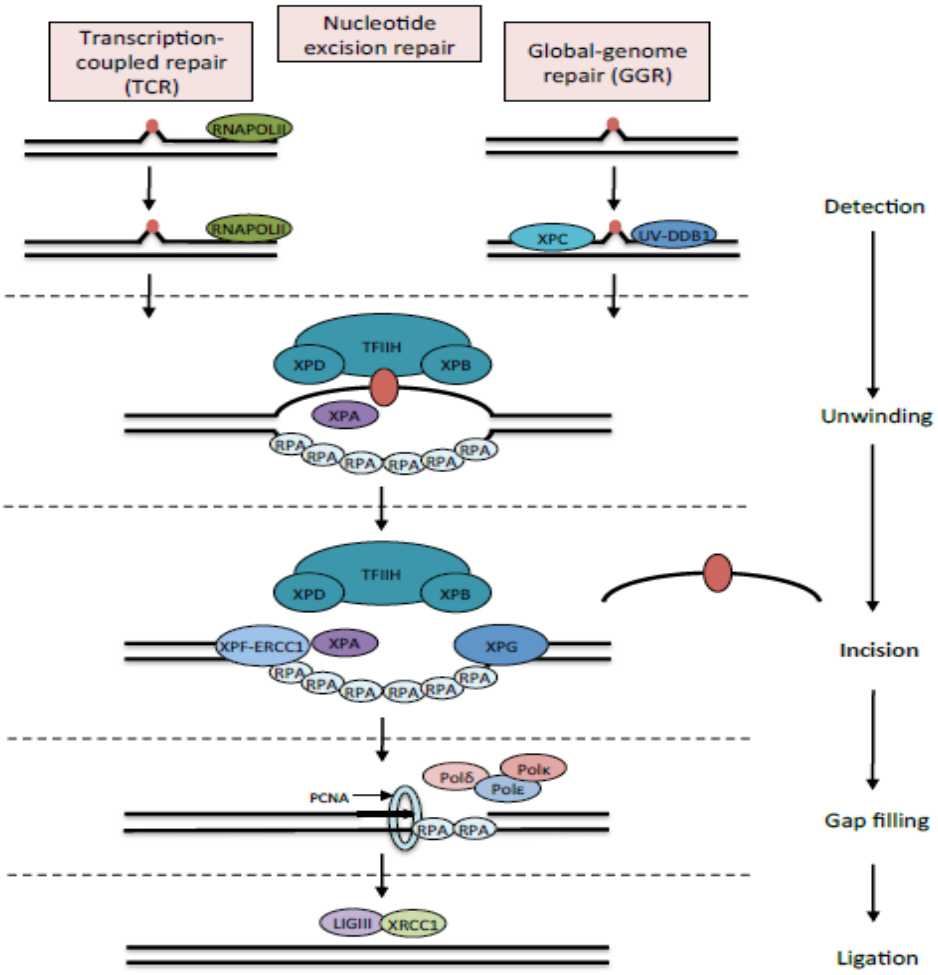

Figure 1.14 The molecular mechanisms of GG-NER and TC-NER in mammals.

The NER repair pathway consists of five different steps; DNA damage detection (it differs in GG-NER and TC-NER), unwinding, DNA incision, gap filling and ligation (these are the same in both sub-pathways of NER). Obtained from (Ryan 2016).

Apart from CPDs and DNA bulky adducts, 8-Oxoguanine (8-oxoG) can also be repaired via the TC-NER pathway in a transcription dependent manner. Formation of 8-oxoG is one of the most common consequences of oxidative stress resulting from reactive oxygen species ; this is produced in DNA by normal cellular metabolism (mitochondrial respiration) or after exposure to exogenous damaging agents such as ionizing radiation. Persistence of this lesion in DNA is associated with G > T transversions with deleterious effects on genome stability. 8-OxoG can block transcription mediated by RNA polymerase II by interfering with gene expression, DNA replication and repair of the damage (Tornaletti, Maeda et al. 2004). The base excision repair (BER) of 8-oxoG from an 8-oxoG:C pair is initiated by OGG-1 DNA glycosylase / AP lyase leaving an apurinic-apyrimidinic (AP) site (Lindahl 1974). In mammals, special DNA glycosylases / AP lyases, nuclear α-hOGGl and mitochondrial β-hOggl, identify 8-OxoG and incise DNA resulting in AP site formation. OGGl protein is required for the repair of 8-OxoG in both the transcribing strand (TS) and non-transcribing strand (NTS); however, it has been reported that 8-OxoG removal from TS is faster compared to NTS, suggesting that TC-NER also contributes to 8-OxoG repair (Le Page, Klungland et al. 2000). These authors showed that in OGGl -/- MEFs transcription can progress through oxidative damaged bases on TS. It is also possible that MutY, a DNA glycosylase, excises adenine inserted opposite 8-OxoG, and mismatch repair removes the mutation induced by lesion on NTS (Le Page, Klungland et al. 2000).

Tornaletti, Maeda et al showed that any changes in the dNTP pool influenced the extent of RNA Pol II stalling at the 8-oxoG lesion (Tornaletti, Maeda et al. 2004). These authors have also observed that reduction in the ATP concentration increased RNA Pol II blockage at the 8-oxoG site.

TLS DNA polymerase PrimPol accurately bypasses 8-oxo-dG and catalyses dCMP insertion opposite 8-oxo-dG with 2 to 6-fold greater efficiency than dAMP mis-insertion (Zafar, Ketkar et al. 2014). PrimPol, a recently characterised human primase and TLS polymerase, is capable of using both dNTPs and rNTPs to make primers and reinitiate DNA synthesis after dNTP depletion, which would be rate limiting for DNA replication. Unlike, Pol-α and Pol- ε, which generate a continuous leading strand, PrimPol promotes discontinuous synthesis of the leading strand (Rudd, Bianchi et al. 2014). Expression of PrimPol mRNA is cell cycle-dependent and peaks in G1/S phase; however, protein levels remain unchanged throughout the cell cycle. Unlike the other TLS polymerases, such as Rev 1 and Pol η the recruitment of PrimPol to DNA is not suppressed in the presence of ATR and Chk1 inhibitors (Göhler, Sabbioneda et al. 2011), (Mourón, Rodriguez-Acebes et al. 2013, DeStephanis, McLeod et al. 2015).

1.4.2 Imbalanced rNTP / dNTP pool ratio and DNA polymerase-mediated incorporation errors

Deoxynucleoside triphosphates (dNTPs) are the building blocks of the DNA and are critical in the maintenance of genome stability; therefore, any changes in their structure or levels has an immediate effect on DNA replication, repair and rates of mutagenesis. Ribonucleotide reductase (RNR) catalyses the conversion of ribonucleotides into deoxyribonucleotides by removing the 2'-hydroxyl group of the ribose ring of the nucleoside diphosphates. RNR is a tetrameric protein complex and consists of two catalytic (RRM1) and two regulatory (RRM2, RRM2B) subunits (Niida, Shimada et al. 2010). RRM2 expression is cell-cycle dependent and is approximately threefold more abundant during DNA replication in S phase than in G1; this is to maintain the balance of dNTP pools (Kotsantis, Petermann et al. 2018). In response to

DNA damage ATR is responsible for an increase in the level of RRM2 and consequently the dNTP pools (D'Angiolella, Donato et al. 2012). In addition, in response to replication stress, active ATR phosphorylates Chk1 which, in turn, supresses cyclin F. Cyclin F, an F-box protein, is the substrate binding subunit of SCF (Skp1-Cul1-F-box protein) ubiquitin ligase complexes and indirectly regulates the level of RRM2 by degradation of transcription factor E2F1, which activates the RRM2 gene promoter, in late G2 phase of the cell cycle (D'Angiolella, Donato et al. 2012). Upregulation of cyclin F mRNA, which reversibly decreases the level of RRM2 has been reported in patients with skin cancer (cutaneous melanoma) with poorer prognosis due to increased DNA damage repair and drug resistance. In addition, poorer patient outcome was observed when the high expression of cyclin F mRNA coincided with increased levels of proliferative factors, such as cyclin E, PCNA, pro-survival factors such as p27 or FOXM1 and proteins connected with AKT pathway activation (INPP4B) (Gagat, Krajewski et al. 2018). Thus, Chk1-mediated inhibition of cyclin F supresses the degradation of both E2F1 and RRM2 (Zhang, Jones et al. 2009). Interestingly, *Buisson, Boisvert et al.* reported that treatment with ATR inhibitor or cyclin F siRNA + ATRi were not able to rescue the level of RRM2. However, overexpression of E2F1 could successfully inhibit degradation of RRM2 in ATRi-treated cell, suggesting reduction of RRM2 by ATRi is a direct consequence of E2F1 degradation (Buisson, Boisvert et al. 2015). Downregulation of RRM2 in response to induction of the activated RAS oncogene is due to an increased binding of the atypical transcriptional repressor E2F7 with the RRM2 gene promoter region and a simultaneous reduction in association of transcriptional activator E2F1 to the RRM2 gene promoter. This gives rise to dNTP pool depletion prior to oncogene-induced senescence (Aird, Zhang et al. 2013). Very recently, using a CRISPR screen the synthetic lethality between ATR or Chk1 inhibition and cyclin F loss has been reported. However, cyclin F knockout cells showed more vulnerability to inhibition

of Chk1 than ATR and this is consistent with the fact that inhibition of Chk1 has more deleterious effect on cycling cells than ATR inhibition (D'Angiolella, Yang et al. 2019). Exhaustion of dNTP pools, following downregulation of RRM2, reduces replication fork progression. Interestingly, the yeast Ccr4-Not complex is required for transcription activation of the RNR subunits by facilitating the recruitment of TBP, RNA pol II and the methyltransferase Set1p to the promoter site of RNR3 following replication stress and DNA damage in yeast (Mulder, Winkler et al. 2005). DNA replication under normal dNTP levels will increase the presence of embedded ribonucleoside monophosphates (rNMPs) in genomic DNA (gDNA). The mis-insertion rate of rNMPs by Family B replicases (Pol α, δ, and ε) has been reported to be surprisingly high (1 in 625, 5000, and 1250 for each polymerase, respectively) despite effective nucleotide discrimination by their active site; this is likely to be aggravated by decreased level of dNTP (McElhinny, Watts et al. 2010). Incorporation of rNMPs in the genome constitutes the most abundant DNA lesion occurring during DNA replication and it is predicted that 1 million rNMPs or more may be incorporated for each replication cycle in the mouse genome (Reijns, Rabe et al. 2012). The pyrimidine rCTP is the most frequently inserted nucleotide and rUTP the least (Potenski and Klein 2014). In mammalian cells, an excess of cellular rCTP reduces basal Poly [ADP-ribose] polymerase 1 (PARP-1) activity and consequently disruption of Chk1 activity at the replication fork, leading to under-replicated DNA and ultrafine anaphase bridge (UFBs) formation (Gemble, Buhagiar-Labarchède et al. 2016). An imbalanced rNTP / dNTP pool ratio threatens genome stability due to an increased mutation rate leading to growth retardation (Bester, Roniger et al. 2011). *Chen, Zhang et al* showed that regulation of the dNTP pool and senescent autophagy are reciprocally linked, so that suppression of RNR induces autophagy and autophagy reduces the dNTP source (Chen, Zhang et al. 2014).

1.4.3 Repair of mis-inserted rNMPs in genomic DNA by ribonucleotide excision repair (RER)

The proofreading of mis-inserted rNMPs is less efficient than the monitoring of incorrect bases by DNA polymerases; rNMP removal post-replication is performed by ribonucleotide excision repair (RER) (Sparks, Chon et al. 2012, Williams, Clausen et al. 2012). The presence of rNMPs in gDNA increases the number of alkali-sensitive sites; indeed, the 2'-hydroxyl group in the ribonucleotide makes RNA chemically more unstable and susceptible to hydrolysis compared to DNA (Reijns, Rabe et al. 2012). RNase H2-dependent RER repair can incise the 5’ phosphodiester bond of the ribonucleotide incorporated within DNA. The eukaryotic RNase H2 complex consists of one catalytic subunit, RNase H2A, and two non-catalytic subunits, RNase H2B and RNase H2C, which are likely involved in interaction with the other proteins such as PCNA localised at the replication sites. Cells lacking RNase H2 show accumulated mono- and polyubiquitylated PCNA, whereas no significant effect is observed in PCNA sumoylation (Lazzaro, Novarina et al. 2012). In addition, these authors have shown that loss of RNase H2 had a synthetic effect when a second deletion occurs in RAD18 E3 ligase, responsible for conjugating ubiquitin to PCNA. In the absence of RNase H2-mediated repair of rNTPs, the TLS polymerases can bypass them (Lazzaro, Novarina et al. 2012).

In yeast strains with a defective RNase H2-initiated ribonucleotide excision repair (RER) pathway, an alternative repair system incises rNMPs incorporated into DNA. In this TOP1-dependent pathway, a nick produces 5’-OH and cyclic 2’-3’ phosphate terminated chains. Since such nicks cannot be extended by DNA polymerases or sealed by ligases, this results in single strand break formation. If a TOP1-dependent cyclic 2’-3’ phosphate nick is opposite a second TOP1 cleavage complex (TOP1cc) on the other strand a DSB could result. As a consequence of erroneous and abortive activity of TOP1 this alternative pathway is

significantly mutagenic although the targets are not all yet characterised (Kim, Shar-yin et al. 2011, Sparks, Chon et al. 2012).

TOP1-associated SSBs are predicted to involve PARP1. The rapid binding of PARP1 to the site of a break is crucial for the re-ligation of SSBs (Murai, Shar-yin et al. 2012). In a recent CRISPR screen of genes whose mutation causes increased PARP inhibitor sensitivity the RNase H2 enzyme complex (RNase H2A, RNase H2B and RNase H2C) and several CNOT genes were identified (Zimmermann, Murina et al. 2018). TOP1-associated PARP1-trapping DNA lesions increase the sensitivity of RNaseH2A-depleted Chronic Lymphocytic Leukaemia (CLL) cells to PARPi. Depletion of TOP1 could decrease the number of γ-H2AX foci in RNase H2-deficient CLL primary cancer cells (Zimmermann, Murina et al. 2018). In another CRISPR screen it was shown that RNase H2 and CNOT complex deficiency are synthetically lethal with ATR inhibition both *in vitro* and *in vivo* (Wang, Wang et al. 2018). These authors have shown that RNase H2-depleted HeLa cells exhibit increased levels of DNA damage; in combination with ATR inhibitor (AZD6738) treatment (short time), the cells underwent apoptosis; however, prolonged treatment (6 days) with ATRi induced a senescence pathway.

1.4.4 Repair of TOP1-dependent single-stranded DNA (ssDNA) nicks

Approximately one hundred and fifty thousand oxidative adducts per cell are generated from endogenous ROS each day and this represents a huge source of modified DNA bases. Insertion of rNMPs into the gDNA by replicative and repair DNA polymerases vastly outnumbers oxidative lesions, with up to one ribonucleotide embedded per thousand bases during normal replication in yeast. It is now well- established that many DNA alterations have been processed by topoisomerase reactions, which in return increases the levels of TOPcc and DNA damage.

TOP1 relieves DNA hyper-negative supercoiling during transcription and DNA replication that would otherwise accumulate and disrupt transcription elongation and DNA replication fork progression (Baranello, Wojtowicz et al. 2016). The function of TOP1 is to reduce super helical torsion. In doing this it creates a 'nick' transiently in the DNA but itself remains covalently attached at the 3'-side of the nick. Generally, TOP1 functions to generate an immediate resealing of the 'nick' in the DNA backbone. If the cleavage–re-ligation cycle is inhibited, this results in the formation of abortive TOP1–DNA complexes that are known as TOP1cc (Pommier, Sun et al. 2016). TOP1 inhibitors, such as camptothecin, inhibit TOP1 re-ligation activity, leading to the enzyme being trapped on a nicked DNA intermediate in the replicating cell. Indeed, replication fork collapse at a pre-existing nicked DNA may result in a replication run-off in close vicinity to the TOP1-trapped site which is frequently linked to DSB generation during DNA replication (Chaudhuri, Hashimoto et al. 2012). Two pathways are involved in TOP1cc removal; firstly, one involving a ubiquitous enzyme, tyrosyl-DNA phosphodiesterase 1 (TDP1), and secondly, one based on the activities of the endonucleases, XPF–ERCC1 and Mre11. At TOP1cc sites, TDP1 also associates with, and is stabilised by, PARP1, which also implicates the role of TDP1 in the repair of TOP1-associated PARP1 trapping DNA lesions. The removal of TOP1cc by TDP1 leaves a 3'phosphate end, which is dephosphorylated by polynucleotide kinase phosphatase (PNKP) (Pommier, Sun et al. 2016, Kawale and Povirk 2017). The Auto-PARylation of PARP1 and its target proteins allows the recruitment of a number of proteins that have roles in BER to the SSB. One such protein is X-ray repair cross complementing protein (XRCC1), which is a partner of DNA ligase III (El-Khamisy, Masutani et al. 2003). In the other pathway, TOP1cc can be released by the 3'flap endonuclease complex (XPF–ERCC1) and the 3'–5' exonuclease Mre11 (Postel-Vinay, Bajrami et al. 2013). The choice between repair by TDPs or by endonucleases needs further investigation (Figure 1.15).

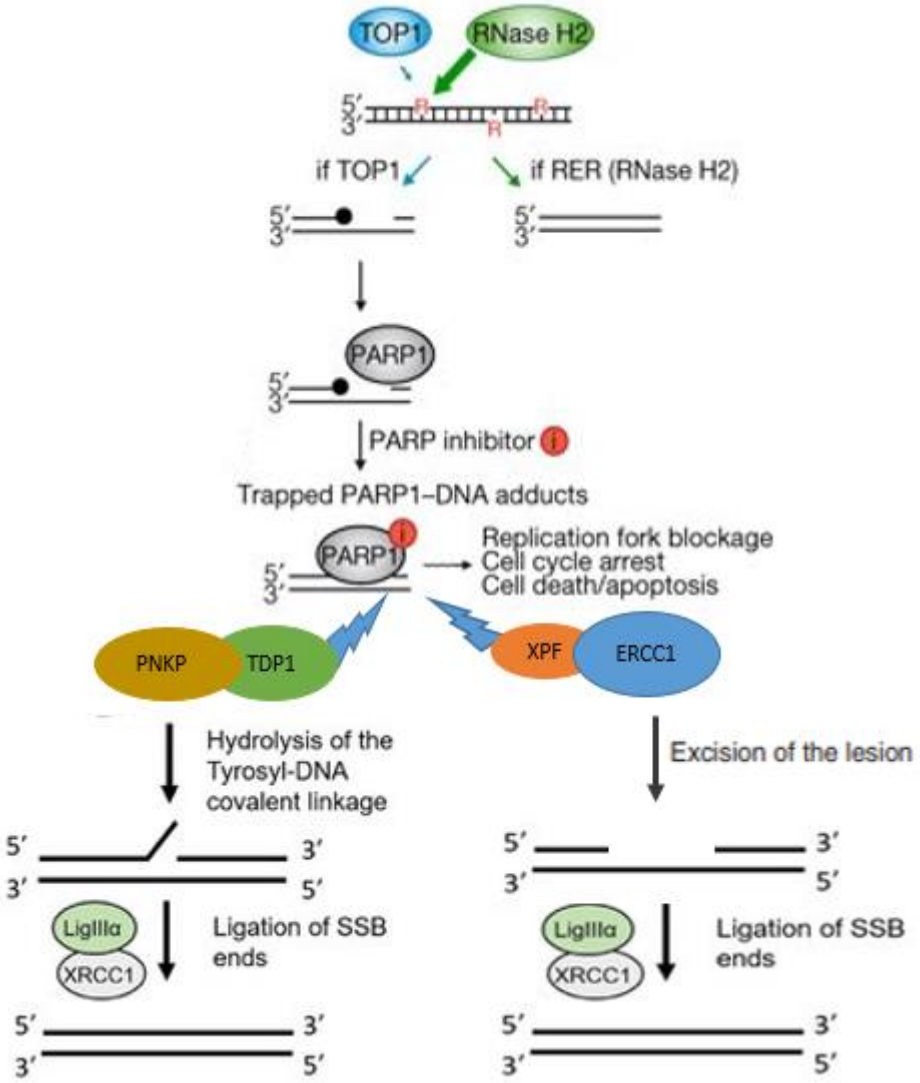

Figure 1.15 Repair of TOP1-PARP trapping lesions.

TOP1-PARP trapping lesions are repaired by two different pathways. ***1)*** *The TDP1-dependent pathway of hydrolysis of the tryosyl-DNA covalent linkage and completion of repair via the BER pathway.* ***2)*** *The endonuclease complex (XPF–ERCC1)-dependent pathway of excision of the lesion and completion of repair via the NER pathway. Modified from (Zimmermann, Murina et al. 2018), (Postel-Vinay, Bajrami et al. 2013, Kawale and Povirk 2017).*

1.4.5 Repair of R-Loop-dependent genome instability

RNA-DNA hybrids (R-loops) may be formed in a variety of circumstances; for example, they can be directly associated with the transcription-blocking DNA lesions seen in trapped TOP1cc sites (Das, Huang et al. 2014) and / or as a consequence of collision between replication forks and the transcription machinery (Lin and Pasero 2012). In these circumstances if replication restarts downstream of the prolonged arrested RNA Pol II at trapping sites this gives rise to the accumulation of gaps in the DNA. In these gaps the template DNA could then be hybridised with a nascent RNA, while the homologous ssDNA is displaced and R-loops could result (Dutta, Shatalin et al. 2011). Transcription may affect genome integrity if co-transcriptional products such as R-loops are not efficiently removed behind RNA polymerase II. R-loops threaten genome integrity by colliding with replication and transcription complexes and by increasing the rate of mutagenesis over transcribed regions, such as ribosomal genes (Kantidakis, Saponaro et al. 2016). It has been shown that induction of DSBs through processing of R-loops by components of the TC-NER pathway is due to the action of the endonucleases XPF and XPG (Sollier, Stork et al. 2014). Finally, R-loops are associated with trinucleotide expansion $(GAA)_{n-}$ promoting gene silencing in Friedriech's Ataxia and Fragile X Syndrome through enrichment of the histone modification H3K9me2 which is strongly associated with transcriptional repression (Groh, Lufino et al. 2014, Neil, Liang et al. 2018).

Genome stability is protected against R-loop formation via two groups of surveillance factors; the first group prevents R-loops forming and the second group actively resolves the R-loop structures. DNA topoisomerase enzymes suppress R-loop formation by the relaxation of transcription-induced negative supercoiling behind moving RNA Pol II. The THO/TREX complex prevents R-loop formation by binding to transcripts or by packaging nascent RNA

into heterogeneous nuclear ribonucleoprotein (hnRNP) complexes (Reese 2013). Splicing and 3' end processing factors that interact with nascent RNA are also believed to suppress R loop formation (Skourti-Stathaki and Proudfoot 2014). It seems that the length of the nascent RNA is an important determinant in forward translocation of stalled RNA Pol II by the CNOT complex (Collart 2016). RNA/DNA helicases such as Senataxin (SETX) and/or Aquarius (AQR) and RNase H enzymes remove R loops once they are formed (Mischo, Gómez-González et al. 2011)and (Wahba, Amon et al. 2011) (Figure 1.16). The potential for R-loops to act as replication primers was originally reported by (Itoh and Tomizawa 1980). In certain regions of the genome, as seen in rDNA, replication forks can reinitiate replication from stalled DNA-RNA polymerase; the replisome then uses the nascent RNA as a primer to restart synthesis of the leading-strand after removing a co-directional RNA polymerase from the DNA (Pomerantz and O'donnell 2008). This action results in a discontinuous leading strand while the replisome remains associated with DNA during the entire process (Pomerantz and O'donnell 2008). The genome–wide mapping of R-loop formation during transcription in 2013 by the Chedin group introduced R-loops for the first time as potential regulators of gene expression; this was based on the observation that they were enriched at the 5' and 3' ends of human genes, where they form and disappear following transcriptional activity (Ginno, Lim et al. 2013). Soon after, (Skourti-Stathaki, Kamieniarz-Gdula et al. 2014) showed that R-loop formation at the 3' end of genes promotes the Ago2-dependent H3K9me2 chromatin architecture which facilitates RNA Pol II pausing before efficient termination of transcription. More recently, it was shown that R-loop formation at the 5' end of genes regulates the recruitment of two key chromatin-regulatory complexes, histone acetyltransfrase TIP60-p400 and polycomb repressive complex 2 (PRC2) which keep the chromatin in an open conformational state facilitating transcription (Chen, Chen et al. 2015).

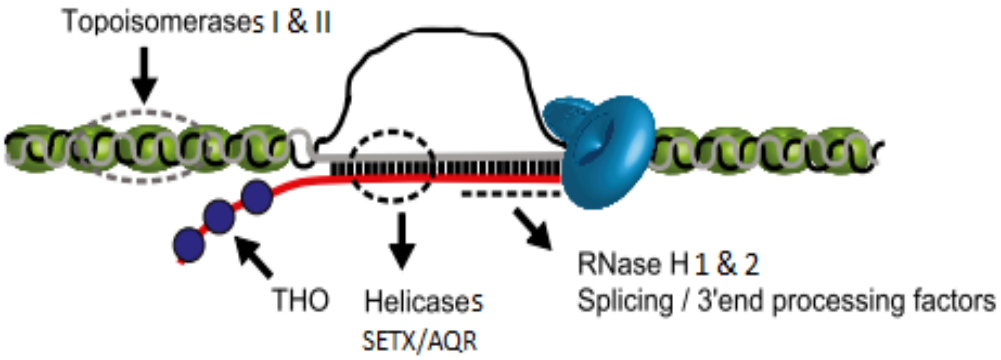

Figure 1.16 R-loop resolution

Two groups of surveillance factors are involved in R-loop removal; the first group prevents R-loops forming; these include proteins such as DNA topoisomerase enzymes, the THO/TREX complex and Splicing and 3' end processing factors. The second group actively removes the R-loop structures; for example, the RNA/DNA helicases such as Senataxin (SETX) and/or Aquarius (AQR) and RNase H enzymes. Adapted from (Skourti-Stathaki and Proudfoot 2014). This article is published under an open access license (published material can be re-used without obtaining permission as long as a correct citation to the original publication is given).

1.5 Double-strand break repair

The cellular genome is subjected to thousands of DNA lesions per day, arising from both endogenous and environmental sources. In order to maintain the integrity of the genome cells have evolved mechanisms known collectively as the DNA damage response (DDR). The DDR employs different repair mechanisms to deal with various types of damage, such as photoreactivation, base excision repair (BER), nucleotide excision repair (NER), and mismatch repair (MMR) (Rastogi, Kumar et al. 2010). DNA double-strand breaks (DSBs) are considered to be the most lethal form of DNA damage, mainly caused by UV or IR, and they can be repaired by two main pathways; either by homologous recombination (HR) or by non-homologous end-joining (NHEJ) (Rapp and Greulich 2004). As the complementary DNA strand is required for HR it can only occur in S, G2 and early M phases of the cell cycle. NHEJ can operate throughout the cell cycle predominately in G1 phase where there is no homologous chain available (Figure 1.17). A better understanding of how these two major DSB repair mechanisms (HR and NHEJ) function can help with the therapeutic purposes of radiation used in tumour radiotherapy by differentially targeting HR and NHEJ function in tumour and normal tissues (Khanna and Jackson 2001).

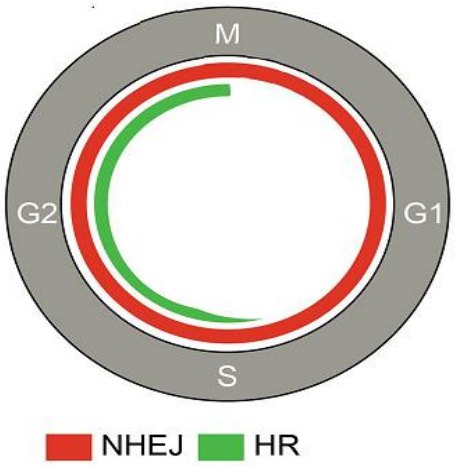

Figure 1.17 The choice between HR and NHEJ at DSBs.

NHEJ can be performed throughout the cell cycle and is the predominant pathway of DNA repair in G1 and early S phase. This is due to the presence of haploid DNA and there is no possibility of repair using a homologous chain. By progression through S phase, the cellular DNA becomes diploid and provides a template strand to allow HR to become more dominant. Obtained from (Krajewska, Fehrmann et al. 2015). This article is published under an open access license (published material can be re-used without obtaining permission as long as a correct citation to the original publication is given).

1.5.1 Homologous recombination (HR) pathway

Rad51 –mediated homologous recombination is the major pathway for repairing DNA double-strand breaks in mammalian cells in S and G2 phases of the cell cycle, although, overall, non-homologous end joining plays the predominant role in the repair of IR and HU-induced DSBs (Bai and Symington 1996). Homologous recombination involves the exchange of molecules of DNA between sequences with similar or identical homology with hundreds of base pairs coverage. However, NHEJ repairs the breaks with no need for a homologous template (Takata, Sasaki et al. 1998). In mammalian cells, the MRN (Mre11-Rad50-NBS1) complex recognises the break and recruits ATM at blunt or minimally processed DNA ends (Williams, Williams et al. 2007). DNA blunt ends undergo 5'–3' nucleolytic degradation, resulting in 3'-single-stranded DNA overhangs which enable repair of DSBs by HR. This process is regulated by 5'-Mre11-Rad50 nuclease-ATPase and CtIP removing small oligonucleotides from the DNA ends to form an early intermediate (DNA end resection) (Limbo, Chahwan et al. 2007). Immediately after this, the Exo1 endonuclease, DNA2 and BLM helicase complete this intermediate and generate extensive tracts of single-stranded DNA (Zhu, Chung et al. 2008). The 3'-ended ssDNA is coated by the replication protein A (RPA) complex, removing the hairpin-containing DNA structures and serving 3'-ssDNA as a substrate for the recombinase RAD51. Paradoxically, the RPA supresses the binding of RAD51, while recombination mediators resolve this inhibitory effect of RPA (Sugiyama and Kowalczykowski 2002). RAD51 displaces RPA from the ssDNA-RPA in a BRCA2-dependent manner and forms a presynaptic filament with ATP and ssDNA. The ssDNA-RAD51-ATP complex is now active and able to undertake homology searches and DNA strand exchange, although the precise role of RAD51 ATPase activity in filament assembly is still somewhat unclear (Baumann, Benson et al. 1996). Once the RAD51 nucleoprotein filaments are assembled the second DNA strand is able to bind

and exchange DNA with the paired homologous region and form a “Holliday junction” structure. How the exchange mechanism really works between paired chromosomes is still under debate. It is thought that a rare random collision juxtaposes complementary nucleotide sequences on two matching ssDNA strands (Alberts, Johnson et al. 2002) (Figure 1.18). NBS1 facilitates the translocation of ATM to the site of the DNA break (Waterworth, Altun et al. 2007). ATM is an essential protein required for phosphorylation of H2AX at serine 139 residue, however, it is not well-understood whether the binding of ATM to NBS1 promotes this phosphorylation or ATM is recruited in its active form (Kinner, Wu et al. 2008). The phosphorylated form of H2AX (γ-H2AX) binds to MDC1 (mediator of DNA damage checkpoint) which is thought to bridge the binding of the MRN complex to γ-H2AX. Moreover, (Saito, Fujimoto et al. 2013) have reported the interaction between H2AX and NBS1 is necessary for NBS1 focus formation, as NBS1 focus formation was not observed in response to DSB damage, neither in H2AX-/- mouse cells nor siRNA-depleted H2AX human cells.

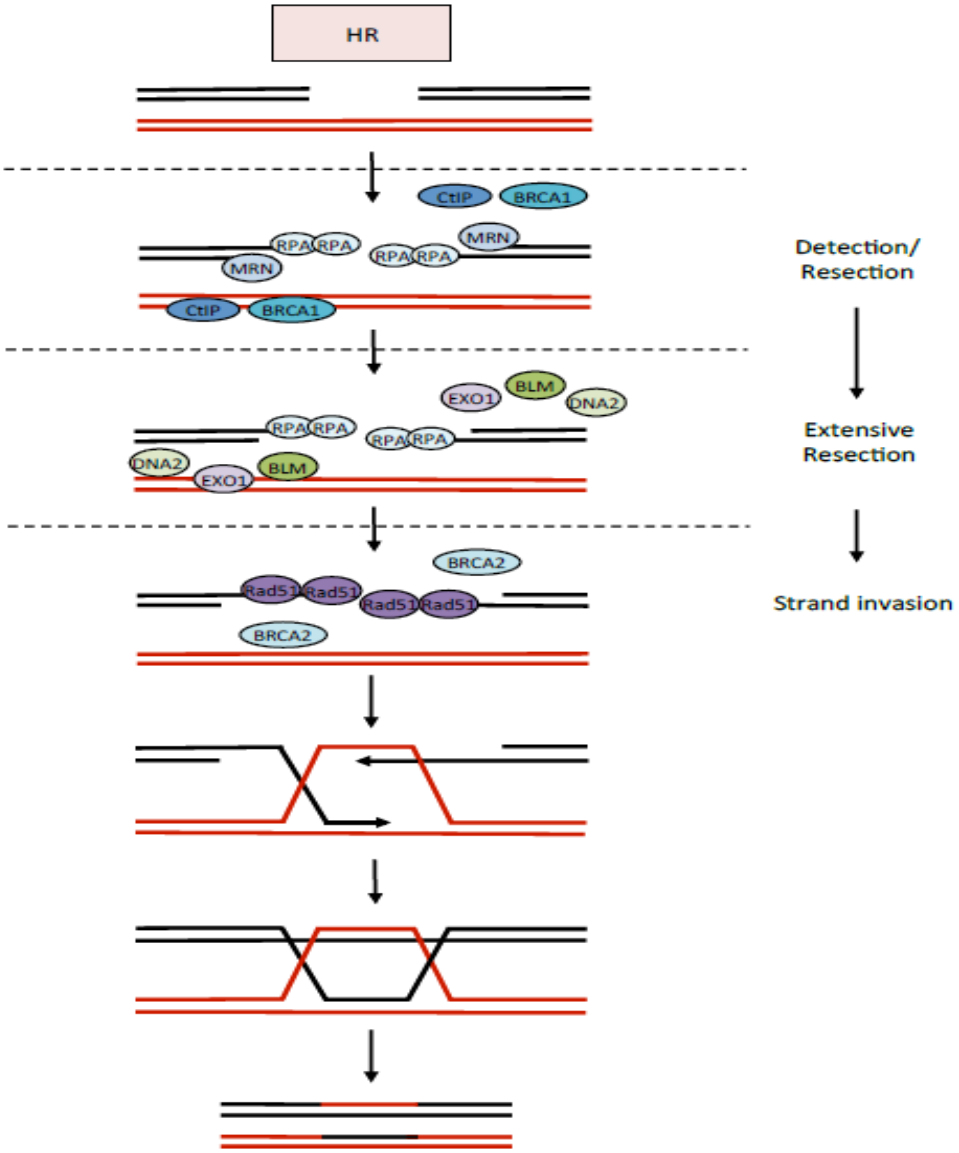

Figure 1.18 The mechanism of HR repair pathway.

Initial endo-cleavage step is mediated by MRN in conjunction with CtIP and BRCA1. Further resection is performed by either EXO1 or DNA2 *in concert with BLM, generating the 3' overhang ssDNA. RPA rapidly binds the 3' overhang ssDNA, which is displaced by the recombinase Rad51 in a BRCA2-dependent manner, generating a presynaptic filament with the ssDNA. The nucleoprotein filament begins homology searches and DNA strand exchange. HR intermediate "Holliday junction" structures can be resolved by the endonucleases MUS81, EME1, SLX1/SLX4 and GEN1 (Ryan 2016).*

1.5.2 Non-Homologous End Joining

The process of NHEJ initiates with an immediate recognition of the DSB by the Ku70/80 heterodimer, which forms a ring-like structure around each end of the DSB with high affinity. The formation of the ring-like structure is imperative as it protects DNA ends from degradation. Recruitment of 53BP1 antagonises resection of the DNA, thus promoting NHEJ. Ku70/80 heterodimer promotes the recruitment and activation of the DNA-PK catalytic subunit (DNA-PKcs). Formation of DNA-PK holoenzyme activates its kinase activity, resulting in auto-phosphorylation; DNA-PK also phosphorylates a number of downstream NHEJ proteins, such as Ku70/80, XRCC4 and Artemis. Similar to HR, H2AX is phosphorylated to γH2AX by DNA-PKcs. The auto-phosphorylation of DNA-PK provides an accessible platform for the other NHEJ mediators to the site of the DSB, such as Artemis and the DNA ligase IV complex (ligase IV, XRCC4 and XLF) once the holoenzyme is removed. The end-processing enzyme Artemis, using its endonuclease activity of 5'- and 3'-DNA overhangs and DNA hairpins, returns the DNA ends of the DSB to their conventional 3'OH and 5'P DNA termini before they are re-ligated by DNA ligase IV complex. Once the blunt ends are in place, the ligase IV complex performs the final crucial ligation step to join the DNA ends together (Figure 1.19).

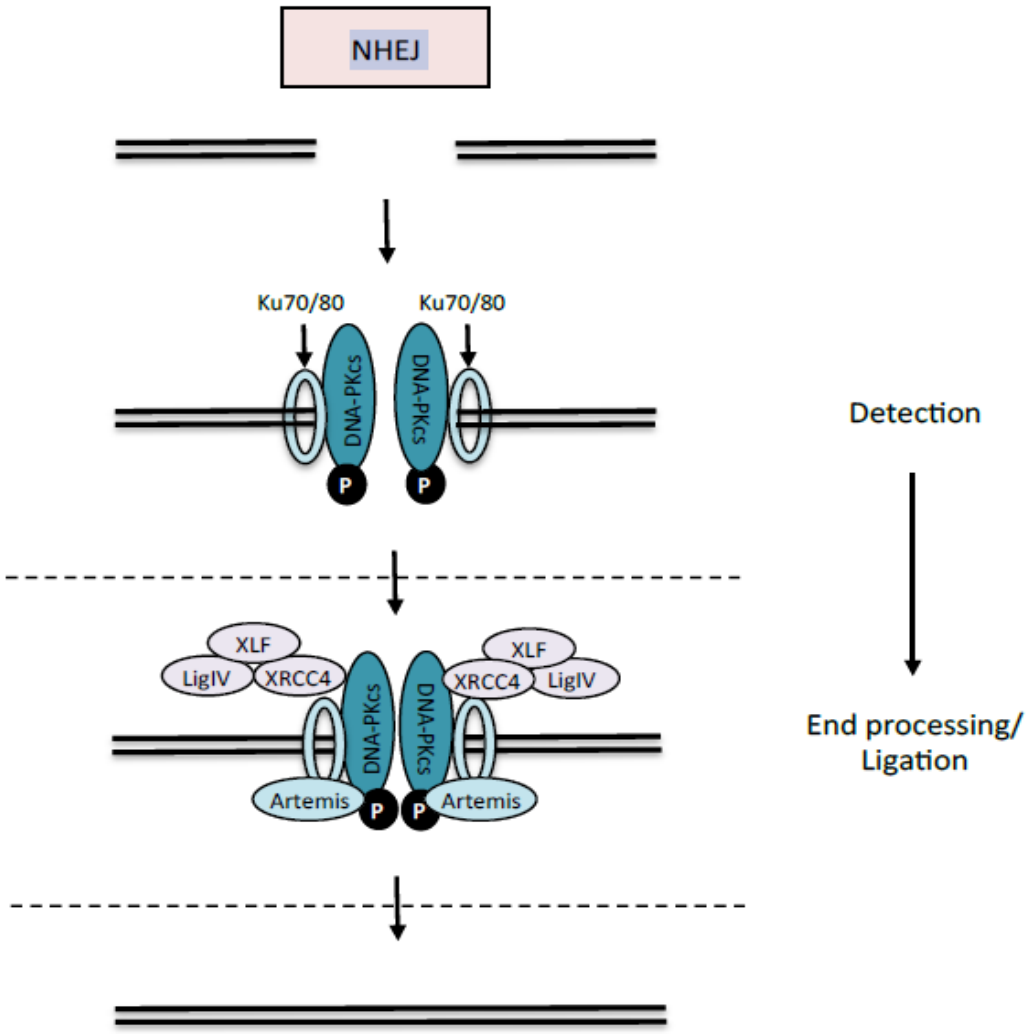

Figure 1.19 The mechanism of NHEJ repair pathway.

DSB structures are recognised by Ku70/Ku80 heterodimer that orchestrates the recruitment and activity of DNA-PKcs. DNA-PKcs phosphorylates and activates additional repair mediators, including itself and the endonuclease Artemis. Artemis processes the DNA ends prior to ligation. The blunt ends are joined by the activity of DNA ligase IV, XRCC4 and XLF (Ryan 2016).

1.5.3 Fanconi anaemia pathway and interstrand cross-links

The Fanconi anaemia (FA) pathway comprises in excess of 20 proteins and is activated in response to interstrand crosslinks (ICLs) (Niraj et al., 2019; Walden and Deans, 2014; Kim and D'Andrea, 2012). ICLs arise following exposure to chemicals such as cisplatin and mitomycin C and result in the covalent cross linking of two DNA strands, inhibiting transcription and imposing a block on replication. They can also occur due to the effect of endogenous metabolic intermediates, such as formaldehyde and acetaldehyde, which result from lipid peroxidation and alcohol metabolism. The FA core complex, comprising nine components, constitutes an E3 ubiquitin ligase which ubiquitylates FANCI and FANCD2 (the ID complex) in response to ICLs. FANCL is the E3 enzyme and FANCT, the E2 ubiquitin conjugating enzyme. The FA anchor complex containing a number of proteins such as FANCM (Walden and Deans, 2014) recognises the ICL. The monoubiquitylated ID2 complex binds to chromatin and recruits various DNA repair proteins such as structure specific nucleases (FANCP and FANCQ) that cleave the DNA and 'unhook' the cross-link. HR proteins are engaged in the later stages of ICL repair, resolving the DSBs, which arise (Walden and Deans, 2014). FANCD1 (BRCA2) and FANCJ (BACH1) are involved in the process at this stage.

1.6 Hypothesis and aims

We hypothesise that the mammalian CNOT complex is required for regulation of steady-state level of mRNAs including those are involved in the cell cycle progression. Furthermore, we suggest that depletion of CNOT1, a scaffold protein for the complex, will may increase the level of mRNA synthesis and decrease the mRNA decay, resulting in disruption of the cell cycle and transcription-induced replication stress and genome instability with low DNA repair response.

The aims of the investigation are:

1. To determine the effects of CNOT1 depletion on the cell cycle progression throughout the difference phases.
2. To investigate whether depletion of CNOT1 can result in cell death via apoptosis or senescence.
3. To study the role of CNOT1 in regulation of global transcription activity.
4. To examine the effects of CNOT1 depletion on global gene expression using RNA-Seq analysis.
5. To examine the effects of CNOT1 depletion on DNA replication using DNA fibre assays
6. To investigate possible different forms of genome instability caused by depletion of CNOT1.
7. To determine the effect of CNOT1 depletion on the ATM and ATR pathways.

CHAPTER TWO

MATERIALS & METHODS

2 MATERIALS AND METHODS

2.1 CELL CULTURE TECHNIQUES

2.1.1 Human Cell Lines

Cell line	Supplier and Cat No	Information
HeLa S3 cells	ATCC-CCL-2.2 ™	Adherent epithelial cell line derived from a human cervical cancer expressing human papilloma virus (HPV-18) proteins
U2OS	ATCC® HTB-96™	Adherent epithelial cell line derived from a human osteosarcoma
H1299	ATCC® CRL-5803™	Adherent epithelial cell line derived from a human lung metastatic site: lymph node

Table 2.1 List of cell lines used in this study

HeLa cells were used in all experiments throughout this project apart from the homologous recombination (HR) assay, in which U2OS was used.

2.1.2 Tissue Culture Media

Cells were grown in Dulbecco's Modified Eagle's Medium-high glucose (Sigma) with 10% FCS (Sigma) in 5% CO_2 at 37 °C. When necessary, media was supplemented with Gentamicin 100 µg/ml. For 70-80% confluency, 5×10^6 cells were plated in 10-cm cell culture dishes (Corning) 24 h before use.

2.1.3 Maintenance of Human Cell Lines

Cells were split when they reached 70-80% confluency by removing existing media rinsing once with Dulbecco's Phosphate Buffered Saline (PBS) and incubating with 0.05% trypsin (Invitrogen) at 37 °C until cells had detached. Detached cells were collected in fresh warm culture medium and centrifuged at 470 x g for 3 minutes. Medium was discarded without

disrupting the cell pellet and fresh warm medium was added to the cells which were re-plated at the desired confluency.

2.1.4 Cryopreservation of human cell Lines

Cells were detached and pelleted as mentioned in section 2.1.3. Cell pellets were re-suspended in freezing medium containing 10% dimethylsulphoxide (DMSO) (Sigma-Aldrich) and 10% FCS. Cells were transferred into cryovials and placed inside a freezing container filled with isopropanol for overnight incubation at 80 °C. The following day, frozen vials were transferred to the vapour phase of a liquid nitrogen for long-term storage at -180 °C. When needed, cells were retrieved by thawing at 37 °C followed by centrifugation at 470 x g for 3 minutes and resuspension in fresh DMEM media.

2.2 CELL BIOLOGY TECHNIQUES

2.2.1 siRNA transfection of cell lines

On-target plus siRNA-SMART pools were obtained from GE Dharmacon; all were designed to reduce gene expression of human CNOT1, CNOT2, CNOT4, CNOT6, CNOT6L, CNOT7, CNOT8, Tab182 and BRCA2. A list of all the siRNAs used in this project is summarised in Table 2.2. Oligofectamine™ (Invitrogen) was used as the cationic lipid cell transfection reagent. A transfection complex of 10 µL of siRNA (0.2nmoles) and 8 µL of Oligofectamine was added to 1 mL Opti-MEM® (Invitrogen-31985-047) and mixed thoroughly by pipetting. Following 30 minutes incubation at room temperature the mixture was added to cells in a 6 cm dish supplemented with 1 mL Opti-MEM. After 5-6 hours, incubation at 37 °C the Opti-MEM transfection mixture was removed and replaced with fresh DMEM medium containing 10% FCS. Cells were incubated until harvested or split.

Target	siRNA	Sense sequence	Antisense sequence	Supplier
lacZ 198-non silencing control	Custom	CGUACGCGGAAUACUUCGAdTdT	AhAhUCGAAG UAUUCCGCGUACG	Dharmacon
CNOT1	SMARTpool	CUAUAAAGAGGGAACGAGA CCAGAAACUUUGGCGACAA GGCCAAAUUGUCUCGAAUA CAAGUUAGCACUAUGGUAA	UCUCGUUCCCUCUUUAUAG UUGUCGCCAA AGUUUCUGG UAUUCGAGAC AAUUUGGCC UUACCAUAGU GCUAACUUG	Dharmacon
CNOT2	SMARTpool	CAUGAAUGGAGGAGACGUA GGCAAUUGGCUUACGCAAA GGCAAGUUUAUACGGGCAA GCACUCAGUUACCGAGCCA	UACGUCUCCUCCAUUCAUG UUUGCGUAAGCCAAUUGCC UUGCCCGUAUAAACUUGCC UGGCUCGGUAACUGAGUGC	Dharmacon
CNOT4	SMARTpool	CCAAUUCUCUCAAUAGUAC CGUCUUUGUUGUAGGUUUA UAACAGAGUCACAGUCGUU GGUAGUAGAUGGCAGAACA	GUACUAUUGA GAGAAUUGG UAAACCUACA ACAAAGACG AACGACUGUG ACUCUGUUA UGUUCUGCCA UCUACUACC	Dharmacon
CNOT6	SMARTpool	GAAAGAACGUGGCUAUAAU GGGCAGAGCUUGAAAUAAG GAGCACAGGUGGAGUAGAA GCUAUAAUGUUCUUUGUGA	AUUAUAGCCA CGUUCUUUC CUUAUUUCAA GCUCUGCCC UUCUACUCCA CCUGUGCUC UCACAAAGAA CAUUAUAGC	Dharmacon
CNOT6L	SMARTpool	UGACAGCGCUGCACCUAAA GAGCAGGUAUGAAGCCUAU CCAAUUACACCUUUGAUUU GGUAUUAGAGGUCCACAAA	UUUAGGUGCA GCGCUGUCA AUAGGCUUCA UACCUGCUC AAAUCAAAGG UGUAAUUGG UUUGUGGACC UCUAAUACCA	Dharmacon
CNOT7	SMARTpool	CAGCUAGGACUGACAUUUA GGAGAAUUCAGGAGCAAUG UCAUAGCGGUUACGACUUU GUUAGAGCUGGAACGGAUA	UAAAUGUCAGUCCUAGCUG CAUUGCUCCUGAAUUCUCC AAAGUCGUAACCGCUAUGA UAUCCGUUCCAGCUCUAAC	Dharmacon
CNOT8	SMARTpool	UUUCGUAGUUCCAUAGAUU AAUAUCAGCUUCUGCGGUG GAGAUAGCCAGGUUAUCU CCAUAGAUCUCCUUGCUAA	AAUCUAUGGA ACUACGAAA CACCGCAGAA GCUGAUAUU AGAUAACCUG GCUAUCUC UUAGCAAGGA GAUCUAUGG	Dharmacon
TAB182	SMARTpool	GAGUUUGGGAAGAGCGCUU CAGAAGCUUUGGAACGAGA AGGACCAGGAAUUCGGAAA CACCAAGGCCUGCGGUUGA	AAGCGCUCUU CCCAAACUC UCUCGUUCCA AAGCUUCUG UUUCCGAAUU CCUGGUCCU UCAACCGCAG GCCUUGGUG	Dharmacon
BRCA2	SMARTpool	GAAACGGACUUGCUAUUUA GGUAUCAGAUGCUUCAUUA GAAGAAUGCAGGUUUAAUA UAAGGAACGUCAAGAGAUA	UAAAUAGCAAGUCCGUUUC UAAUGAAGCAUCUGAUACC UAUUAAACCUGCAUUCUUC UAUCUCUUGACGUUCCUUA	Dharmacon

Table 2.2 List of siRNAs used in the study

The siRNAs used to study the gene function of various candidate proteins belonging to CNOT complex components and BRCA2 are shown.

2.2.2 Transient transfection of DNA

Cells were treated with siRNA 48 hours prior to DNA plasmid transfection. On day three, the transfection complex was prepared by diluting DNA as indicated below and 9 µl of Lipofectamine 2000 (Invitrogen) into 250 µl of Opti-MEM in two separate tubes. Both tubes were mixed by pipetting and then left at room temperature for 5 minutes. The two solutions were then mixed together and incubated for another 25 minutes at room temperature. 500 µl transfection mixture was added to cells in DMEM, without changing the medium, for overnight incubation at 37 °C. Opti-MEM transfection complex was removed and replaced with warm DMEM medium supplemented with 10% FCS and incubated until needed.

Cloning vectors	Doses used for 6cm dishes/ 6 well plates	Manufacturer
pCMV6-AC-RNase H1-GFP	2.5 µg/µl	Origene-PS100010
I-SceI-GFP (Moynahan, Pierce et al. 2001)	3 µg/µl	A gift from G. Stewart lab
pcDNA 3.1	2 µg/µl	Invitrogen-V79020

Table 2.3 A List of DNA plasmids used during this study

Their doses and sources are indicated.

2.2.3 Cytotoxic Agents

All drugs used in this study are outlined in Table 2.4.

Reagents	Stock concentration	Working concentration	Time of treatment	Manufacturer	Information
5, 6-Dichlorobenzimidazole 1-β-D-ribofuranoside (DRB)	50 mg/mL	100 µm	100 min	Sigma-D1916	Transcription inhibitor that prevents activating phosphorylation of the RNA Pol II C-terminal domain.
1,5,6,7-Tetrahydro-2-(4-pyridinyl)-4H-pyrrolo[3,2-c]pyridin-4-one hydrochloride, 2-Pyridin-4-yl-1,5,6,7-tetrahydro-pyrrolo[3,2-c]pyridin-4-one hydrochloride, (PHA-767491)	50 mg/mL	10 µm	60 min	Tocris Bioscience-767491	Dual DNA replication and transcription elongation inhibitor. Cdc7/cdk9 inhibitor.
RNase H1	5,000 units/ml	2 U per µg of DNA	120 min	NEB - M0297S	Endoribonuclease that catalyses the cleavage of RNA in an RNA-DNA hybrid.
Mitomycin C (MMC)	25 0ug/mL	1 µm	24 hours	Sigma	Inhibits DNA synthesis by formation of DNA crosslinks
Hydroxyurea	10 g	1, 2.5, 5, 10 & 20 mM	2 hours	Sigma	Inhibits DNA synthesis by dNTP pool depletion.
Nocodazole	1 mg/mL	200 ng/mL	18 hours	Sigma	Inhibits mitosis by disruption of mitotic spindle function.
AZD6738	1 mM	2 µm	2 hours	Astrazeneca	ATR kinase inhibitor

Table 2.4 A List of all cytotoxic components used during this study

Their stock and working concentration, exposure time, source and brief information about their function are shown.

2.2.4 Buffers Recipes

All buffers and their recipes used for cell biology in this study are summarised in Table 2.5.

Buffer Name	Recipe
Comet Lysis Buffer	2.5 M NaCl, 0.1 M EDTA pH8, 10 mM Tris pH10, adjusted to pH 10 with 10 M NaOH
Comet Electrophoresis Buffer	1 mM EDTA pH8 and 50 mM NaOH
Fibre Spreading Buffer	0.2 M Tris-HCl pH 7.4, 50 mM EDTA and 0.5% SDS
Fibre Blocking solution	1% BSA, 0.01% Tween 20 in PBS
PBST Buffer (Phosphate Buffered Saline Tween-20)	Phosphate buffered saline containing 1%Tween 20.
NETN Buffer	1% NP-40, 0.15 M NaCl, 50 mM Tris-HCl pH 7.4, 5 mM EDTA
CBF Buffer A	10 mM Hepes pH 7.2, 10 mM KCL, 1.5 mM $MgCl_2$, 0.34 M Sucrose, 10% Glycerol and 1 mM DTT
CBF Buffer B	3 mM EDTA, 5 mM EGTA and1 mM DTT
SDS sample Buffer	5% SDS, 5 M urea, 20 mM Tris HCL pH 7.4 and 0.1 M β-mercaptoethanol
Western blot Running Buffer	100 mM Tris/Bicine and 1% SDS
Western blot Transferring Running Buffer	200 mM Tris, 190 mM Glycine and 20% v/v methanol
TBST Buffer	50 mM Tris-HCl pH 7.4, 0.15 M NaCI, 1% Tween 80
SSC Buffer (Saline and Sodium Citrate)	0.30 M NaCl, 30 mM trisodium citrate, pH7
10 X TBE Buffer	1 M Tris, 1M Boric acid, 20mM EDTA
Alkaline Running Buffer	50 mM NaOH, 1 mM EDTA
Alkaline Neutralizing Buffer	1M Tris HCl pH 8.0, 1.5 M NaCl
Deadenylation Buffer	50 Mm Hepes-NaOH pH 8.0, 0.15 M NaCl, 2 mM MgCl2, 10% glycerol
RNA Loading Buffer	95% formamide, 0.025% SDS, 5 mM EDTA, Blue-orange loading dye (Promega)

Table 2.5 A List of all buffers used during this study

Their concentration and recipes are indicated. The source of all chemicals are from Sigma-Aldrich

2.2.5 Colony Survival Assays

CNOT1 siRNA-transfected and control siRNA-transfected HeLa cells were plated at appropriate concentration into 6 cm dishes. On the following day, cells were mock-treated or treated with HU or MMC with different dosages. After treatments, cells were washed twice with PBS and incubated with fresh DMEM medium. Cells were incubated in a humidified atmosphere with 5% CO_2 for 2 weeks until large colonies formed > 1 mm (Colonies of more than 50 cells were counted). Colonies were rinsed with PBS, stained with 0.5% crystal violet in 20% ethanol and counted.

2.2.6 Natural Comet Assay

On day one, comet slides (X-tra® Slides from Leica Biosystem) were prepared. The slides were scratched with an engraving pen. 0.6% normal agarose (Sigma) was prepared by dissolving 120 mg agarose in 20 mL PBS and microwaving for 1-3 minutes. The melted agarose was placed in a 42°C water bath during slide preparation. 600 µl of melted agarose was added to each slide and spread over the scored area to make an agarose layer of 2-3 mm thickness. After the agarose was set on the slides, they were placed in a slide box and left in at 4 °C overnight. On day two, 1.2% LMP agarose (Sigma) was made up by dissolving 240 mg agarose in 20 mL PBS and incubated in a 42 °C water bath. 5×10^5 cells/mL final concentration was calculated for each control and CNOT1 siRNA-transfected sample (each sample was in triplicate). The cells were placed in universal tubes on ice and kept in the cold until electrophoresis was completed. Samples were washed twice with sterile cold PBS at 4 °C, and dispensed so that 600 µL (at 5×10^5cells/mL) of each sample was placed into a 1.5 mL tube on ice. Agarose covered slides from day one were placed on a slide tray on ice. 600

µL LMP agarose was pipetted into each sample and mixed well by pipetting up and down 2 or 3 times. 600 µL of mixture of LMP Agarose and sample was spotted onto slides quickly and stored at 4 °C for ≥ 30 minutes. Comet lysis buffer was prepared (Table 2.5)**.** DMSO and Triton X-100 (Sigma) were added to the lysis buffer to a final concentration of 1% for each ≤ 20 minutes before use. Slides were transferred to a blacked-out Coplin jar with lysis buffer and left for 60 minutes in the dark. The comet tank was refrigerated, and electrophoresis buffer was completed by adding 10 mL DMSO < 20 minutes before use. Slides were washed 3 times with ice cold water and submerged in the comet tank with electrophoresis buffer for 45 minutes in the darkness. Electrophoresis was performed for 25 minutes at 21 V. Slides were removed from the electrophoresis tank, rinsed quickly with ice-cold water and transferred to the Coplin jar with 1 M Tris pH 7 for ≥ 30 minutes. Slides were rinsed in ice-cold water and heated at 42 °C overnight and then placed at 4 °C. Slides were stained with 1 mL of SYBR Green in PBS (1: 10,000) and cover slips were applied. Excess SYBR Green was removed and 200 Comets viewed at 20X magnification. Mean Tail moment were calculated using Open Comet plugin ImageJ bundle.

2.2.7 DNA Fibre Assay

24 hours prior to labelling, control and siRNA-transfected HeLa cells were plated in 6 cm dishes. Exponentially growing cells at 40-50% confluency were pulse labelled with 20 µl 2.5 mM 5-Chloro-2'-deoxyuridine (CldU) (Sigma) (final concentration 25 µM) for 20 minutes at 37 °C. Cells were treated with RNase H1, DRB, and PHA for 24 hours, 100 minutes and 60 minutes, respectively, if required (Table 2.4). In order to remove excess CIdU, cells were rinsed 2 times with warm DMEM. Cells were pulse-labelled with 222 µl CO_2-equilibrated 2.5 mM 5-Iodo-2'-deoxyuridine (IdU) (Sigma) (final concentration 250 µM) for 20 minutes at 37 °C. DMEM / IdU

solution was removed and cells were washed twice with ice-cold sterile PBS. Cells were trypsinised, re-suspended in 1 mL ice cold PBS to a concentration of 5×10^4 cells/mL cells/mL and transferred to ice cold 1.5 mL Eppendorf tubes. 2 µl of each re-suspended sample in PBS was placed on a slide, near to the frosting, and left for 4 minutes until the edges of the drops became crinkly, lysis occurred after 7 µl of spreading buffer was added (Table 2.5). The two together were stirred 5 times and left for 2 minutes at room temperature until lysis was accomplished. Slides were briefly tilted to start the DNA moving down the slide; excess liquid was allowed to run off the end, and the slide left to air-dry for 10 minutes. DNA fibre spreads were fixed in methanol / acetone (3:1) for 15 minutes and air-dried for 10 minutes. Slides were stored at 4 °C and were stable for up to 1 year.

2.2.8 Homologous Recombination Assay

The U2OS DNA homologous recombination reporter cell line was transfected with control siRNA or CNOT1-siRNA. 24 hours prior to transfection of the plasmid DNA, cells (1×10^6/mL) were plated in 6 well plates supplemented with DMEM plus 10% FCS. 3 µl of I-SceI DNA and 9 µl Lipofectamine™ 2000 (Invitrogen) were added to 250 µl of Opti-MEM in a 1.5 mL eppendorf tube (per reaction). The contents of the tube were mixed thoroughly by pipetting and left at room temperature for 30 minutes. The transfection complex was added to cells plated in 6 well plates supplemented with 250 µl of DMEM plus 10% FCS and incubated at 37 °C overnight. The following day, medium was removed and replaced with fresh DMEM and incubated at 37 °C for another 5-6 hours. Cells were trypsinised, pelleted by centrifugation at 410 x g for 5 minutes and washed with sterile PBS (all media and washes were kept at every step and transferred to a 50 mL Falcon tube to avoid losing any mitotic cells). Cells were re-suspended in 3 mL ice-cold PBS and 7 mL of ice-cold absolute ethanol was added drop-wise

while vortexing at medium speed. Cells were stored at -20 °C for up to 2 weeks (a minimum of 24 hours fixation is required). Cells were removed from the freezer and pelleted by centrifugation at 535 x g for 5 minutes. Ethanol was removed from the loosely attached cell pellet and 10 mL of PBS was added to the dehydrated cells and left for 30 minutes on ice. Cells were pelleted by centrifugation at 535 x g for 5 minutes. The PBS wash was repeated. The supernatant from the final wash was discarded and cells were re-suspended in PBS. Cells were permeabilised in 10 mL of ice-cold 0.25% Triton- X100 in PBS for 15 minutes. Cells were incubated in 1 µg/mL propidium iodide together with 0.1 µg/mL RNase A in PBS and for at least 30 minutes at room temperature. Cells were analysed on a BD Accuri C6 flow cytometer using FL-2 channel on slow flow setting.

2.2.9 Cell Growth Assay

HeLa Cells were transfected with control or siRNAs of the CCR4-NOT subunits (CNOT1, 2, 6, 6L, 7, 8 and TAB182). 200 µl of 2×10^4 $\mathrm{cells/mL}$ suspension in DMEM were seeded (final concentration of 2×10^3 $\mathrm{cells/well}$) per well in 96-well solid white polystyrene microplates in triplicate and incubated for the indicated times. Control wells containing DMEM without cells were also set up in triplicate to obtain a value for background luminescence. CellTiter-Glo® Luminescent reagent (Promega) and the 96-well microplate were both equilibrated at room temperature for 30 minutes. 50 µl CellTitre Glo reagent was added to each well followed by gentle agitation on a shaker for 2 minutes to complete cell lysis. In order to stabilise the luminescent signal, cells were incubated at room temperature for 30 minutes. Relative luminescence unit (RLU) was measured with a Pherastar Plate Reader (BMG LABTECH). The RLU mean was calculated for the medium-only wells and subtracted from the RLU mean of wells with CellTitre Glo reagent. In order to calculate the relative survival fraction for each

CNOT siRNA, the RLU mean corresponding to the CNOT siRNA was divided by the RLU mean of the control siRNA-treated wells.

2.2.10 Cell Cycle Analysis

2.2.10.1 Synchronizing cells with mitotic shake-off method

CNOT1 siRNA-transfected and control siRNA-transfected HeLa cells were grown in T75 flasks 24 hours prior to nocodazole treatment. Cells were synchronised in mitosis using nocodazole (200 ng/mL) for 18h. Mitotic cells were visualised using an EVOS fluorescence inverted digital microscope from Advanced Microscopy Group (AMG). Loose round mitotic cells were mechanically detached by tapping the flask on a hard surface and collected. Cells were rinsed once in PBS (all media and washes were kept to avoid losing any mitotic cells). The flattened cells remaining attached after shaking off, were trypsinzed and transferred to a separate tube for further investigation. Nocodazole shake-off cells were centrifuged at 470 x g for 5 minutes. Medium was removed and pellet was washed once with PBS. Mitotic cells were released from the G2/M block into fresh media and sub-cultured into 6 cm dishes and were harvested at 0, 1, 2, 4, 8, and 24 hours later. The pellet obtained from the trypsinised cells was retained for further investigation. Cell pellets obtained from different time points were washed once with PBS and lysed in UTB lysis buffer (whole cell lysate) or subjected to sub cellular fractionation as explained below in section 2.3.1.

2.2.10.2 FACS analysis

Cell culture medium was removed from 72 hours CNOT1 siRNA-transfected and control siRNA-transfected HeLa cells. Following the ethanol-fixation step as explained above in section 2.2.8 cells were rehydrated with 10 mL ice-cold PBS on ice for 30 minutes. Cells were

centrifuged at 535 x g for 4 minutes and PBS /ethanol was discarded. 10 mL ice-cold PBS was added to cell pellets and transferred to 25 mL universal tubes. Cells were centrifuged at 535 x g for 4 minutes and PBS was discarded. Cell pellets were re-suspended in remaining PBS and incubated with 10 mL ice-cold 0.25% Triton-X100 in PBS on a rocker at 4 °C for 15 minutes. Cells were centrifuged at 535 x g for 4 minutes and rinsed once with 1% BSA in PBS. In order to discriminate between G2 and M phase cells, simultaneous staining of DNA with PI and the mitotic marker, anti-phospho-histone H3 serine 10 (pH3) antibody was performed. Cells were incubated in 200 µl of 1% BSA/PBS containing 1:500 dilution of pH3 antibody at room temperature and transferred to 1.5 mL Eppendorf tubes. Tubes were gently flicked occasionally to re-suspend cells with the antibody. After 1 hour incubation with antibody cells were washed with 1% BSA/PBS twice and centrifuged at 677 x g for 5 minutes. Cells were incubated in 200 µl of 1% BSA/PBS containing 1:50 dilution of secondary antibody Alexa fluor® 488 at room temperature in the dark for 1 hour. Tubes were gently flicked occasionally. Cells were washed once with 1% BSA/PBS followed by one PBS wash. Cells were incubated in 1mL PI (final concentration 10 µg / mL) in PBS containing 0.1 mg / mL RNase A at room temperature in the dark for 30 minutes. Cells were transferred to BD FACS™ tubes and analysed on a BD LSRFortessa™ X-20 flow cytometer on slow flow setting.

2.3 PROTEIN BIOCHEMISTRY TECHNIQUES

2.3.1 Protein Extraction

Cell lysates were prepared for Western blotting as follow. 80% confluent CNOT1 siRNA-transfected and control-transfected cells were washed twice with ice-cold PBS and lysed in 250-500 µl of UTB lysis buffer (8 M **U**rea, 50 mM **T**ris HCl pH7.4 and 0.15 M **β**-mercaptoethanol) depending on the cell number. Cells were scrapped off the culture dish and

collected in 1.5 mL tubes. Cells were sonicated (5 watts for 15 seconds) and pelleted at 535 x g for 4 minutes at 4 °C. The supernatants containing the proteins were collected and transferred to new tubes.

Cell lysate preparation for **C**o-**I**mmuno**p**recipitation (CIP) and **S**ubcellular **C**hromatin **F**ractionation (SCF) assays was carried out as follow. Medium was removed from cell culture dishes; cells were washed with pre-warmed PBS once and trypsinzed as before. Cells were pelleted by centrifugation at 470 x g for 4 minutes. Culture medium containing trypsin was removed and pellets were washed with ice-cold PBS twice. Once PBS was removed from the final wash, for CIP assay cells were lysed in 1 mL NETN buffer (Table 2.5). The lysis was completed by adding 50 µL of 5 M NaCl per 1 mL NETN buffer, vortexing and homogenising using a Wheaton-Dounce homogeniser. Homogenised cell lysates were centrifuged at 100,000 x g for 5 minutes at 4 °C. The supernatant was retained at every step of the preparation and the pellet discarded. The supernatant from each sample was carefully removed and dispensed into 1.5 mL Eppendorf tubes (500 µL per tube). Eppendorf tubes were centrifuged at 364 x g for 8 minutes at 4 °C. The supernatant was transferred into new tubes and centrifuged at 100,000 x g for 30 minutes at 4 °C using an Optima MAX-TL Beckman Coulter ultracentrifuge. The final supernatant was transferred into the new tubes for antibody incubation overnight.

For SCF assays, cell pellets were washed twice with ice-cold PBS as described above and lysed in 1 mL Buffer A (Table 2.5) supplemented with 100 µL 10% Triton on ice for 8 minutes. 200 µL of this suspension was retained as a **W**hole **C**ell lysate **F**raction (WCF). The remaining suspension was centrifuged at 10,000 x g for 5 minutes at 4 °C. Both supernatant and pellet were collected as crude cytoplasmic fraction (S1) and nuclear fraction (P1), respectively. S1 was subjected to additional centrifugation at 364 x g for 15 minutes; the supernatant was the

cytoplasm (S2) and the pellet contained the organelles (P2). P1 fraction was washed with buffer A without Triton and centrifuged at 535 x g for 5 minutes at 4 °C. The supernatant was discarded, and the pellet was lysed in buffer B (Table 2.5) on ice for 30 minutes. The lysed P1 fraction was centrifuged at 10,000 x g at 4 °C and two fractions were designated nucleoplasm (S3) and chromatin (P3). P3 fraction was solubilised in UBT buffer and centrifuged at 535 x g for 5 minutes at 4 °C. The supernatant containing Chromatin-bound proteins was collected into the new tubes.

2.3.2 Protein Determination (Bradford Assay)

Cell lysates were prepared as explained above (section 2.3.1). A range of bovine serum albumin (BSA) concentrations was used to produce a standard protein curve and were made up of 0, 2, 4, 6, 8 and 10 µg BSA in 1 mL diluted Bradford reagent (Bio-Rad) (1:5 in water). 1 µL of each experimental cell lysate was added to 1 mL diluted Bradford reagent. Absorbance readings were measured using Eppendorf Biospectrometer at a wavelength of 595 nm. Protein concentation was calculated using a BSA standard curve.

2.3.3 SDS-Polyacrylamide Gel Electrophoresis (SDS-PAGE)

Proteins were fractionated on polyacrylamide gels based on their molecular weight. For low molecular weight proteins (15 kDa-120 kDa), a 10% acrylamide gel was used and for high molecular weight proteins (> 120 kDa) an 8% acrylamide gel was used (Table 2.6). The gel was set in a Hoefer Studier apparatus. Generally, 30 µg of each protein sample per well was denatured in SDS sample buffer (Table 2.5) and heated at 90 °C for 5 minutes. Samples were loaded onto the gel along with molecular weight markers (BlueEasy Pre-Stained Protein

Ladder, (6.5 – 270 kDa) from GenFlow. Gels were run at 20 mA for 4-5 hours or overnight at 10 mA in running buffer (Table 2.5).

Ingredients	Supplier	8% Gel	10% Gel
H_20	---	42 mL	39 mL
1 M Tris 1MBicine	Sigma	6 mL	6 mL
40% Acrylamide (N,N' -methylene-bis-acrylamide)	Severn Biotech	12 mL	15 mL
10% SDS (sodium dodecyl sulphate)	Severn Biotech	I mL	1 mL
TEMED (N, N, N'. N'-tetra-methyl-ethylenediamine)	Melford	200 µl	200 µL
10 % APS (ammonium persulphate)	Sigma	150 µl	150 µl

Table 2.6 Polyacrylamide Gel Recipe

Polyacrylamide gel recipe used for western blot in this study are listed.

2.3.4 Electrophoretic Transfer of Protein

Once fractionation was completed on SDS-PAGE, proteins were electrophoretically transferred onto a nitrocellulose membrane (Biotrace). The gel and membrane were held together between two sponges and pre-soaked Whatman filter paper and placed into a 5 L Hoefer transfer gel electrophoresis tank within a gel holder cassette. Transfer was overnight at 200 mA or 6 hours at 300 mA in the buffer described (Table 2.5).

2.3.5 Visualisation of Protein Bands on Nitrocellulose Membranes

In order to confirm success of the protein transfer, Ponceau S stain (0.1% Ponceau S in 3% trichloroacetic acid (TCA)) was applied to the nitrocellulose membrane and agitated for 2 minutes. The Ponceau S stain was removed and membrane washed with distilled H_2O a few times to remove excess dye. The quality of protein loading and transferring procedure were

checked and the result noted. Nitrocellulose membrane was cut according to the protein ladder and the size of proteins being investigated. The cut membranes were completely destained in TBST buffer (Table 2.5). The membranes were incubated in blocking buffer (3-5% skimmed milk powder in TBST or 3-5% BSA in TBST depending on the protein being investigate) on a shaker for 30 minutes.

2.4 IMMUNOCHEMISTRY TECHNIQUES

2.4.1 Antibodies

All the antibodies used in this study are listed in Table 2.7 and 2.8.

2.4.2 Immunodetection of proteins

After blocking the membranes (2.3.5 section), solutions of primary antibodies were prepared in 5% milk or 5% BSA to the appropriate concentration (Table 2.7). The nitrocellulose membranes were then incubated in primary antibodies in a sealed bag at 4 °C overnight with gentle agitation. On the following day, membranes were washed in TBST buffer six times for 5 minutes each. Membranes were then incubated in the secondary antibodies diluted in 5% milk to the appropriate concentration (Table 2.8) for two hours at room temperature while rocking. Following incubation, membranes were washed in TBST buffer six times for 5 minutes each. Membranes were incubated in **E**nhanced **C**hemical **L**uminescence (ECL) (GE Healthcare) solution for 1 minute. Blots were exposed to X-ray film (Kodak) for different lengths of time. Protein bands were developed and visualised using the X-ray film processor ECOMAXTM.

Primary Antibody	Species	Application	Dilution	Supplier
CNOT1	Rabbit	WB/IP	1:1000	Proteintech
CNOT2	Rabbit	WB	1:500	SantaCruz
CNOT4	Rabbit	WB	1:500	SantaCruz
CNOT6	Rabbit	WB	1:500	SantaCruz
CNOT7	Rabbit	WB	1:500	SantaCruz
CNOT10	Rabbit	WB	1:500	SantaCruz
Tab182	Rabbit	WB/IP	1:3000	In house
Pan3	Rabbit	WB	1:500	SantaCruz
ATR	Goat	WB/IP	1:1000	SantaCruz
ATM	Mouse	WB	1:1000	Gift from P. Byrd
pATM (S1981)	Rabbit	WB	1:500	R & D Systems
KAP1	Rabbit	WB	1:1000	Bethyl Laboratories
pKAP1 (S824)	Rabbit	WB	1:1000	Bethyl Laboratories
53BP1	Rabbit	IF/WB	1:1000	Novus
p53 (DO1)	Mouse	WB	1:2000	Gift from D. Lane
H2AX	Rabbit	WB	1:1000	Millipore
γH2AX (S139)	Mouse	WB/IF	1:1000	Millipore
H2B	Rabbit	WB	1:2000	Abcam
Rad51	Rabbit	WB	1:1000	Millipore
Cdc25A	Mouse	WB	1:1000	SantaCruz
TOPBP1	Rabbit	WB	1:1000	Bethyl
MCM2	Rabbit	WB/IP	1:500	SantaCruz
MCM3	Rabbit	WB/IP	1:500	SantaCruz
MCM7	Rabbit	WB/IP	1:500	SantaCruz
ORC3	Rat	WB/IP	1:500	SantaCruz
PCNA	Mouse	WB	1:1000	SantaCruz
TOP1	Mouse	WB	1:1000	SantaCruz
TOP2α	Mouse	WB	1:1000	SantaCruz
TOP2β	Mouse	WB	1:1000	SantaCruz
RNase H1	Rabbit	WB/IF	1:500	Proteintech
RNase H2A	Rabbit	WB	1:500	Gift from A. Agathanggelou
SETX	Rabbit	WB	1:500	SantaCruz
CSB	Rabbit	WB	1:500	Bethyl
XPG	Rabbit	WB	1:500	Bethyl
XPF	Mouse	WB	1:500	NeoMarkers
XPC	Rabbit	WB	1:500	SantaCruz
Chk1	Mouse	WB	1:1000	Santa Cruz
pChk1(S345)&(S317)	Rabbit	WB	1:1000	Cell Signalling
Chk2	Rabbit	WB	1:1000	Steve Elledge
pChk2 (T68)	Rabbit	WB	1:1000	Cell Signalling
RPA32	Mouse	WB/IF	1:1000	Calbiochem
pRPA32 (S4/S8)	Rabbit	WB	1:1000	Bethyl
PARP1	Mouse	WB	1:1000	SantaCruz
DNAPK	Mouse	WB	1:1000	Santa Cruz
FANCD2	Mouse	WB	1:500	SantaCruz
IdU	Mouse	DNA fibres	1:500	Becton Dickinson
CldU	Rat	DNA fibres	1:750	AbD SeroTec

Cyclin A	Rabbit	WB/IF	1:500	SantaCruz
Cyclin B	Rabbit	WB	1:500	SantaCruz
Cyclin E	Rabbit	WB	1:500	Abcam
Cyclin D1	Mouse	WB	1:500	SantaCruz
p27Kip1	Rabbit	WB	1:500	SantaCruz
p21Cip1	Rabbit	WB	1:500	Abcam
TBP	Rabbit	WB	1:1000	SantaCruz
RNA Poll C-terminal domain (CTD)	Rabbit	WB	1:1000	SantaCruz
Histone H3	Rabbit	WB	1:3000	Abcam
pHistone H3 (Ser-10)	Rabbit	WB	1:100	Cell signalling
H3K4me3	Rabbit	WB	1:1000	Abcam
Mre11	Mouse	WB	1:1000	Genetex
NBS1	Rabbit	WB	1:10000	Genetex
pNBS1 (Ser-343)	Rabbit	WB	1:1000	Abcam
β-Actin	Mouse	WB	1:1000	Sigma-Aldrich
GAPDH	Mouse	WB	1:500	SantaCruz
R-loop (S9.6)	Mouse	WB	1:1000	Gift from E.Peterman
CENPF	Rabbit	WB/IF	1:1000	Abcam
SSDNA	Mouse	WB	1:5000	Millipore
Cdc7	Mouse	WB	1:500	SantaCruz
LC3β	Mouse	WB/IF	1:4,000	Novus Biologicals

Table 2.7 Table demonstrates the primary antibodies used in this study including species, application, dilution and supplier

Secondary Antibody	Species	Application	Dilution	Supplier
Mouse IgG (Green)	Goat	WB	1:2000	DAKO Laboratories
Rabbit IgG (Red)	Swine	WB	1:3000	DAKOLaboratories
Rabbit IgG Alexa fluor® 488 (Red)	Goat	IF	1:1000	Invitrogen
Mouse IgG Alexa fluor® 546 (Green)	Goat	IF	1:1000	Invitrogen
Rat IgG Alexa fluor® 555 (Red)	Goat	DNA fibres	1:500	Invitrogen
Mouse IgG Alexa fluor® 488 (Green)	Goat	DNA fibres	1:500	Invitrogen

Table 2.8 Table demonstrates the secondary antibodies in used this study including species, application, dilution and supplier

2.4.3 Co-Immunoprecipitation

The final supernatants obtained from 2.3.1 section were incubated with 10µl of primary CNOT1 and Tab182 antibodies at 4 °C overnight. On the following day, the antibody-containing lysates were centrifuged at 10,000 x g at 4 °C for 15 minutes and the supernatant collected to the new tubes. The immunocomplexes were captured by incubating on a rotator with 40 µl of protein G-Sepharose beads for 1 hour at 4 °C. Immunocomplexes on the Sepharose beads were centrifuged at 10,000 x g for 1 minute at 4°C and the supernatant removed. Following this, beads-bound immunocomplexes were washed four times in NETN buffer, centrifuging at 10,000 x g for 1 minute at 4 °C each time. The supernatant was removed between each wash. Washed beads were boiled in 40 µl SDS sample buffer. The samples were centrifuged at 360 x g for 2 minutes and the supernatants loaded onto SDS-PAGE gels. Proteins were detected by immunoblotting as described above in sections 2.3.4/5 and 2.4.2, respectively.

2.4.4 Subcellular Chromatin Fractionation (SCF) assay

The supernatant containing chromatin-bound proteins obtained from 2.3.1 section were separated by SDS-PAGE and developed by immunoblotting as described above in sections 2.3.4/5 and 2.4.2, respectively.

2.4.5 Immunofluorescence

Poly-L-lysine coated circular cover slips (Dixon Glass Ltd Marketplace) were dipped in absolute ethanol for 20 seconds and placed in 24-well plates and washed once with 2 mL warm DMEM. Control and CNOT1-KD cells were aliquoted (4×10^4 cells/well) on the coverslips in 24 well plates and incubated at 37 °C overnight. If required, cells were transfected with DNA plasmid (pCMV6-AC-RNase H1-GFP / pcDNA 3.1) (refer to section 2.2.2) and incubated at 37 °C overnight. Growth medium was removed from cells and coverslips were washed once with ice-cold PBS. Cells were fixed in 500 µl of ice-cold paraformaldehyde (4% PFA in PBS, pH 7.2) for 10 minutes followed by a PBS wash and 10 minutes permeabilization in 0.5% Triton X-100 in PBS. For R-loop (S.96 antibody) immunofluorescence labelling, cells were fixed and permeabilised in 500 µl of ice-cold absolute methanol at -20 °C for 15 minutes.

In all cases cells were washed with ice-cold PBS once and blocked in 5% FCS in PBS at room temperature for 30 minutes - 1 hour. Blocking solution was removed from each well and replaced with the primary antibodies from Table 2.7 diluted in 5% FCS/PBS for overnight incubation at 4 °C. Primary antibodies were removed and coverslips were washed three times with 5% FCS/PBS. Cells were incubated in the dark with secondary antibodies (Alexa fluor® 546 & 488 from Invitrogen) diluted to the required concentration in 5% FCS/PBS

(Table 2.8) at room temperature for 1 hour. Excess secondary antibodies were discarded followed by three PBS washes. Cells were stained with 4', 6-diamidino-2-phenylindole (DAPI) for 15 minutes in the dark at room temperature. Excess DAPI stain was removed with two PBS washes. A drop of immune-mount mounting medium (Vectashield Mounting Medium from Vector Laboratories) was added onto rectangular slides (Surgipath). The coverslips were removed using tweezers and located on the slides. In order to seal the edges of the coverslips, a gentle pressure was applied and the edges of the coverslips were sealed using colourless nail polish. Glass slides were stored at 4 °C in a slide box. Cells were visualised using a Nikon Eclipse E600 microscope and analysed using Velocity software version 4.

2.4.6 Immunostaining of DNA Fibres

Methanol / acetone fixed DNA fibres on slides (from section 2.2.7) were placed horizontally in a humidified blackout chamber. Slides were washed twice with deionised water, rinsed once in 2.5 M hydrochloric acid (HCl) and immersed in 2.5M HCl for 1 hour 15 minutes. Upon completion of denaturation, slides were washed once in PBS, followed by two washes in blocking solution (Table 2.5). Additional blocking solution was applied on each slide for 30 minutes-1 hour. Blocking solution were tipped off and slides were incubated with 200 µl primary antibodies (rat anti-BrdU to detect CIdU and 200 µl mouse anti-BrdU to detect IdU) diluted in blocking solution at the required ratio (Table 2.8) for 1 hour. Slides were gently covered with a coverslip to spread the primary antibodies solution evenly. Primary antibodies were tipped off and coverslips were discarded, followed by three washes with PBST (Table 2.5). Slides were fixed with 500 µl of ice-cold 4% PFA for 10 minutes. Slides

were then washed three times with PBST followed by three washes with blocking solution. Slides were incubated with 200 µl secondary antibodies (anti- rat Alexa fluor® 555 [Red] and 200 µl anti-mouse Alexa fluor® 488 [green]) diluted in blocking solution at the required ratio (Table 2.8) for 1.5 hour. Slides were gently covered with a coverslip to spread the secondary antibodies solution evenly. Slides were washed twice in PBST, followed by three washes in blocking solution and then twice in PBS. 2 drops of mounting medium were spread over the surface and a long rectangular coverslip was applied. Slides were left to dry for 10-15 minutes and sealed using nail varnish. DNA fibres were viewed using a Nikon Eclipse E600 microscope and analysed using Image J software.

2.4.7 Transcription Assay

Coverslips and 24 well plates were prepared as explained in section 2.4.5. Cells were incubated with 500 µl of 1 mM 5-ethynyl uridine (EU) (Click-iT® RNA Imaging Kit) diluted in pre-warmed complete medium for 1 hour at 37 °C. Inhibition of transcription was achieved by treating cells with DRB (Table 2.4). DRB and EU were added to the cells at the same time and cells were maintained at 37 °C for 100 minutes. Culture medium including EU or EU / DRB was removed and cells were washed twice with ice-cold PBS. Cells were fixed in 500 µl of ice-cold 4% PFA in PBS for 10 minutes, followed by 10 minutes permeabilization in 0.5% Triton X-100 in PBS with a PBS wash in between. Click-iT reaction cocktail was freshly prepared according to the manufacturer's instructions. Permeabilization solution was removed and cells were washed once with PBS. Cells were incubated with 500 µl Click-iT reaction cocktail while protected from light for 30 minutes. Click-iT reaction cocktail was removed and cells were washed with 1 mL Click-iT reaction rinse buffer. Click-iT reaction rinse buffer was discarded and cells were incubated with 500 µl diluted Hoechst (DAPI)

(1:1000 in PBS) protected from light for 10 minutes, followed by two washes with PBS. Images were viewed using a Nikon Eclipse E600 microscope and analysed using Image J software. Based on DAPI staining a nuclear mask was generated in Image J and the mean Alexa fluor® 594 fluorescence intensities per pixel were quantified per nucleus.

2.4.8 Deadenylase Assay

The method was adapted from (Mittal, Aslam et al. 2011). The whole cell lysates from control, CNOT1, CNOT7 and TAB182-depleted HeLa cells were washed twice with deadenylation buffer. 2 µl of 5'-fluorescein-labeled RNA substrate (Flc-5'-CCUUUCCAAAAAAA-3' final concentration 0.2 µM, Sigma-Aldrich) was incubated with equal amounts of whole cell lysates of control, CNOT1, TAB182 and CNOT7-depleted cells for 10, 30, 60 and 120 minutes at 37 °C. The reaction was stopped by addition of 10µl RNA loading buffer (for buffer recipe refer to section 2.2.4) and heating for 3 minutes at 85 °C. Aliquots of the assay mixtures were fractionated on 20% polyacrylamide gel containing 8 M urea and TBE. Flc-labeled RNAs were visualised using a FUSION-FX imaging system.

2.5 MOLECULAR BIOLOGY TECHNIQUES

2.5.1 Total Nucleic Acid Isolation

72 hours post siRNA transfection total nucleic acid was extracted using a FlexiGene Kit (Qiagen). 1×10^7 Cells per 6 cm dish were pelleted and washed once with PBS. The cell pellet was re-suspended in 300 µl Buffer FG1 and mixed by pipetting up and down. 300 µl Buffer FG2 and 3 µl QIAGEN Protease K were added to cell lysates. The tube was inverted 3 times and placed in a heating block at 65 °C for 5-6 hours. 600 µl absolute isopropanol was

added to each cell lysate and mixed thoroughly by inverting until the white thread-like strands of DNA formed a visible clump. Tubes were centrifuged at 360 x g for 5 minutes. Supernatants were carefully removed and the tubes inverted onto a clean piece of absorbent paper for 5-10 minutes. 600 µl 70% ethanol was added to the DNA pellet and the tube vortexed for few seconds. Centrifugation was repeated and supernatants discarded, this was followed by inversion of the tube onto a clean piece of absorbent paper for 10-15 minutes. DNA pellets were air-dried until all the liquid had evaporated. The DNA pellet was dissolved in 100 µl Buffer FG3 for 5-6 hours at 65 °C in a heating block. DNA samples containing RNA were stored at -20 °C.

2.5.2 DNA Concentration Quantification

Purity of DNA was determined using a Nanodrop 1000 spectrophotometer (Thermo-Fisher Scientific) and ratio OD260 /OD280 was calculated. DNA concentrations were measured in ng/µL.

2.5.3 Densitometric quantification of DNA

Equal amount of nucleic acid measured by Nanodrop from each sample and a 1 KB DNA ladder (New England Biolabs) were fractionated on 0.85% agarose gel (0.85 g agarose, 100 mL TBE buffer (Table 2.5) microwaved for 1 minutes). Staining of gels using ethidium bromide at a concentration of 0.5 µg per mL was performed for 1 hour. DNA bands were visualised using UV illumination FUSION-FX (Vilber) and images collected. Densitometric readings were obtained using Image J software for DNA samples and the DNA ladder separately. Intensity of

each DNA sample was normalised against its equivalent DNA ladder band intensity and the results compared between two samples.

2.5.4 Alkaline Hydrolysis of Genomic DNA

Total nucleic acids extracted as described in section 2.5.1 were heated in 40 µl 0.3 M NaOH for 2 hours at 55 °C and fractionated on 1% alkaline agarose gel (1 g agarose, 100mL 50 mM NaOH, 1 mM EDTA) with alkaline running buffer (Table 2.5). Electrophoresis was performed at 10 V/cm overnight. Following electrophoresis, the gel was neutralised by soaking in neutralizing buffer (Table 2.5) for 1 hour, and then post-staining was carried out using 0.5 µg/ml ethidium bromide in neutralizing buffer for an additional hour. The density of the 1kb DNA ladder (Invitrogen) and each samples were measured and plotted using Image J software as described above in section 2.5.3.

2.5.5 Slot Blots

In order to give an equal loading of DNA determined by densitometry sufficient volume of nucleic acid for each control siRNA and CNOT1 siRNA treated sample (46 ng/µl and 161 ng/µl respectively) was incubated with +/- 2 U of RNase H (New England Biolabs) per µg of gDNA for 2 hours at 37 °C. One piece of Whatman filter paper and nitrocellulose membrane were cut according to the dimensions of the slot blot apparatus. Filter paper and membrane were first rinsed with deionised H_20 and then with 2 X SSC buffer (Table 2.5). The slot blot apparatus was assembled and air bubbles removed. Each well was washed twice with 200 µL 2 X SSC buffer. All samples were loaded twice and sucked through the apparatus under vacuum. Each well was washed twice with 200 µL 2 X SSC buffer. The apparatus was dissembled and the membrane was cross-linked using a Stratalinker (UV irradiation of 0.12

J/M^2). The membrane was blocked with 1% BSA/TBST for 30 minutes - 1 hour. The membrane was then cut in half and one half was blotted with S9.6 antibody (for R-loops) and the other half for ssDNAs (Table 2.7) overnight at 4 °C. For a loading control the membrane was first denatured in (0.5 N NaOH, 1.5 M NaCl) for 10 minutes and neutralised in (1 M NaCl, 0.5 M Tris-HCl pH 7.0) for 10 minutes and then blotted with ssDNA antibody. The next day, primary antibodies were removed and the blots were washed 6 times with TBST buffer. Following TBST washes, blots were incubated with the secondary antibodies (Table 2.5) for 1 hour with gentle agitation at room temperature. Blots were washed 6 times with TBST buffer and proteins were visualised with ECL reagent and detected on X-ray film.

2.5.6 Isolation of Total RNA

72 hours post siRNA transfection total RNA was extracted using RNeasy Plus Mini (Qiagen). 1×10^7 Cells per 6 cm dish were pelleted and washed once with PBS. Cell pellets were disrupted by adding 600 µl lysis buffer RLT Plus. Cell lysis was completed by vortexing or vigorous pipetting of the cell lysate. Cells were homogenised by passing the cell lysate a few times through a 20G needle fitted to a syringe. The homogenised lysate was transferred to a gDNA Eliminator spin column placed in a 2 ml collection tube and centrifuged for 1 minute at 360 x g. The flow-through in the collection tube was saved and the spin column was discarded. 600 µl of 70% ethanol was added to the flow-through and mixed thoroughly by pipetting. 600 µl of flow-through was transferred to an RNeasy spin column placed in a new 2 ml collection tube and centrifuged for 1 minute at 360 x g. This time the flow-through was discarded and spin column was saved. The spin column was washed once with 600 µl buffer RW1, followed by additional two washes with 500 µl Buffer RPE. In order to eliminate residual flow-through the spin column was placed in a new 2 mL collection tube and centrifuged at 535 x g for one

minute. The spin column was placed in a new 1.5 mL collection tube and 30-50 µl RNAse-free water was directly added to the spin column membrane and left for 2 minutes at room temperature. The spin column was centrifuged for 1 minute at 360 x g and eluted RNA was stored at -80 °C.

2.5.7 RNA Quality Control

The quality and quantity of extracted RNA were measured using a Qubit 2.0 Fluorometer (Life Technologies) and an Agilent 2200 TapeStation system, respectively. RNA concentrations and purity were measured in pg/µL and RIN (RNA Integrity Number), respectively and results were recorded (Table 2.9). The RIN 7 was set as the cut off value for sequencing (the highest score for RIN is 10). The 28S:18S rRNA ratio was also calculated as a marker for RNA quality (Table 2.9). A 28S:18S rRNA ratio of 2:1 was considered as a representative of good-quality RNA.

Well	Conc. (pg/µl)	RINe	Sample ID	28S/18S (Area)
A0	3850	---	Electronic Ladder	---
A1	4430	9.5	Con siRNA	3.7
B1	4770	9.7	CNOT1 siRNA	3.9

Table 2.9 RNA concentration and purity measured by Qubit 2.0 and TapeStation system

2.5.8 Total RNA-Sequencing

Dual-indexed, strand-specific RNA-Seq library was prepared from submitted total RNA, using RiboZero (Illumina) rRNA depletion and the NEBNext Ultra Directional RNA library preparation kit (NEB). RNA-Seq was performed on 2 lanes of HiSeq4000 (paired-end, 2x150bp) platform to generate ~80M reads per sample.

2.5.9 Bioinformatics data analysis

2.5.9.1 RNA-Sequencing data

The raw data files were generated in binary base call (BCL) format and converted to FASTQ format using bcl2fastq Conversion Software (Illumina). FASTQ format readings were transferred to BaseSpace® Sequence Hub (Illumina). The assay was run in 4 lanes in paired-end and 76-cycle mode. The FASTQ files were aligned using HISAT2 (Kim, Langmead et al. 2015), and the resulting mRNA transcripts were assembled using StringTie (Pertea, Pertea et al. 2015) as described in (Pertea, Kim et al. 2016). All RNA-seq data was uploaded to the GEO database (https://www.ncbi.nlm.nih.gov/geo/query/acc.cgi?acc=GSE141496) with the accession number GSE141496.

2.5.9.2 Differential Gene Expression Analysis

Taking the Control siRNA sample as reference, log2-transformed fold changes (log2FC) of CNOT1 siRNA samples were calculated. Genes with positive log2FC were considered “upregulated” while those with negative log2FC were considered “downregulated”. To determine if the change in the expression of a particular gene was significant, we used empirical p-values. After correcting p-values for false positive rate in multiple testing problem using false discovery rate as proposed in (Benjamini and Hochberg 1995), we analysed the enrichment of the up/down-regulated gene sets for each sample using Enrichr (Kuleshov, Jones et al. 2016). Finally, significant biological processes reported by Enrichr were extracted for further consideration.

CHAPTER THREE

CNOT1 & The CELL CYCLE PROGRESSION

3 CNOT1 AND CELL CYCLE PROGRESSION

3.1 INTRODUCTION

Previous studies by Dronamraju *et al.* (2018) had proposed a novel role for Ccr4-Not in the regulation of mRNAs involved in cell cycle progression in yeast (Dronamraju, Hepperla et al. 2018). They showed that the interaction between Spt6, a histone chaperone, and RNA PoII promotes the recruitment of the Ccr4-Not complex at the site of transcription in order to facilitate the degradation of mRNAs required for cell-cycle progression. This recruitment possibly occurs during G1 phase as suggested by *Morel* et al. (2003), who showed that the CNOT complex is concentrated in the nucleus in early G1 cells, but by the time the cells enter S phase much of it becomes cytoplasmic. In addition, Westmoreland *et al.* (2004) showed that yeast CCR4 (hCNOT6/hCNOT6L) regulates cell cycle progression through G1 and S phases following radiation or replication stress (Westmoreland, Marks et al. 2004). In an earlier study by (Liu, Toyn et al. 1997) it has been shown that, during M/G1 phase transition, Dbf2p (metaphase cell cycle-regulated protein kinase), is dephosphorylated to initiate degradation of mRNAs required for cell cycle progression, possibly through regulation of the Ccr4-Not complex. In agreement with these studies, our results have revealed that depletion of CNOT1 leads to much reduced cell cycle progression through S and G2/M phases and subsequent arrest of the cell cycle in G1. At later times, the cells appear to senesce and /or undergo autophagy.

Based on our results we propose the repertoire of CCR4-NOT complex mRNA homeostasis to include a function in cell cycle progression in mammalian cells. Indeed, it has already been shown that the CNOT complex is involved in the stability of cell cycle-associated mRNAs such as CLB2 (cyclin B human orthologue) (Kadyrova, Habara et al. 2007), cyclins CLN2 (cyclin E

human orthologue) and CLB5 (cyclin A2 human orthologue), histone H2A.1 (H1A human orthologue) (Dronamraju, Hepperla et al. 2018), DBF2 and SW15 (Johnston, Eberly et al. 1990) in *Saccharomyces cerevisiae.*

3.2 RESULTS

3.2.1 Depletion of CNOT1 leads to reduction in level of the other CNOT subunits

HeLa cells were treated with CNOT1 siRNA and control siRNA and the efficiency of knock down was judged by western blot at different times: 0, 24, 48, 72, 96 and 120 hours (Figure 3.1.A). On the basis of this result, 72 hours post CNOT1 siRNA transfection was used for most subsequent experiments. The expression level of the other CNOT subunits was analysed in control and CNOT1-depleted HeLa cells 72 hours post siRNA transfection. Depletion of CNOT1 leads to reduction in the level of other CNOT subunits (Figure 3.1.B).

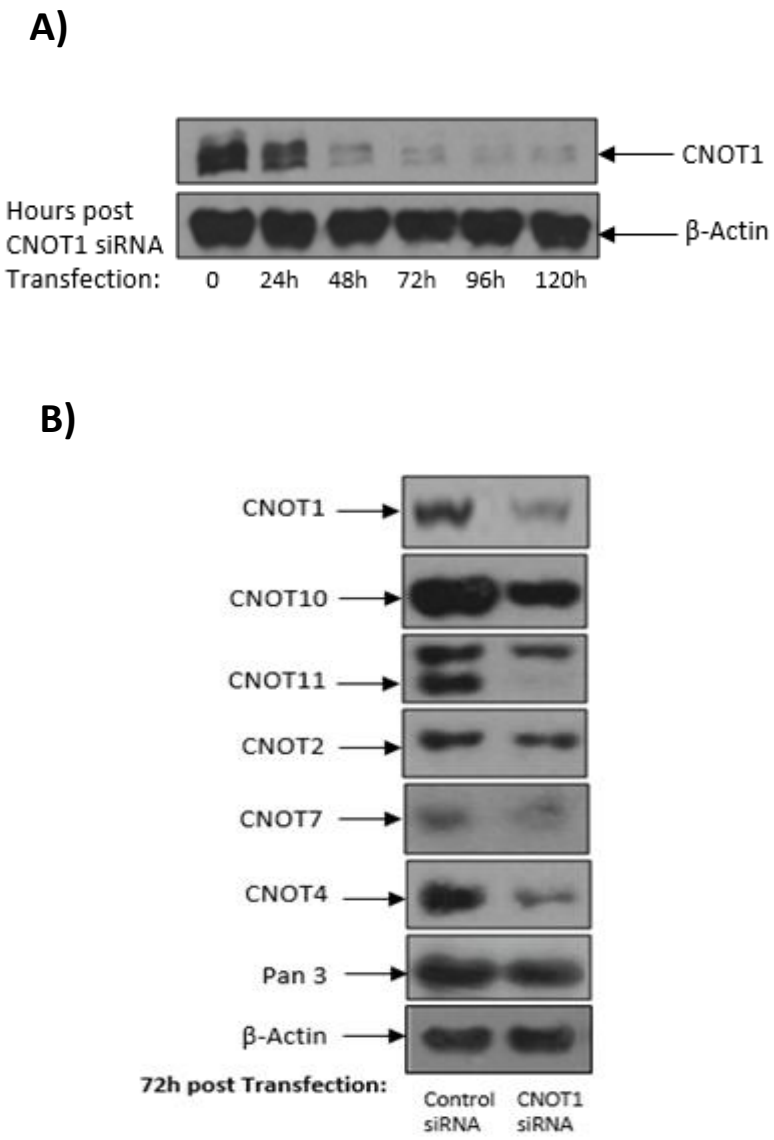

Figure 3.1 Depletion of CNOT1 leads to reduction in the other CNOT subunits

A) *Representative immunoblot shows the CNOT1-dependent depletion at different time points, 0, 24h, 48h, 72h, 96h and 120h (0.2nmol siRNA/6cm culture dish).* ***HeLa*** *cells were transfected with control or CNOT1 siRNA.* ***B)*** *Cells were lysed and the lysates assessed by immunoblotting with the indicated antibodies against different CNOT subunits and Pan 3 72hours post siRNA transfection.*

3.2.2 Depletion of CNOT1 disrupts the cell cycle progression in HeLa cells

Activation of the DDR can result in cell cycle arrest and, therefore, a number of DDR proteins can directly affect the cell cycle following their activation. To assess whether the depletion of CNOT1 had any effect on cell cycle progression in HeLa cells, cells were stained with the DNA stain PI and the cell cycle profiles were investigated using FACS analysis 0, 4, 8, 24 and 32h post siRNA transfection (Figures 3.2.A and B). In comparison to the control cells, CNOT1-depleted cells gradually accumulated in G1 phase, whereas very few cells were observed in the S and G2 phases. The data are represented in a graphical format, where the average cell cycle was plotted from three independent experiments (Figures 3.2.C).

A)

Control siRNA

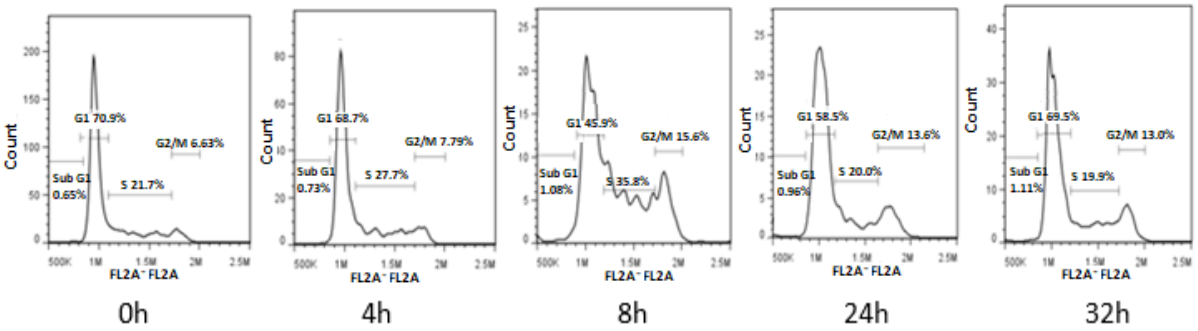

0h 4h 8h 24h 32h

B)

CNOT1 siRNA

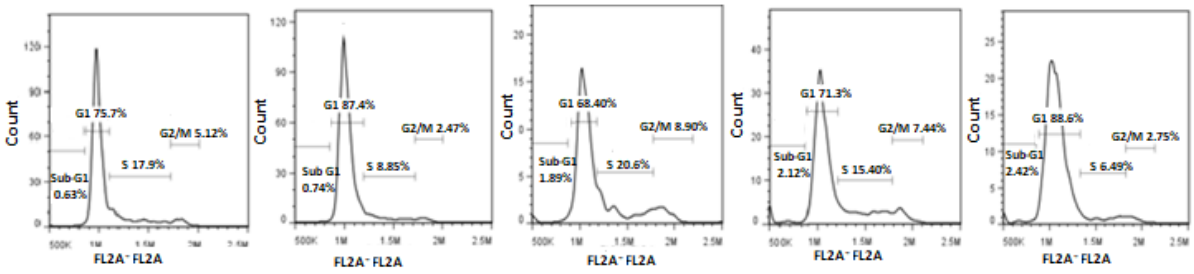

0h 4h 8h 24h 32h

C)

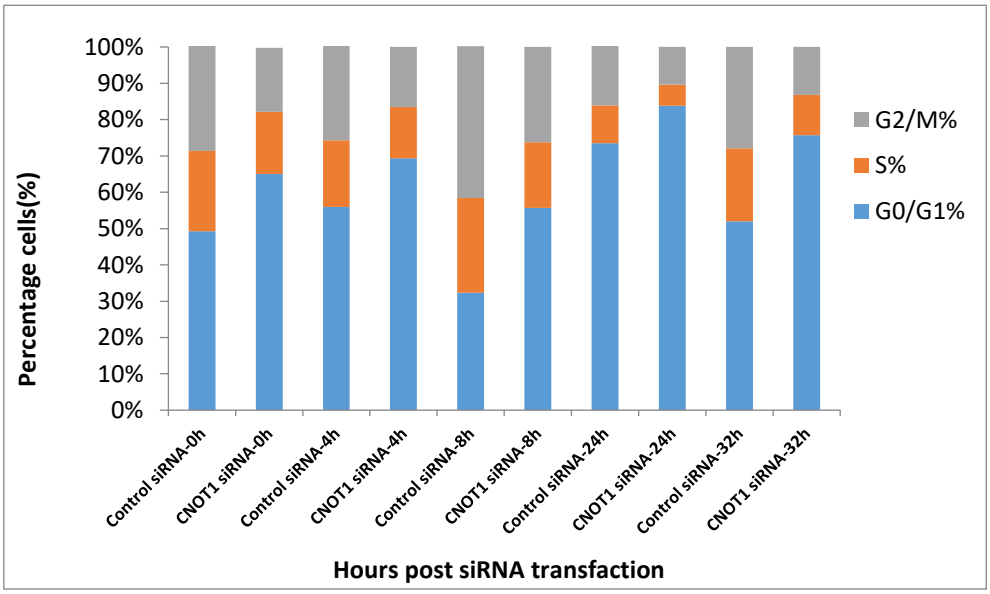

Figure 3.2 Ablation of CNOT1 expression leads to G1-cell cycle arrest

HeLa cells were transfected with either control or CNOT1 siRNA and stained with PI and the cell cycle profiles analysed by flow cytometry at different time-points post-transfection. ***A & B)*** *are representatives of a typical flow cytometry plots observed.* ***C)*** *Multiple stacked graph depicts the average cell cycle profile observed in three independent experiments. Relative DNA content were analysed using an Accuri C6 flow cytometer (BD) and FlowJo software (Tree Star Inc.)*

3.2.3 Depletion of CNOT1 reduces the S-phase indices in HeLa cells

EdU labelling was used to determine a full S phase of a fraction of cells in asynchronous HeLa cells. HeLa cells were transfected with either control or CNOT1 siRNA. Cells were incubated with 10 μM EdU for 20 minutes at 24, 48 and 72 hours post siRNA transfection. Cells were fixed using 3.7% formadehyde diluted in PBS followed by a 0.5% Triton X-100 permeabilisation. Cells were incubated with the fluorescent EdU detection cocktail for 30 minutes at room temperature and protected from light. Nuclei were stained with DAPI and proceed for microscopic imaging (Figure 3.3 A). The percentage of cells with positive EdU labelling in CNOT1-depleted cells was lower than their control counterparts, suggesting the progression through S phase is reduced in CNOT1-depleted cells (Figure 3.3 B).

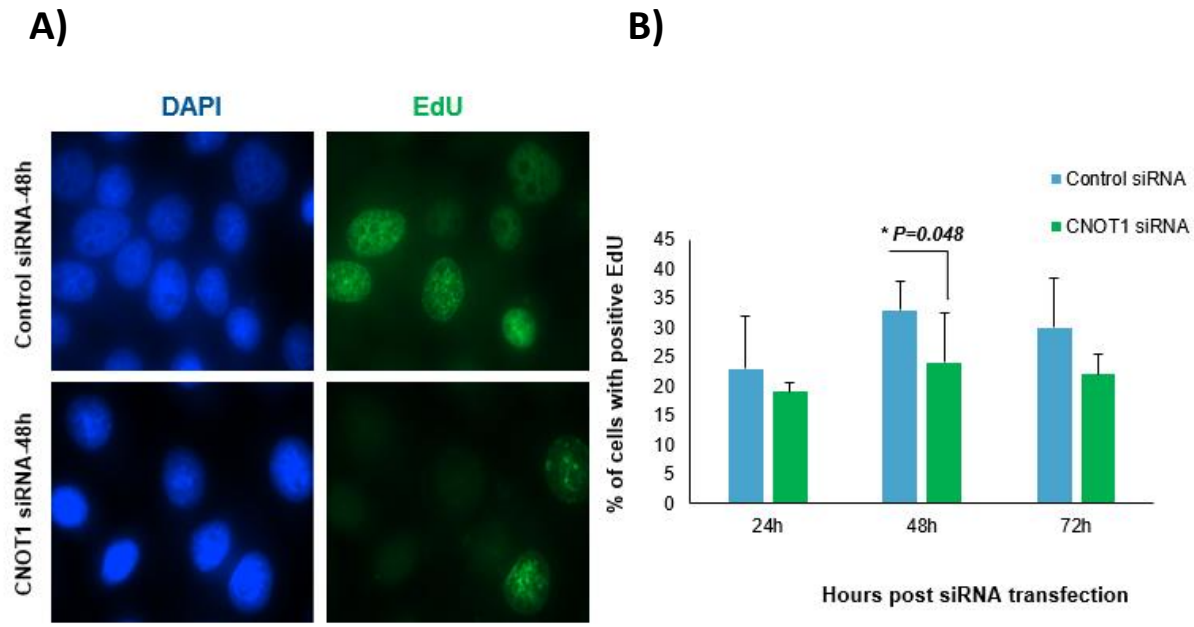

Figure 3.3 Ablation of CNOT1 expression reduces the S-phase indices in HeLa cells

HeLa cells were transfected with either control or CNOT1 siRNA and processed at the indicated time points. Cells were labelled with 10 µM EdU for 20 minutes. Cells were incubated with the fluorescent EdU detection cocktail for 30 min. Cells were visualized using a Nikon Eclipse E600 microscope and analysed using Velocity software version 4. ***A)*** *The immunofluorescence images illustrate both positive and negative EdU-labelled cells in control and CNOT1-depleted cells.* ***B)*** *Representative bar graphs show % cells present in S phase. 200 cells were counted in each experimental repeat (n = 3 independent experiments). Statistical analyses were performed using a two-tailed and unpaired Student t test, *P <0.05, **, P<0.01; ***, P<0.001. Error bars represent the StDev. Scale bars, 10 µm.*

3.2.4 Depletion of CNOT1 remarkably reduced the G2/M cell cycle transition

In further experiments, in order to discriminate between G2 and M phase cells, simultaneous staining of DNA with PI and the mitotic marker, pH3 (Serine 10), was performed at different time points (24, 32, 48, 56, and 7 2hours). A distinct cell cycle profile was gated to determine the percentage of cells present in each phase (Figures 3.4.A and B). Very few cells were observed in the G2 phase and pH3-positive cells were hardly detected in CNOT1-depleted cells, further evidence confirming that depletion of CNOT1 disrupts the cell cycle progression beyond G1 phase (Figure 3.4.C)

A)

Control siRNA-32h post siRNA transfection

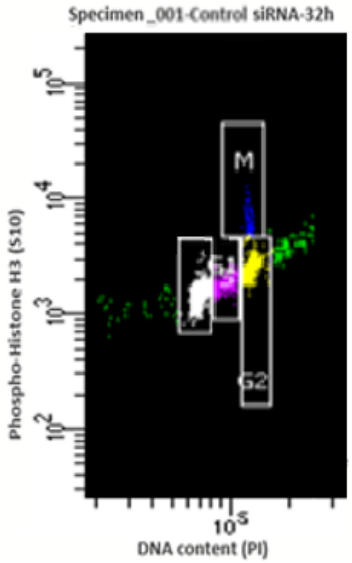

Tube: Control siRNA-32h

Population	#Events	%Parent	%Total
All Events	10,000	####	100.00
P1	5,878	58.8	58.8
P2	3,324	56.5	33.2
M	94	2.8	0.9
G1	2,284	68.7	22.8
S	297	8.9	3.0
G2	517	15.6	5.2

B)

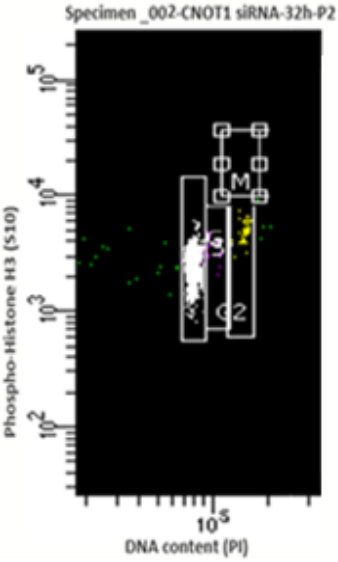

Tube: CNOT1 siRNA 32h

Population	#Events	%Parent	%Total
All Events	10,000	####	100.00
P1	2,077	20.8	20.8
P2	1,641	79.0	16.4
M	3	0.2	0.0
G1	1,332	81.2	13.3
S	128	7.8	1.3
G2	75	4.6	0.8

C)

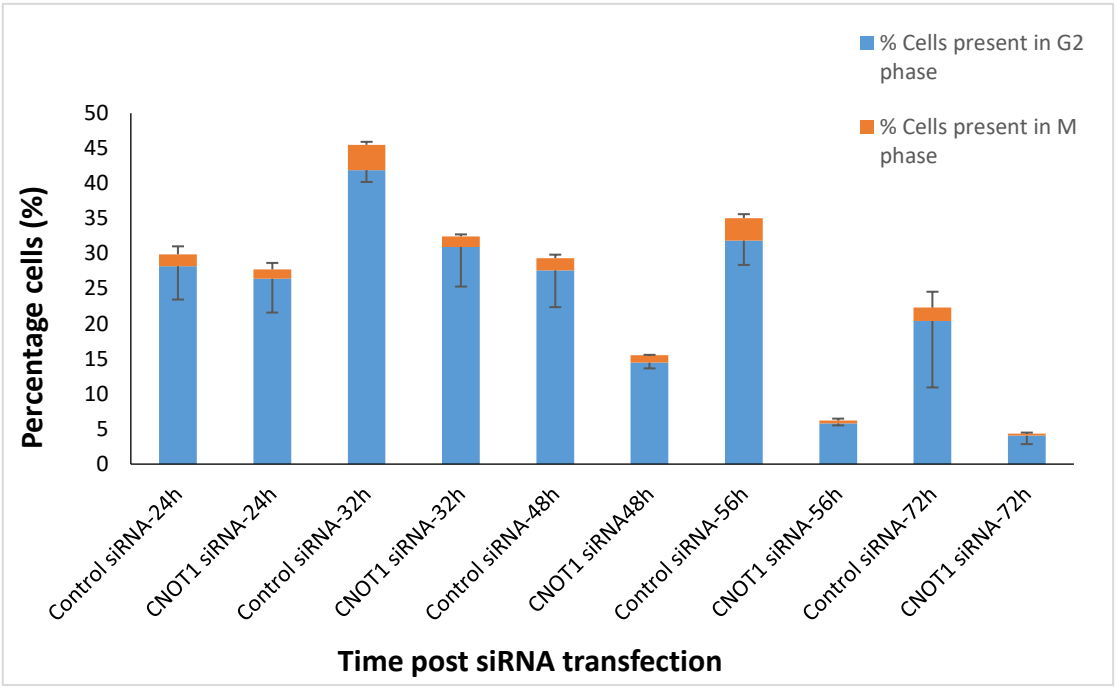

Figure 3.4 Ablation of CNOT1 expression remarkably reduced the G2/M cell cycle transition A & B) *HeLa cells were transfected with either control or CNOT1 siRNA, stained with simultaneous staining of DNA with PI and pH3 (with an antibody) was performed and the cell cycle profiles in control and CNOT1-depleted cells were analysed at different time points after siRNA treatment (24, 32, 48, 56 and 72 hours) on a BD LSRFortessa™ X-20 flow cytometer.* ***C)*** *Representative stacked bar graphs showing % cells present in each phase of the cell cycle (G1, S, G2 and M respectively). Percentages of cell cycle phase distribution represent the average of three independent experiments. The results are statistically significant but t-test results have been omitted for clarity).*

3.2.5 Depletion of CNOT1 disrupts the cell cycle progression beyond the G1/S boundary

The impact of depletion of CNOT1 on cell cycle progression was further assessed by synchronizing cells in mitosis using nocodazole (200 ng/ml), which blocks cells in pro-metaphase by inhibiting the mitotic spindle formation, for 18h, 72 hours post CNOT1 depletion. Mitotic cells were visualised using an EVOS fluorescence inverted digital microscope from Advanced Microscopy Group (AMG). Figures 3.5.A and B show HeLa cells 18 hours after nocodazole treatment. Mitotic cells are round and weakly adherent cells, whereas those cells that have not entered mitosis are still flat and adhere to the tissue culture plastic. The dominant cell population in CNOT1-depleted cells were adherent interphase cells, suggesting progression into and through mitosis is inhibited in CNOT1-depleted cells. Control and CNOT1-depleted mitotic cells were collected by shake-off and released from the G2/M block by washing with fresh media. Cells were harvested at the indicated times and analysed by western blotting using the indicated antibodies as listed in (Figure 3.5.C). β-actin was used as a loading control. Separately, adherent cells were harvested by trypsinization from the flask and collected. Strikingly, high-level expression of cyclin E, which is responsible for cell cycle transition from G1 to S phase, was seen in CNOT1-depleted cells up to 24 hours after nocodazole release (Figure 3.5.C). Increase in expression of cyclin inhibitors p21 and p27 was also observed in CNOT1-depleted cells (Figure 3.5.C). Cyclin D1 was weakly expressed in CNOT1-depleted cells compared to controls (4 hours post G2/M release). These cells were considered to be in G1 phase (Figure 3.5.C). In control HeLa cells the expression level of cyclin B1 peaked in M phase and by entry into G1 phase was substantially reduced 2 hours post nocodazole washout. The level then gradually increased as the cells progressed through the cell cycle. However, the expression of cyclin B1 was reduced in G2/M CNOT1-depleted cells and into the following cycles (Figure 3.5.C). Moreover, in CNOT1- depleted cells

phosphorylation of the metaphase marker histone H3 (pH3) on serine 10 was lost 2 hours after removal of nocodazole. No further evidence of H3 phosphorylation was seen even at later time points (Figure 3.5.C). It is also worth noting that the CNOT1-depleted cells appear to progress out of mitosis more rapidly than the controls as evidenced by the absence of pH3 after 1 hour in normal media; pH3 can be seen in control cells up to 4 hours. Cyclin A, which is responsible for progression through S phase, was expressed at low level during late G1 (from 6 to 8 hours), S (at 8 hours) and G2 (at 24 hours) in CNOT1-depleted cells, suggesting that progression through S and G2 phases had been hindered in CNOT1-depleted cells.

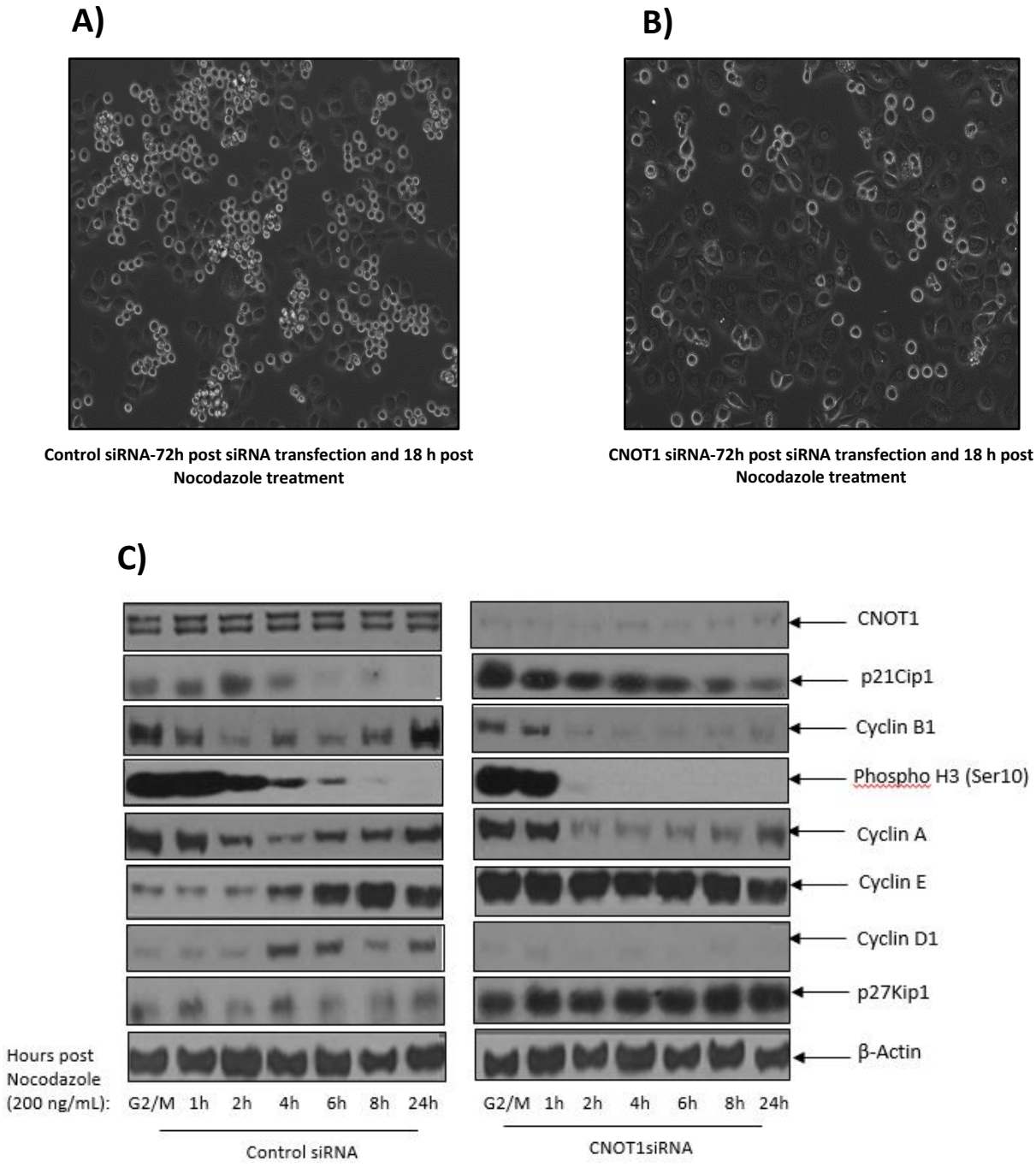

Figure 3.5 Depletion of CNOT1 disrupts cell cycle progression beyond the G1/S boundary

A & B) *Control and CNOT1-depleted HeLa cells 18 hours after 200 ng/mL nocodazole treatment. Images were collected using an EVOS fluorescence inverted digital microscope.* ***C)*** *Representative immunoblot shows the comparative protein expression between control (left panel) and CNOT1-depleted cells (right panel). β-actin was used as a loading control. The expression level of cell cycle regulators at different time points up to 24 hours post nocodazole release is shown. The siRNA-mediated gene suppression was performed 48 h before nocodazole treatment.*

3.2.6 p53-independent upregulation of p21 and p27 promote the G1-cell cycle upregulation in CNOT1-depleted HeLa and U2OS cells

Since CNOT1 depletion disrupts the cell cycle progression beyond the G1/S boundary in the absence of DNA damage in HeLa cells, we next investigated the activation of the G1 checkpoint in two different cell lines, HeLa and U2OS, up to 4 days post siRNA transfection. We have shown that the expression of cyclin inhibitors p21 (log2FoldChange in gene expression= + 1.073303) and p27 (no difference in gene expression was observed) gradually increased in CNOT1-depleted HeLa and U2OS cells (Figures 3.6.A and B). It seems that Chk2, independently of p53, is responsible for p21 induction in HeLa cells as no difference in p53 gene (assessed by RNA-Seq results and it is not included) and its protein expression (assessed by western blot and it is included) was observed between control and CNOT1-depleted cells (Figures 3.6.A and B).

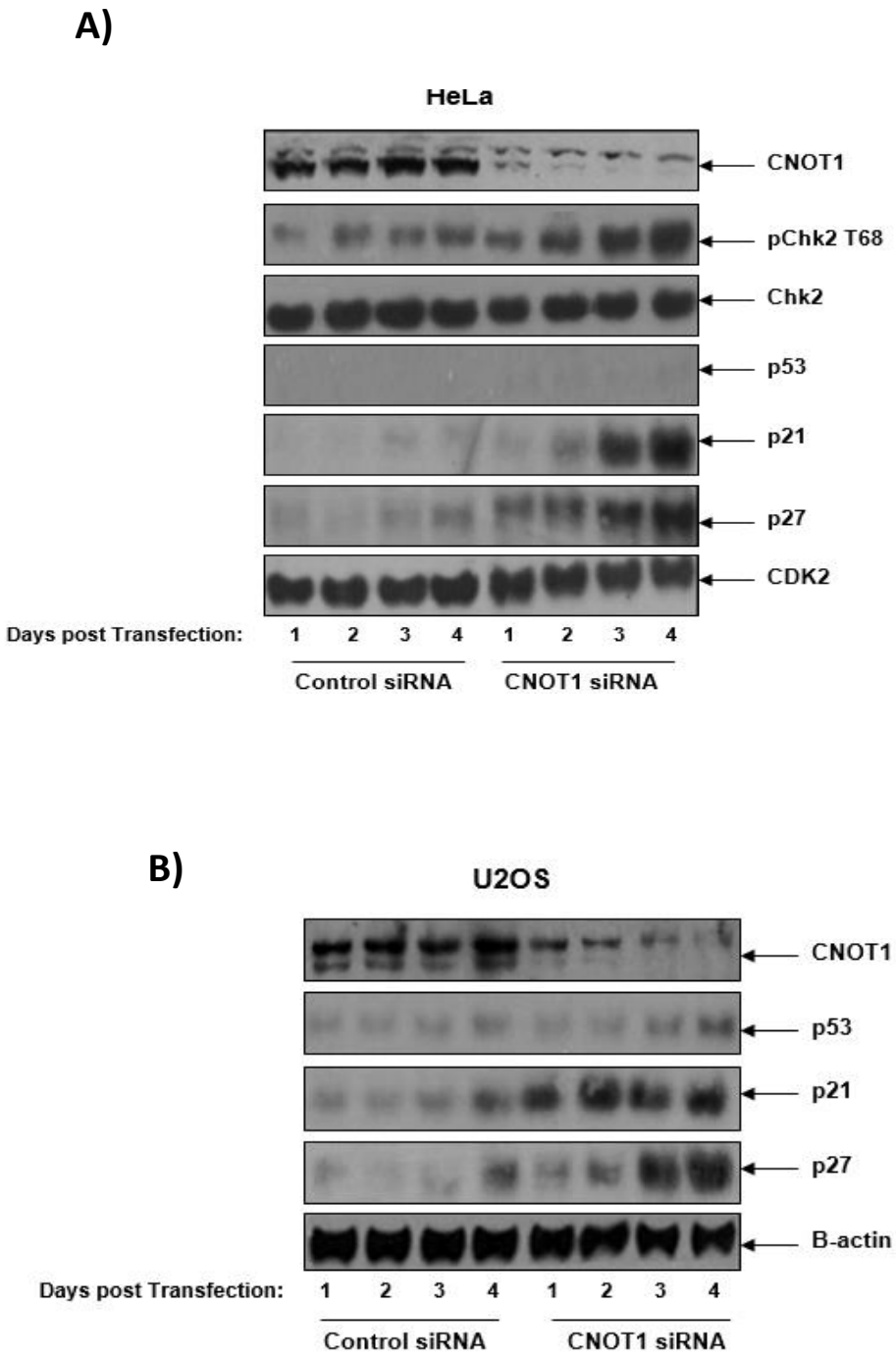

Figure 3.6 p53-independent upregulation of p21 and p27 promote the G1-cell cycle upregulation in CNOT1-depleted HeLa and U2OS cells.

A & B) *Representative immunoblots shows the comparative protein expression between control (left panel) and CNOT1-depleted cells (right panel) in HeLa and U2OS cells respectively.CDK2 and β-actin were used as a loading controls. The expression level of indicated proteins at different time points up to 4 days post siRNA transfection is shown.*

3.2.7 Depletion of CNOT1 decreased the expression of genes involved in cell cycle progression

To assess further the cell cycle distribution of CNOT1-depleted cells, we took advantage of our RNA-Seq data processed by GO Enrichr tool. These results showed downregulation of genes involved in cell cycle progression through the S phase (GO: 0044843) (Figure 3.7 A) and G2/M phase transition (GO: 0044839), (GO: 0006285) and (GO: 0044772) (Figure 3.3.1 B). Gene ontology (GO) was applied to identify characteristic biological attributes of RNA-seq data. Separate gene ontology enrichment analysis using Enrichr for up-regulated and down-regulated genes was performed. The GO data is shown in Figures 3.7 C & D. Considering the expression of many of these genes is cell-cycle dependent, any up- or down-regulation in their expression contribute to the G1-cell cycle phenotype observed in CNOT1-depleted HeLa cells.

A)

Gene names	log2FoldChange	P-value	P-adj
CCNA2	-0.90561	0.000196	0.008654
CDK1	-0.90642	0.000179	0.007997263
ORC6	-0.95286	0.000148	0.006969
CDKN3	-0.71543	0.006457	0.086194
RANBP1	-0.58982	0.006463	0.086194
PLK2	-0.76467	0.001049	0.027592
HIST1H2AD	-1.51484	2.59E-07	3.92E-05
HIST1H2BM	-1.09616	0.000175	0.00786615
HIST1H1A	-0.97789	0.000411	0.014855113
HIST1H2AG	-0.84148	0.003343	0.057579212
HIST1H2BD	-0.62675	0.005821	0.080983033
HIST1H2BH	-0.81217	0.001196	0.029836522
HIST1H2BO	-0.8671	0.000878	0.024518918
HIST1H4A	-0.96608	0.000223	0.009486935

B)

Gene names	log2FoldChange	P-value	P-adj
STMN1	-1.26473	7.45E-07	9.16E-05
HMMR	-1.13081	3.78E-06	0.000358865
CEP78	-1.04606	6.03E-05	0.003474465
CCNB2	-0.98241	7.39E-05	0.004051762
CCNB1	-0.66348	0.003436	0.058596404
CDK1	-0.90642	0.000179	0.007997263
CENPF	-0.6527	0.005232	0.076087796
SKP1	-0.71037	0.001915	0.040687284
PLK2	-0.76467	0.001049	0.027591791
PLK4	-0.64781	0.003357	0.057729592
CETN2	-0.68306	0.007499	0.094746499
KIF14	-0.7639	0.001219	0.030223204
NPM1	-0.78059	0.000968	0.026166253
HAUS2	-0.63193	0.005177	0.075519965
PSMD10	-0.90259	0.00042	0.015085895
PSMA2	-0.58802	0.008214	0.099938554
PSME1	-0.648	0.006437	0.086052333
NEK2	-0.84308	0.000319	0.012375474
RPS27A	-0.83297	0.000366	0.013676609
GTSE1	-0.61851	0.005085	0.074733852
ANLN	-0.78993	0.000597	0.019093037
UBE2C	-0.70916	0.001564	0.035612128
NUF2	-0.89424	0.000141	0.006734374
NUSAP1	-0.76365	0.000907	0.02501347
AURKB	-0.70122	0.001962	0.041184251
SPC25	-0.84479	0.000562	0.018235204

C)

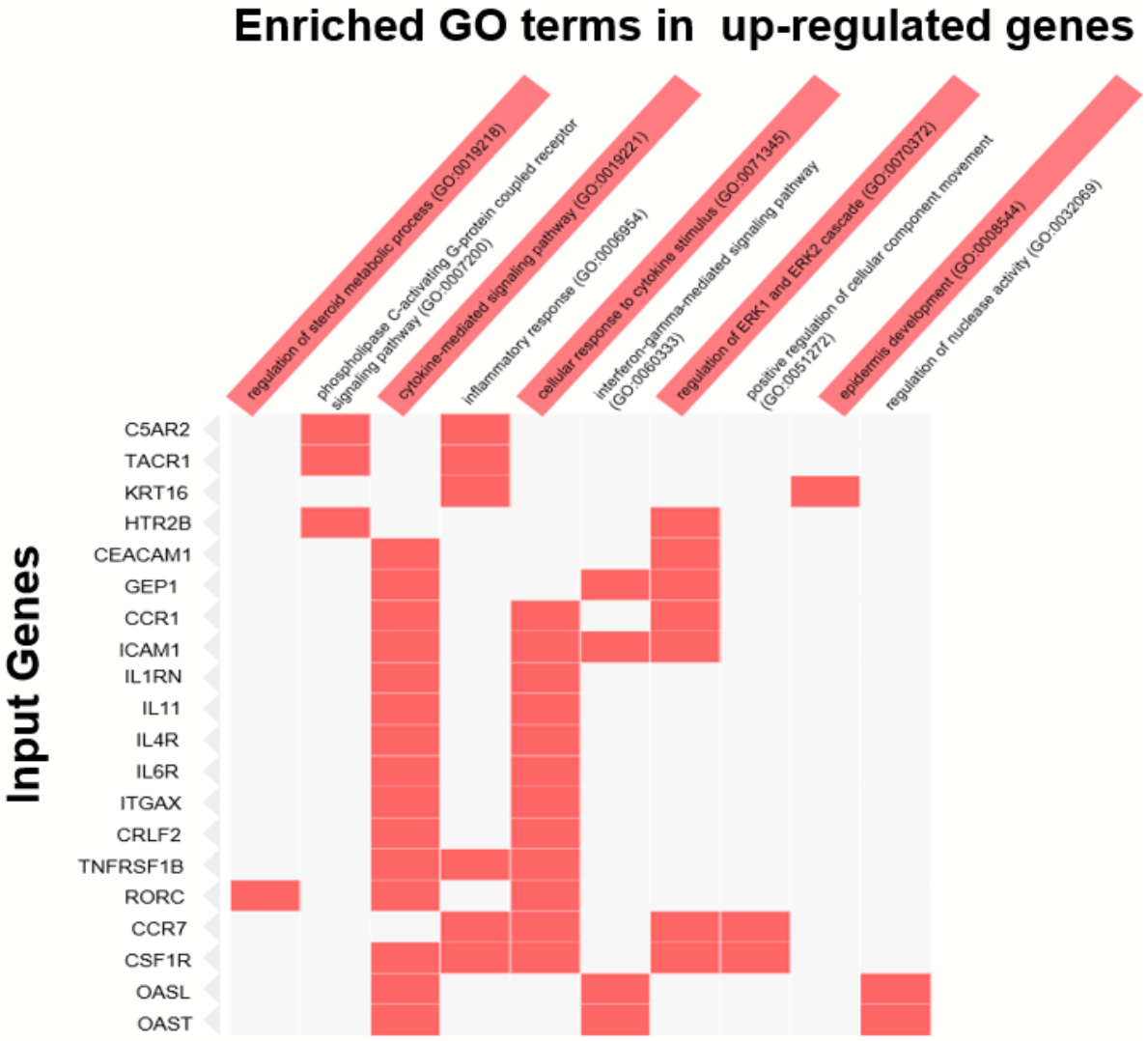
Enriched GO terms in up-regulated genes
regulation of steroid metabolic process (GO:0019218)
phospholipase C-activating G-protein coupled receptor signaling pathway (GO:0007200)
cytokine-mediated signaling pathway (GO:0019221)
inflammatory response (GO:0006954)
cellular response to cytokine stimulus (GO:0071345)
interferon-gamma-mediated signaling pathway (GO:0060333)
regulation of ERK1 and ERK2 cascade (GO:0070372)
positive regulation of cellular component movement (GO:0051272)
epidermis development (GO:0008544)
regulation of nuclease activity (GO:0032069)
Input Genes
C5AR2
TACR1
KRT16
HTR2B
CEACAM1
GEP1
CCR1
ICAM1
IL1RN
IL11
IL4R
IL6R
ITGAX
CRLF2
TNFRSF1B
RORC
CCR7
CSF1R
OASL
OAST

D)

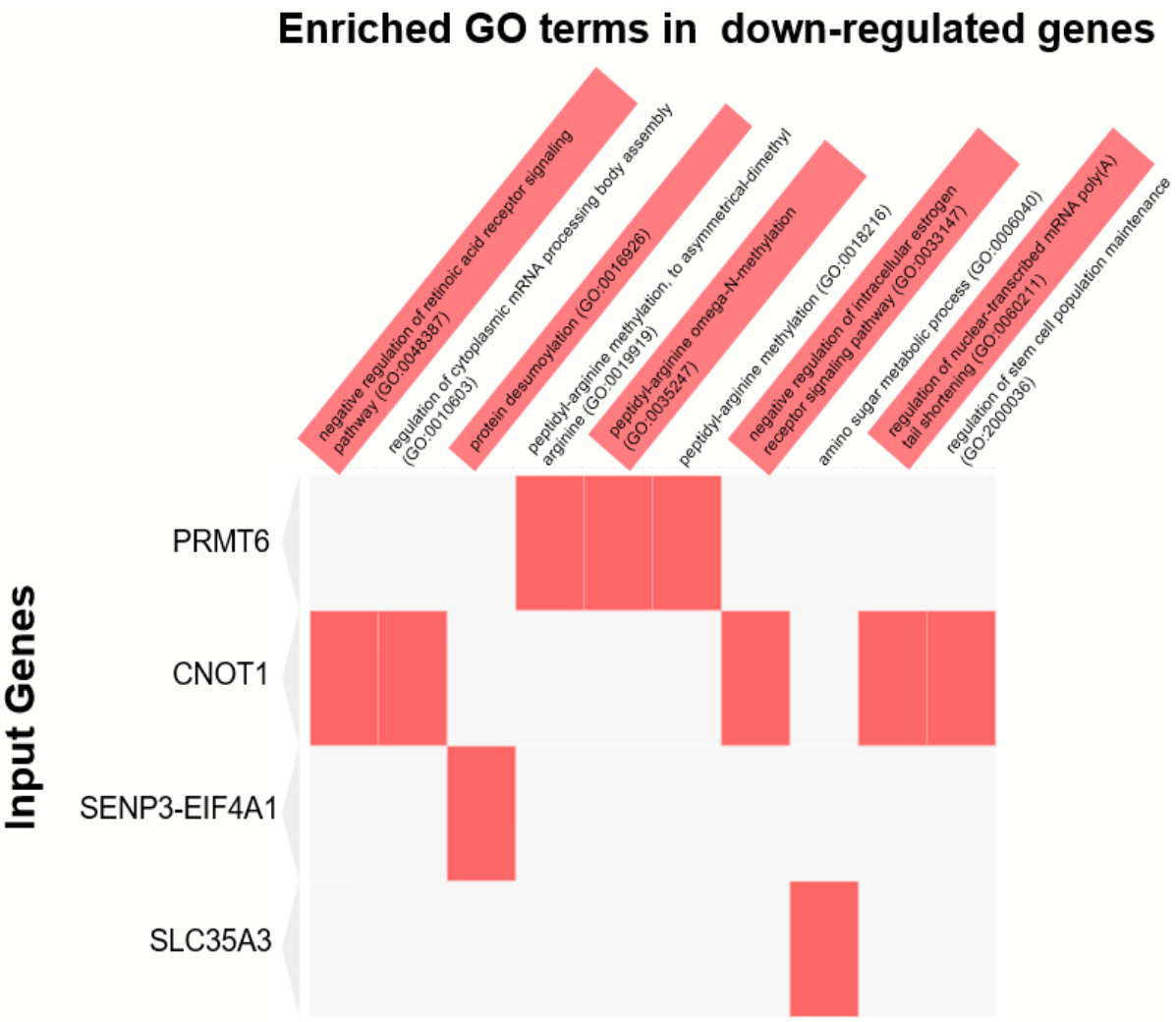

Figure 3.7 Depletion of CNOT1 decreased the expression of genes involved in cell cycle progression through S phase and G2/M phase transition.

A & B) *tables show down-regulation of genes involved in cell cycle progression through S (A) and G2/M transition (B) 72 hours post CNOT1 siRNA treatment. The total RNA was extracted from 3 biological replicates and RNA-Seq was performed on 2 lanes of HiSeq4000 (paired-end, 2x150bp) platform to generate ~80M reads per sample. The Control siRNA sample was*

considered as the reference; log2-transformed fold changes (log2FC) of CNOT1 siRNA samples were calculated. Genes with positive log2FC were considered "upregulated" while those with negative log2FC were considered "downregulated". The empirical p-values were used to determine the change in the expression of a particular gene. ***C & D)*** *Gene Ontology enrichment analysis of molecular function for up- and down-regulated genes between control and CNOT1-depleted HeLa cells using Enrichr platform (combined score). A threshold of 2-fold was used to enumerate a set of most-changed genes between conditions All RNA-seq data was uploaded to the GEO database (https://www.ncbi.nlm.nih.gov/geo/query/acc.cgi?acc=GSE141496) with the accession number GSE141496. RNA-Seq data was generated by the Centre for Genomic Research, which is based at the University of Liverpool. Bioinformatics analysis was carried out by Dr Morteza Chalabi Hajkarim from Biotech Research and Innovation Centre (BRIC), which is based at the University of Copenhagen.*

3.2.8 Autophagy, Senescence or Apoptosis?

Irreversible accumulation of DNA damage drives mitotic cells either to adapt to stress through autophagy and/or senescence or to be eliminated through programmed cell death (Vicencio, Galluzzi et al. 2008). Therefore, we have examined whether depletion of CNOT1 can activate any of these pathways.

3.2.8.1 Autophagy

The cell culture phenotype was assessed in control and CNOT1-depleted HeLa and U2OS cells over a time course of 7 days using an EVOS fluorescence inverted digital microscope. CNOT1-depleted HeLa and U2OS cells were bigger in size, with flattened morphology (between day 4 and 5) and extensive vacuolation especially in HeLa cells at day) (Figures 3.8 A and B). This phenotype is commonly associated with autophagy and/or senescence. Induction of autophagy in CNOT1-depleted cells were confirmed by marked induction of the autophagy markers p16 and LC3β (Figures 3.8 C and D). Degradation of p62 (SQSTM1) during autophagy is another widely used marker to monitor autophagic flux. Since, p62 protein level gradually accumulated in CNOT1-depleted cells, with no change in its gene expression assessed by RNA-Seq, results indicated that degradation of autophagosomes caused by lysosomal acidification is impaired (Figures 3.8 C and D). To confirm that induction of autophagy is p53-independent we monitored the cell culture phenotype and expression of p62 protein in control and CNOT1-depleted H1299 cells, which have a homozygous partial deletion of the TP53 gene and, as a result, do not express the tumour suppressor p53 protein. Similarly depletion of CNOT1 increased the formation of vacuoles in H1299 cells 7 days post siRNA transfection (Figure 3.8

E). Perturbation in autophagy was also monitored by upregulation of p62 protein in CNOT1-depleted H1299 cells (Figure 3.8 F).

A)

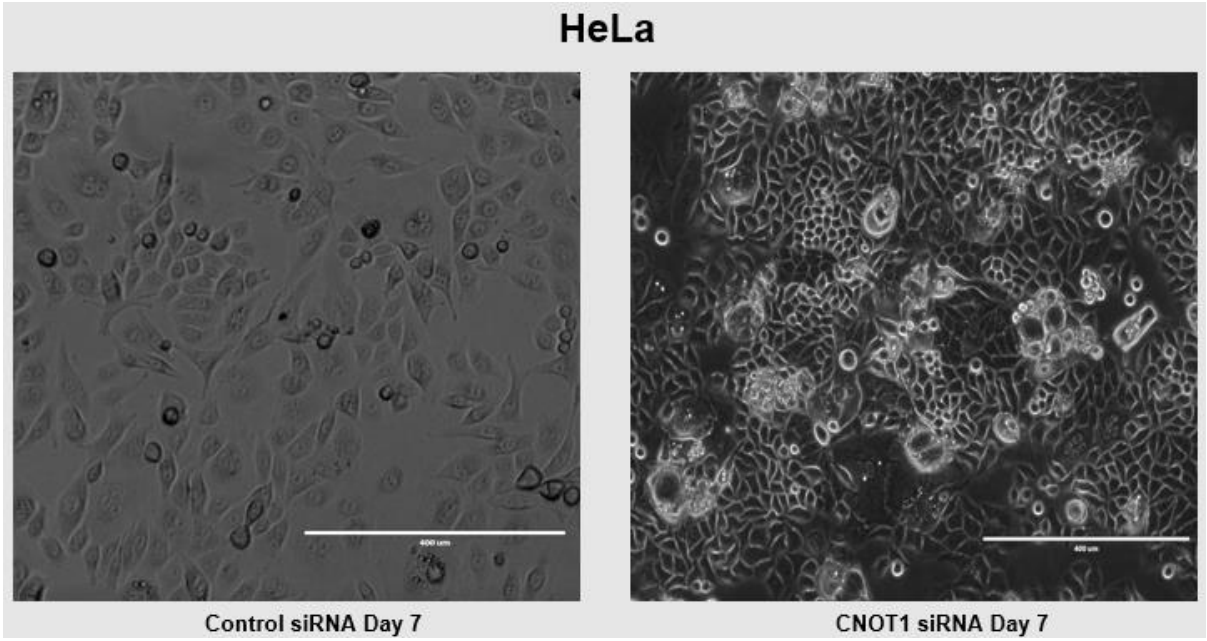
HeLa
Control siRNA Day 7
CNOT1 siRNA Day 7

B)

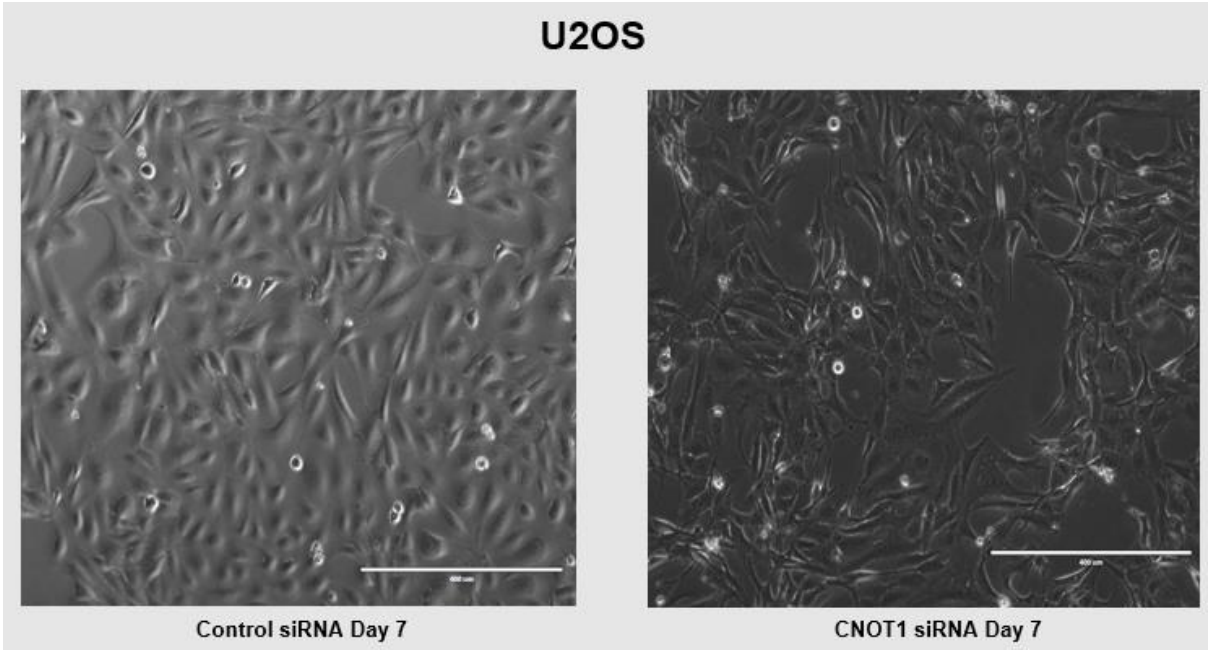
U2OS
Control siRNA Day 7
CNOT1 siRNA Day 7

C)

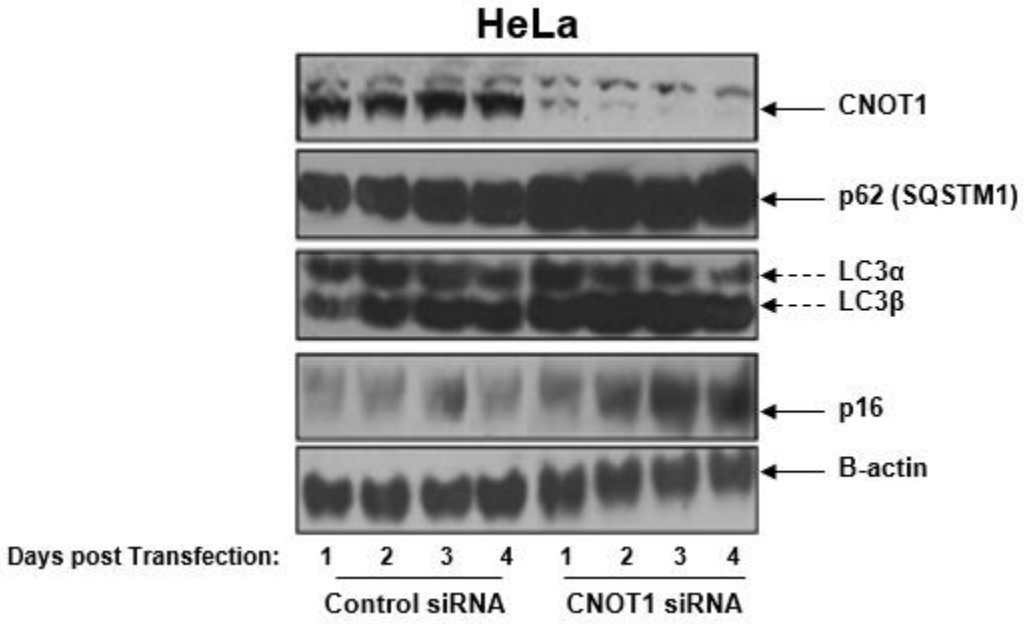
HeLa
CNOT1
p62 (SQSTM1)
LC3α
LC3β
p16
B-actin
Days post Transfection: 1 2 3 4 1 2 3 4
Control siRNA
CNOT1 siRNA

D)

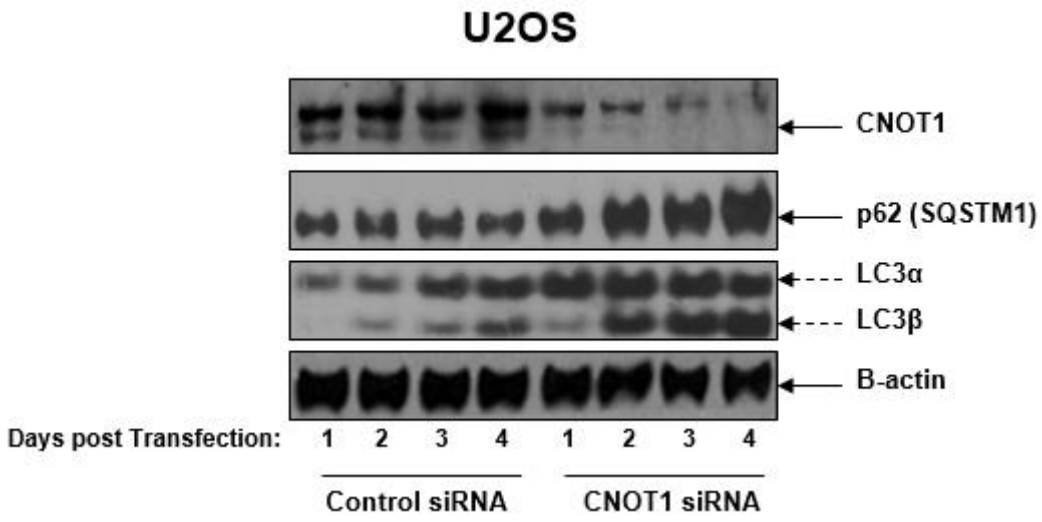
U2OS
CNOT1
p62 (SQSTM1)
LC3α
LC3β
B-actin
Days post Transfection: 1 2 3 4 1 2 3 4
Control siRNA
CNOT1 siRNA

E)

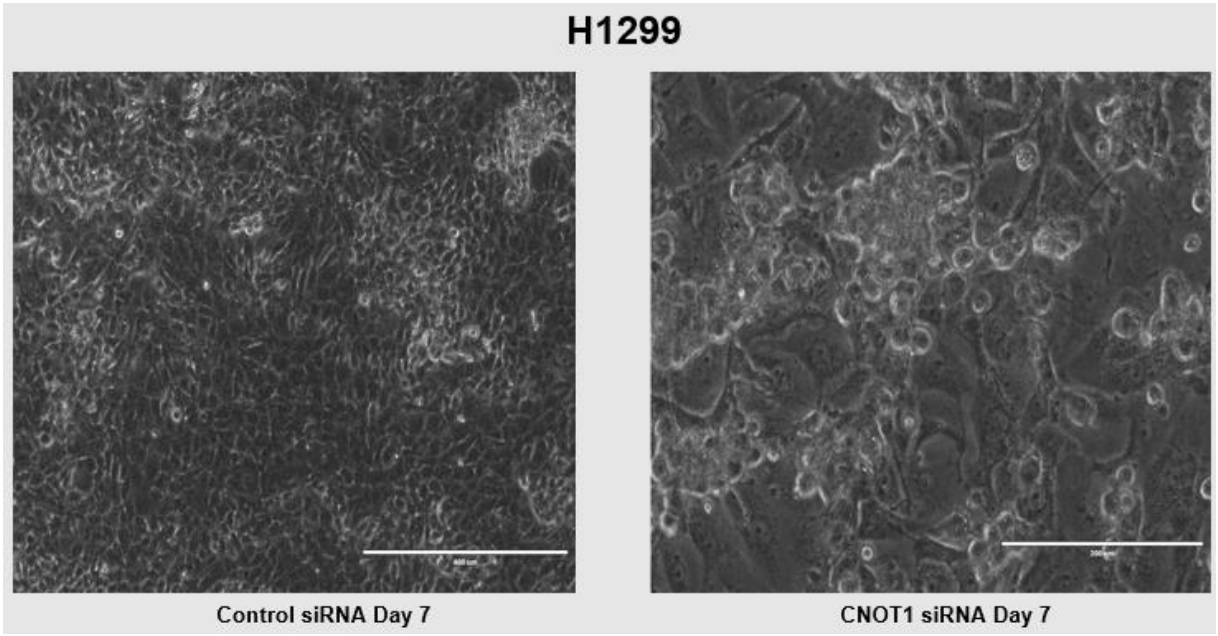

F)

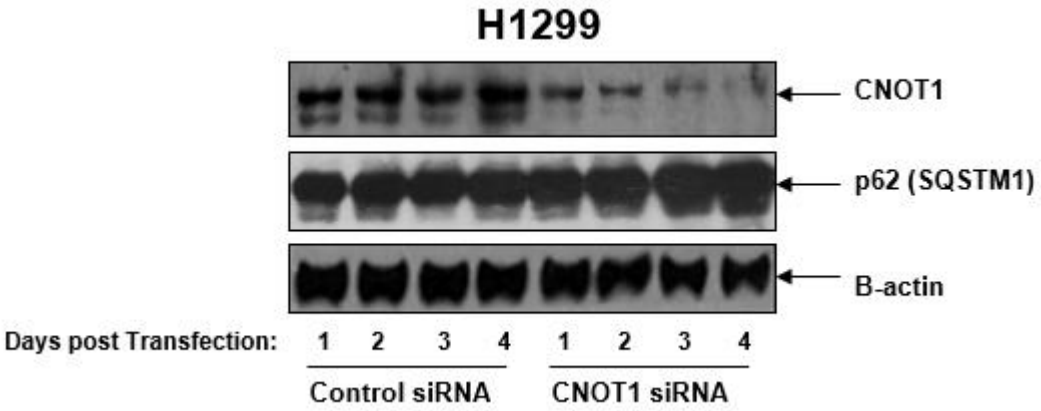

Figure 3.8 Induction of autophagy in CNOT1-depleted HeLa, U2OS and H1299 cells.

A & B) *Representative images compare the cell phenotypes in control HeLa / U2OS cells (left panel) and CNOT1-depleted HeLa / U2OS cells (right panel) 7 days post siRNA transfection. Images were collected using an EVOS fluorescence inverted digital microscope (scale bar of 400 µm).* ***C & D)*** *Representative western blots show expression level of autophagy markers p62 (SQSTM1), LC3Ƃ, p16 between control and CNOT1-depleted HeLa / U2OS cells up to 4 days*

post siRNA depletion. ***E)*** *Representative images compare the cell phenotypes in control (left panel) and CNOT1-depleted H1299 (null-p53) cells (right panel) 7 days post siRNA transfection (scale bar of 400 µm).* ***F)*** *Representative western blot shows expression level of autophagy markers p62 (SQSTM1) between control and CNOT1-depleted H1299 cells up to 4 days post siRNA depletion.*

3.2.8.2 Senescence

It is well known that primary mammalian cells in culture eventually reach a state of 'replicative senescence' where they are metabolically active and still viable but stop dividing. Senescence can also be induced in most cells in response to various forms of stress. Induction of senescence in HeLa cells was confirmed using SA-β-gal staining at 3, 5 and 7 days post CNOT1 siRNA transfection. Based on the results obtained in section 3.2.1 (the knock down efficiency assay) and knowing that induction of senescence without drug administration is not an immediate response, we processed samples from 72 hours post siRNA treatment for both control and CNOT1-depleted HeLa cells. However, we do acknowledge the need of 0 time points for both control and CNOT1-depleted cells for a robust comparison with the later time points. We have shown that at later times, the CNOT1-depleted HeLa cells appeared to senesce (increased senescence-associated β -galactosidase activity) whereas the control; cells did not (Figures 3.9 A & B).

A)

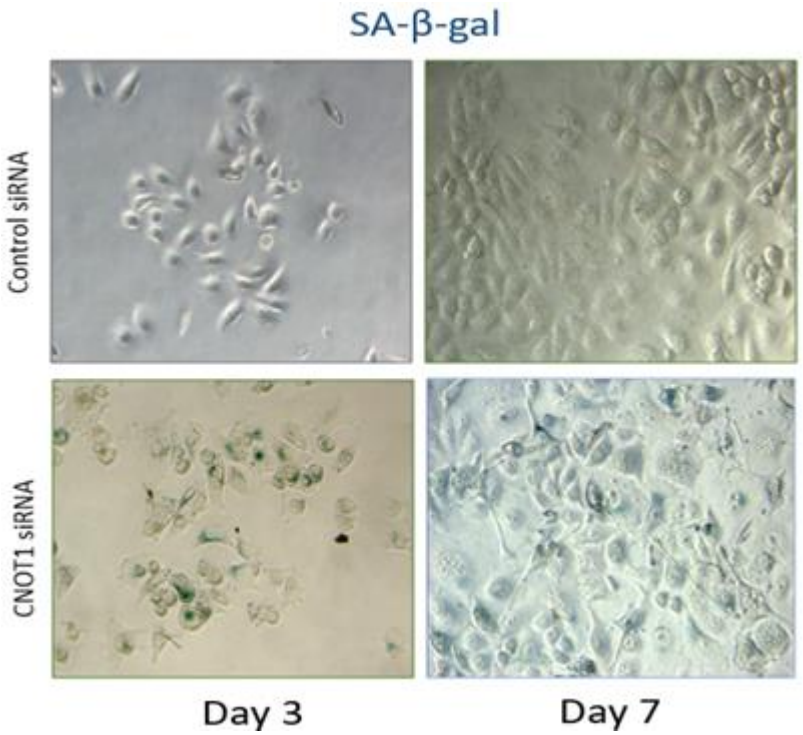
SA-β-gal
Control siRNA
CNOT1 siRNA
Day 3
Day 7

B)

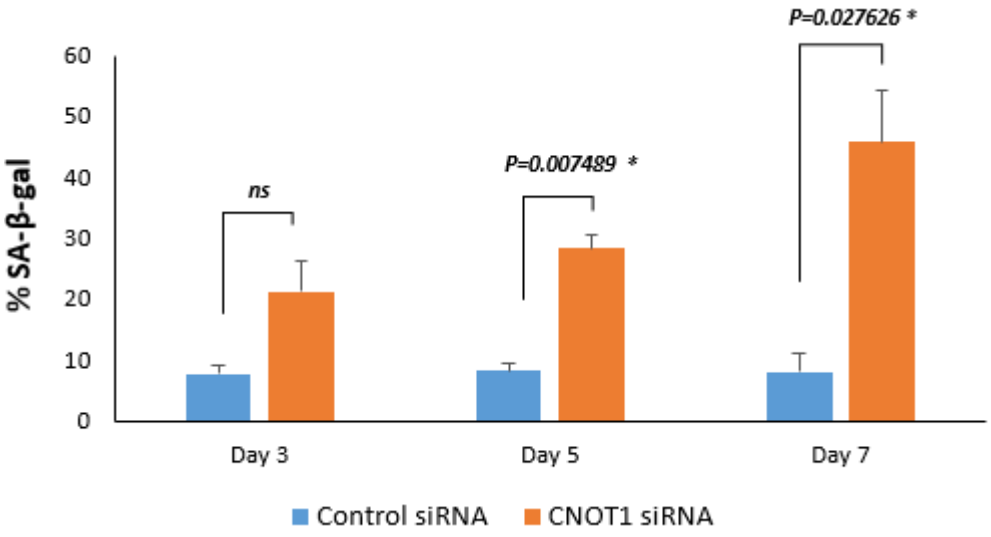
% SA-β-gal
60
50
40
30
20
10
0
ns
P=0.007489 *
P=0.027626 *
Day 3
Day 5
Day 7
Control siRNA
CNOT1 siRNA

Figure 3.9 Induction of senescence in CNOT1-depleted HeLa cells.

A) *Representative images compare the development of SA-β-Gal staining (positive senescent cells) in control HeLa cells (top panel) and CNOT1-depleted HeLa cells (bottom panel) between day 3 (left panel) and day 7(right panel) post siRNA transfection. The blue colour represents senescent cells. Scale bar = 50 µm.* ***B)*** *Representative bar graphs show % SA-β-Gal positive cells in control and CNOT1-depleted cells 3, 5 and 7 days post siRNA depletion (n=3 independent experiments). Statistical analyses were performed using a two-tailed and unpaired Student t test, *P <0.05, **, P<0.01; ***, P<0.001. Error bars represent the StDev.*

3.2.8.3 Apoptosis

As the cells treated with CNOT1 siRNA for a long time (in excess of 6 days) appear to be in 'distress' we considered the possibility that they were undergoing apoptosis. However, no activation of the apoptosis pathway was observed in CNOT1-depleted HeLa cells at least via procaspase-3 activation or PARP1 degradation (Figure 3.10 A). Control HeLa cells treated with cisplatin (10 μg/mL) wereused as a positive apoptotic control. PARP1 cleavage was observed following cisplatin treatment for 24 h, depletion of CNOT1 did not affect PARP cleavage in HeLa cells.

In a further experiment, using CellTiter-Glo Luminescent Cell Viability Assay to measure ATP level as an indication of cell viability we have demonstrated that CNOT1-depleted HeLa cells showed decreased level of cell proliferation (negative slope) (Figure 3.10 B)., consistent with the other data presented here. Depletion of other CNOT components also reduced cell growth but not to the same extent as loss of CNOT1. In addition, we have shown that depletion of CNOT1 significantly reduced the ability of colony formation in CNOT1-depleted cells (0h) 14 days after the plating of cells in the absence of DNA damaging agents (Figures 3.10 C & D).

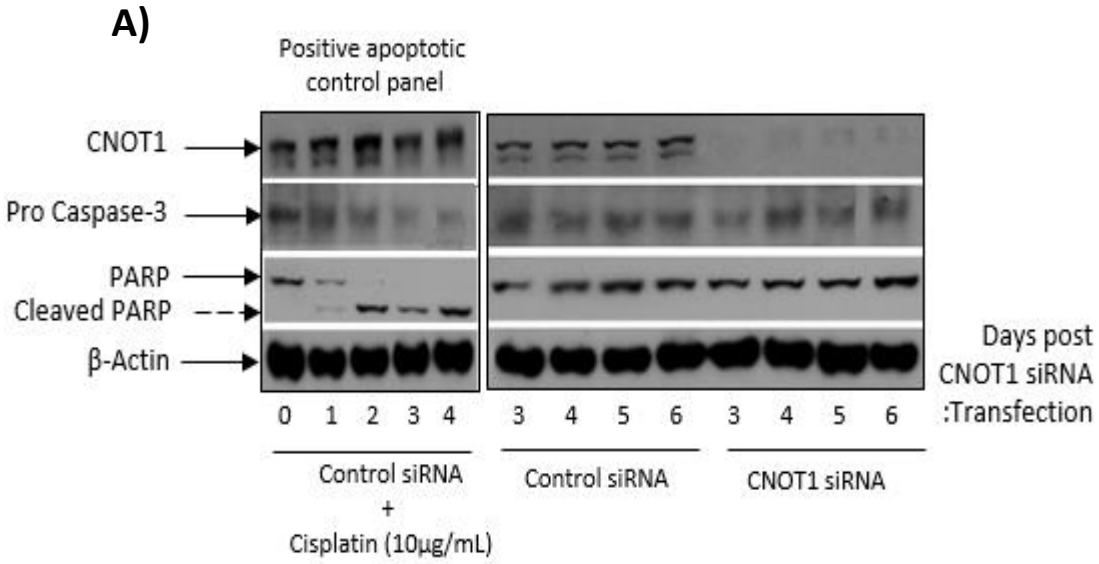
A)
Positive apoptotic control panel
CNOT1
Pro Caspase-3
PARP
Cleaved PARP
β-Actin
0 1 2 3 4
3 4 5 6
3 4 5 6
Days post CNOT1 siRNA :Transfection
Control siRNA + Cisplatin (10µg/mL)
Control siRNA
CNOT1 siRNA

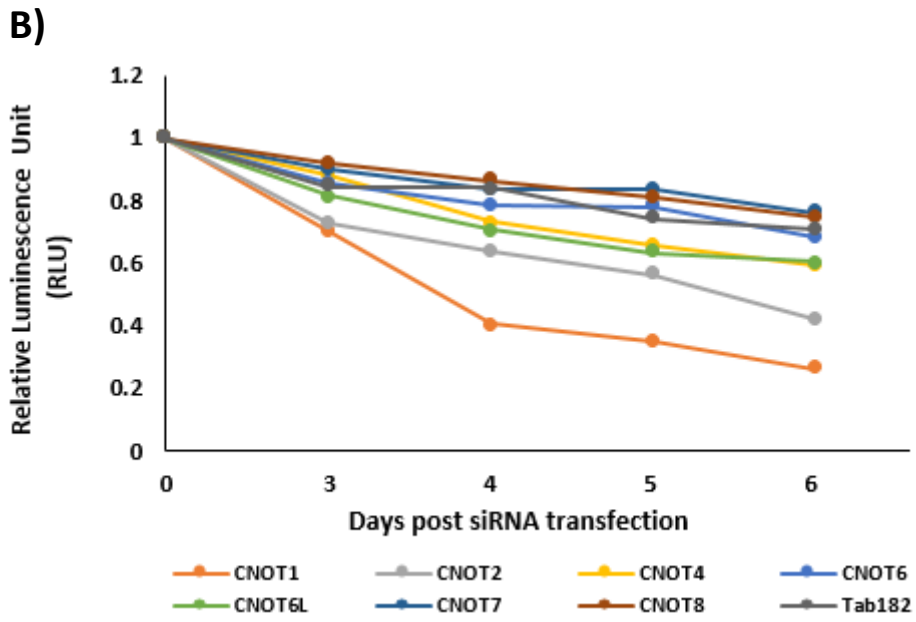
B)
Relative Luminescence Unit (RLU)
1.2
1
0.8
0.6
0.4
0.2
0
0
3
4
5
6
Days post siRNA transfection
CNOT1
CNOT2
CNOT4
CNOT6
CNOT6L
CNOT7
CNOT8
Tab182

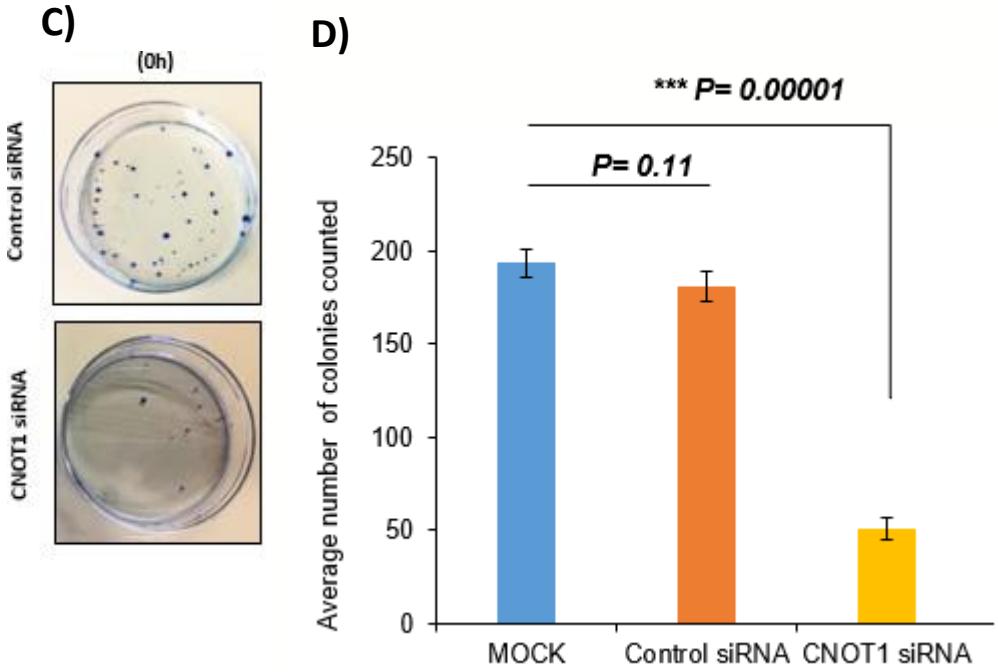

Figure 3.10 Reduced cell proliferation and viability in CNOT1-depleted HeLa cells in the absence of activated apoptosis via procaspase-3 activation or PARP1 degradation.

A) *Representative western blot showing the activation of apoptosis (as judged by the loss of procaspase 3 and degradation of PARP1) between cisplatin (10µg/mL)-treated control HeLa cells and untreated control and CNOT1-depleted HeLa cells.* ***B)*** *The diagram shows the number of viable cells treated with different CNOT subunit siRNAs in culture based on quantitation of the ATP present, an indicator of metabolically active cells. All values (for each siRNA-treated sample) were calculated relative to cells treated with control siRNA at the appropriate time point.* ***C)*** *HeLa cells were plated at appropriate concentration 72 hours post siRNA transfection. At day 14, large colonies were stained with crystal violet and counted (thanks to Dr Katarzyna Leszczynska and Professor Ester Hammond at University of Oxford for doing this experiment for us).* ***D)*** *Representative bar graph shows the plating efficiency of the cells at day 14 after staining with crystal violet and counting (N=3 independent experiments). Statistical analyses were performed using a two-tailed and unpaired Student t test, *P <0.05, **, P<0.01; ***, P<0.001. Error bars represent the StDev.*

3.3 DISCUSSION

Taken together, we have shown that depletion of CNOT1 impairs cell cycle progression beyond the G1/S boundary judged by FACS analysis and western blotting after synchronization of cells in the G2/M phase. The FACS analysis showed the accumulation of a G1 population in CNOT1-depleted HeLa cells, whereas, very few cells were observed in the S and G2/M phases. In further FACS analysis, simultaneous staining of DNA with PI and the mitotic marker, pH3 (Serine 10) allowed us to determine the percentage of cells present in G2 and M phases separately. pH3-positive cells were hardly detected in CNOT1-depleted cells confirming G2/M transition is inhibited. In support of the FACS results, we also assessed the expression level of proteins involved in cell cycle progression following synchronization of cells into the G2/M phase using nocodazol treatment. In line with our FACS analysis, the expression level of cyclins A2 and B1 and pH3 were all downregulated in CNOT1-depleted cells. In contrast, the expression of cyclin E was appreciably higher in CNOT1-depleted cells during G1 and beyond. We have also shown that the expression levels of the CDK inhibitors p21 and p27 were both upregulated in CNOT1-depleted cells, which may explain the G1-cell cycle arrest phenotype. This is further evidence confirming that depletion of CNOT1 disrupts the cell cycle progression beyond G1 phase. Upregulation of p21 and p27 appeared to be independent of p53 as its gene and protein expressions were not affected in CNOT1-depleted cells. Moreover, it is possible that Chk2, independently of p53, was responsible for p21 induction in HeLa cells. It has been previously reported that a novel p53-independent role for Chk2 in p21 induction and senescence may contribute to tumour suppression (Aliouat-Denis, Dendouga et al. 2005). In addition, Phalke *et al*. (2012) have shown that PRMT6 depletion induces the p21 levels by a p53-independent mechanism (Phalke, Mzoughi et al. 2012).

Interestingly, the gene expression of PRMT6 was downregulated in CNOT1-depleted HeLa cells (log2FoldChange= -2.71). It is worth mentioning that the expression of PRMT6 could be affected by G1-cell cycle arrest in CNOT1-depleted cells.

Since the gene expression of p27 was not affected by CNOT1 depletion we assume this upregulation in its protein level was due to increased stability of its mRNA poly (A) tail which was already reported by Morita *et al.* (2007). These authors have shown that depletion of CNOT6L elevates the expression level of p27 protein due to increased stability of its mRNA poly (A) tail when deadenylase activity of CNOT complex is compromised (Morita, Suzuki et al. 2007). Upregulation of both p21 and p27 protein may exert the growth inhibitory effects through the induction of G1 arrest. It is also possible that increased half-life contributes to the additional protein observed.

In addition, depletion of CNOT1 downregulated the expression of those genes involved in cell cycle progression through the S phase and G2/M phase transition. For example; downregulation of genes involved in nucleosome assembly and organization (GO: 0034728) such as histones was observed in CNOT1-depleted cells. Downregulation of chromatin re-modellers which are required during replication to deal with the addition of DNA associated proteins to the newly synthesised DNA can also contribute to decreased S phase progression. Interestingly, (Alabert, Bukowski-Wills et al. 2014) Alabert *et al*. (2014) using the nascent chromatin capture (NCC) technique, have shown that mammalian CNOT1 protein was among 3995 proteins enriched in nascent newly synthesized chromatin (Alabert, Bukowski-Wills et al. 2014). The other important genes, which are responsible for progression through S phase, such as cyclin A, CDK1 and ORC6 were downregulated in CNOT1-depleted HeLa cells. In addition, using the immunofluorescence detection of EdU, we demonstrated that depletion of CNOT1 reduces the S phase indices in HeLa cells.

G2/M cyclin B1 and B2 gene expression was downregulated in CNOT1-depleted HeLa cells. Cell viability assay showed the low level of cellular ATP in CNOT1-depleted cells. In addition, depletion of other CNOT components also reduced cell growth but not to the same extent as loss of CNOT1. We have also demonstrated that depletion of CNOT1 significantly reduced the ability of colony formation in CNOT1-depleted cells 14 days after the plating of cells in the absence of DNA damaging agents. Together these observations confirm the necessity of CNOT1 and the CNOT complex for continued cell viability and proliferation.

Different studies have shown that depletion or mutation of different CNOT subunits contributes to apoptosis, senescence and autophagy (Morita, Suzuki et al. 2007, Ito, Takahashi et al. 2011, Mittal, Aslam et al. 2011, Yamaguchi, Suzuki et al. 2018). In agreement with these studies, we have shown that at later time (day 7), when we expect the effects of siRNA-mediated silencing of CNOT1 to be markedly decreased, CNOT1-depleted HeLa cells appeared to senesce and /or undergo autophagy. Extensive vacuolation that is a common phenotype associated with autophagy, senescence and/or endoplasmic reticulum ER stress was observed in CNOT1-depleted cell. In addition, depletion of CNOT1 caused the marked induction of the autophagy markers p16 and LC3β. Degradation of p62 (SQSTM1) during autophagy is another marker, widely used to monitor autophagic flux. We observed that the protein expression level of p62 gradually accumulated in CNOT1-depleted cells with no change in its gene expression indicating that the degradation of autophagosomes caused by lysosomal acidification was impaired. We confirmed that induction of autophagy is p53-independent using CNOT1-depleted H1299 cells ($p53^{-}$) showing induction of p62 and vacuoles formation at later time points.

We have also shown that at later times, the CNOT1-depleted HeLa cells senesce, as demonstrated by increasing the senescence-associated β -galactosidase activity. We do

acknowledge the need of 0 time points for both control and CNOT1-depleted cells for a robust comparison with the later time points.

No activation of caspase-3 pathway or degradation of PARP1, which are normally taken as diagnostic markers of apoptosis, was not seen in CNOT1-depleted HeLa cells. However, the gene expression of caspase types 1 and 4 were both upregulated in CNOT1-depleted HeLa cells. Ito *et al*. (2011) had shown that the sub G1 apoptotic fraction was increased in CNOT1-depleted HeLa cells. They further showed that CNOT1 depletion increased CHOP mRNA levels and activated caspase-4, which is associated with ER stress-induced apoptosis (Ito, Takahashi et al. 2011). ER stress induces intrinsic apoptosis independent from the DDR in the unfolded protein and is characterized by extensive cytoplasmic vacuolation in cancer cells.

Overall, these results indicate that the CNOT complex is required for progression through S phase and G2/M. In the absence of an active CNOT complex, or at least of CNOT1, cells accumulate in G1 phase, undergo, over time, senescence and probably cell death by autophagy or apoptosis.

CHAPTER FOUR

CNOT1 & DNA REPLICATION STRESS

4 CNOT1 AND DNA REPLICATION STRESS

4.1 INTRODUCTION

The CNOT complex regulates “Transcript Buffering” by controlling the steady-state level of mRNA. On the one hand, it controls the transcription initiation / elongation, and on the other, it regulates the mRNA degradation (Timmers and Tora 2018).

Consistent with this, various studies have described positive and negative roles of the CNOT complex during transcription. The CNOT complex is the negative transcription regulator of TATA-less genes which in human and yeast includes 80% of genes (Anish, Hossain et al. 2009, Yang, Wang et al. 2014). These genes are mostly involved in energy metabolism and the inflammatory response. In fact, the CNOT complex is also the positive transcription regulator of TATA-containing genes, which in human includes 20% of genes. These genes are mostly involved in the cellular stress response.

Results from in vivo protein-DNA cross-linking studies in yeast indicate that the NOT1-NOT5, and Ccr4 subunits associate with the 5′ region of mRNA, reflecting a role for the CNOT complex in transcription initiation (Lee, Wyrick et al. 1998, Badarinarayana, Chiang et al. 2000, Deluen, James et al. 2002, Swanson, Qiu et al. 2003, Kruk, Dutta et al. 2011). It has been shown that the Ccr4 (CNOT6L) protein strongly binds to promoter regions and resides in a large cluster of proteins involved in transcription elongation by RNA Pol II; this may indicate the role of Ccr4 in transcription elongation (Kruk, Dutta et al. 2011, Sohrabi-Jahromi 2019). The ubiquitin E3 ligase NOT4 appears to contribute to transcription elongation by regulation of histone H3 K4 tri-methylation, which positively regulates transcription elongation, through ubiquitin-dependent protein degradation of histone demethylase Jhd2; this results in forward translocation of a stalled RNA Pol II (Reese 2013). This requires the association between the

Rpb4/7 module of the polymerase RNA Pol II and both NOT3 and NOT5 in *Saccharomyces cerevisiae* (Babbarwal, Fu et al. 2014). Stalled RNA Pol II at DNA lesions can be also removed by NOT4-mediated polyubiquitylation and proteasome-dependent degradation of the largest RNA Pol II subunit Rpb1 (Jiang, Wolgast et al. 2019).

NOT1 negatively regulates the transcription of TATA-less promotors such as seen in the *HIS3* gene (Oberholzer and Collart 1999). CNOT1 is a ligand-dependent repressor of estragon ERα-mediated transcription of target genes such *c-Myc* (Winkler, Mulder et al. 2006). Among those proteins involved in controlling major histocompatibility complex class II (MHC-II) transcription and transport, CNOT1 and CNOT2 were identified using a genome-wide RNAi screen (Paul, van den Hoorn et al. 2011). For the first time, Zwartjes et al. (2004) showed that the NOT-Box motif of the CNOT2 and CNOT3 subunits can directly repress the association of the promoter sequence TATA-box with RNA Pol II (Zwartjes, Jayne et al. 2004).

Increased global transcription activity can become a potentially hazardous process promoting replication stress, which would ultimately cause genome instability, a hallmark of cancer cells. Importantly, the link between CNOT1 and cancer has been previously reported by several studies. Gain-of-function mutation of CNOT1 functions as an oncogene in osteosarcoma progression (Cheng, Li et al. 2017). Single nucleotide polymorphisms (SNPs) within the CNOT1 and CNOT6 genes are associated with B-cell paediatric lymphoblastic leukaemia (B-ALL) (Gutierrez-Camino, Lopez-Lopez et al. 2014). In addition, missense mutations, which are dominant mutations in the CNOT1 have been frequently reported in colorectal, melanoma and uterine cancers (cBoPortal & Gene online projects).

In this chapter we first show that depletion of CNOT1 increases global transcription which is a well-known mechanism of oncogene-induced replication stress in cancer (Kotsantis, Silva et al. 2016). We also show that depletion of CNOT1 increases formation of transcription-

dependent R-loop intermediates, which impair the progression of replication forks. We also demonstrate that another source of replication stress in CNOT1-depleted cells is depletion of the dNTP pool as the CNOT complex is required for transcription of RNR genes (Mulder, Winkler et al. 2005). We also show that the level of embedded rNTP into genomic DNA increases in CNOT1-depleted cells following dNTP pool depletion and reduced protein expression of RNase H2A and B. In a recent CRISPR screen of genes whose mutation causes increased PARP inhibitor sensitivity the RNase H2 enzyme complex (RNase H2A, RNase H2B and RNase H2C) and several CNOT genes were identified (Zimmermann, Murina et al. 2018). In another CRISPR screen it was shown that RNase H2 and CNOT complex deficiency is synthetically lethal with ATR both *in vitro* and *in vivo* (Wang, Wang et al. 2018). It is noteworthy that we show that two subunits CNOT1 and Tab182 have physical interaction with ATR and different pre-RC components (MCM2, MCM7 and ORC3). Finally, we show that the deadenylase activity of CNOT complex is compromised when CNOT1 is depleted.

4.2 RESULTS

4.2.1 CNOT1-depleted cells show increased transcription activity

The effect of CNOT1 depletion on transcription activity was assessed by quantifying the level of RNA-specific labelled nucleoside 5-ethynyl uridine (EU) incorporated into nascent RNA (Figure 4.1.A). RNA synthesis (EU incorporation) was elevated 48 hours post CNOT1 depletion and was slightly decreased on day 3 and increased further on day 4; this incorporation was significantly greater than the level seen in control cells (Figure 4.1.B). Increased level of transcription activity in CNOT1-depleted cells was also indicated by western blotting results showing increased expression level of TATA-binding protein (TBP) and phospho-RNA Poll (C-terminus) at serine 5 compared to the control cells (Figure 4.1.C).

A)

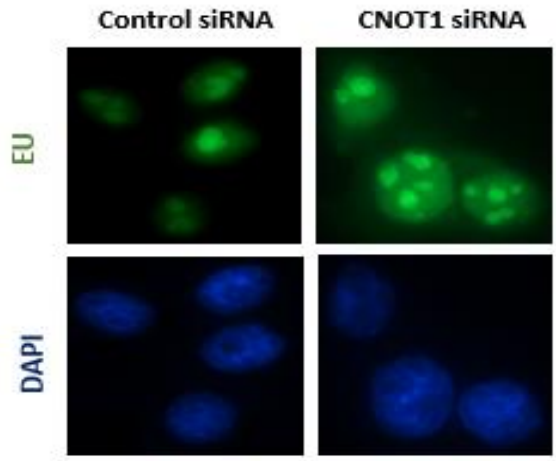
Control siRNA
CNOT1 siRNA
EU
DAPI

B)

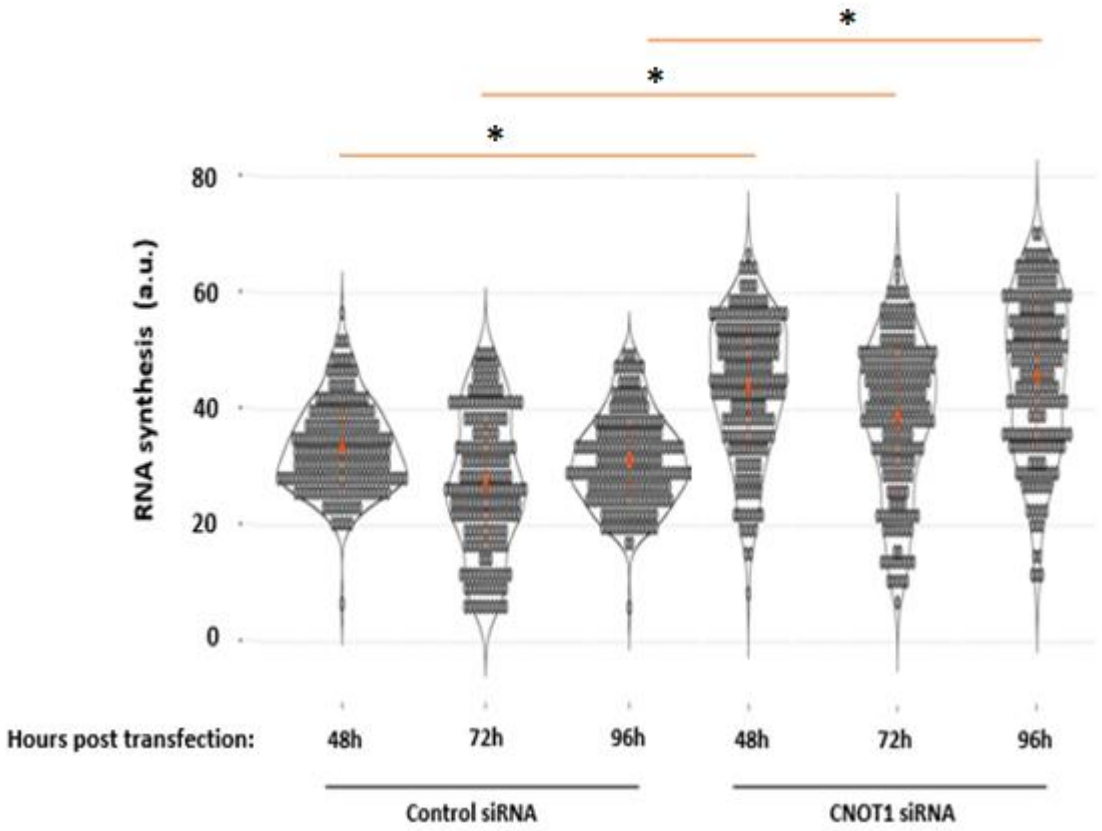
*
*
*
RNA synthesis (a.u.)
80
60
40
20
0
Hours post transfection:
48h
72h
96h
48h
72h
96h
Control siRNA
CNOT1 siRNA

C)

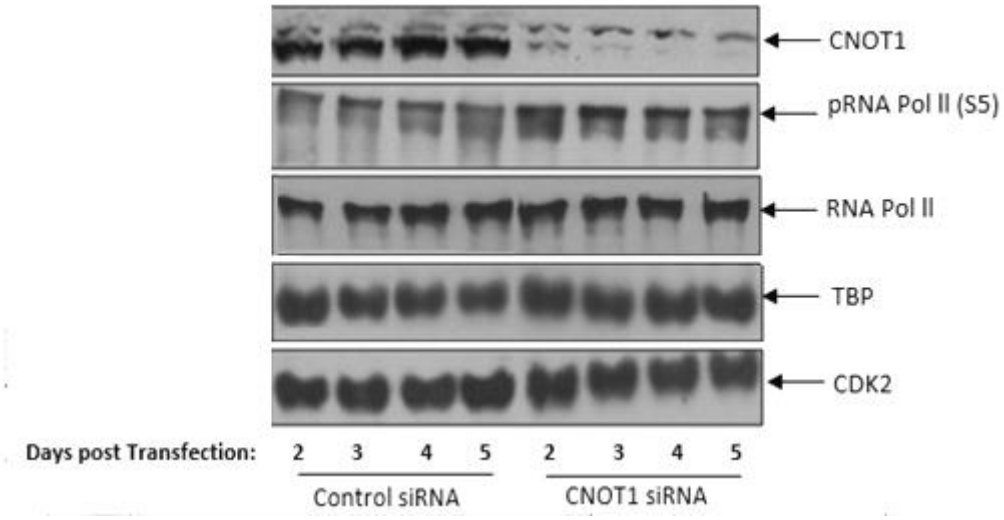

Figure 4.1 CNOT1 depletion increases transcription

A) *HeLa cells were depleted with CNOT1 siRNA or control siRNA. Transcription elongation was measured after EU incorporation (1 hour) shown after 48, 72 and 92 hours.* ***B)*** *To quantitate EU incorporation, Hoechst was used to stain the nucleus of cells, generating a nuclear mask. Then Adobe Photoshop was used to adjust the levels of all panels equally. Quantification of EU signal per nucleus was performed by RStudio statistical software and shown (n=3 independent experiments, Stats: Mann-Whitney Wilcoxon Rank Sum).* ***C)*** *Representative western blot shows the expression level of TBP and the phosphorylation of RNA Poll (S5) in each experimental condition. CDK2 was used as a loading control.*

4.2.2 Depletion of CNOT1 induces replication stress through ongoing transcription

To test the hypothesis that an increase in transcription level observed in CNOT1-depleted cells may underlie replication stress in CNOT1-depleted cells, RNA synthesis was inhibited using 100 μM DRB (100 minutes). DRB inhibits RNA polymerase II elongation by inhibition of CDK-activating kinase associated with the general transcription factor TFIIH (Yankulov, Yamashita et al. 1995). Treatment with DRB significantly reduced the nuclear EU intensity in both control and CNOT1-depleted cells, consistent with decreased level of RNA synthesis (Figure 4.2.A & B). In a further experiment, we went on to investigate the effect of CNOT1 depletion on DNA replication directly. Using DNA fibre analysis, as described in section 2.2.7 and 2.4.6, we examined DNA replication fork speeds in the absence of CNOT1. Depletion of CNOT1 was seen to reduce fork speeds appreciably (Figure 4.2.C). However, DRB treatment increased replication fork speeds specifically in CNOT1-depleted cells (Figure 4.2.C). Similarly, treatment with PHA-767491 (CDC7/CDK9 inhibitor) which is a dual replication and transcription inhibitor significantly rescued replication fork progression, presumably by reduction in replication initiation or transcription elongation by inhibition of CDC7 or CDK9, respectively, in CNOT1-depleted cells (Figure 4.2.D). These data suggest that replication stress in CNOT1-depleted cells is associated with increased active RNA synthesis.

A)

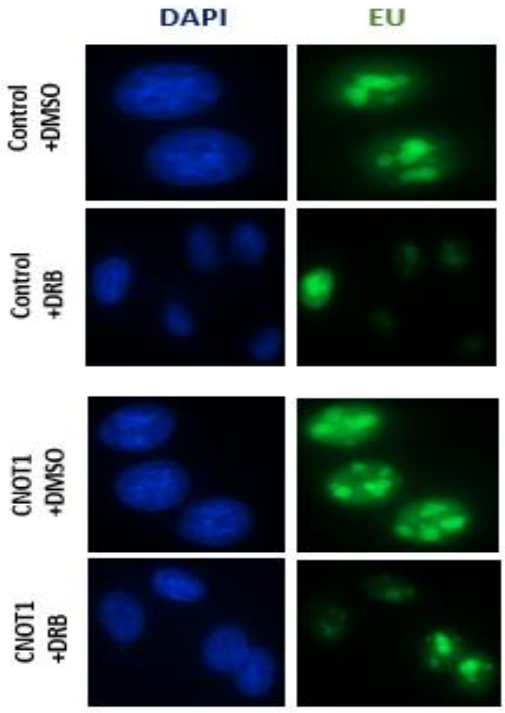
DAPI
EU
Control +DMSO
Control +DRB
CNOT1 +DMSO
CNOT1 +DRB

B)

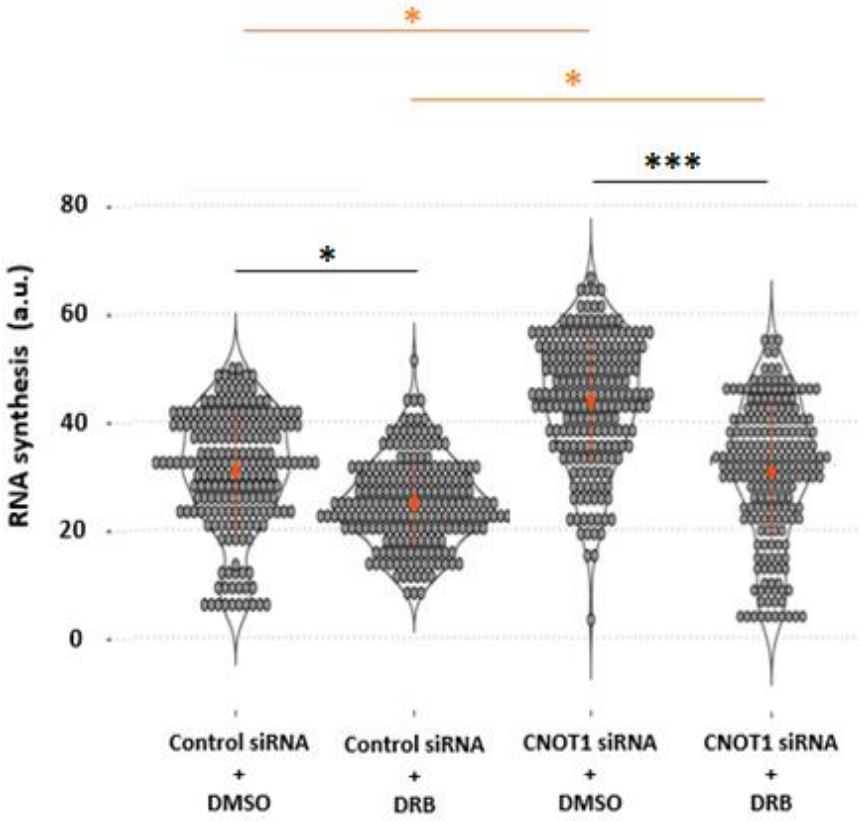
*
*
***
*
RNA synthesis (a.u.)
80
60
40
20
0
Control siRNA + DMSO
Control siRNA + DRB
CNOT1 siRNA + DMSO
CNOT1 siRNA + DRB

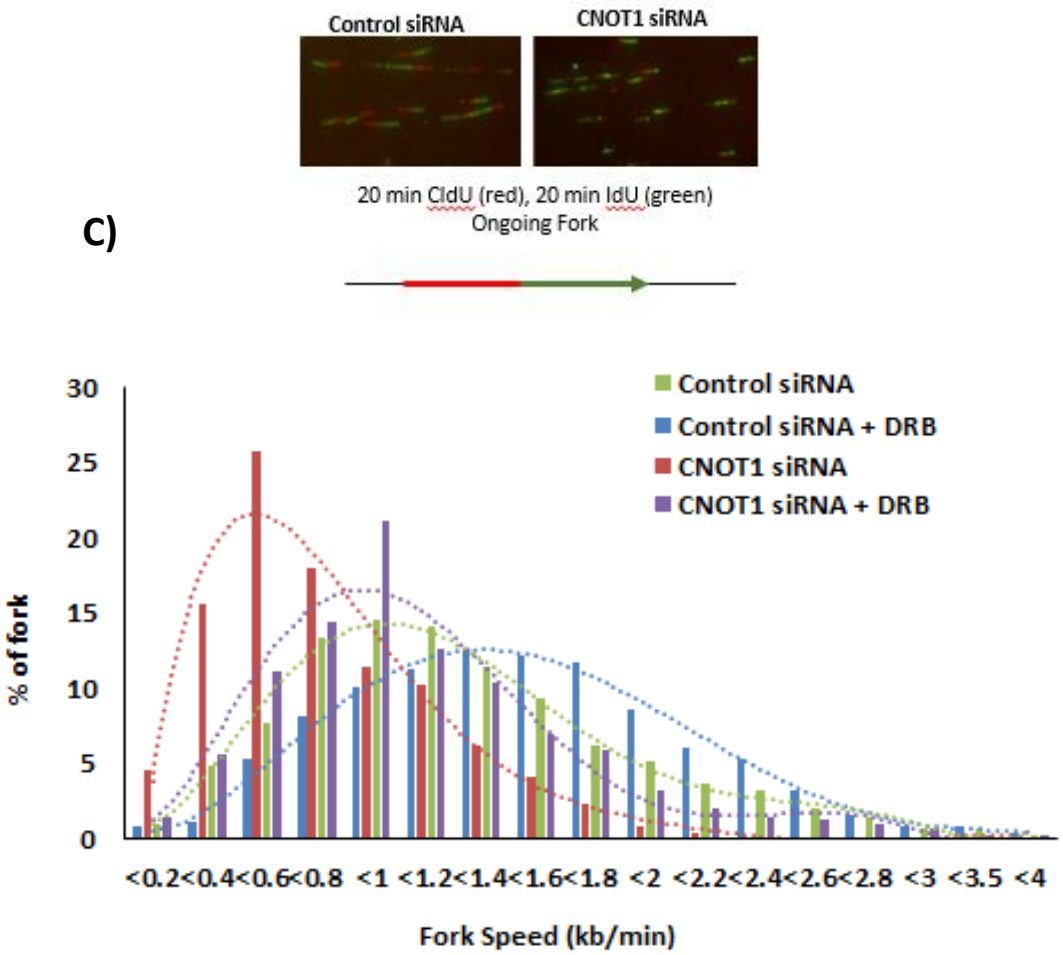
Control siRNA
CNOT1 siRNA
20 min CldU (red), 20 min IdU (green)
Ongoing Fork
C)
Control siRNA
Control siRNA + DRB
CNOT1 siRNA
CNOT1 siRNA + DRB
% of fork
30
25
20
15
10
5
0
<0.2 <0.4 <0.6 <0.8 <1 <1.2 <1.4 <1.6 <1.8 <2 <2.2 <2.4 <2.6 <2.8 <3 <3.5 <4
Fork Speed (kb/min)

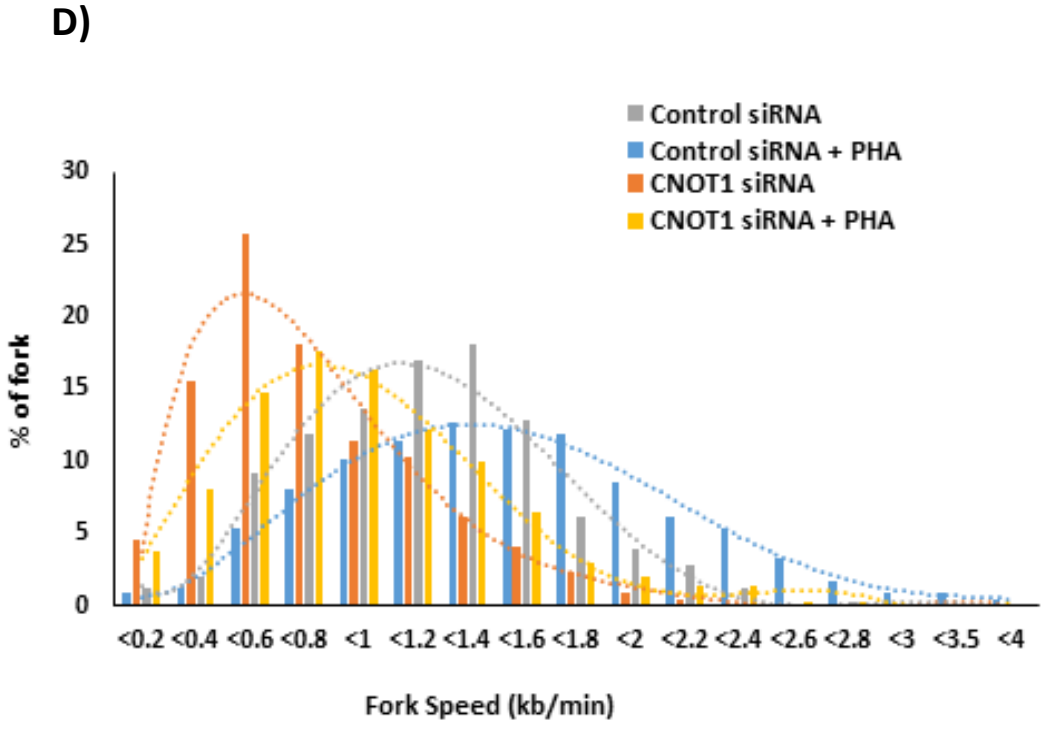
D)
Control siRNA
Control siRNA + PHA
CNOT1 siRNA
CNOT1 siRNA + PHA
% of fork
30
25
20
15
10
5
0
<0.2 <0.4 <0.6 <0.8 <1 <1.2 <1.4 <1.6 <1.8 <2 <2.2 <2.4 <2.6 <2.8 <3 <3.5 <4
Fork Speed (kb/min)

Figure 4.2 CNOT1-induced replication stress is promoted by ongoing transcription

A) *Inhibition of RNA synthesis with DRB in CNOT1 depleted HeLa cells. Cells were treated with CNOT1 or control siRNA. On days 2, 3 and 4 cells were exposed to DRB or the solvent DMSO for 100 min during EU labelling.* ***B)*** *Quantification of EU signal per nucleus treated with transcription inhibitor DRB was performed by RStudio statistical software and shown (n=3 independent experiments). Stats: Mann-Whitney Wilcoxon Rank Sum.* ***C)*** *Distribution of replication fork speeds 72 h after CNOT1 depletion; cells were treated with transcription inhibitor DRB (450 replication forks from 3 independent experiments).* ***D)*** *Distribution of replication fork speeds 72 h after CNOT1 depletion in HeLa cells treated with 10 µM pha-767491 for 1 h (450 replication forks from 3 independent experiments). The lengths obtained in Image J were converted into micrometres using the scale bars on the microscope.*

4.2.3 Depletion of CNOT1 causes replication stress through R-loop formation in HeLa cells

Transcription may affect genome integrity if co-transcriptional products such as RNA-DNA hybrids (R-loops) are not efficiently removed behind RNA polymerase II (Skourti-Stathaki and Proudfoot 2014). Therefore, we investigated whether elevated transcription activity in CNOT1-depleted cells leads to increased R-loop formation; to examine this slot blot analysis of gDNA isolated from control and CNOT1-depleted Hela cells was performed. Samples were generated as described in Chapter 2 (section 2.5.5) and nitrocellulose membranes from the slot blot were incubated with S9.6 antibody, which detects the RNA-DNA hybrid, or antibody against single stranded DNA (ssDNA). R-loops were significantly enriched in CNOT1 depleted cells compared to the control cells. The S9.6 signal was diminished by pre-treatment of gDNA with RNase H1 enzyme for 2 hours, demonstrating that the signal derived from RNA (Figure 4.3.A).

In more detailed investigations, we examined the expression levels of proteins known to be involved in R-loop resolution, such as RNase H1, RNase H2A or B, Senataxin (SETX) and TOP I (Sollier, Stork et al. 2014). If any of these enzymes fails to operate properly, R-loops may persist and accumulate behind the transcription machinery and cause DSBs and genome instability (Sollier, Stork et al. 2014).Immunoblotting of control and CNOT1-depleted cells showed no difference in RNase H1 expression between two experimental conditions; however, there was a noticeable downregulation of RNase H2A in CNOT1 knocked down cells. TOP I and SETX protein, which are also involved in R-loop removal, were upregulated, presumably to deal with the increased level of R-loops in CNOT1-depleted cells (Figure 4.3.B). In a further experiment, the intensity of nuclear S9.6 signal was quantified by confocal microscopy. Cells were co-labelled with S9.6 antibody and an antibody against the nucleolar

protein nucleolin (NCL). The S9.6 signal was decreased after transfection of RNase H1 cDNA for 24 hours. The ability of endogenous RNase H1 enzyme to remove R-loops from gDNA appeared to be somewhat more efficient than the transiently transfected recombinant RNase H1 (Figure 4.3.C and D). This could be due to the presence of RNase H-resistant hybrids or incomplete nuclease activity in the nucleolus, which is rich in DNA-RNA hybrids. It is also very likely that transfection efficiency of the construct was less than 100% (transfection efficiency of 20-25%). To investigate the contribution of R-loops to replication fork slowing in CNOT1-depleted cells, recombinant RNase H1-GFP was transfected into CNOT1-depleted and control cells. RNase H1-GFP did not have a significant effect on replication initiation (Figure 4.3.E), although it rescued the replication fork progress in CNOT1-depleted cells to a limited extent, but not in control cells. This observation supports the suggestion that replication stress in CNOT1 depleted cells is promoted by increased R-loop formation following increased RNA synthesis (Figure 4.3.F).

A)

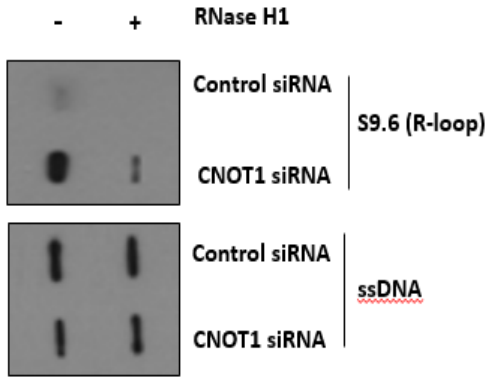
- +
RNase H1
Control siRNA
CNOT1 siRNA
S9.6 (R-loop)
Control siRNA
CNOT1 siRNA
ssDNA

B)

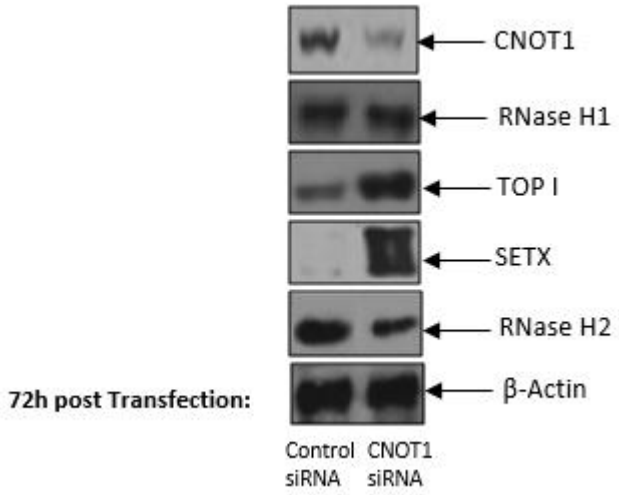
CNOT1
RNase H1
TOP I
SETX
RNase H2
β-Actin
72h post Transfection:
Control siRNA
CNOT1 siRNA

C)

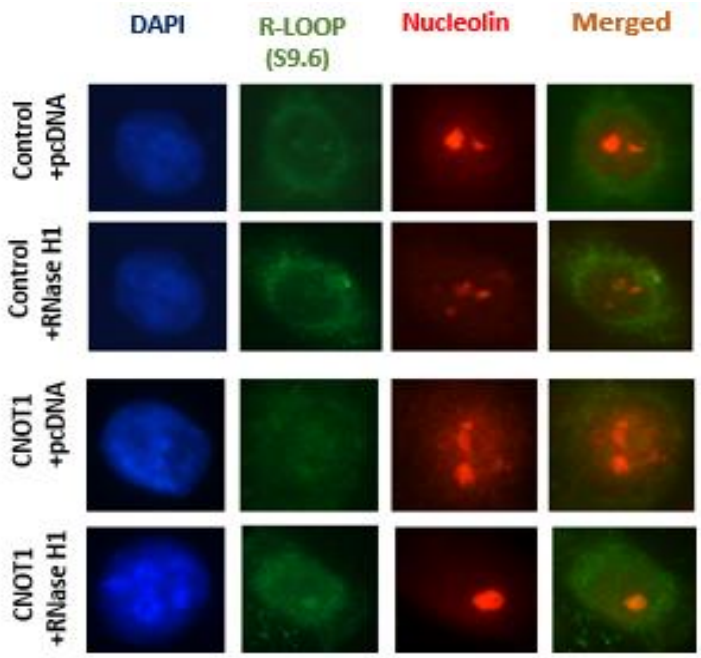
DAPI
R-LOOP (S9.6)
Nucleolin
Merged
Control +pcDNA
Control +RNase H1
CNOT1 +pcDNA
CNOT1 +RNase H1

D)

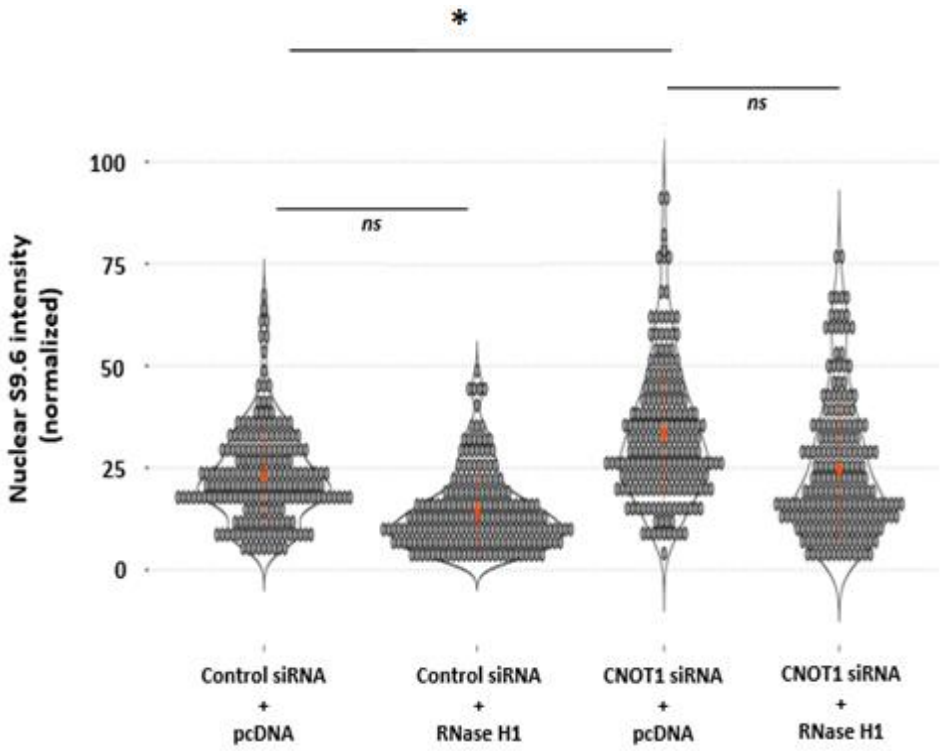
*
ns
ns
Nuclear S9.6 intensity (normalized)
100
75
50
25
0
Control siRNA + pcDNA
Control siRNA + RNase H1
CNOT1 siRNA + pcDNA
CNOT1 siRNA + RNase H1

E)

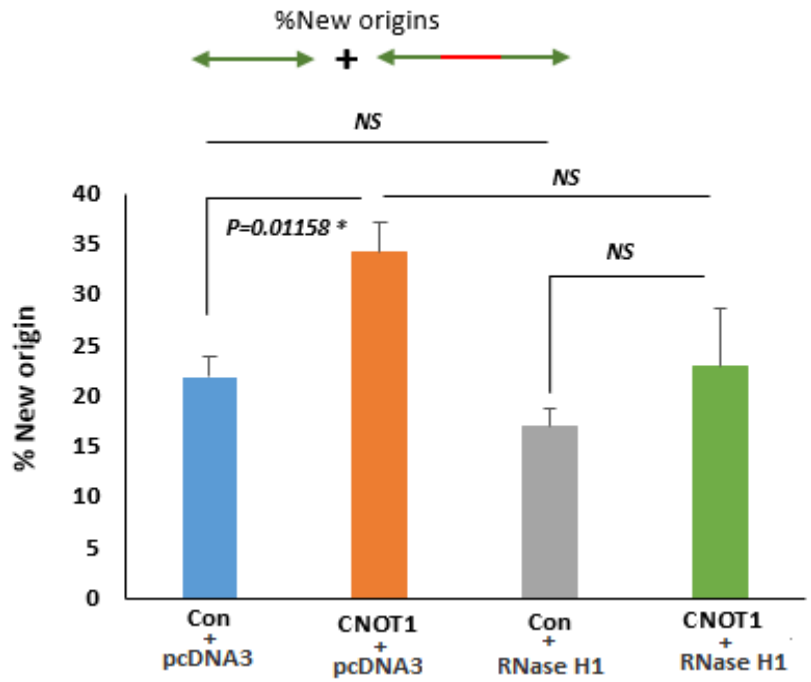
%New origins
+
NS
NS
P=0.01158 *
NS
% New origin
40
35
30
25
20
15
10
5
0
Con + pcDNA3
CNOT1 + pcDNA3
Con + RNase H1
CNOT1 + RNase H1

F)

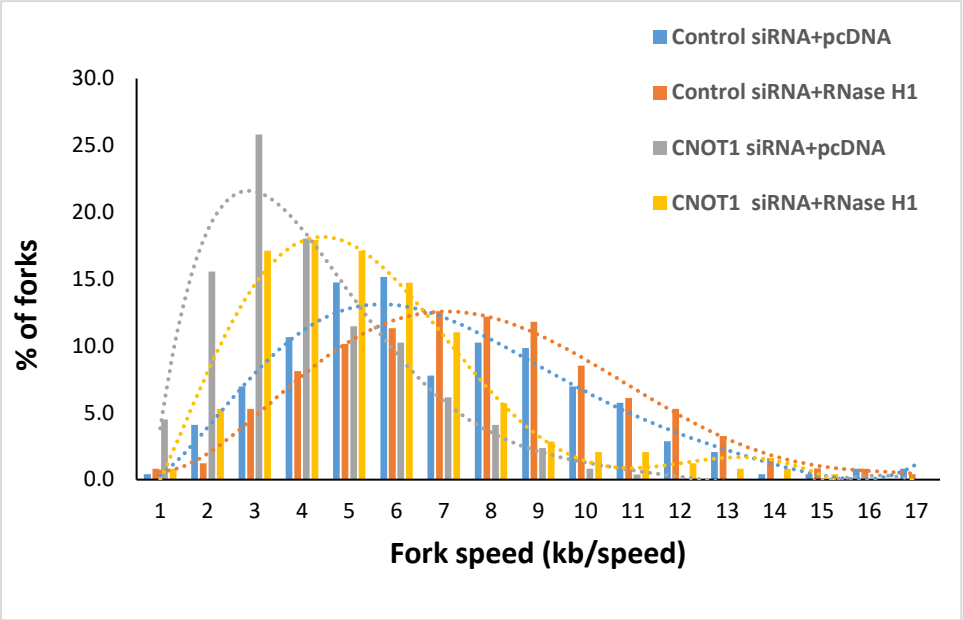

Figure 4.3 CNOT1-depleted HeLa cells have increased R-loop accumulation

A) *Detection of RNA-DNA hybrids using slot blot and S9.6 antibody on gDNA isolated from HeLa cells 72 hours post CNOT1 depletion. A ssDNA antibody was used as a loading control (lower panel).* ***B)*** *Representative immunoblot shows the expression level of RNase H1, RNase H2A, TOP I and SETX in each experimental condition. β-Actin was used as a loading control.* ***C)*** *Co-immunostaining of HeLa cells with S9.6 (green) and nucleolin (red) antibodies 72 hours post siRNA transfection and 24 hours after recombinant RNase H1 transfection. The nuclear DNA was stained with DAPI.* ***D)*** *Quantification of S9.6 antibody signal per nucleus after subtraction of nucleolar staining using Image J. Statistical analysis was performed using RStudio statistical software. (n=3 independent experiments, Stats: Mann-Whitney Wilcoxon Rank Sum).* ***E)*** *Representative bar graph shows the percentage of new origins during DNA fibre labelling 72 hours post CNOT1 depletion and 24 h post transfection with pCMV6-AC-RNase H1-GFP or pcDNA 3.1 (450 replication forks from three independent experiments).* ***F)*** *Distribution of replication fork speeds 24 h post transfection with pCMV6-AC-RNase H1-GFP or pcDNA 3.1 following 72 h CNOT1 depletion (450 replication forks from two independent experiments. The lengths obtained in Image J were converted into micrometres using the scale bars on the microscope.*

4.2.4 Depletion of CNOT1 causes replication stress by an increase in embedded rNTP into genomic DNA following dNTP pool reduction

Knowing that the CNOT complex is required for transcription of RNR genes (Mulder, Winkler et al. 2005) and depletion of the dNTP pool impairs discrimination between rNTP and dNTP by DNA polymerases during DNA replication (McElhinny, Watts et al. 2010), we first confirmed that the protein expression level of catalytic subunit RRM2 and non-catalytic subunit p53R2 is downregulated in CNOT1-depleted cells (Figure 4.4.A). This downregulation was also seen at the gene expression level of RRM2 confirmed by RNA-Seq results (log2FoldChange= -0.79974). Treatment with the RNR inhibitor, HU slightly reduced the ability of CNOT1-depleted HeLa cells in colony formation, 14 days post siRNA transfection (Figure 4.4.B).

Next, we speculated that the level of mis-incorporated ribonucleotides into gDNA is increased in CNOT1 depleted cells. To investigate this, the sensitivity of gDNA to alkaline hydrolysis was examined as the presence of ribonucleotides in gDNA increases its susceptibility to hydrolysis at high pH. For this, sufficient volume of each DNA sample was treated with 0.3 M NaOH for 2 hours at 55°C and fractionated on a 1% alkaline agarose gel. Genomic DNA isolated from CNOT1-depleted cells displayed markedly increased sensitivity to alkaline hydrolysis and migrated faster compared to that from control cells (the DNA peak was shifted from left to right as seen in the densitometric intensity distribution), suggesting a high level of ribonucleotide embedded in gDNA in CNOT1-depleted cells (Figure 4.4.C and D). Besides, we observed downregulation of proteins which are involved in the enzymatic removal of mis-incorporated ribonucleotides into gDNA (RNase H2A and B) in CNOT1-depleted cells (Figure 4.4.E)

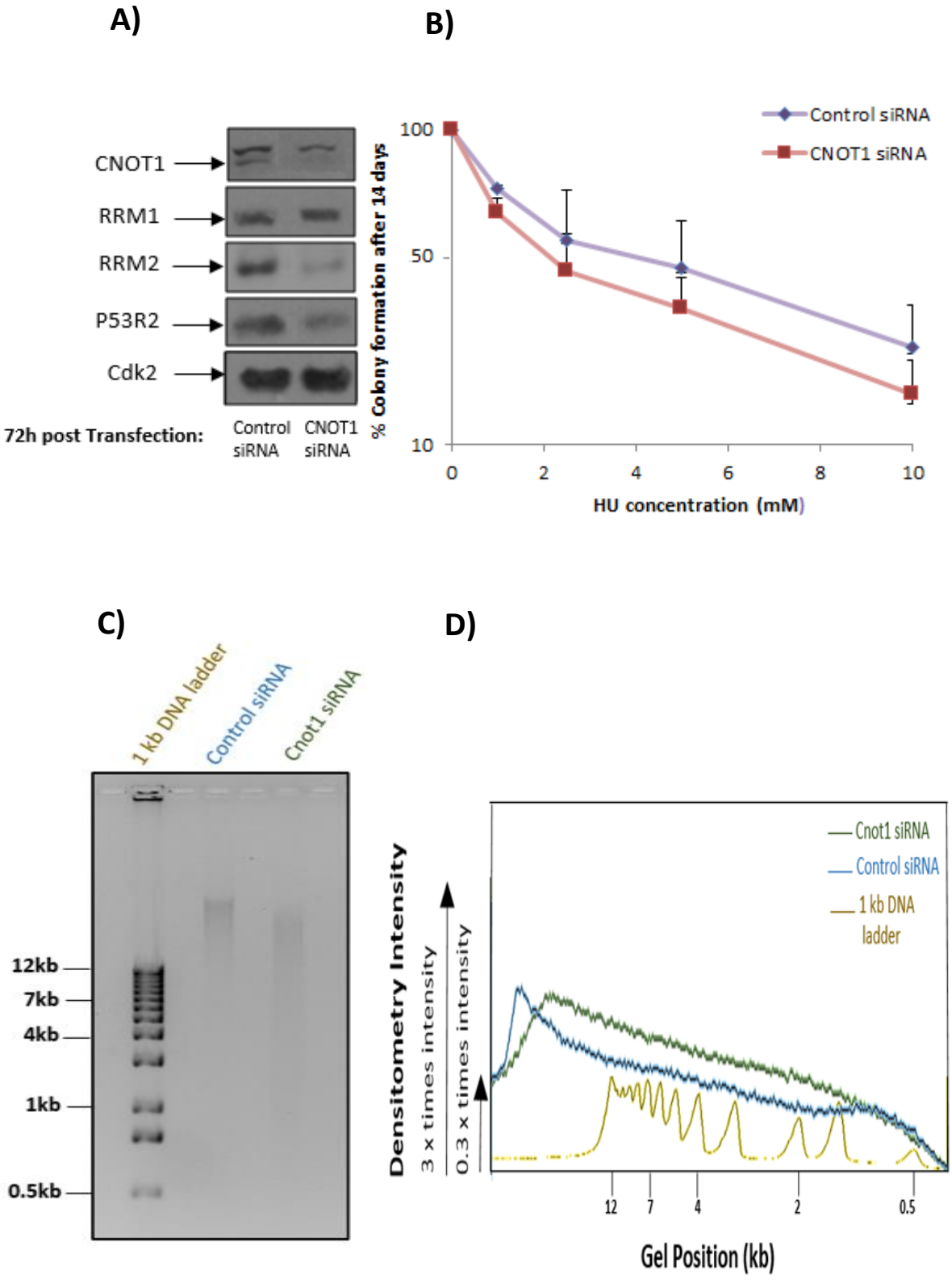
A)
B)
CNOT1
RRM1
RRM2
P53R2
Cdk2
72h post Transfection:
Control siRNA
CNOT1 siRNA
% Colony formation after 14 days
100
50
10
0
2
4
6
8
10
HU concentration (mM)
Control siRNA
CNOT1 siRNA
C)
D)
1 kb DNA ladder
Control siRNA
Cnot1 siRNA
12kb
7kb
4kb
1kb
0.5kb
Densitometry Intensity
3 x times intensity
0.3 x times intensity
Cnot1 siRNA
Control siRNA
1 kb DNA ladder
12
7
4
2
0.5
Gel Position (kb)

E)

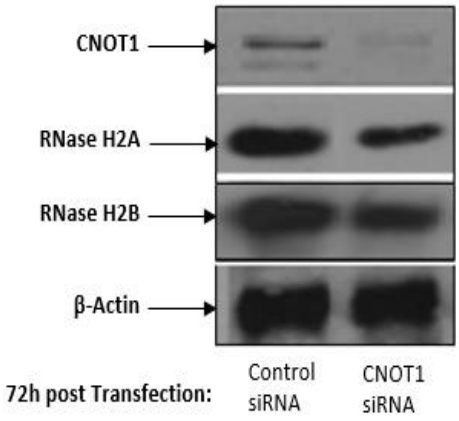

Figure 4.4 CNOT1-depleted HeLa cells show increased embedded ribonucleotide in genomic DNA

A) *Western blot analysis of RNR subunits RRM1/2 and p53R2 in control and CNOT1-depleted cells 72 hours post siRNA transfection. CDK2 was used as a loading control.* ***B)*** *Cells were plated at appropriate concentration 72 hours post siRNA transfection and then exposed to different concentrations of HU (mM). At day 14, large colonies were stained with crystal violet and counted. Clonogenic survival was expressed as a surviving fraction of non-treated controls for each condition and was plotted on a semi-logarithmic scale. Representative graphs were plotted from 3 independent experiments. Statistical analyses were performed using a two-tailed and unpaired Student t test, *P <0.05; **, P<0.01. Error bars represent the SEM.* ***C)*** *Representative 1% alkaline agarose gel of NaOH-treated nucleic acids from control and CNOT1-depleted cells.* ***D)*** *The quantitative estimation of ribonucleotide level from the gel shown in "**C**" using the distribution of DNA densitometry intensity analysis. The intensity of DNA ladder bands shown is decreased by 1/3 and the intensity of the gDNA bands is increased three-fold to make a more obvious comparison.* ***E)*** *Western blot analysis of RNase H2A and B in control and CNOT1-depleted Hela cells 72 hours post siRNA transfection. β-Actin was used as a loading control*

4.2.5 The CNOT complex may function in origin firing

Continuing our investigation of a role for CNOT1 in DNA replication, DNA fibre analysis was performed, and replication structures analysed in siRNA treated cells. CNOT1 depleted HeLa cells showed increased stalling of forks together with an increase in first label origin and a decrease in second label origins (Figure 4.5.A). To gain further insight into the role of the CNOT1 and/or the CNOT complex in DNA replication, a series of co-immunoprecipitation (CIP) assays was conducted with a panel of pre-replication complex (pre-RC) antibodies (MCM2, MCM7 and ORC3). The CIP assays were carried out using HeLa cell lysates, prepared as described in chapter 2 (section 2.4.3) and revealed that MCM2, MCM7 and ORC3 associated with CNOT1 and TAB182 suggesting that the CNOT complex may interact with the pre-RC at DNA replication origins (Figure 4.5.B,C & D). The difference between the amounts of target protein immunoprecipitated with the TAB182 and CNOT1 antibodies is probably a reflection of a much higher titre in the former compared to the latter. Cellular levels of MCM proteins 2, 3, 7 and CDC7 were similar in control and CNOT1-depleted cells 72 hours post siRNA depletion (Figure 4.5.E).

A)

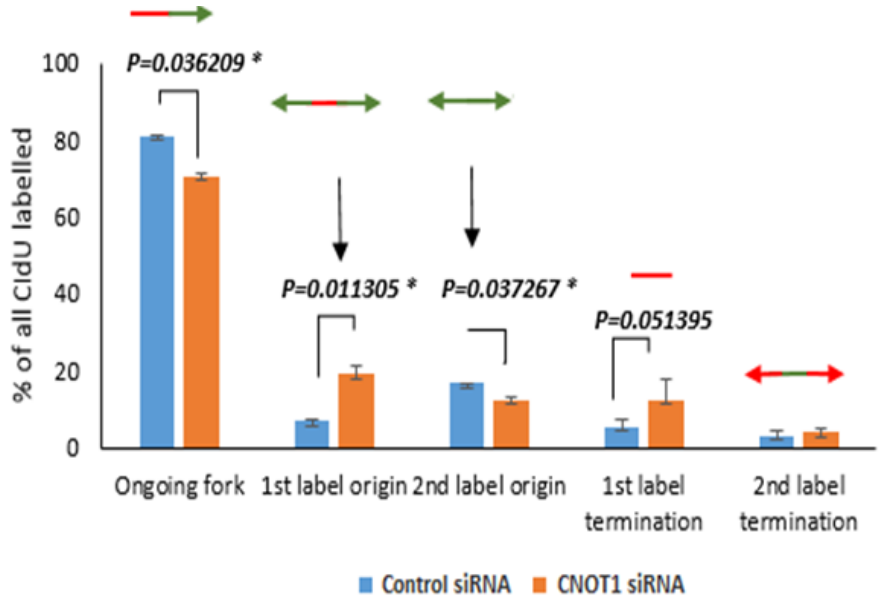
100
80
60
40
20
0
% of all CldU labelled
P=0.036209 *
P=0.011305 *
P=0.037267 *
P=0.051395
Ongoing fork
1st label origin
2nd label origin
1st label termination
2nd label termination
Control siRNA
CNOT1 siRNA

B)

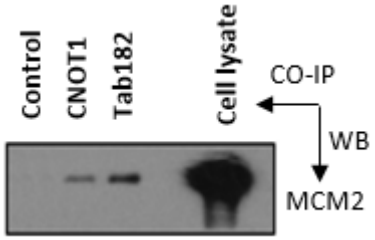
Control
CNOT1
Tab182
Cell lysate
CO-IP
WB
MCM2

C)

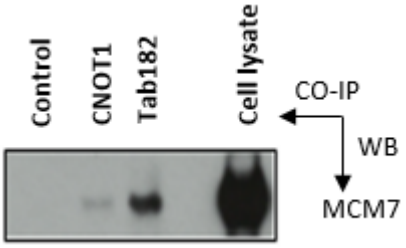
Control
CNOT1
Tab182
Cell lysate
CO-IP
WB
MCM7

D)

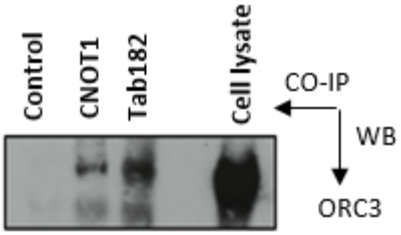
Control
CNOT1
Tab182
Cell lysate
CO-IP
WB
ORC3

E)

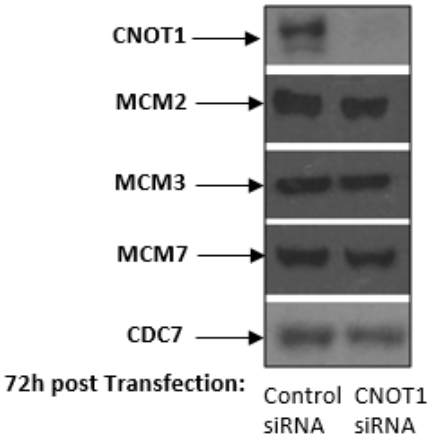
CNOT1
MCM2
MCM3
MCM7
CDC7
72h post Transfection:
Control siRNA
CNOT1 siRNA

Figure 4.5 The CNOT complex regulates replication initiation in Hela cells

DNA fibre labelling was carried out in HeLa cells 72 hours post siRNA transfection. ***A)*** *Representative bar graph of DNA fibre structures 72 h after CNOT1 depletion. (450 replication forks from 3 independent experiments, mean ± SD, *p < 0.05, **p < 0.01 and ***p < 0.001).* ***B, C & D)*** *The CIP assays were conducted using HeLa cell lysates incubated with either CNOT1 or TAB182 or irrelevant antibody (control) overnight. Antibody-bound protein complexes were collected on protein G-agarose beads. The immune-complexes were then fractionated by SDS-PAGE, and western blotting was performed using MCMs 2, 7 and ORC3 antibodies.* ***F)*** *Levels of the indicated MCM proteins 2, 3, 7 and CDC7 were determined by immunoblotting of total HeLa cell extracts 72 h post transfection with control or CNOT1 siRNA.*

4.2.6 CNOT1-depleted cells show reduced deadenylase activity

To ascertain whether the deadenylase activity of the CNOT complex was reduced by depletion of CNOT1, a simple deadenylase assay was performed. 5'-fluorescein-labeled RNA substrate was incubated with equal amounts of whole cell lysates of control and CNOT1-depleted cells for 10, 30, 60 and 120 minutes at 37°C. The reaction was stopped by addition of RNA loading buffer and heating for 3 minutes at 85°C. Aliquots of the assay mixtures were fractionated on 20% polyacrylamide gel in the presence of 8M urea. The data presented suggests that depletion of CNOT1 noticeably decreased the level of deadenylase activity of the CNOT complex compared to the control (Figure 4.6.A, B & C). The deadenylase activity of CNOT7-depleted cells was also measured as a positive control. Surprisingly, depletion of deadenylase subunit CNOT7 increased the level of deadenylated ribonucleotides even greater than the one observed in control, suggesting that other deadenylase subunits catalyze deadenylation in HeLa cells (Figure 4.6.D & E). For instance, Lau *et al*. (2009) reported, in mammalian cells, that the complex contains either CNOT7 or CNOT8 (not both as in yeast), suggesting they compete for binding to CNOT1 (Lau, Kolkman et al. 2009). Depletion of Tab182 did not affect the deadenylase activity of the CNOT complex (Figure 4.6.F & G). The overall reduction in deadenylase activity in HeLa cells following depletion of CNOT1 was also confirmed by RNA-Seq results and GO Enrichr tool (section3.2.7).

A)

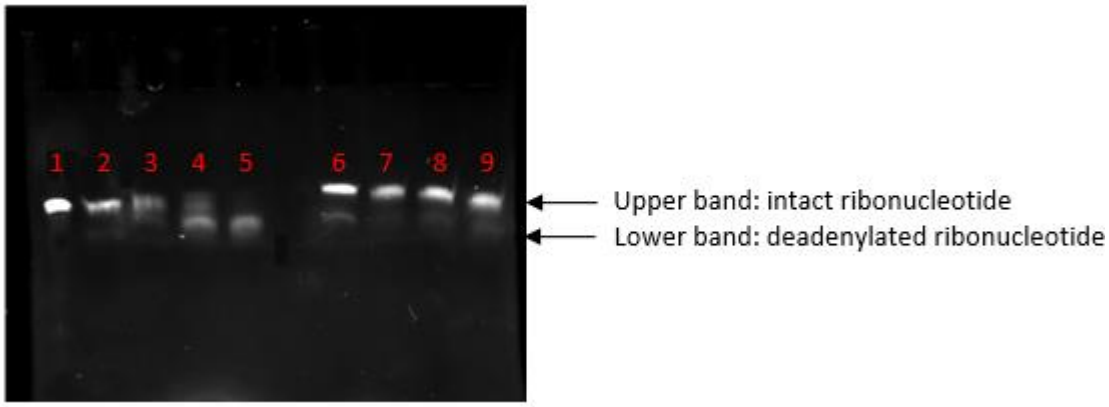
1
2
3
4
5
6
7
8
9
Upper band: intact ribonucleotide
Lower band: deadenylated ribonucleotide

B)

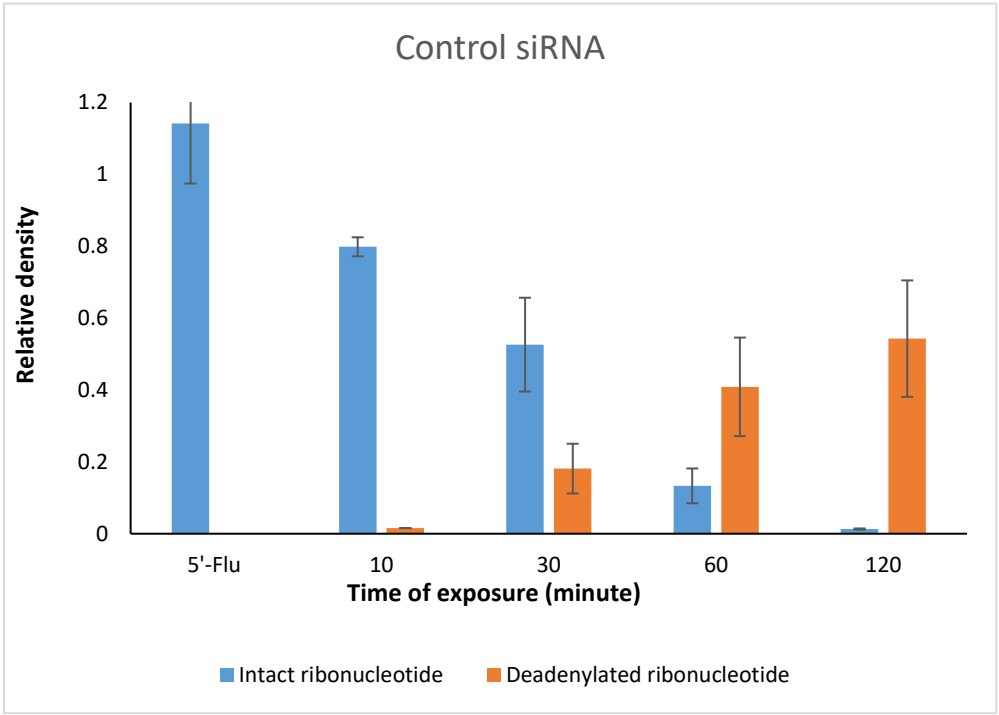
Control siRNA
Relative density
1.2
1
0.8
0.6
0.4
0.2
0
5'-Flu
10
30
60
120
Time of exposure (minute)
Intact ribonucleotide
Deadenylated ribonucleotide

C)

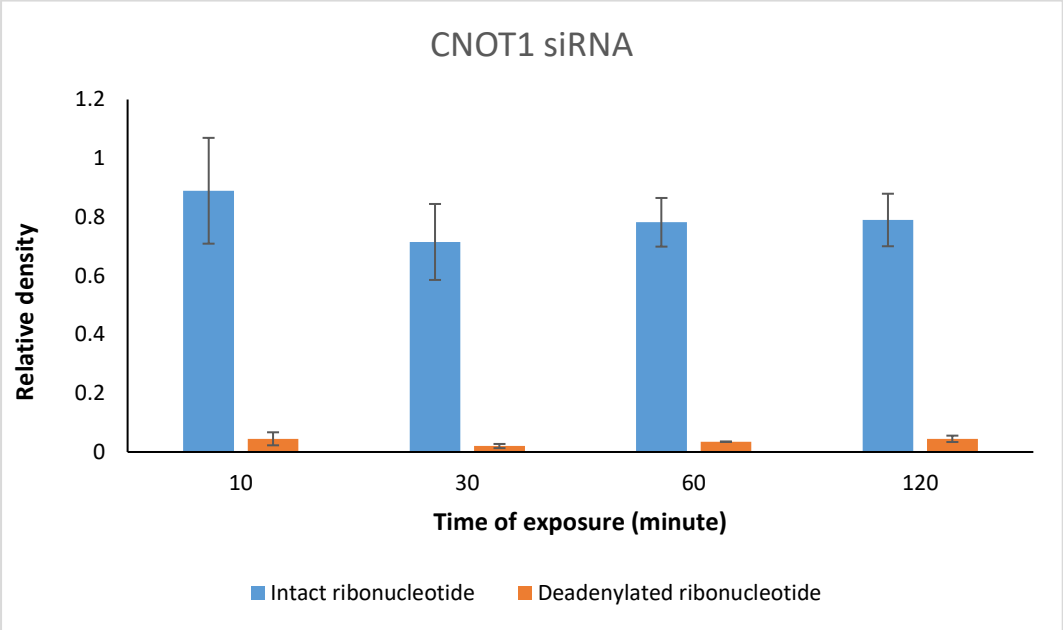
CNOT1 siRNA
Relative density
1.2
1
0.8
0.6
0.4
0.2
0
10
30
60
120
Time of exposure (minute)
Intact ribonucleotide
Deadenylated ribonucleotide

D)

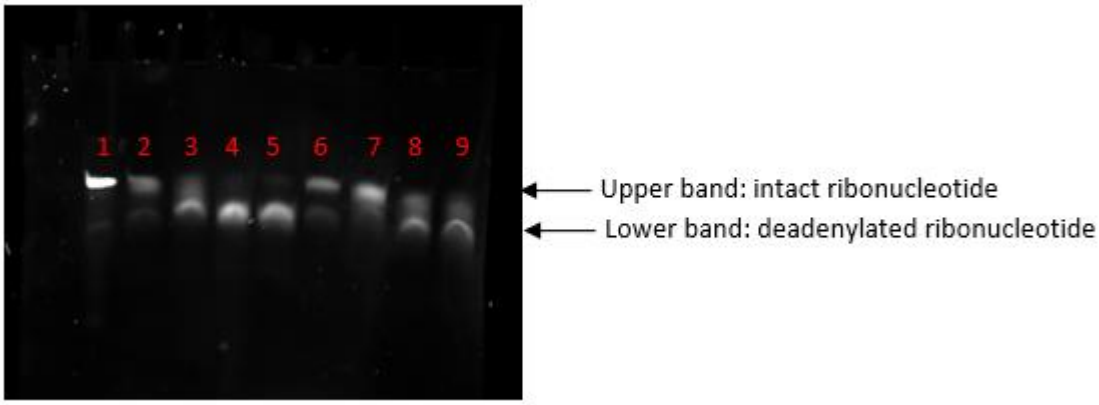
1 2 3 4 5 6 7 8 9
Upper band: intact ribonucleotide
Lower band: deadenylated ribonucleotide

E)

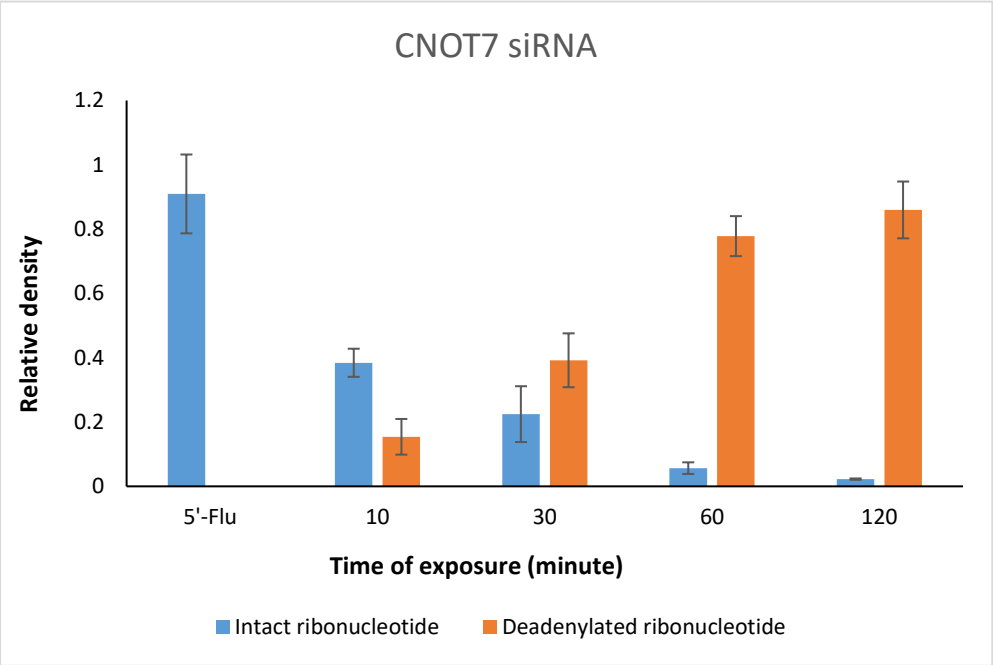
CNOT7 siRNA
1.2
1
0.8
0.6
0.4
0.2
0
Relative density
5'-Flu
10
30
60
120
Time of exposure (minute)
Intact ribonucleotide
Deadenylated ribonucleotide

F)

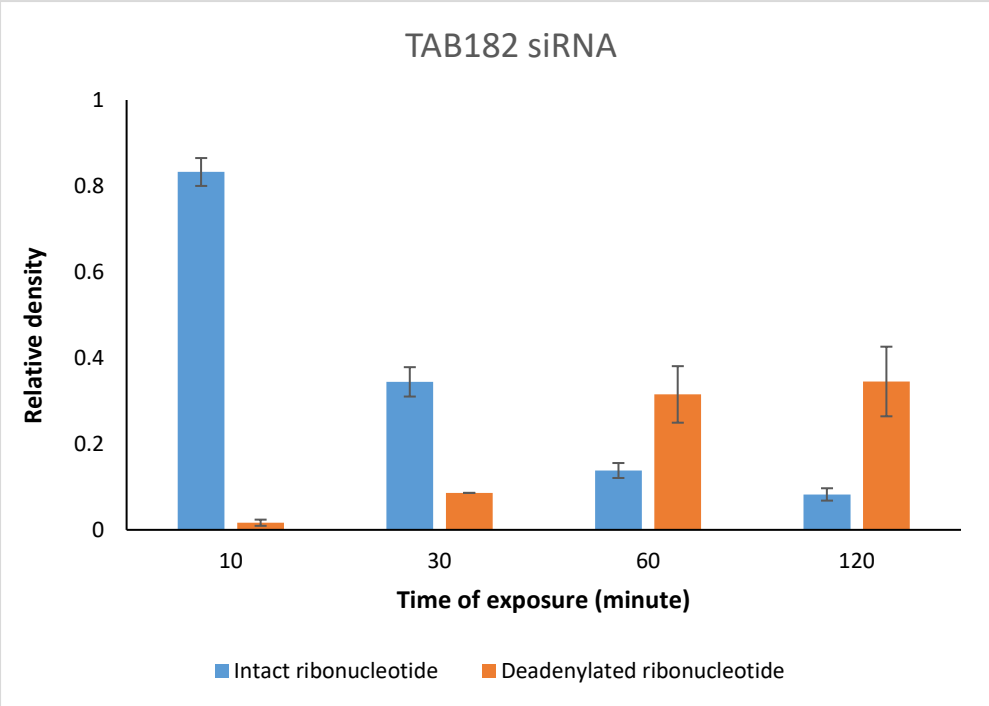
TAB182 siRNA
1
0.8
0.6
0.4
0.2
0
Relative density
10
30
60
120
Time of exposure (minute)
Intact ribonucleotide
Deadenylated ribonucleotide

Figure 4.6 Deadenylase activity is suppressed in CNOT1-depleted HeLa cells, but not in CNOT7 and Tab182 -depleted HeLa cells

2µl of 5'-fluorescein-labeled RNA substrate (Flc-5'-CCUUUCCAAAAAAA-3') was incubated with equal amounts of whole cell lysates (5µg) of control, CNOT1, CNOT7 and Tab182-depleted HeLa cells for 10, 30, 60 and 120 minutes at 37°C. The reaction was stopped by addition of 10µl RNA loading buffer and heating for 3 minutes at 85°C. Aliquots of the assay mixtures were fractionated on 20% polyacrylamide gel containing 8 M urea. 5'-Fluorescein labelled ribonucleotides were visualised using a FUSION-FX imaging system. ***A)*** *1: 5'-Flu, 2: Control siRNA (10min), 3: Control siRNA (30min), 4: Control siRNA (60min), 5: Control siRNA (120min), 6: CNOT1 siRNA (10min), 7: CNOT1 siRNA (30min), 8: CNOT1 siRNA (60min), 9: CNOT1 siRNA (120min).* ***B*** *&* ***C)*** *Representative bar graphs show the relative density of the RNA bands in Control and CNOT1-depleted Hela cells. Bands were quantified using the ImageJ software. Total pixel density for each lane was computed by drawing a rectangle around the bands.* ***D)*** *1: 5'-Flu, 2: CNOT7 siRNA (10min), 3: CNOT7 siRNA (30min), 4: CNOT7siRNA (60min), 5: CNOT7 siRNA (120min), 6: Tab182 siRNA (10min), 7: Tab182 siRNA (30min), 8: Tab182 siRNA (60min), 9: Tab182 siRNA (120min).* ***E*** *&* ***F)*** *Representative bar graphs show the relative density of the RNA bands in CNOT7 and Tab182-depleted Hela cells. This experiment was carried out by a 3rd year BSc Biomedical Science project student Amandeep Jagdev.*

4.3 DISCUSSION

Taken together, we have shown that depletion of CNOT1 increases the RNA synthesis in HeLa cells judged by EU incorporation assay. Treatment with DRB appreciably reduced the nuclear EU intensity in both control and CNOT1-depleted cells, consistent with decreased level of RNA synthesis. Importantly, treatment with transcription inhibitors DRB and PHA significantly increased the replication fork speed in CNOT1-depleted cells, suggesting that replication stress in CNOT1-depleted cells is caused by active RNA synthesis. In addition, the level of general transcription factors TBP and phosphorylation of RNA Poll (C-terminus) at serine 5 were both upregulated in CNOT1-depleted cells 72 hours post siRNA transfection. The level of TOP I, which contributes to transcription elongation by resolving transcription-induced DNA hyper-negative supercoiling downstream of RNA Pol II (Shykind, Kim et al. 1997, Baranello, Wojtowicz et al. 2016), was also upregulated in CNOT1-depleted cells 72 hours post siRNA transfection.

Increased transcription-associated R-loop formation in CNOT1-depleted cells was confirmed using the slot-blot assay and immunoblotting of S9.6 antibody. The S9.6 signal was diminished by pre-treatment of gDNA with RNase H1 enzyme for 2 hours, demonstrating that the signal derived from RNA. In addition, immunofluorescence detection of nuclear S9.6 confirmed the results obtained from the slot-blot assay. Transfection of RNase H1 cDNA for 24 hours decreased the S9.6 intensity in both control and CNOT1-depleted cells. The ability of endogenous RNase H1 enzyme to remove R-loops from gDNA in slot-blot assay was somewhat more efficient than the transiently transfected recombinant RNase H1 in immunofluorescence detection of S9.6.

In more detailed investigations, we examined the expression levels of proteins known to be involved in R-loop resolution, such as RNase H1, RNase H2A or B, Senataxin (SETX) and TOP I. Immunoblotting of control and CNOT1-depleted cells showed no difference in RNase H1 expression between the two experimental conditions; however there was a noticeable downregulation of RNase H2A in CNOT1 depleted cells. TOP I and SETX protein levels were upregulated, presumably to deal with the increased level of R-loops, in CNOT1-depleted cells. We also showed that increased transcription-dependent R-loop formation can be a source of slowed replication forks in CNOT1-depleted cells. Transfection with recombinant RNase H1-GFP did not have a significant effect on replication initiation, although it rescued replication fork progress in CNOT1-depleted cells to a limited extent, but not in control cells.

The results obtained from RNA-Seq data showed downregulation of RRM2 expression in CNOT1-depleted cells. In agreement with this, our western blotting data showed that the expression level of RRM2 protein was also downregulated in CNOT1-depleted cells. Knowing that the expression of RNR-encoded genes are cell cycle dependent (Chabouté, Clément et al. 2000) we cannot confirm whether this reduction observed in RRM2 expression levels is the direct effect of CNOT1 depletion or as a consequence of the cell cycle arrest phenotype in CNOT1-depleted cells. Treatment with different doses of RNR inhibitor HU slightly decreased the ability of CNOT1-depleted HeLa cells to form colonies 14 days post siRNA transfection. Interestingly, (Aird, Zhang et al. 2013) showed that RRM2-mediated suppression of nucleotide biosynthesis maintains cancer cells in stable cell growth arrest leading to senescence. In addition, suppression of RRM2 expression by siRNA or treatment with HU significantly induces autophagy (Chen, Zhang et al. 2014). As discussed in chapter 3 (section 3.2.8), both autophagy and senescence phenotypes were noticeably induced in CNOT1-depleted HeLa cells.

Ribonucleotides can be mis-incorporated into gDNA in two ways; firstly, depletion of the dNTP pool impairs discrimination between rNTP and dNTP by DNA polymerases during DNA replication, such that in order to complete DNA replication DNA polymerases erroneously incorporate rNTPs instead of dNTPs (McElhinny, Watts et al. 2010). Secondly, during DNA replication, DNA polymerases incorporate RNA primers into the 5' end of Okazaki-lagging fragments which must eventually be removed and replaced with DNA after completion of DNA replication (Liu, Hu et al. 2017). The RNase H2 complex can recognise and degrade the embedded ribonucleotides to gDNA; failure to accomplish this is associated with genomic instability (Lindsey-Boltz, Kemp et al. 2015). In mammalian cells, an excess of cellular rCTP reduces basal Poly [ADP-ribose] polymerase 1 (PARP-1) activity and consequently disruption of Chk1 activity at the replication fork, leading to under-replicated DNA and ultrafine anaphase bridge (UFBs) formation (Gemble, Buhagiar-Labarchède et al. 2016). The 2'-hydroxyl group makes RNA chemically unstable and susceptible to hydrolysis compared to DNA. Genomic DNA isolated from CNOT1-depleted cells displayed increased sensitivity to alkaline hydrolysis and migrated faster in gel electrophoresis compared to that from control cells. This suggests a high level of ribonucleotides embedded in gDNA in CNOT1-depleted cells. Considering that the gene expression of RNase H2, but not RNase H1, is cell cycle dependent (Lockhart, Pires et al. 2019) we observed downregulation of RNase H2 A and B in CNOT1-depleted HeLa cells.

To gain further insight into the role of the CNOT1 and/or the CNOT complex in DNA replication we analysed different fibre structures in control and CNOT1-depleted cells. CNOT1 depleted-HeLa cells showed increased stalling of forks together with an increase in first label origins and a decrease in second label origins. Increase in the level of new origin firing in CNOT1-depleted cells may lead to reduced replication fork speed (judged by the distribution of

replication fork speeds). Besides, CIP assay has revealed that CNOT1 and TAB182 interact with pre-RC subunits MCM2, MCM7 and ORC3. This association seems to be essential for protecting replication forks as depletion of CNOT1 leads to reduced replication fork speeds. Cellular levels of MCM proteins 2, 3, 7 and CDC7 were similar in control and CNOT1-depleted cells 72 hours post siRNA depletion. These results indicate that CNOT1 may function at replication origins.

The final step to assess the steady-state level of mRNA in CNOT1-depleted cells was to measure the overall level of deadenylase activity of HeLa cells. We showed that depletion of CNOT1 noticeably decreased the level of deadenylase activity of the CNOT complex compared to the control. We take this to indicate that depletion of CNOT1 results in a general inhibition of the activity of the CNOT complex, although we have no evidence of effects on the ubiquitin E3 ligase activity.

All in all, we have shown that the steady-state level of mRNA is disrupted when the CNOT complex loses control of transcription and mRNA stability in HeLa cells, after CNOT1 depletion. Moreover, we have shown that the increase in transcription synthesis in CNOT1-depleted cells promotes transcription-induced replication stress through R-loop formation. We also showed that another source of replication stress in CNOT1-depleted is increased rNTP mis-incorporation into gDNA.

CHAPTER 5

CNOT1 & DNA DAMAGE RESPONSE

5 CNOT1 AND DNA DAMAGE RESPONSE

5.1 INTRODUCTION

The Ccr4-Not complex has been reported to be involved in DNA repair in yeast. Many IR resistance genes involved in DDR pathways have been shown by Westmoreland *et al.* (2004) to have an interconnection with Ccr4 (hCNOT6/hCNOT6L), a major catalytic subunit of the Ccr4-Not and RNA polymerase-associated factor 1 (PAF1)-CDC73 transcription complexes (Westmoreland, Marks et al. 2004). A systematic interaction has been observed between the CCR4-CAF1 subunits with the cell cycle checkpoint genes DUN1, MRC1, RAD9, and RAD17 following treatment with hydroxyurea or methylmethane sulfonate (MMS). Yeast cells lacking NOT2, NOT4, NOT5 and CCR4 or CAF1 genes were shown to be sensitive to HU (Westmoreland, Marks et al. 2004). In the response to replication stress the RING-finger-dependent ubiquitin-protein ligase Not4 modulates the Ubc4p/Ubc5p-mediated stress responses (Mulder, Inagaki et al. 2007). In mammalian cells depletion of CNOT6 in HEK293 T cells resulted in remarkable resistance to cisplatin-mediated apoptosis following induction of Chk2T68 phosphorylation, while overexpression of CNOT6, increased the sensitivity of cells, not only to cisplatin but to bleomycin (Sanchez-Perez, Manguan-Garcia et al. 2009).

In addition, deficiency in transcription-coupled repair (TC-NER), a sub-pathway of NER , is associated with mutations in the Ccr4-Not complex in yeast, suggesting additional functions in DNA repair during transcription elongation (Gaillard, Tous et al. 2009). Zou *et al.* (2015) have shown that TAB182 contributes to radiation-induced DNA double-strand break repair through facilitating the interaction between DNA-PKcs and PARP1. The PARP1-mediated PARylation of DNA-PKcs leads to activation of DNA-PKcs auto-phosphorylation during DNA DSB repair (Zou, Shang et al. 2015). Moreover, in the mammalian system TAB182 was

identified in a screen of proteins which are highly phosphorylated at SQ/TQ sites by ATM or ATR in response to ionising radiation-induced DNA damage (Matsuoka, Ballif et al. 2007).

In this chapter, we show that depletion of CNOT1 in HeLa cell increases induction of spontaneous genome instability and this has been confirmed by several different methods.

We also show that two CNOT complex subunits, CNOT1 and Tab182, associate with ATR; in addition, a lack of CNOT1 appears to be associated with reduced level of ATR.

5.2 RESULTS

5.2.1 Increased spontaneous genome instability in CNOT1-depleted cells

Here we have assessed the extent of DNA damage generated after CNOT1 depletion over several days using different assays. Firstly, we have shown that CNOT1 protein is present in the nucleus but does not localise to DNA damage foci following IR (3Gy) treatment (Figure 5.1.A).

The level of DSBs in control and CNOT1-depleted HeLa cells was measured using neutral comet assays. An increase in tail moment was observed in CNOT1-depleted HeLa cells, confirming increased DSB formation 120 hours post siRNA transfection (Figure 5.1.B). In a second set of experiments the number of cells with more than 5 micronuclei was found to be significantly elevated in CNOT1-depleted HeLa cells at later time points (5 days) post siRNA transfection (Figure 5.1.C and D). In addition, a significant increase in 53BP1 foci formation was observed in G1 positive CNOT1-depleted HeLa cells, 72 hours post siRNA transfection (Figure 5.1.E and F).

A)

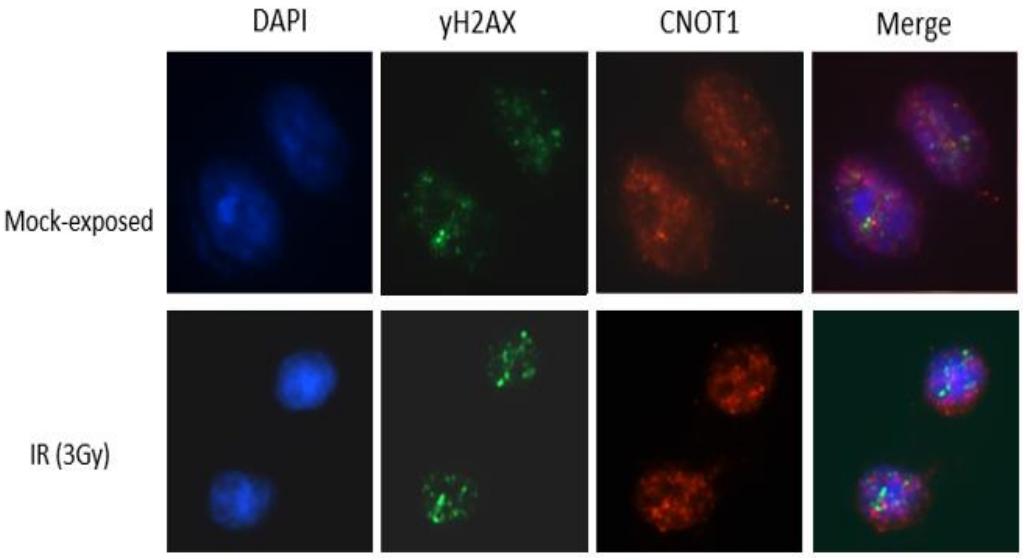
DAPI
γH2AX
CNOT1
Merge
Mock-exposed
IR (3Gy)

B)

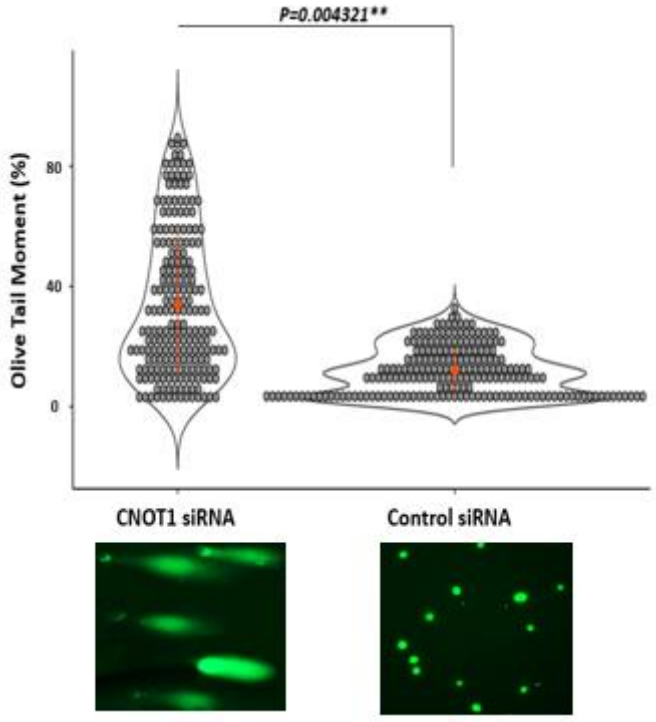
P=0.004321**
Olive Tail Moment (%)
80
40
0
CNOT1 siRNA
Control siRNA

C)

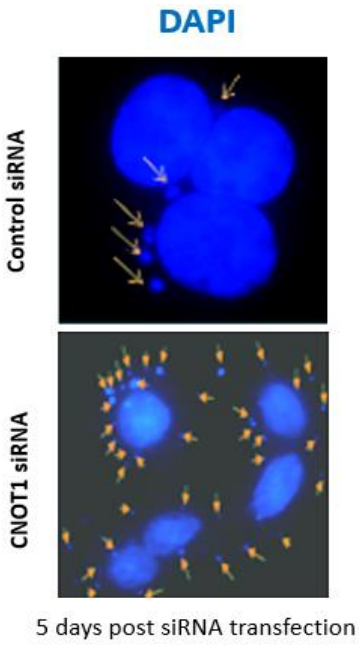
DAPI
Control siRNA
CNOT1 siRNA
5 days post siRNA transfection

D)

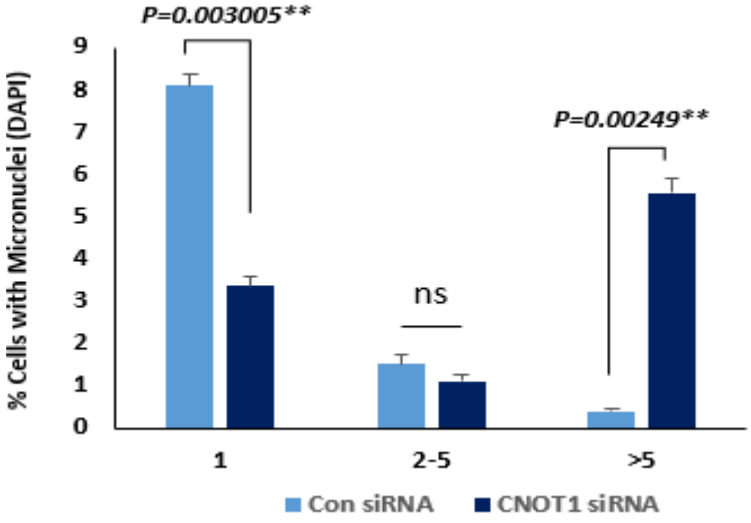
P=0.003005**
P=0.00249**
ns
% Cells with Micronuclei (DAPI)
0
1
2
3
4
5
6
7
8
9
1
2-5
>5
Con siRNA
CNOT1 siRNA

E)

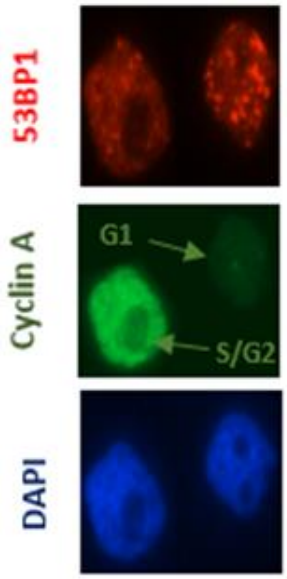
53BP1
Cyclin A
G1
S/G2
DAPI

F)

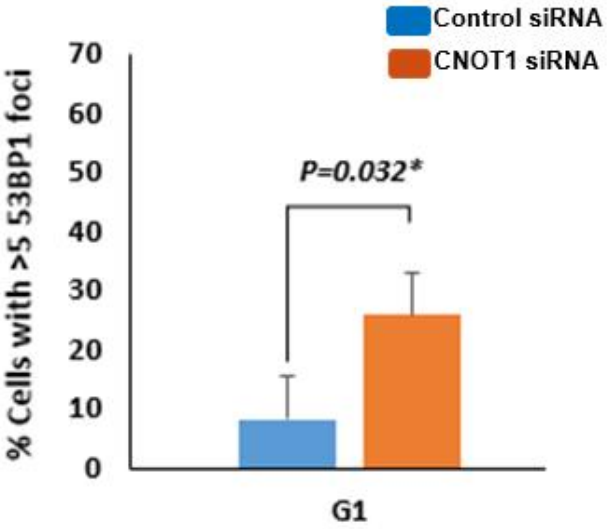
Control siRNA
CNOT1 siRNA
P=0.032*
% Cells with >5 53BP1 foci
0
10
20
30
40
50
60
70
G1

Figure 5.1 Increased genome instability in CNOT1-depleted cells

A) *HeLa cells were mock-exposed or irradiated to 3 Gy IR. 5 hours post irradiation the cells were permeabilised twice in CSK buffer including 0.3 mg/ml RNAse A for 3 minutes per each time. Cells were washed twice with PBS and fixed with 2% PFA for 15 minutes followed by one PBS wash. Cells were then stained with antibodies against yH2AX and CNOT1. The immunofluorescence images are representative of 3 independent experiments.* ***B)*** *DNA damage was evaluated using the Olive tail moment in control and CNOT1-depleted HeLa cells. Neutral comet assay was performed 120 hours post siRNA transfection. Dot plot of Olive tail moments was performed by RStudio statistical software and shown (n=3 independent experiments; >100 cells analysed per repeat, mean ± SD, *p < 0.05, **p < 0.01 and ***p < 0.001).* ***C & D)*** *Quantification of cells with micronuclei classified in three categories; (=1 micronuclei per cell), (2- 5 micronuclei per cell) and (> 5 micronuclei per cell). Scale bars, 10µm. (n=3 independent experiments; >100 cells counted per repeat, mean ± SD, *p < 0.05, **p < 0.01 and ***p < 0.001).****E & F)*** *Quantification of cells with >5 53BP1 foci in G1 positive control and CNOT1-depleted HeLa cells as judged by co-staining of with Cyclin A.*

5.2.2 Downregulation of ATR signalling in CNOT1-depleted cells

Co-immunoprecipitation (CIP) assays were conducted using HeLa cell lysates with CNOT1 and Tab182 antibodies. A western blot showed that ATR associated with CNOT1 and Tab182, possibly indicating an interaction with the intact CNOT complex (Figure 5.2.A). The difference between the amounts of target protein immunoprecipitated with the Tab182 and CNOT1 antibodies is probably a reflection of a much higher titre in the former compared to the latter. These interactions were not supressed in the presence of the ATR kinase inhibitor AZD6738 (Figure 5.2.B). We have also shown that the expression of ATR and its binding partner ATRIP were both down regulated in CNOT1-depleted cells, 72 hours post siRNA transfection (Figure 5.2.C). However, no difference was observed in level of the ATR activator protein TopBP1 between control and CNOT1-depleted cells. It also appears that ATR loading onto chromatin was reduced in the absence of CNOT1 (Figure 5.2.D). A further experiment was performed to examine the activation of ATR substrates, between control and CNOT1-depleted HeLa cells up to 4 days post siRNA depletion. As expected, following downregulation of ATR, the phosphorylation of both Chk1 (S345) and RPA (S4/S8) was decreased in CNOT1-depleted HeLa cells (Figure 5.2.E). Finally, RPA foci formation was shown to be reduced in S-G2/M positive CNOT1-depleted HeLa cells compared to control cells (Figure 5.1.F and G).

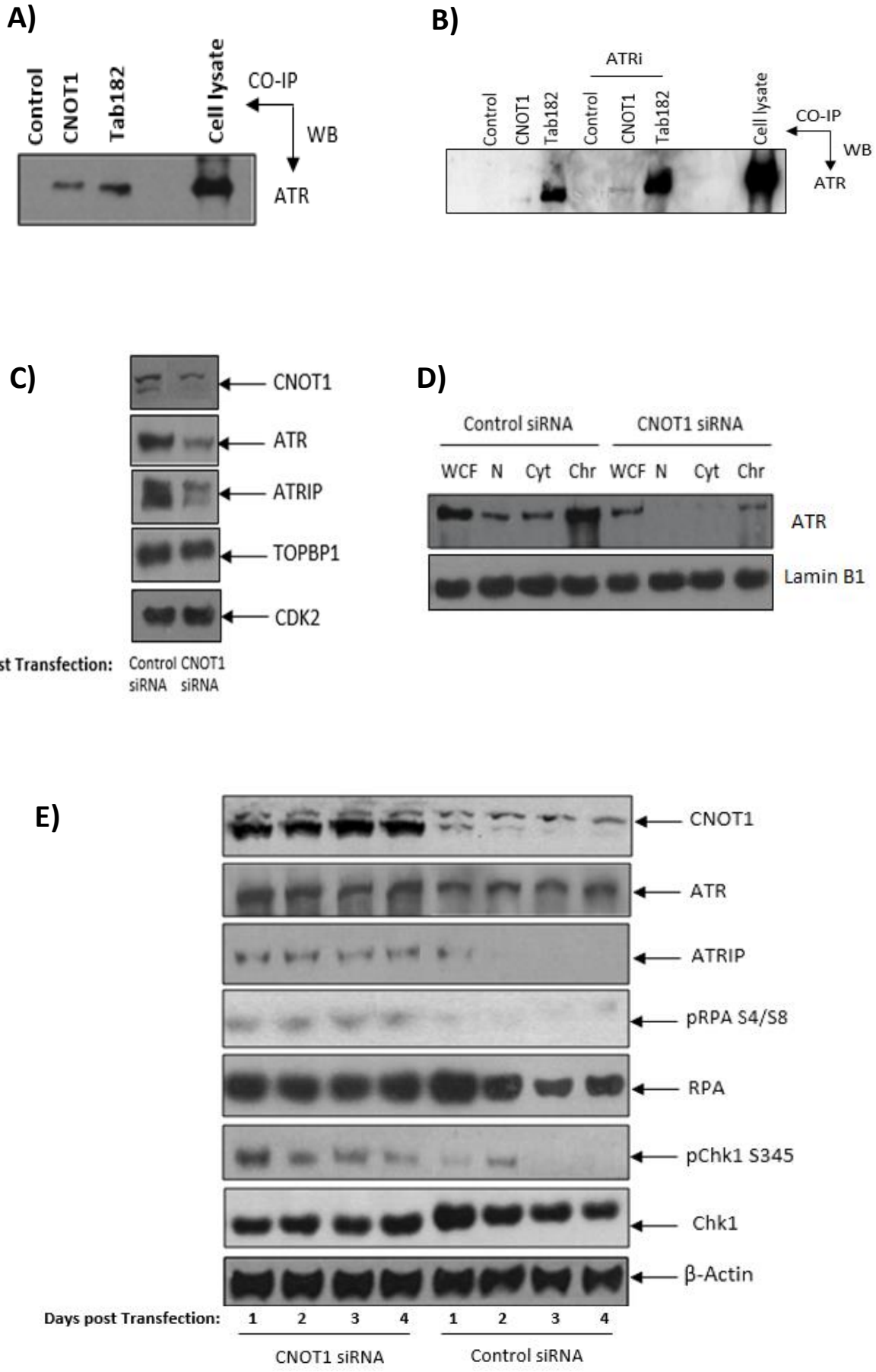
A)
Control
CNOT1
Tab182
Cell lysate
CO-IP
WB
ATR
B)
ATRi
Control
CNOT1
Tab182
Control
CNOT1
Tab182
Cell lysate
CO-IP
WB
ATR
C)
CNOT1
ATR
ATRIP
TOPBP1
CDK2
72h post Transfection:
Control siRNA
CNOT1 siRNA
D)
Control siRNA
CNOT1 siRNA
WCF N Cyt Chr WCF N Cyt Chr
ATR
Lamin B1
E)
CNOT1
ATR
ATRIP
pRPA S4/S8
RPA
pChk1 S345
Chk1
β-Actin
Days post Transfection:
1 2 3 4 1 2 3 4
CNOT1 siRNA
Control siRNA

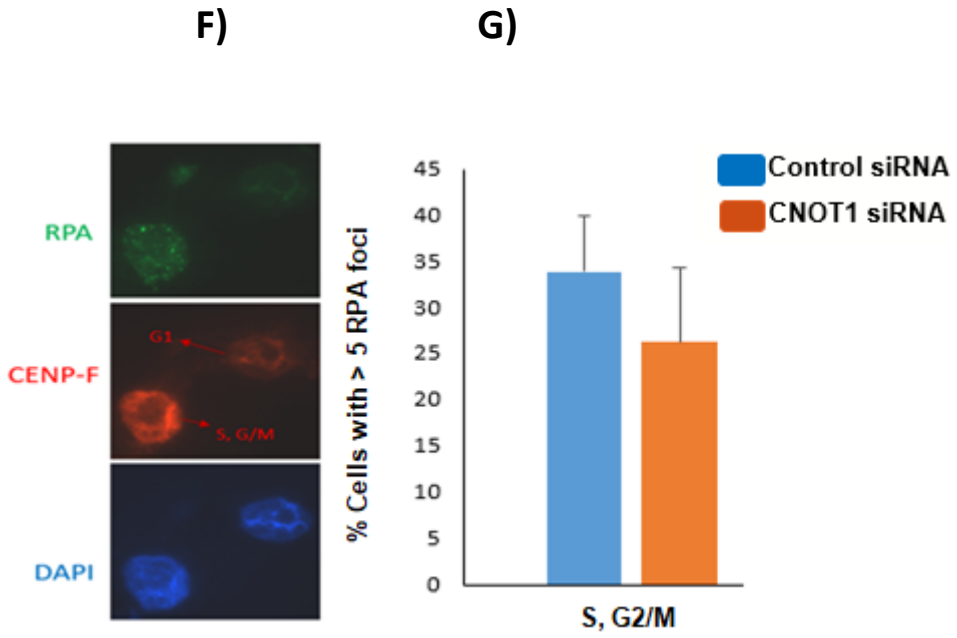

Figure 5.2 Downregulation of ATR signalling in CNOT1-depleted cells

A) *The CIP assays were conducted using HeLa cell lysates incubated with either CNOT1 or Tab182 or irrelevant antibody (control) overnight. Antibody-bound protein complexes were collected on protein G-agarose beads. The immune-complexes were then fractionated by SDS-PAGE, and western blotting was performed using an ATR antibody.* ***B)*** *The CIP assays were conducted using HeLa cell lysates treated with and without ATR inhibitor AZD6738 (2 µM) for 2 hours and incubated with either CNOT1 or Tab182 or irrelevant antibody (control) overnight.* ***C)*** *Total levels of the indicated ATR, ATRIP and TOPBP1 proteins were determined by immunoblotting of total HeLa cell extracts 72 h post transfection with control or CNOT1 siRNA. CDK2 was used as a loading control.* ***D)*** *Representative immunoblot shows the expression level of total ATR in different fractions (whole cell fraction (WCF), cytoplasm (Cyt), nucleoplasm (N) and chromatin (Chr)) in control and CNOT1-depleted cells 72 hours post siRNA transfection after sub -cellular fractionation. Lamin B1 was used as a positive loading control.* ***E)*** *Expression of total ATR, ATRIP, pChk1, Chk1, RPA and pRPA were analysed between control and CNOT1-depleted HeLa cells up to 4 days post siRNA transfection. ß-actin was used as a loading control. The longer time points were used to let the CNOT1-mediated DSBs become detectable and trigger the threshold damage response.* ***F)*** *RPA foci in S and G2/M positive (positive CENPF staining) HeLa cells 72 hours post siRNA transfection.* ***G)*** *Quantification of cells with >5 Rad51*

*and RPA foci (n=3 independent experiments; >100 cells counted per repeat, Statistical analyses were performed using a two-tailed and unpaired Student t test, *P <0.05; **, P<0.01. Error bars represent the SEM. Scale bars, 10µm.*

5.2.3 Reduced homologous recombination (HR) repair in CNOT1-depleted HeLa cells

Since CNOT1-depleted cells showed the G1-cell cycle arrest phenotype, we assumed that the HR repair should be also inactive in those cells. To confirm this, the efficiency of HR repair in CNOT1-depelted cells was assessed using the recombinant I-SceI-GFP plasmid assay. BRAC2-depleted cells were used as a positive control for the assay. As we expected, the same level of deficiency was observed in BRAC2 and CNOT1- depleted cells compared to control cells (Figure 5.3.A, B, C and D). In addition, the Rad51 foci formation was significantly reduced in S/G2 positive CNOT1-depleted HeLa cells compared to control cells (Figure 5.3 E and F).

A)

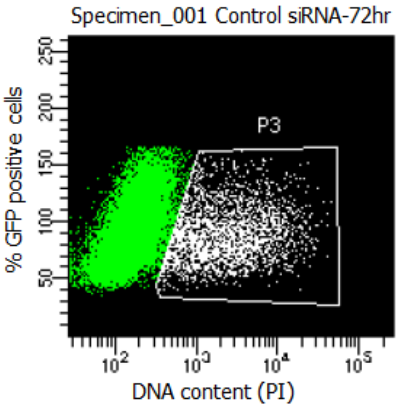

Tube: Control siRNA-72h

Population	#Events	%Parent	%Total
All Events	34,502	####	100.0
P1	20,000	58.0	58.0
P2	19,894	99.5	57.7
P3	2,255	11.3	6.5

B)

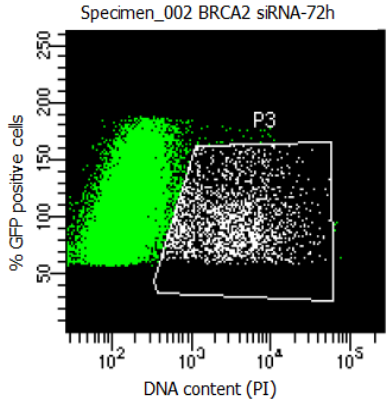

Tube: BRCA2 siRNA-72h

Population	#Events	%Parent	%Total
All Events	67,637	####	100.0
P1	38,477	56.9	56.9
P2	37,549	97.6	55.5
P3	1,622	4.3	2.4

C)

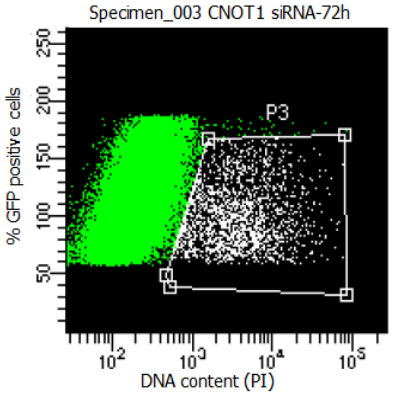

Tube: CNOT1 siRNA-72h

Population	#Events	%Parent	%Total
All Events	95,592	####	100.0
P1	48,477	50.7	50.7
P2	47,259	97.5	49.4
P3	1,721	3.6	1.8

D)

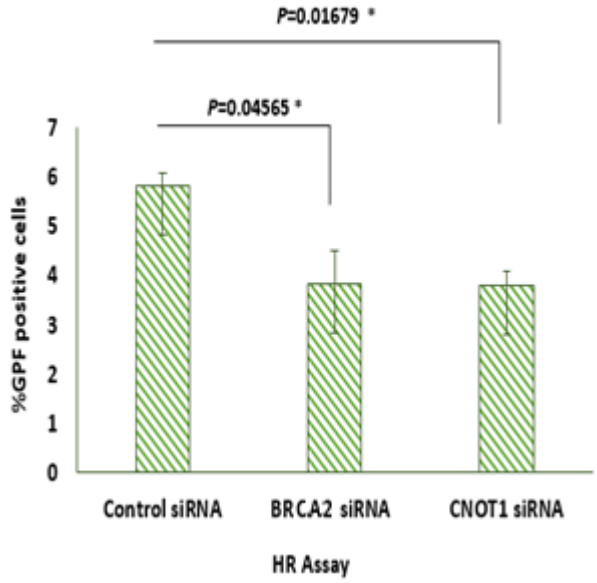
P=0.01679 *
P=0.04565 *
%GPF positive cells
0
1
2
3
4
5
6
7
Control siRNA
BRCA2 siRNA
CNOT1 siRNA
HR Assay

E)

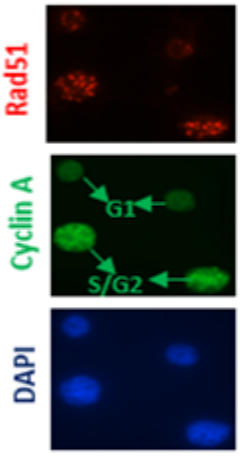
Rad51
Cyclin A
G1
S/G2
DAPI

F)

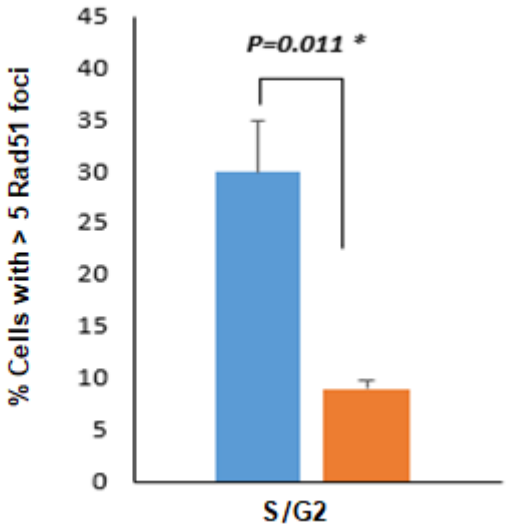
% Cells with > 5 Rad51 foci
P=0.011 *
0
5
10
15
20
25
30
35
40
45
S/G2

Figure 5.3 Reduced homologous recombination (HR) repair in CNOT1-depleted HeLa cells

A, B, and C) *HR repair of the I-SceI-induced DSB in control, BRAC2 and CNOT1 siRNA transfected U2OS cells. % Parent for sub-population of P3 (GFP positive cells) was obtained for each experimental condition using a BD LSRFortessa™ flow cytometer.* ***D)*** *Representative bar graph shows % GFP positive cells in each sample 72 h post siRNA transfection. (n=3 independent experiments, Statistical analyses were performed using a two-tailed and unpaired Student t test, *, P<0.05; ***, P<0.001. Error bars represent the SEM).* ***E)*** *Rad51 foci in S/G2 positive (positive cyclin A staining) HeLa cells 72 hours post siRNA transfection.* ***F)*** *Quantification of cells with >5 Rad51 foci (n=3 independent experiments; >100 cells counted per repeat, statistical analyses were performed using a two-tailed and unpaired Student t test, *, P<0.05; ***, P<0.001. Error bars represent the SEM. Scale bars, 10µm.*

5.2.4 CNOT1-depleted HeLa cells show resistance to MMC treatment

Use of the CRISPR-Cas9-mediated knockout HAP1 cell line with individual mutations in five FA genes has shown that CNOT1 was among those genes whose inactivation can reduce the chromosomal instability following MMC treatment (Velimezi, Robinson-Garcia et al. 2018). Besides, knowing that progression through S phase is required for efficient induction of MMC-mediated DNA damage and CNOT1-depleted cells exhibit the G1-cell cycle arrest phenotype we speculated that depletion of CNOT1 allows HeLa cells to tolerate MMC-induced replication stress. As expected, the results from the colony survival assay showed that the control HeLa cells formed fewer colonies than CNOT1-depleted cells 14 days post treatment with MMC, indicating that the absence of an active CNOT complex is advantageous to HeLa cells to tolerate MMC-dependent DNA intra-crosslinking damage (Figure 5.4.A and B).

In western blotting studies, it was seen that cells lacking CNOT1 exhibited delayed or defective activation of ATR signalling in response to MMC treatment, suggesting that sensing and repairing DNA double-strand breaks was delayed (Figure 5.4.C). However, by 24 hours the level of phosphorylation was comparable in control and CNOT1-depleted cells. Mono-ubiquitination of FA core complex FANCD2 was also delayed in CNOT1-depleted HeLa cells. Since, in G1, ICL bypass repair is carried out by nucleotide excision repair (NER) we also assessed the expression of NER factors STEX, CSB, XPC, XPG and XPF and all were upregulated in CNOT1-depleted cells (Figure5.3.D).

A)

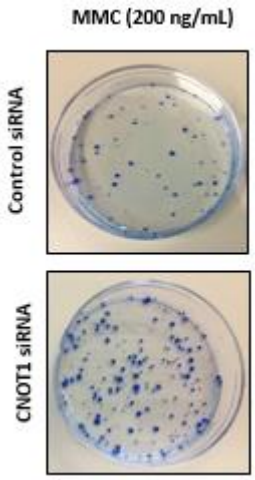
MMC (200 ng/mL)
Control siRNA
CNOT1 siRNA

B)

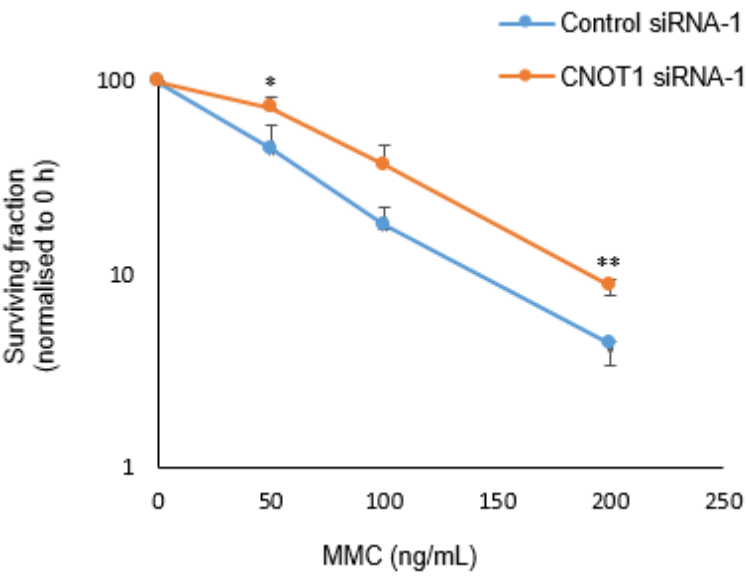
Control siRNA-1
CNOT1 siRNA-1
Surviving fraction (normalised to 0 h)
100
10
1
*
**
0
50
100
150
200
250
MMC (ng/mL)

C)

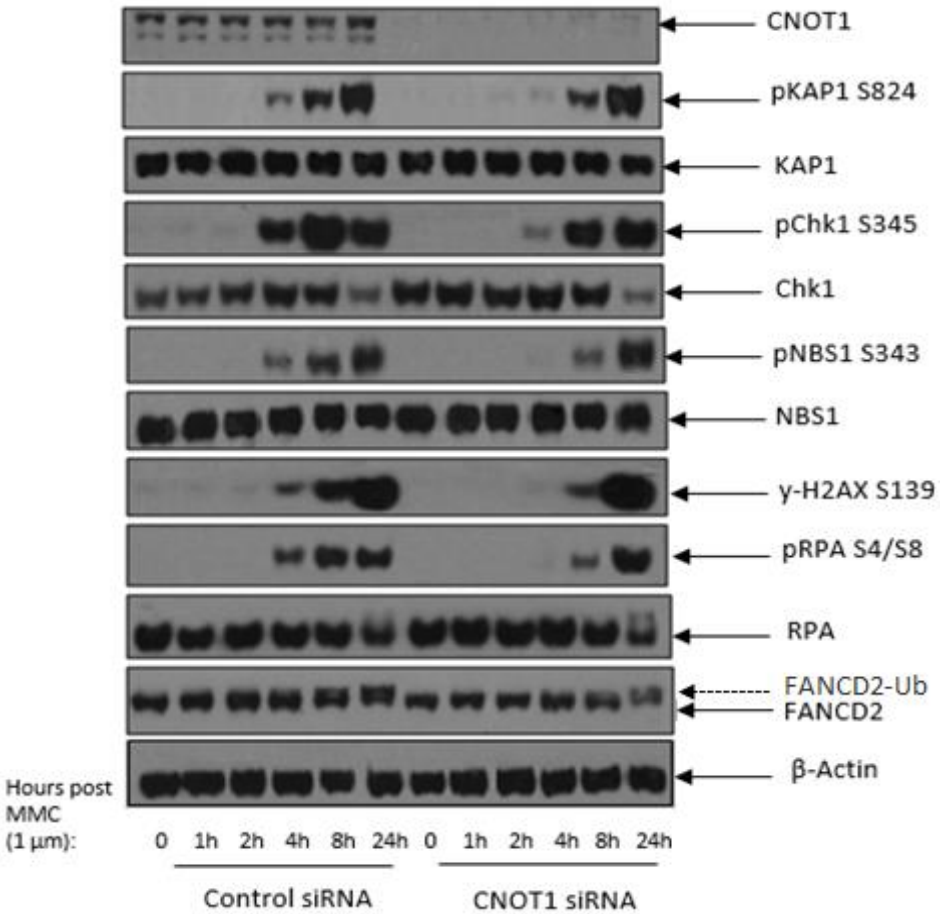
CNOT1
pKAP1 S824
KAP1
pChk1 S345
Chk1
pNBS1 S343
NBS1
γ-H2AX S139
pRPA S4/S8
RPA
FANCD2-Ub
FANCD2
β-Actin
Hours post MMC (1 μm):
0 1h 2h 4h 8h 24h 0 1h 2h 4h 8h 24h
Control siRNA
CNOT1 siRNA

D)

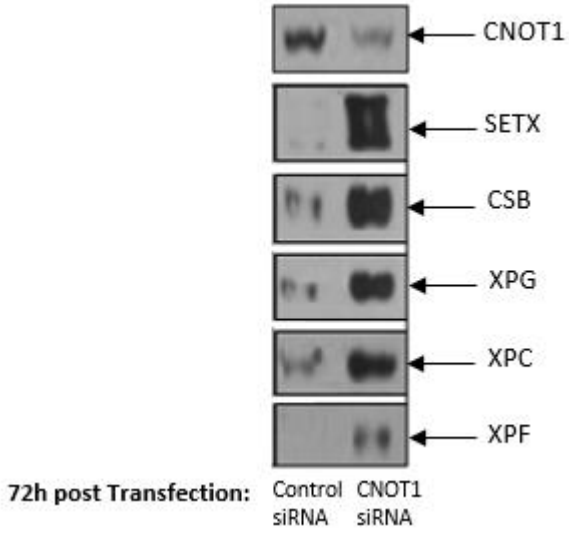

Figure 5.4 CNOT1-depleted HeLa cells show resistance to MMC treatment

A) *Cells were plated at appropriate concentration 72 hours post siRNA transfection and then exposed to different concentrations of MMC (ng/mL). At day 14, large colonies were stained with crystal violet and counted.* ***B)*** *Clonogenic survival was expressed as a surviving fraction of non-treated controls for each condition and was plotted on a semi-logarithmic scale. The graph shown was plotted from 3 independent experiments, mean ± SD, *p < 0.05, **p < 0.01 and ***p < 0.001.* ***C)*** *Western blot analysis of activation of ATR substrates performed after treatment of HeLa cells with MMC (1 µm) 72 post siRNA transfection. Samples were processed at the indicated time points and blotted using the antibodies shown. β-Actin was used as a loading control.* ***D)*** *Western blot analysis of NER proteins in HeLa cell lysate 72 hours post siRNA transfection in in control and CNOT1-depleted HeLa cells.*

5.3 DISCUSSION

The maintenance of genome integrity during DNA replication is crucial for cell proliferation and survival. The sensor kinase ATR acts as a safeguard to detect replication blocks and subsequent generation of double-strand breaks. We have shown that the CNOT complex may associate with ATR. A recent CRISPR screen revealed that CNOT complex deficiency is synthetically lethal with ATR both *in vitro* and *in vivo* (Wang, Wang et al. 2018). The CIP assays showed that ATR associates with CNOT1 and Tab182, possibly indicating an interaction with the intact CNOT complex. Interestingly, the ATR kinase inhibitor AZD6738 only reduced the interactions between CNOT1 or Tab182 and ATR slightly. Noteworthy, the ATR inhibitor can block the kinase activity of ATR by interacting with, and inhibiting, its kinase domains. This changes the configuration of ATR and inhibits its interaction with binding proteins, such as Chk1 and RPA. It seems likely, therefore, that the binding site on ATR for CNOT is located well away from the kinase domain. We have also shown that phosphorylation of effector kinase Chk1 at serines-345 and 317 and RPA at serines 4/8 were reduced following CNOT1 depletion in HeLa cells. These are considered usual ATR substrates. Furthermore, depletion of CNOT1 also results in reduced NBS1 and KAP1 phosphorylation, possibly indicating an effect on DNA-PK and/or ATM. These data suggest the existence of truncated ATR and perhaps other PIKK signalling pathways in response to DNA damage in CNOT1-depleted cells.

Induction of DSBs in CNOT1-depleted HeLa cells was confirmed by increased Olive Tail Moment, micronuclei formation and 53BP1 foci formation (in G1 positive cells). In contrast, phosphorylation of H2AX and its recruitment to the site of DNA damage were delayed in CNOT1-depleted HeLa cells (data is not presented). This may be due to reduced expression of histone proteins which take place in S phase.

We also assessed the DDR response in CNOT1-depleted HeLa cells in combination with DNA damaging agent MMC, which can block DNA replication during S phase. Colony survival assays confirmed that the G1-arrested HeLa cells, following depletion of CNOT1, displayed reduced MMC sensitivity compared to control cells. In all likelihood, CNOT1-depleted cells were able to tolerate the deleterious effect of MMC-dependent replication stress by staying in G1 phase. Initial phosphorylation of DDR proteins H2AX, Chk1, KAP1, RPA1, and NBS1 was delayed after MMC treatment in CNOT1-depleted cells, suggesting that sensing and repairing DNA double-strand breaks was delayed.

Knowing that in G1, ICL bypass repair is carried out by nucleotide excision repair (NER) and translesion DNA synthesis (TLS) (Deans and West 2011) we analysed the expression of proteins involved in NER repair in CNOT1-depleted cells. The results showed upregulation of STEX, CSB, XPC, XPG and XPF in CNOT1-depleted cells compared to control.

All in all, it seems that two main factors contribute to CNOT1-depleted HeLa cells' ability to tolerate the MMC-mediated DNA damage compared to control cells: G1-cell cycle arrest and activation of NER repair.

CHAPTER SIX

CONCLUSIONS

6 CONCLUSIONS

6.1 Proposed Model

We have shown that depletion of CNOT1, a scaffold to the CNOT complex, disrupts cellular transcription buffering. On the one hand, by increasing the level of transcription synthesis, and on the other, by decreasing the mRNA decay rates. In this study, the first result of CNOT1 depletion was disruption of cell cycle progression and G1 arrest. It seems two factors contribute to the G1-cell cycle arrest phenotype in HeLa cells. Firstly, the role of CNOT1 in transcription and mRNA stability of genes involved in cell cycle transition through different phases as suggested by various studies in yeast (Johnston, Eberly et al. 1990, Kadyrova, Habara et al. 2007, Dronamraju, Hepperla et al. 2018). Secondly, upregulation of CDK inhibitors p21 and p27, independently of p53 following induction of DNA damage in CNOT1-depleted cells.

It seems that phosphorylation of Chk2 (T68) correlated with the increased expression of p21 in CNOT1-depleted cells. In case of p27, Morita et al. (2007) has shown that depletion of CNOT6L elevates the expression level of p27 protein due to increased stability of its mRNA poly (A) tail (Morita, Suzuki et al. 2007). Since, increased p27 protein levels did not result from an increase in p27 gene expression in CNOT1-depleted cells we assume disruption of deadenylase activity of CNOT complex is responsible for p27 upregulation. It is also possible that increased half-life contributes to the additional p27 protein observed following downregulation of E3 ubiquitin ligase (CNOT4) activity of CNOT complex.

“Why are p21 and p27 levels increased in CNOT1 depleted cells?”

We propose two possible scenarios below;

1) Increased transcription-induced replication stress through R-loops formation
2) Increased mis-incorporation of rNTPs into gDNA following depletion of dNTP pool resulting from:
    a) Reduction in activity of the RNR complex following downregulation of RRM2 and p53R2

    and/or

    b) Increased level of origin firing following overexpression of cyclin E.

Either of these scenarios or a combination of them leads to increased DSB formation (judged by increased level of micronuclei, 53BP1 bodies and an increase in comet tail moment) in CNOT1-depleted cells and activation of Chk2-dependent G1/S cell cycle arrest. Irreversible accumulation of DNA damage drives mitotic cells either to adapt to stress through autophagy and/or senescence or to be eliminated through programmed cell death. In fact, CNOT1-depleted cells showed induction of autophagy, senescence and apoptosis (independent of Caspase-3), perhaps with some overlapping with one other. The following cartoon shows a summary of pathways dysregulated during CNOT1 depletion that may lead to genomic instability and cell death in HeLa cells (Figure 6.1).

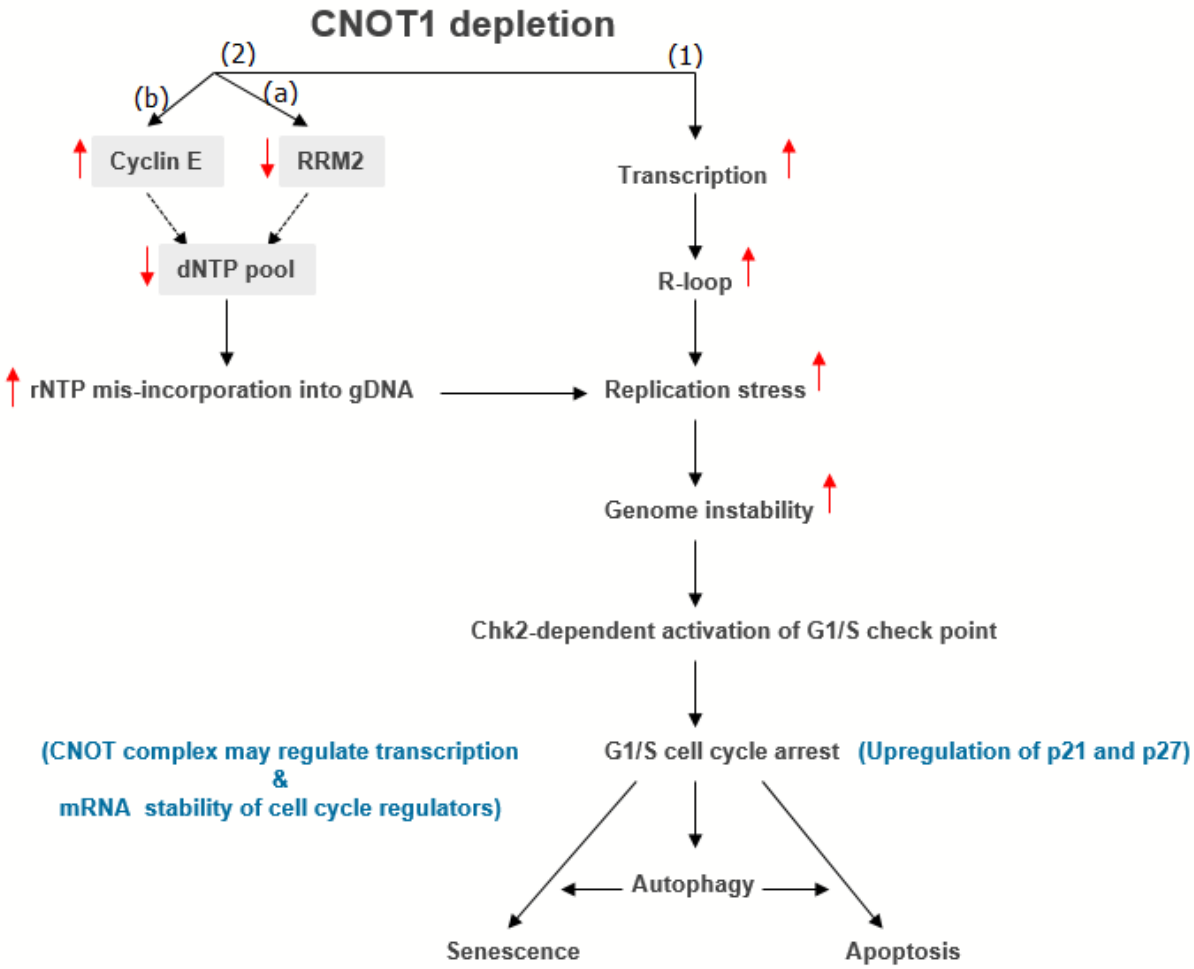

Figure 6.1 Model for the action of CNOT1 in mammalian cells

*The cartoon shows a summary of pathways dysregulated during CNOT1 depletion that may lead to genomic instability and cell death in HeLa cells. Pathway **(1)** shows Transcription-induced replication stress in CNOT1-depleted HeLa cells. Pathway **(2)** shows increased level of rNTP mis-corporation into gDNA following reduction of RNR activity **(a)** and overexpression of cyclin E **(b)** in CNOT1-depleted HeLa cells.*

6.2 Unanswered questions and future work

The findings presented in this thesis raise several interesting questions for possible future investigation. Firstly, because some of the effects we have observed as a result of CNOT1 siRNA-mediated depletion could be due to 'off-target' effects, we will carry out a range of complementation experiments to examine this. A cell line will be generated containing an inducible siRNA resistant form of CNOT1 under the control of tetracycline-inducible promoter. For this we will make use of U2OS 'flip-in' cells.

Secondly, as the results from RNA-Seq did not show an upregulation of CCNE1 gene expression in CNOT1-depleted cells, we will look at its mRNA stability by measuring the mRNA half-life at different time points after treatment with a transcription inhibitor such as actinomycin D or DRB. In addition, we will determine the half-life of the cyclin E protein after CNOT1 depletion. Given that the dysregulation of the oncogene cyclin E has been shown to increase transcription and replication interference (Jones, Mortusewicz et al. 2013), we will investigate the cyclin E-dependent replication stress in CNOT1-depleted HeLa cells in more detail.

Thirdly, we will also measure the nuclear intensity of pRNA poII (S5) by IF microscopy to support our pRNA poII (S5) western blot data.

As separate projects, we will investigate in more detail the ATR-CNOT complex-RNase H2 complex and ATR-CNOT complex-RNR complex axes.

Finally, we will investigate the other phosphorylation sites in ATR and ATM substrates in CNOT1-dependent DDR and the involvement of DNA-PK in the DDR in CNOT1-depleted cells.

REFERENCES

Abraham, K. J., J. N. Chan, J. S. Salvi, B. Ho, A. Hall, E. Vidya, R. Guo, S. A. Killackey, N. Liu and J. E. Lee (2016). "Intersection of calorie restriction and magnesium in the suppression of genome-destabilizing RNA–DNA hybrids." Nucleic acids research **44**(18): 8870-8884.

Abraham, R. T. (2001). "Cell cycle checkpoint signaling through the ATM and ATR kinases." Genes & development **15**(17): 2177-2196.

Aguilera, M., L. Delgui, P. Romano and M. Colombo (2018). "Chronic infections: a possible scenario for autophagy and senescence cross-talk." Cells **7**(10): 162.

Aird, K. M., G. Zhang, H. Li, Z. Tu, B. G. Bitler, A. Garipov, H. Wu, Z. Wei, S. N. Wagner and M. Herlyn (2013). "Suppression of nucleotide metabolism underlies the establishment and maintenance of oncogene-induced senescence." Cell reports **3**(4): 1252-1265.

Alabert, C., J.-C. Bukowski-Wills, S.-B. Lee, G. Kustatscher, K. Nakamura, F. de Lima Alves, P. Menard, J. Mejlvang, J. Rappsilber and A. Groth (2014). "Chromatin dynamics during DNA replication and uncharacterized replication factors determined by nascent chromatin capture (NCC) proteomics." Nature cell biology **16**(3): 281.

Alberts, B., A. Johnson, J. Lewis, M. Raff, K. Roberts and P. Walter (2002). DNA replication mechanisms. Molecular Biology of the Cell. 4th edition, Garland Science.

Alberts, B., A. Johnson, J. Lewis, M. Raff, K. Roberts and P. Walter (2002). "Molecular Biology of the Cell (Garland Science, New York, 2002)." There is no corresponding record for this reference.

Aliouat-Denis, C.-M., N. Dendouga, I. Van den Wyngaert, H. Goehlmann, U. Steller, I. van de Weyer, N. Van Slycken, L. Andries, S. Kass and W. Luyten (2005). "p53-independent regulation of p21Waf1/Cip1 expression and senescence by Chk2." Molecular cancer research **3**(11): 627-634.

Allsopp, R. C., H. Vaziri, C. Patterson, S. Goldstein, E. V. Younglai, A. B. Futcher, C. W. Greider and C. B. Harley (1992). "Telomere length predicts replicative capacity of human fibroblasts." Proceedings of the National Academy of Sciences **89**(21): 10114-10118.

Andreassen, P. R., A. D. D'Andrea and T. Taniguchi (2004). "ATR couples FANCD2 monoubiquitination to the DNA-damage response." Genes & development **18**(16): 1958-1963.

Anish, R., M. B. Hossain, R. H. Jacobson and S. Takada (2009). "Characterization of transcription from TATA-less promoters: identification of a new core promoter element XCPE2 and analysis of factor requirements." PloS one **4**(4): e5103.

Azzouz, N., O. O. Panasenko, C. Deluen, J. Hsieh, G. Theiler and M. A. Collart (2009). "Specific roles for the Ccr4-Not complex subunits in expression of the genome." Rna **15**(3): 377-383.

Babbarwal, V., J. Fu and J. C. Reese (2014). "The Rpb4/7 module of RNA polymerase II is required for carbon catabolite repressor protein 4-negative on TATA (Ccr4-not) complex to promote elongation." Journal of Biological Chemistry **289**(48): 33125-33130.

Badarinarayana, V., Y.-C. Chiang and C. L. Denis (2000). "Functional interaction of CCR4-NOT proteins with TATAA-binding protein (TBP) and its associated factors in yeast." Genetics **155**(3): 1045-1054.

Bahassi, E. M., R. F. Hennigan, D. L. Myer and P. J. Stambrook (2004). "Cdc25C phosphorylation on serine 191 by Plk3 promotes its nuclear translocation." Oncogene **23**(15): 2658.

Bai, Y. and L. S. Symington (1996). "A Rad52 homolog is required for RAD51-independent mitotic recombination in Saccharomyces cerevisiae." Genes & Development **10**(16): 2025-2037.

Balakrishnan, L. and R. A. Bambara (2013). "Okazaki fragment metabolism." Cold Spring Harbor Perspectives in Biology **5**(2): a010173.

Banin, S., L. Moyal, S.-Y. Shieh, Y. Taya, C. Anderson, L. Chessa, N. Smorodinsky, C. Prives, Y. Reiss and Y. Shiloh (1998). "Enhanced phosphorylation of p53 by ATM in response to DNA damage." Science **281**(5383): 1674-1677.

Bansbach, C. E., R. Bétous, C. A. Lovejoy, G. G. Glick and D. Cortez (2009). "The annealing helicase SMARCAL1 maintains genome integrity at stalled replication forks." Genes & development **23**(20): 2405-2414.

Baranello, L., D. Wojtowicz, K. Cui, B. N. Devaiah, H.-J. Chung, K. Y. Chan-Salis, R. Guha, K. Wilson, X. Zhang and H. Zhang (2016). "RNA polymerase II regulates topoisomerase 1 activity to favor efficient transcription." Cell **165**(2): 357-371.

Bartek, J., C. Lukas and J. Lukas (2004). "Checking on DNA damage in S phase." Nature reviews Molecular cell biology **5**(10): 792.

Bartkova, J., N. Rezaei, M. Liontos, P. Karakaidos, D. Kletsas, N. Issaeva, L.-V. F. Vassiliou, E. Kolettas, K. Niforou and V. C. Zoumpourlis (2006). "Oncogene-induced senescence is part of the tumorigenesis barrier imposed by DNA damage checkpoints." Nature **444**(7119): 633.

Bass, T. E., J. W. Luzwick, G. Kavanaugh, C. Carroll, H. Dungrawala, G. G. Glick, M. D. Feldkamp, R. Putney, W. J. Chazin and D. Cortez (2016). "ETAA1 acts at stalled replication forks to maintain genome integrity." Nature cell biology **18**(11): 1185.

Baumann, P., F. E. Benson and S. C. West (1996). "Human Rad51 protein promotes ATP-dependent homologous pairing and strand transfer reactions in vitro." Cell **87**(4): 757-766.

Bawankar, P., B. Loh, L. Wohlbold, S. Schmidt and E. Izaurralde (2013). "NOT10 and C2orf29/NOT11 form a conserved module of the CCR4-NOT complex that docks onto the NOT1 N-terminal domain." RNA biology **10**(2): 228-244.

Beauséjour, C. M., A. Krtolica, F. Galimi, M. Narita, S. W. Lowe, P. Yaswen and J. Campisi (2003). "Reversal of human cellular senescence: roles of the p53 and p16 pathways." The EMBO journal **22**(16): 4212-4222.

Benjamini, Y. and Y. Hochberg (1995). "Controlling the False Discovery Rate: A Practical and Powerful Approach to Multiple Testing." Journal of the Royal Statistical Society. Series B (Methodological) **57**(1): 289-300.

Berti, M., A. R. Chaudhuri, S. Thangavel, S. Gomathinayagam, S. Kenig, M. Vujanovic, F. Odreman, T. Glatter, S. Graziano and R. Mendoza-Maldonado (2013). "Human RECQ1 promotes restart of replication forks reversed by DNA topoisomerase I inhibition." Nature structural & molecular biology **20**(3): 347.

Bester, A. C., M. Roniger, Y. S. Oren, M. M. Im, D. Sarni, M. Chaoat, A. Bensimon, G. Zamir, D. S. Shewach and B. Kerem (2011). "Nucleotide deficiency promotes genomic instability in early stages of cancer development." Cell **145**(3): 435-446.

Bétous, R., G. G. Glick, R. Zhao and D. Cortez (2013). "Identification and characterization of SMARCAL1 protein complexes." PloS one **8**(5): e63149.

Bétous, R., A. C. Mason, R. P. Rambo, C. E. Bansbach, A. Badu-Nkansah, B. M. Sirbu, B. F. Eichman and D. Cortez (2012). "SMARCAL1 catalyzes fork regression and Holliday junction migration to maintain genome stability during DNA replication." Genes & development **26**(2): 151-162.

Bhatia, V., S. I. Barroso, M. L. García-Rubio, E. Tumini, E. Herrera-Moyano and A. Aguilera (2014). "BRCA2 prevents R-loop accumulation and associates with TREX-2 mRNA export factor PCID2." Nature **511**(7509): 362.

Bodnar, A. G., M. Ouellette, M. Frolkis, S. E. Holt, C.-P. Chiu, G. B. Morin, C. B. Harley, J. W. Shay, S. Lichtsteiner and W. E. Wright (1998). "Extension of life-span by introduction of telomerase into normal human cells." science **279**(5349): 349-352.

Boland, A., Y. Chen, T. Raisch, S. Jonas, D. Kuzuoğlu-Öztürk, L. Wohlbold, O. Weichenrieder and E. Izaurralde (2013). "Structure and assembly of the NOT module of the human CCR4–NOT complex." Nature structural & molecular biology **20**(11): 1289.

Boos, D., L. Sanchez-Pulido, M. Rappas, L. H. Pearl, A. W. Oliver, C. P. Ponting and J. F. Diffley (2011). "Regulation of DNA replication through Sld3-Dpb11 interaction is conserved from yeast to humans." Current Biology **21**(13): 1152-1157.

Bornstein, G., J. Bloom, D. Sitry-Shevah, K. Nakayama, M. Pagano and A. Hershko (2003). "Role of the SCFSkp2 ubiquitin ligase in the degradation of p21Cip1 in S phase." Journal of Biological Chemistry **278**(28): 25752-25757.

Braun, J. E., E. Huntzinger, M. Fauser and E. Izaurralde (2011). "GW182 proteins directly recruit cytoplasmic deadenylase complexes to miRNA targets." Molecular cell **44**(1): 120-133.

Brown, C. E. and A. B. Sachs (1998). "Poly (A) tail length control in Saccharomyces cerevisiae occurs by message-specific deadenylation." Molecular and cellular biology **18**(11): 6548-6559.

Brown, E. J. (2003). "The ATR-independent DNA replication checkpoint." Cell Cycle **2**(3): 187-188.

Brown, E. J. and D. Baltimore (2000). "ATR disruption leads to chromosomal fragmentation and early embryonic lethality." Genes & development **14**(4): 397-402.

Brueckner, F., U. Hennecke, T. Carell and P. Cramer (2007). "CPD damage recognition by transcribing RNA polymerase II." Science **315**(5813): 859-862.

Bugreev, D. V., M. J. Rossi and A. V. Mazin (2010). "Cooperation of RAD51 and RAD54 in regression of a model replication fork." Nucleic acids research **39**(6): 2153-2164.

Buisson, R., J. L. Boisvert, C. H. Benes and L. Zou (2015). "Distinct but concerted roles of ATR, DNA-PK, and Chk1 in countering replication stress during S phase." Molecular cell **59**(6): 1011-1024.

Bulavin, D. V., Y. Higashimoto, I. J. Popoff, W. A. Gaarde, V. Basrur, O. Potapova, E. Appella and A. J. Fornace Jr (2001). "Initiation of a G2/M checkpoint after ultraviolet radiation requires p38 kinase." Nature **411**(6833): 102.

Campisi, J. (2013). "Aging, cellular senescence, and cancer." Annual review of physiology **75**: 685-705.

Canman, C. E., D.-S. Lim, K. A. Cimprich, Y. Taya, K. Tamai, K. Sakaguchi, E. Appella, M. B. Kastan and J. D. Siliciano (1998). "Activation of the ATM kinase by ionizing radiation and phosphorylation of p53." Science **281**(5383): 1677-1679.

Chabouté, M.-E., B. Clément, M. Sekine, G. Philipps and N. Chaubet-Gigot (2000). "Cell cycle regulation of the tobacco ribonucleotide reductase small subunit gene is mediated by E2F-like elements." The Plant Cell **12**(10): 1987-1999.

Chan, G., S. Jablonski, V. Sudakin, J. Hittle and T. Yen (1999). "Human BUBR1 is a mitotic checkpoint kinase that monitors CENP-E functions at kinetochores and binds the cyclosome/APC." The Journal of cell biology **146**(5): 941-954.

Chaudhuri, A. R., Y. Hashimoto, R. Herrador, K. J. Neelsen, D. Fachinetti, R. Bermejo, A. Cocito, V. Costanzo and M. Lopes (2012). "Topoisomerase I poisoning results in PARP-mediated replication fork reversal." Nature structural & molecular biology **19**(4): 417.

Chen, C. Y. A., N. Ezzeddine and A. B. Shyu (2008). "Messenger RNA half-life measurements in mammalian cells." Methods in enzymology **448**: 335-357.

Chen, P. B., H. V. Chen, D. Acharya, O. J. Rando and T. G. Fazzio (2015). "R loops regulate promoter-proximal chromatin architecture and cellular differentiation." Nature structural & molecular biology **22**(12): 999.

Chen, W., L. Zhang, K. Zhang, B. Zhou, M.-L. Kuo, S. Hu, L. Chen, M. Tang, Y.-R. Chen and L. Yang (2014). "Reciprocal regulation of autophagy and dNTP pools in human cancer cells." Autophagy **10**(7): 1272-1284.

Chen, Y., A. Boland, D. Kuzuoğlu-Öztürk, P. Bawankar, B. Loh, C.-T. Chang, O. Weichenrieder and E. Izaurralde (2014). "A DDX6-CNOT1 complex and W-binding pockets in CNOT9 reveal direct links between miRNA target recognition and silencing." Molecular cell **54**(5): 737-750.

Cheng, D. d., J. Li, S. j. Li, Q. c. Yang and C. y. Fan (2017). "CNOT 1 cooperates with LMNA to aggravate osteosarcoma tumorigenesis through the Hedgehog signaling pathway." Molecular oncology **11**(4): 388-404.

Cogoi, S. and L. E. Xodo (2006). "G-quadruplex formation within the promoter of the KRAS proto-oncogene and its effect on transcription." Nucleic acids research **34**(9): 2536-2549.

Collart, M. A. (2003). "Global control of gene expression in yeast by the Ccr4-Not complex." Gene **313**: 1-16.

Collart, M. A. (2016). "The Ccr4-Not complex is a key regulator of eukaryotic gene expression." Wiley Interdisciplinary Reviews: RNA.

Collart, M. A., O. O. Panasenko and S. I. Nikolaev (2013). "The Not3/5 subunit of the Ccr4-Not complex: a central regulator of gene expression that integrates signals between the cytoplasm and the nucleus in eukaryotic cells." Cellular signalling **25**(4): 743-751.

Collart, M. A. and K. Struhl (1994). "NOT1 (CDC39), NOT2 (CDC36), NOT3, and NOT4 encode a global-negative regulator of transcription that differentially affects TATA-element utilization." Genes & development **8**(5): 525-537.

Coppé, J.-P., P.-Y. Desprez, A. Krtolica and J. Campisi (2010). "The senescence-associated secretory phenotype: the dark side of tumor suppression." Annual Review of Pathological Mechanical Disease **5**: 99-118.

Cortez, D., S. Guntuku, J. Qin and S. J. Elledge (2001). "ATR and ATRIP: partners in checkpoint signaling." Science **294**(5547): 1713-1716.

Cuervo, A. M. and J. F. Dice (1998). "How do intracellular proteolytic systems change with age." Front Biosci **3**: d25-d43.

Cui, Y., D. B. Ramnarain, Y.-C. Chiang, L.-H. Ding, J. S. McMahon and C. L. Denis (2008). "Genome wide expression analysis of the CCR4-NOT complex indicates that it consists of three modules with the NOT module controlling SAGA-responsive genes." Molecular Genetics and Genomics **279**(4): 323-337.

D'Angiolella, V., V. Donato, F. M. Forrester, Y.-T. Jeong, C. Pellacani, Y. Kudo, A. Saraf, L. Florens, M. P. Washburn and M. Pagano (2012). "Cyclin F-mediated degradation of ribonucleotide reductase M2 controls genome integrity and DNA repair." Cell **149**(5): 1023-1034.

D'Angiolella, V., H. Yang, R. Faedda, S. Hume, D. Ebner, S. B. Hatch, B. Kessler, K. Burdova, I. Vendrell and D. H. Drewry (2019). "Cyclin F-Chk1 synthetic lethality mediated by E2F1 degradation." bioRxiv: 509810.

Das, B. B., S.-y. N. Huang, J. Murai, I. Rehman, J.-C. Ame, S. Sengupta, S. K. Das, P. Majumdar, H. Zhang and D. Biard (2014). "PARP1–TDP1 coupling for the repair of topoisomerase I–induced DNA damage." Nucleic acids research **42**(7): 4435-4449.

De Duve, C. and R. Wattiaux (1966). "Functions of lysosomes." Annual review of physiology **28**(1): 435-492.

Deans, A. J. and S. C. West (2011). "DNA interstrand crosslink repair and cancer." Nature reviews cancer **11**(7): 467.

Deluen, C., N. James, L. Maillet, M. Molinete, G. Theiler, M. Lemaire, N. Paquet and M. A. Collart (2002). "The Ccr4-Not complex and yTAF1 (yTafII130p/yTafII145p) show physical and functional interactions." Molecular and cellular biology **22**(19): 6735-6749.

Denis, C. L. and J. Chen (2003). "The CCR4–NOT complex plays diverse roles in mRNA metabolism." Progress in nucleic acid research and molecular biology **73**: 221-250.

Denoyelle, C., G. Abou-Rjaily, V. Bezrookove, M. Verhaegen, T. M. Johnson, D. R. Fullen, J. N. Pointer, S. B. Gruber, L. D. Su and M. A. Nikiforov (2006). "Anti-oncogenic role of the endoplasmic reticulum differentially activated by mutations in the MAPK pathway." Nature cell biology **8**(10): 1053.

DeStephanis, D., M. McLeod and S. Yan (2015). "REV1 is important for the ATR-Chk1 DNA damage response pathway in Xenopus egg extracts." Biochemical and biophysical research communications **460**(3): 609-615.

di Fagagna, F. d. A., P. M. Reaper, L. Clay-Farrace, H. Fiegler, P. Carr, T. von Zglinicki, G. Saretzki, N. P. Carter and S. P. Jackson (2003). "A DNA damage checkpoint response in telomere-initiated senescence." Nature **426**(6963): 194.

Di Marco, S., Z. Hasanova, R. Kanagaraj, N. Chappidi, V. Altmannova, S. Menon, H. Sedlackova, J. Langhoff, K. Surendranath and D. Hühn (2017). "RECQ5 helicase cooperates with MUS81 endonuclease in processing stalled replication forks at common fragile sites during mitosis." Molecular cell **66**(5): 658-671. e658.

Di Micco, R., M. Fumagalli, A. Cicalese, S. Piccinin, P. Gasparini, C. Luise, C. Schurra, P. G. Nuciforo, A. Bensimon and R. Maestro (2006). "Oncogene-induced senescence is a DNA damage response triggered by DNA hyper-replication." Nature **444**(7119): 638.

Dirac, A. M. and R. Bernards (2003). "Reversal of senescence in mouse fibroblasts through lentiviral suppression of p53." Journal of Biological Chemistry **278**(14): 11731-11734.

Dominguez-Sola, D., C. Y. Ying, C. Grandori, L. Ruggiero, B. Chen, M. Li, D. A. Galloway, W. Gu, J. Gautier and R. Dalla-Favera (2007). "Non-transcriptional control of DNA replication by c-Myc." Nature **448**(7152): 445.

Dronamraju, R., A. J. Hepperla, Y. Shibata, A. T. Adams, T. Magnuson, I. J. Davis and B. D. Strahl (2018). "Spt6 Association with RNA Polymerase II Directs mRNA Turnover During Transcription." Molecular Cell **70**(6): 1054-1066. e1054.

Du, S., X. Liu and Q. Cai (2018). "Viral-Mediated mRNA Degradation for Pathogenesis." Biomedicines **6**(4): 111.

Dumaz, N. and D. W. Meek (1999). "Serine 15 phosphorylation stimulates p53 transactivation but does not directly influence interaction with HDM2." The EMBO journal **18**(24): 7002-7010.

Dutta, D., K. Shatalin, V. Epshtein, M. E. Gottesman and E. Nudler (2011). "Linking RNA polymerase backtracking to genome instability in E. coli." Cell **146**(4): 533-543.

Ekholm-Reed, S., J. Méndez, D. Tedesco, A. Zetterberg, B. Stillman and S. I. Reed (2004). "Deregulation of cyclin E in human cells interferes with prereplication complex assembly." The Journal of cell biology **165**(6): 789-800.

El-Khamisy, S. F., M. Masutani, H. Suzuki and K. W. Caldecott (2003). "A requirement for PARP-1 for the assembly or stability of XRCC1 nuclear foci at sites of oxidative DNA damage." Nucleic acids research **31**(19): 5526-5533.

Ericsson, J. (1969). "Studies on induced cellular autophagy: I. Electron microscopy of cells with in vivo labelled lysosomes." Experimental cell research **55**(1): 95-106.

Fish, R. N. and C. M. Kane (2002). "Promoting elongation with transcript cleavage stimulatory factors." Biochimica et Biophysica Acta (BBA)-Gene Structure and Expression **1577**(2): 287-307.

Forment, J. V., M. Blasius, I. Guerini and S. P. Jackson (2011). "Structure-specific DNA endonuclease Mus81/Eme1 generates DNA damage caused by Chk1 inactivation." PloS one **6**(8): e23517.

Fousteri, M. and L. H. Mullenders (2008). "Transcription-coupled nucleotide excision repair in mammalian cells: molecular mechanisms and biological effects." Cell research **18**(1): 73.

Fragkos, M., O. Ganier, P. Coulombe and M. Méchali (2015). "DNA replication origin activation in space and time." Nature Reviews Molecular Cell Biology **16**(6): 360.

Franza Jr, B. R., K. Maruyama, J. I. Garrels and H. E. Ruley (1986). "In vitro establishment is not a sufficient prerequisite for transformation by activated ras oncogenes." Cell **44**(3): 409-418.

Fugger, K., M. Mistrik, K. J. Neelsen, Q. Yao, R. Zellweger, A. N. Kousholt, P. Haahr, W. K. Chu, J. Bartek and M. Lopes (2015). "FBH1 catalyzes regression of stalled replication forks." Cell reports **10**(10): 1749-1757.

Gagat, M., A. Krajewski, D. Grzanka and A. Grzanka (2018). "Potential role of cyclin F mRNA expression in the survival of skin melanoma patients: Comprehensive analysis of the pathways altered due to cyclin F upregulation." Oncology reports **40**(1): 123-144.

Gaillard, H., C. Tous, J. Botet, C. González-Aguilera, M. J. Quintero, L. Viladevall, M. L. García-Rubio, A. Rodríguez-Gil, A. Marín and J. Ariño (2009). "Genome-wide analysis of factors affecting transcription elongation and DNA repair: a new role for PAF and Ccr4-not in transcription-coupled repair." PLoS genetics **5**(2): e1000364.

Gari, K., C. Décaillet, M. Delannoy, L. Wu and A. Constantinou (2008). "Remodeling of DNA replication structures by the branch point translocase FANCM." Proceedings of the National Academy of Sciences **105**(42): 16107-16112.

Gemble, S., G. Buhagiar-Labarchède, R. Onclercq-Delic, D. Biard, S. Lambert and M. Amor-Guéret (2016). "A balanced pyrimidine pool is required for optimal Chk1 activation to prevent ultrafine anaphase bridge formation." J Cell Sci **129**(16): 3167-3177.

Gilad, O., B. Y. Nabet, R. L. Ragland, D. W. Schoppy, K. D. Smith, A. C. Durham and E. J. Brown (2010). "Combining ATR suppression with oncogenic Ras synergistically increases genomic instability, causing synthetic lethality or tumorigenesis in a dosage-dependent manner." Cancer research **70**(23): 9693-9702.

Ginno, P. A., Y. W. Lim, P. L. Lott, I. Korf and F. Chédin (2013). "GC skew at the 5′ and 3′ ends of human genes links R-loop formation to epigenetic regulation and transcription termination." Genome research **23**(10): 1590-1600.

Godon, C., S. Mourgues, J. Nonnekens, A. Mourcet, F. Coin, W. Vermeulen, P. O. Mari and G. Giglia-Mari (2012). "Generation of DNA single-strand displacement by compromised nucleotide excision repair." The EMBO journal **31**(17): 3550-3563.

Göhler, T., S. Sabbioneda, C. M. Green and A. R. Lehmann (2011). "ATR-mediated phosphorylation of DNA polymerase η is needed for efficient recovery from UV damage." The Journal of cell biology **192**(2): 219-227.

Groh, M., M. M. Lufino, R. Wade-Martins and N. Gromak (2014). "R-loops associated with triplet repeat expansions promote gene silencing in Friedreich ataxia and fragile X syndrome." PLoS genetics **10**(5): e1004318.

Guainazzi, A. and O. D. Schärer (2010). "Using synthetic DNA interstrand crosslinks to elucidate repair pathways and identify new therapeutic targets for cancer chemotherapy." Cellular and molecular life sciences **67**(21): 3683-3697.

Gutierrez-Camino, A., E. Lopez-Lopez, I. Martin-Guerrero, M. A. Piñan, P. Garcia-Miguel, J. Sanchez-Toledo, A. C. Bañeres, J. Uriz, A. Navajas and A. Garcia-Orad (2014). "Noncoding RNA–related polymorphisms in pediatric acute lymphoblastic leukemia susceptibility." Pediatric research **75**(6): 767.

Hagkarim, N. C., E. L. Ryan, P. J. Byrd, R. Hollingworth, N. J. Shimwell, A. Agathanggelou, M. Vavasseur, V. Kolbe, T. Speiseder and T. Dobner (2018). "Degradation of a novel DNA damage response protein, tankyrase 1 binding protein 1, following adenovirus infection." Journal of virology **92**(12): e02034-02017.

Hammond, E. M., C. L. Brunet, G. D. Johnson, J. Parkhill, A. E. Milner, G. Brady, C. D. Gregory and R. J. Grand (1998). "Homology between a human apoptosis specific protein and the product of APG5, a gene involved in autophagy in yeast." FEBS letters **425**(3): 391-395.

Hamperl, S., M. J. Bocek, J. C. Saldivar, T. Swigut and K. A. Cimprich (2017). "Transcription-replication conflict orientation modulates R-loop levels and activates distinct DNA damage responses." Cell **170**(4): 774-786. e719.

Hashimoto, Y., A. R. Chaudhuri, M. Lopes and V. Costanzo (2010). "Rad51 protects nascent DNA from Mre11-dependent degradation and promotes continuous DNA synthesis." Nature structural & molecular biology **17**(11): 1305.

Hatchi, E., K. Skourti-Stathaki, S. Ventz, L. Pinello, A. Yen, K. Kamieniarz-Gdula, S. Dimitrov, S. Pathania, K. M. McKinney and M. L. Eaton (2015). "BRCA1 recruitment to transcriptional pause sites is required for R-loop-driven DNA damage repair." Molecular cell **57**(4): 636-647.

Hawkins, M., J. U. Dimude, J. A. L. Howard, A. J. Smith, M. S. Dillingham, N. J. Savery, C. J. Rudolph and P. McGlynn (2019). "Direct removal of RNA polymerase barriers to replication by accessory replicative helicases."

Hayflick, L. (1965). "The limited in vitro lifetime of human diploid cell strains." Experimental cell research **37**(3): 614-636.

Hayflick, L. and P. S. Moorhead (1961). "The serial cultivation of human diploid cell strains." Experimental cell research **25**(3): 585-621.

Hermeking, H., C. Lengauer, K. Polyak, T.-C. He, L. Zhang, S. Thiagalingam, K. W. Kinzler and B. Vogelstein (1997). "14-3-3σIs a p53-regulated inhibitor of G2/M progression." Molecular cell **1**(1): 3-11.

Higgins, N., K. Kato and B. Strauss (1976). "A model for replication repair in mammalian cells." Journal of molecular biology **101**(3): 417-425.

Homma, Y., M. Tsunoda and H. Kasai (1994). "Evidence for the accumulation of oxidative stress during cellular aging of human diploid fibroblasts." Biochemical and biophysical research communications **203**(2): 1063-1068.

Hu, G., J. Kim, Q. Xu, Y. Leng, S. H. Orkin and S. J. Elledge (2009). "A genome-wide RNAi screen identifies a new transcriptional module required for self-renewal." Genes & development **23**(7): 837-848.

Itakura, E., C. Kishi-Itakura and N. Mizushima (2012). "The hairpin-type tail-anchored SNARE syntaxin 17 targets to autophagosomes for fusion with endosomes/lysosomes." Cell **151**(6): 1256-1269.

Ito, K., A. Takahashi, M. Morita, T. Suzuki and T. Yamamoto (2011). "The role of the CNOT1 subunit of the CCR4-NOT complex in mRNA deadenylation and cell viability." Protein & cell **2**(9): 755-763.

Itoh, T. and J.-I. Tomizawa (1980). "Formation of an RNA primer for initiation of replication of ColE1 DNA by ribonuclease H." Proceedings of the National Academy of Sciences **77**(5): 2450-2454.

Jiang, H., M. Wolgast, L. M. Beebe and J. C. Reese (2019). "Ccr4–Not maintains genomic integrity by controlling the ubiquitylation and degradation of arrested RNAPII." Genes & Development.

Joazeiro, C. A. and A. M. Weissman (2000). "RING finger proteins: mediators of ubiquitin ligase activity." Cell **102**(5): 549-552.

Johnson, S. A., N. Mandavia, H.-D. Wang and D. L. Johnson (2000). "Transcriptional regulation of the TATA-binding protein by Ras cellular signaling." Molecular and cellular biology **20**(14): 5000-5009.

Johnston, L., S. Eberly, J. Chapman, H. Araki and A. Sugino (1990). "The product of the Saccharomyces cerevisiae cell cycle gene DBF2 has homology with protein kinases and is periodically expressed in the cell cycle." Molecular and Cellular Biology **10**(4): 1358-1366.

Jones, R., O. Mortusewicz, I. Afzal, M. Lorvellec, P. Garcia, T. Helleday and E. Petermann (2013). "Increased replication initiation and conflicts with transcription underlie Cyclin E-induced replication stress." Oncogene **32**(32): 3744.

Kadyrova, L. Y., Y. Habara, T. H. Lee and R. P. Wharton (2007). "Translational control of maternal Cyclin B mRNA by Nanos in the Drosophila germline." Development **134**(8): 1519-1527.

Kai, T., R. Matsunaga, M. Eguchi, H. Kamiya, H. Kasai, M. Suzuki and S. Izuta (2002). "An oxidized nucleotide affects DNA replication through activation of protein kinases in Xenopus egg lysates." Nucleic acids research **30**(2): 569-573.

Kang, C., Q. Xu, T. D. Martin, M. Z. Li, M. Demaria, L. Aron, T. Lu, B. A. Yankner, J. Campisi and S. J. Elledge (2015). "The DNA damage response induces inflammation and senescence by inhibiting autophagy of GATA4." Science **349**(6255): aaa5612.

Kantidakis, T., M. Saponaro, R. Mitter, S. Horswell, A. Kranz, S. Boeing, O. Aygün, G. P. Kelly, N. Matthews and A. Stewart (2016). "Mutation of cancer driver MLL2 results in transcription stress and genome instability." Genes & development **30**(4): 408-420.

Kawale, A. S. and L. F. Povirk (2017). "Tyrosyl–DNA phosphodiesterases: rescuing the genome from the risks of relaxation." Nucleic acids research **46**(2): 520-537.

Khanna, K. K. and S. P. Jackson (2001). "DNA double-strand breaks: signaling, repair and the cancer connection." Nature genetics **27**(3): 247-254.

Kim, D., B. Langmead and S. L. Salzberg (2015). "HISAT: a fast spliced aligner with low memory requirements." Nature methods **12**(4): 357.

Kim, N., N. H. Shar-yin, J. S. Williams, Y. C. Li, A. B. Clark, J.-E. Cho, T. A. Kunkel, Y. Pommier and S. Jinks-Robertson (2011). "Mutagenic processing of ribonucleotides in DNA by yeast topoisomerase I." Science **332**(6037): 1561-1564.

Kinner, A., W. Wu, C. Staudt and G. Iliakis (2008). "γ-H2AX in recognition and signaling of DNA double-strand breaks in the context of chromatin." Nucleic acids research **36**(17): 5678-5694.

Klionsky, D. J. and Y. Ohsumi (1999). "Vacuolar import of proteins and organelles from the cytoplasm." Annual review of cell and developmental biology **15**(1): 1-32.

Kobayashi, K., T. A. Guilliam, M. Tsuda, J. Yamamoto, L. J. Bailey, S. Iwai, S. Takeda, A. J. Doherty and K. Hirota (2016). "Repriming by PrimPol is critical for DNA replication restart downstream of lesions and chain-terminating nucleosides." Cell Cycle **15**(15): 1997-2008.

Komatsu, M., H. Kurokawa, S. Waguri, K. Taguchi, A. Kobayashi, Y. Ichimura, Y.-S. Sou, I. Ueno, A. Sakamoto and K. I. Tong (2010). "The selective autophagy substrate p62 activates the stress

responsive transcription factor Nrf2 through inactivation of Keap1." Nature cell biology **12**(3): 213.

Kops, G. J., B. A. Weaver and D. W. Cleveland (2005). "On the road to cancer: aneuploidy and the mitotic checkpoint." Nature Reviews Cancer **5**(10): 773.

Kotsantis, P., E. Petermann and S. J. Boulton (2018). "Mechanisms of oncogene-induced replication stress: jigsaw falling into place." Cancer discovery **8**(5): 537-555.

Kotsantis, P., L. M. Silva, S. Irmscher, R. M. Jones, L. Folkes, N. Gromak and E. Petermann (2016). "Increased global transcription activity as a mechanism of replication stress in cancer." Nature communications **7**: 13087.

Krajewska, M., R. S. Fehrmann, E. G. de Vries and M. A. van Vugt (2015). "Regulators of homologous recombination repair as novel targets for cancer treatment." Frontiers in genetics **6**: 96.

Kruk, J. A., A. Dutta, J. Fu, D. S. Gilmour and J. C. Reese (2011). "The multifunctional Ccr4–Not complex directly promotes transcription elongation." Genes & development **25**(6): 581-593.

Kuilman, T., C. Michaloglou, W. J. Mooi and D. S. Peeper (2010). "The essence of senescence." Genes & development **24**(22): 2463-2479.

Kuilman, T. and D. S. Peeper (2009). "Senescence-messaging secretome: SMS-ing cellular stress." Nature reviews cancer **9**(2): 81.

Kuleshov, M. V., M. R. Jones, A. D. Rouillard, N. F. Fernandez, Q. Duan, Z. Wang, S. Koplev, S. L. Jenkins, K. M. Jagodnik, A. Lachmann, M. G. McDermott, C. D. Monteiro, G. W. Gundersen and A. Ma'ayan (2016). "Enrichr: a comprehensive gene set enrichment analysis web server 2016 update." Nucleic Acids Research **44**(W1): W90-W97.

Kumagai, A. and W. G. Dunphy (1999). "Binding of 14-3-3 proteins and nuclear export control the intracellular localization of the mitotic inducer Cdc25." Genes & development **13**(9): 1067-1072.

Ladha, M. H., K. Y. Lee, T. M. Upton, M. F. Reed and M. E. Ewen (1998). "Regulation of exit from quiescence by p27 and cyclin D1-CDK4." Molecular and cellular biology **18**(11): 6605-6615.

Lamark, T., S. Svenning and T. Johansen (2017). "Regulation of selective autophagy: the p62/SQSTM1 paradigm." Essays in biochemistry **61**(6): 609-624.

Land, H., L. F. Parada and R. A. Weinberg (1983). "Tumorigenic conversion of primary embryo fibroblasts requires at least two cooperating oncogenes." Nature **304**(5927): 596.

Lara-Gonzalez, P., F. G. Westhorpe and S. S. Taylor (2012). "The spindle assembly checkpoint." Current biology **22**(22): R966-R980.

Lau, N., A. Kolkman, F. van Schaik, K. Mulder, W. Pijnappel, A. Heck and H. Timmers (2009). "Human Ccr4-Not complexes contain variable deadenylase subunits." Biochem. J **422**: 443-453.

Lazzaro, F., D. Novarina, F. Amara, D. L. Watt, J. E. Stone, V. Costanzo, P. M. Burgers, T. A. Kunkel, P. Plevani and M. Muzi-Falconi (2012). "RNase H and postreplication repair protect cells from ribonucleotides incorporated in DNA." Molecular cell **45**(1): 99-110.

Le Page, F., A. Klungland, D. E. Barnes, A. Sarasin and S. Boiteux (2000). "Transcription coupled repair of 8-oxoguanine in murine cells: the ogg1 protein is required for repair in nontranscribed sequences but not in transcribed sequences." Proceedings of the National Academy of Sciences **97**(15): 8397-8402.

Lee, T. I., J. J. Wyrick, S. S. Koh, E. G. Jennings, E. L. Gadbois and R. A. Young (1998). "Interplay of positive and negative regulators in transcription initiation by RNA polymerase II holoenzyme." Molecular and cellular biology **18**(8): 4455-4462.

Li, A. and J. J. Blow (2005). "Cdt1 downregulation by proteolysis and geminin inhibition prevents DNA re-replication in Xenopus." The EMBO journal **24**(2): 395-404.

Libri, D., K. Dower, J. Boulay, R. Thomsen, M. Rosbash and T. H. Jensen (2002). "Interactions between mRNA export commitment, 3'-end quality control, and nuclear degradation." Molecular and cellular biology **22**(23): 8254-8266.

Limbo, O., C. Chahwan, Y. Yamada, R. A. de Bruin, C. Wittenberg and P. Russell (2007). "Ctp1 is a cell-cycle-regulated protein that functions with Mre11 complex to control double-strand break repair by homologous recombination." Molecular cell **28**(1): 134-146.

Lin, C. Y., J. Lovén, P. B. Rahl, R. M. Paranal, C. B. Burge, J. E. Bradner, T. I. Lee and R. A. Young (2012). "Transcriptional amplification in tumor cells with elevated c-Myc." Cell **151**(1): 56-67.

Lin, Y.-L. and P. Pasero (2012). "Interference between DNA replication and transcription as a cause of genomic instability." Current genomics **13**(1): 65-73.

Lindahl, T. (1974). "An N-glycosidase from Escherichia coli that releases free uracil from DNA containing deaminated cytosine residues." Proceedings of the National Academy of Sciences **71**(9): 3649-3653.

Lindsey-Boltz, L. A., M. G. Kemp, J. Hu and A. Sancar (2015). "Analysis of ribonucleotide removal from DNA by human nucleotide excision repair." Journal of Biological Chemistry: jbc. M115. 695254.

Liu, B., J. Hu, J. Wang and D. Kong (2017). "Direct visualization of RNA-DNA primer removal from Okazaki fragments provides support for flap cleavage and exonucleolytic pathways in eukaryotic cells." Journal of Biological Chemistry **292**(12): 4777-4788.

Liu, H., S. Takeda, R. Kumar, T. D. Westergard, E. J. Brown, T. K. Pandita, E. H.-Y. Cheng and J. J.-D. Hsieh (2010). "Phosphorylation of MLL by ATR is required for execution of mammalian S-phase checkpoint." Nature **467**(7313): 343.

Liu, H. Y., J. H. Toyn, Y. C. Chiang, M. P. Draper, L. H. Johnston and C. L. Denis (1997). "DBF2, a cell cycle-regulated protein kinase, is physically and functionally associated with the CCR4 transcriptional regulatory complex." The EMBO journal **16**(17): 5289-5298.

Ljungman, M. and F. Zhang (1996). "Blockage of RNA polymerase as a possible trigger for uv light-induced apoptosis." Oncogene **13**(4): 823-832.

Lockhart, A., V. B. Pires, F. Bento, V. Kellner, S. Luke-Glaser and B. Luke (2019). "RNase H1 and H2 are differentially regulated to eliminate RNA-DNA hybrids." bioRxiv: 593152.

Maillet, L., C. Tu, Y. K. Hong, E. O. Shuster and M. A. Collart (2000). "The essential function of Not1 lies within the Ccr4-Not complex." Journal of molecular biology **303**(2): 131-143.

Manchado, E., M. Eguren and M. Malumbres (2010). The anaphase-promoting complex/cyclosome (APC/C): cell-cycle-dependent and-independent functions, Portland Press Limited.

Mannava, S., V. Grachtchouk, L. J. Wheeler, M. Im, D. Zhuang, E. G. Slavina, C. K. Mathews, D. S. Shewach and M. A. Nikiforov (2008). "Direct role of nucleotide metabolism in C-MYC-dependent proliferation of melanoma cells." Cell Cycle **7**(15): 2392-2400.

Marteijn, J. A., H. Lans, W. Vermeulen and J. H. Hoeijmakers (2014). "Understanding nucleotide excision repair and its roles in cancer and ageing." Nature reviews Molecular cell biology **15**(7): 465.

Masai, H., S. Matsumoto, Z. You, N. Yoshizawa-Sugata and M. Oda (2010). "Eukaryotic chromosome DNA replication: where, when, and how?" Annual review of biochemistry **79**.

Matsuoka, S., B. A. Ballif, A. Smogorzewska, E. R. McDonald, K. E. Hurov, J. Luo, C. E. Bakalarski, Z. Zhao, N. Solimini and Y. Lerenthal (2007). "ATM and ATR substrate analysis reveals extensive protein networks responsive to DNA damage." science **316**(5828): 1160-1166.

Mauxion, F., B. Prève and B. Séraphin (2013). "C2ORF29/CNOT11 and CNOT10 form a new module of the CCR4-NOT complex." RNA biology **10**(2): 267-276.

Mazumder, S., E. DuPree and A. Almasan (2004). "A dual role of cyclin E in cell proliferation and apotosis may provide a target for cancer therapy." Current cancer drug targets **4**(1): 65-75.

McElhinny, S. A. N., B. E. Watts, D. Kumar, D. L. Watt, E.-B. Lundström, P. M. Burgers, E. Johansson, A. Chabes and T. A. Kunkel (2010). "Abundant ribonucleotide incorporation into DNA by yeast replicative polymerases." Proceedings of the National Academy of Sciences **107**(11): 4949-4954.

Mersman, D. P., H.-N. Du, I. M. Fingerman, P. F. South and S. D. Briggs (2009). "Polyubiquitination of the demethylase Jhd2 controls histone methylation and gene expression." Genes & development.

Minocherhomji, S., S. Ying, V. A. Bjerregaard, S. Bursomanno, A. Aleliunaite, W. Wu, H. W. Mankouri, H. Shen, Y. Liu and I. D. Hickson (2015). "Replication stress activates DNA repair synthesis in mitosis." Nature **528**(7581): 286.

Miron, K., T. Golan-Lev, R. Dvir, E. Ben-David and B. Kerem (2015). "Oncogenes create a unique landscape of fragile sites." Nature communications **6**: 7094.

Mischo, H. E., B. Gómez-González, P. Grzechnik, A. G. Rondón, W. Wei, L. Steinmetz, A. Aguilera and N. J. Proudfoot (2011). "Yeast Sen1 helicase protects the genome from transcription-associated instability." Molecular cell **41**(1): 21-32.

Mittal, S., A. Aslam, R. Doidge, R. Medica and G. S. Winkler (2011). "The Ccr4a (CNOT6) and Ccr4b (CNOT6L) deadenylase subunits of the human Ccr4–Not complex contribute to the prevention of cell death and senescence." Molecular biology of the cell **22**(6): 748-758.

Mizushima, N., T. Yoshimori and Y. Ohsumi (2011). "The role of Atg proteins in autophagosome formation." Annual review of cell and developmental biology **27**: 107-132.

Morita, M., T. Suzuki, T. Nakamura, K. Yokoyama, T. Miyasaka and T. Yamamoto (2007). "Depletion of mammalian CCR4b deadenylase triggers elevation of the p27Kip1 mRNA level and impairs cell growth." Molecular and cellular biology **27**(13): 4980-4990.

Moser, J., H. Kool, I. Giakzidis, K. Caldecott, L. H. Mullenders and M. I. Fousteri (2007). "Sealing of chromosomal DNA nicks during nucleotide excision repair requires XRCC1 and DNA ligase IIIα in a cell-cycle-specific manner." Molecular cell **27**(2): 311-323.

Mourón, S., S. Rodriguez-Acebes, M. I. Martínez-Jiménez, S. García-Gómez, S. Chocrón, L. Blanco and J. Méndez (2013). "Repriming of DNA synthesis at stalled replication forks by human PrimPol." Nature structural & molecular biology **20**(12): 1383.

Moyer, S. E., P. W. Lewis and M. R. Botchan (2006). "Isolation of the Cdc45/Mcm2–7/GINS (CMG) complex, a candidate for the eukaryotic DNA replication fork helicase." Proceedings of the National Academy of Sciences **103**(27): 10236-10241.

Moynahan, M. E., A. J. Pierce and M. Jasin (2001). "BRCA2 is required for homology-directed repair of chromosomal breaks." Molecular cell **7**(2): 263-272.

Mulder, K. W., A. B. Brenkman, A. Inagaki, N. J. van den Broek and H. T. Marc Timmers (2007). "Regulation of histone H3K4 tri-methylation and PAF complex recruitment by the Ccr4-Not complex." Nucleic acids research **35**(7): 2428-2439.

Mulder, K. W., A. Inagaki, E. Cameroni, F. Mousson, G. S. Winkler, C. De Virgilio, M. A. Collart and H. T. M. Timmers (2007). "Modulation of Ubc4p/Ubc5p-mediated stress responses by the

RING-finger-dependent ubiquitin-protein ligase Not4p in Saccharomyces cerevisiae." Genetics **176**(1): 181-192.

Mulder, K. W., G. S. Winkler and H. T. M. Timmers (2005). "DNA damage and replication stress induced transcription of RNR genes is dependent on the Ccr4–Not complex." Nucleic acids research **33**(19): 6384-6392.

Muniandy, P. A., J. Liu, A. Majumdar, S.-t. Liu and M. M. Seidman (2010). "DNA interstrand crosslink repair in mammalian cells: step by step." Critical reviews in biochemistry and molecular biology **45**(1): 23-49.

Muniandy, P. A., D. Thapa, A. K. Thazhathveetil, S.-t. Liu and M. M. Seidman (2009). "Repair of laser-localized DNA interstrand cross-links in G1 phase mammalian cells." Journal of Biological Chemistry **284**(41): 27908-27917.

Murai, J., N. H. Shar-yin, B. B. Das, A. Renaud, Y. Zhang, J. H. Doroshow, J. Ji, S. Takeda and Y. Pommier (2012). "Trapping of PARP1 and PARP2 by clinical PARP inhibitors." Cancer research **72**(21): 5588-5599.

Nakatogawa, H., K. Suzuki, Y. Kamada and Y. Ohsumi (2009). "Dynamics and diversity in autophagy mechanisms: lessons from yeast." Nature reviews Molecular cell biology **10**(7): 458.

Nakazawa, Y., K. Sasaki, N. Mitsutake, M. Matsuse, M. Shimada, T. Nardo, Y. Takahashi, K. Ohyama, K. Ito and H. Mishima (2012). "Mutations in UVSSA cause UV-sensitive syndrome and impair RNA polymerase IIo processing in transcription-coupled nucleotide-excision repair." Nature genetics **44**(5): 586.

Nallamshetty, S., M. Crook, M. Boehm, T. Yoshimoto, M. Olive and E. G. Nabel (2005). "The cell cycle regulator p27Kip1 interacts with MCM7, a DNA replication licensing factor, to inhibit initiation of DNA replication." FEBS letters **579**(29): 6529-6536.

Narita, M., A. R. Young, S. Arakawa, S. A. Samarajiwa, T. Nakashima, S. Yoshida, S. Hong, L. S. Berry, S. Reichelt and M. Ferreira (2011). "Spatial coupling of mTOR and autophagy augments secretory phenotypes." Science **332**(6032): 966-970.

Nasertorabi, F., C. Batisse, M. Diepholz, D. Suck and B. Böttcher (2011). "Insights into the structure of the CCR4-NOT complex by electron microscopy." FEBS letters **585**(14): 2182-2186.

Neil, A. J., M. U. Liang, A. N. Khristich, K. A. Shah and S. M. Mirkin (2018). "RNA–DNA hybrids promote the expansion of Friedreich's ataxia (GAA) n repeats via break-induced replication." Nucleic acids research **46**(7): 3487-3497.

Nie, Z., G. Hu, G. Wei, K. Cui, A. Yamane, W. Resch, R. Wang, D. R. Green, L. Tessarollo and R. Casellas (2012). "c-Myc is a universal amplifier of expressed genes in lymphocytes and embryonic stem cells." Cell **151**(1): 68-79.

Niida, H., M. Shimada, H. Murakami and M. Nakanishi (2010). "Mechanisms of dNTP supply that play an essential role in maintaining genome integrity in eukaryotic cells." Cancer science **101**(12): 2505-2509.

Oberholzer, U. and M. A. Collart (1999). "In vitro transcription of a TATA-less promoter: negative regulation by the Not1 protein." Biological chemistry **380**(12): 1365-1370.

Panepinto, J. C., E. Heinz and A. Traven (2013). "The cellular roles of Ccr4-NOT in model and pathogenic fungi–implications for fungal virulence." Frontiers in genetics **4**: 302.

Patschan, S., J. Chen, A. Polotskaia, N. Mendelev, J. Cheng, D. Patschan and M. S. Goligorsky (2008). "Lipid mediators of autophagy in stress-induced premature senescence of endothelial cells." American Journal of Physiology-Heart and Circulatory Physiology **294**(3): H1119-H1129.

Paul, P., T. van den Hoorn, M. L. Jongsma, M. J. Bakker, R. Hengeveld, L. Janssen, P. Cresswell, D. A. Egan, M. van Ham and A. ten Brinke (2011). "A Genome-wide multidimensional RNAi screen reveals pathways controlling MHC class II antigen presentation." Cell **145**(2): 268-283.

Peng, W., C. Togawa, K. Zhang and S. K. Kurdistani (2008). "Regulators of cellular levels of histone acetylation in Saccharomyces cerevisiae." Genetics **179**(1): 277-289.

Pertea, M., D. Kim, G. M. Pertea, J. T. Leek and S. L. Salzberg (2016). "Transcript-level expression analysis of RNA-seq experiments with HISAT, StringTie and Ballgown." Nature Protocols **11**: 1650.

Pertea, M., G. M. Pertea, C. M. Antonescu, T.-C. Chang, J. T. Mendell and S. L. Salzberg (2015). "StringTie enables improved reconstruction of a transcriptome from RNA-seq reads." Nature Biotechnology **33**: 290.

Petermann, E. and K. W. Caldecott (2006). "Evidence that the ATR/Chk1 pathway maintains normal replication fork progression during unperturbed S phase." Cell cycle **5**(19): 2203-2209.

Petermann, E., M. L. Orta, N. Issaeva, N. Schultz and T. Helleday (2010). "Hydroxyurea-stalled replication forks become progressively inactivated and require two different RAD51-mediated pathways for restart and repair." Molecular cell **37**(4): 492-502.

Petit, A.-P., L. Wohlbold, P. Bawankar, E. Huntzinger, S. Schmidt, E. Izaurralde and O. Weichenrieder (2012). "The structural basis for the interaction between the CAF1 nuclease and the NOT1 scaffold of the human CCR4–NOT deadenylase complex." Nucleic acids research **40**(21): 11058-11072.

Petit, A.-P., L. Wohlbold, P. Bawankar, E. Huntzinger, S. Schmidt, E. Izaurralde and O. Weichenrieder (2012). "The structural basis for the interaction between the CAF1 nuclease and the NOT1 scaffold of the human CCR4–NOT deadenylase complex." Nucleic acids research: gks883.

Phalke, S., S. Mzoughi, M. Bezzi, N. Jennifer, W. C. Mok, D. H. Low, A. A. Thike, V. A. Kuznetsov, P. H. Tan and P. M. Voorhoeve (2012). "p53-Independent regulation of p21Waf1/Cip1 expression and senescence by PRMT6." Nucleic acids research **40**(19): 9534-9542.

Pomerantz, R. T. and M. O'donnell (2008). "The replisome uses mRNA as a primer after colliding with RNA polymerase." Nature **456**(7223): 762.

Pommier, Y., Y. Sun, N. H. Shar-yin and J. L. Nitiss (2016). "Roles of eukaryotic topoisomerases in transcription, replication and genomic stability." Nature reviews Molecular cell biology **17**(11): 703.

Postel-Vinay, S., I. Bajrami, L. Friboulet, R. Elliott, Y. Fontebasso, N. Dorvault, K. Olaussen, F. André, J. Soria and C. Lord (2013). "A high-throughput screen identifies PARP1/2 inhibitors as a potential therapy for ERCC1-deficient non-small cell lung cancer." Oncogene **32**(47): 5377.

Postow, L., C. Ullsperger, R. W. Keller, C. Bustamante, A. V. Vologodskii and N. R. Cozzarelli (2001). "Positive torsional strain causes the formation of a four-way junction at replication forks." Journal of Biological Chemistry **276**(4): 2790-2796.

Potenski, C. J. and H. L. Klein (2014). "How the misincorporation of ribonucleotides into genomic DNA can be both harmful and helpful to cells." Nucleic acids research **42**(16): 10226-10234.

Prado, F. and A. Aguilera (2005). "Impairment of replication fork progression mediates RNA polII transcription-associated recombination." The EMBO journal **24**(6): 1267-1276.

Quintanilla-Martinez, L., T. Davies-Hill, F. Fend, J. Calzada-Wack, L. Sorbara, E. Campo, E. S. Jaffe and M. Raffeld (2003). "Sequestration of p27Kip1 protein by cyclin D1 in typical and blastic variants of mantle cell lymphoma (MCL): implications for pathogenesis." Blood **101**(8): 3181-3187.

Rai, P., T. T. Onder, J. J. Young, J. L. McFaline, B. Pang, P. C. Dedon and R. A. Weinberg (2009). "Continuous elimination of oxidized nucleotides is necessary to prevent rapid onset of cellular senescence." Proceedings of the National Academy of Sciences **106**(1): 169-174.

Ralf, C., I. D. Hickson and L. Wu (2006). "The Bloom's syndrome helicase can promote the regression of a model replication fork." Journal of biological chemistry **281**(32): 22839-22846.

Rapp, A. and K. O. Greulich (2004). "After double-strand break induction by UV-A, homologous recombination and nonhomologous end joining cooperate at the same DSB if both systems are available." Journal of cell science **117**(21): 4935-4945.

Rastogi, R. P., A. Kumar, M. B. Tyagi and R. P. Sinha (2010). "Molecular mechanisms of ultraviolet radiation-induced DNA damage and repair." Journal of nucleic acids **2010**.

Reese, J. C. (2013). "The control of elongation by the yeast Ccr4–Not complex." Biochimica et Biophysica Acta (BBA)-Gene Regulatory Mechanisms **1829**(1): 127-133.

Reijns, M. A., B. Rabe, R. E. Rigby, P. Mill, K. R. Astell, L. A. Lettice, S. Boyle, A. Leitch, M. Keighren and F. Kilanowski (2012). "Enzymatic removal of ribonucleotides from DNA is essential for mammalian genome integrity and development." Cell **149**(5): 1008-1022.

Reynolds, J. J., L. S. Bicknell, P. Carroll, M. R. Higgs, R. Shaheen, J. E. Murray, D. K. Papadopoulos, A. Leitch, O. Murina and Ž. Tarnauskaitė (2017). "Mutations in DONSON disrupt replication fork stability and cause microcephalic dwarfism." Nature genetics **49**(4): 537.

Rubinsztein, D. C., T. Shpilka and Z. Elazar (2012). "Mechanisms of autophagosome biogenesis." Current Biology **22**(1): R29-R34.

Rudd, S. G., J. Bianchi and A. J. Doherty (2014). "PrimPol—A new polymerase on the block." Molecular & cellular oncology **1**(2): e960754.

Ryan, E. L. (2016). Investigating the role of TAB182 in the DNA damage response and replication stress pathways, University of Birmingham.

Saito, Y., H. Fujimoto and J. Kobayashi (2013). "Role of NBS1 in DNA damage response and its relationship with cancer development." Translational Cancer Research **2**(3): 178-189.

Saldivar, J. C., D. Cortez and K. A. Cimprich (2017). "The essential kinase ATR: ensuring faithful duplication of a challenging genome." Nature Reviews Molecular Cell Biology **18**(10): 622.

Sanchez-Perez, I., C. Manguan-Garcia, M. Menacho-Marquez, J. R. Murguía and R. Perona (2009). "hCCR4/cNOT6 targets DNA-damage response proteins." Cancer letters **273**(2): 281-291.

Sandler, H., J. Kreth, H. T. M. Timmers and G. Stoecklin (2011). "Not1 mediates recruitment of the deadenylase Caf1 to mRNAs targeted for degradation by tristetraprolin." Nucleic acids research **39**(10): 4373-4386.

Saponaro, M., T. Kantidakis, R. Mitter, G. P. Kelly, M. Heron, H. Williams, J. Söding, A. Stewart and J. Q. Svejstrup (2014). "RECQL5 controls transcript elongation and suppresses genome instability associated with transcription stress." Cell **157**(5): 1037-1049.

Schmitt, E., R. Boutros, C. Froment, B. Monsarrat, B. Ducommun and C. Dozier (2006). "CHK1 phosphorylates CDC25B during the cell cycle in the absence of DNA damage." Journal of cell science **119**(20): 4269-4275.

Schoppy, D. W., R. L. Ragland, O. Gilad, N. Shastri, A. A. Peters, M. Murga, O. Fernandez-Capetillo, J. A. Diehl and E. J. Brown (2012). "Oncogenic stress sensitizes murine cancers to hypomorphic suppression of ATR." The Journal of clinical investigation **122**(1): 241-252.

Schwab, R. A., J. Nieminuszczy, F. Shah, J. Langton, D. L. Martinez, C.-C. Liang, M. A. Cohn, R. J. Gibbons, A. J. Deans and W. Niedzwiedz (2015). "The Fanconi anemia pathway maintains genome stability by coordinating replication and transcription." Molecular cell **60**(3): 351-361.

Serrano, M., A. W. Lin, M. E. McCurrach, D. Beach and S. W. Lowe (1997). "Oncogenic ras provokes premature cell senescence associated with accumulation of p53 and p16INK4a." Cell **88**(5): 593-602.

Sherr, C. J. and R. A. DePinho (2000). "Cellular senescence: minireview mitotic clock or culture shock?" Cell **102**(4): 407-410.

Shieh, S.-Y., J. Ahn, K. Tamai, Y. Taya and C. Prives (2000). "The human homologs of checkpoint kinases Chk1 and Cds1 (Chk2) phosphorylate p53 at multiple DNA damage-inducible sites." Genes & development **14**(3): 289-300.

Shin, J. H., L. Xu and D. Wang (2017). "Mechanism of transcription-coupled DNA modification recognition." Cell & bioscience **7**(1): 9.

Shirai, Y.-T., T. Suzuki, M. Morita, A. Takahashi and T. Yamamoto (2014). "Multifunctional roles of the mammalian CCR4–NOT complex in physiological phenomena." Frontiers in genetics **5**: 286.

Shykind, B. M., J. Kim, L. Stewart, J. J. Champoux and P. A. Sharp (1997). "Topoisomerase I enhances TFIID-TFIIA complex assembly during activation of transcription." Genes & development **11**(3): 397-407.

Siddiqui-Jain, A., C. L. Grand, D. J. Bearss and L. H. Hurley (2002). "Direct evidence for a G-quadruplex in a promoter region and its targeting with a small molecule to repress c-MYC transcription." Proceedings of the National Academy of Sciences **99**(18): 11593-11598.

Siwaszek, A., M. Ukleja and A. Dziembowski (2014). "Proteins involved in the degradation of cytoplasmic mRNA in the major eukaryotic model systems." RNA biology **11**(9): 1122-1136.

Skourti-Stathaki, K., K. Kamieniarz-Gdula and N. J. Proudfoot (2014). "R-loops induce repressive chromatin marks over mammalian gene terminators." Nature **516**(7531): 436.

Skourti-Stathaki, K. and N. J. Proudfoot (2014). "A double-edged sword: R loops as threats to genome integrity and powerful regulators of gene expression." Genes & development **28**(13): 1384-1396.

Sohrabi-Jahromi, S. (2019). "Transcriptome maps of general eukaryotic RNA degradation factors." eLife.

Solana, J., C. Gamberi, Y. Mihaylova, S. Grosswendt, C. Chen, P. Lasko, N. Rajewsky and A. A. Aboobaker (2013). "The CCR4-NOT complex mediates deadenylation and degradation of stem cell mRNAs and promotes planarian stem cell differentiation." PLoS genetics **9**(12): e1004003.

Sollier, J., C. T. Stork, M. L. García-Rubio, R. D. Paulsen, A. Aguilera and K. A. Cimprich (2014). "Transcription-coupled nucleotide excision repair factors promote R-loop-induced genome instability." Molecular cell **56**(6): 777-785.

Sørensen, C. S., R. G. Syljuåsen, J. Lukas and J. Bartek (2004). "ATR, Claspin and the Rad9-Rad1-Hus1 complex regulate Chk1 and Cdc25A in the absence of DNA damage." Cell cycle **3**(7): 939-943.

Sotiriou, S. K., I. Kamileri, N. Lugli, K. Evangelou, C. Da-Ré, F. Huber, L. Padayachy, S. Tardy, N. L. Nicati and S. Barriot (2016). "Mammalian RAD52 functions in break-induced replication repair of collapsed DNA replication forks." Molecular cell **64**(6): 1127-1134.

Sparks, J. L., H. Chon, S. M. Cerritelli, T. A. Kunkel, E. Johansson, R. J. Crouch and P. M. Burgers (2012). "RNase H2-initiated ribonucleotide excision repair." Molecular cell **47**(6): 980-986.

Spruck, C. H., K.-A. Won and S. I. Reed (1999). "Deregulated cyclin E induces chromosome instability." Nature **401**(6750): 297.

Stork, C. T., M. Bocek, M. P. Crossley, J. Sollier, L. A. Sanz, F. Chedin, T. Swigut and K. A. Cimprich (2016). "Co-transcriptional R-loops are the main cause of estrogen-induced DNA damage." Elife **5**: e17548.

Stubbert, L. J., J. M. Smith and B. C. McKay (2010). "Decreased transcription-coupled nucleotide excision repair capacity is associated with increased p53-and MLH1-independent apoptosis in response to cisplatin." BMC cancer **10**(1): 207.

Sugitani, N., R. M. Sivley, K. E. Perry, J. A. Capra and W. J. Chazin (2016). "XPA: A key scaffold for human nucleotide excision repair." DNA repair **44**: 123-135.

Sugiyama, T. and S. C. Kowalczykowski (2002). "Rad52 protein associates with replication protein A (RPA)-single-stranded DNA to accelerate Rad51-mediated displacement of RPA and presynaptic complex formation." Journal of Biological Chemistry **277**(35): 31663-31672.

Suzuki, A., R. Saba, K. Miyoshi, Y. Morita and Y. Saga (2012). "Interaction between NANOS2 and the CCR4-NOT deadenylation complex is essential for male germ cell development in mouse." PloS one **7**(3): e33558.

Svitkin, Y. V. and N. Sonenberg (2006). "Translational control by the poly (A) binding protein: a check for mRNA integrity." Molecular Biology **40**(4): 611-619.

Swanson, M. J., H. Qiu, L. Sumibcay, A. Krueger, S.-j. Kim, K. Natarajan, S. Yoon and A. G. Hinnebusch (2003). "A multiplicity of coactivators is required by Gcn4p at individual promoters in vivo." Molecular and cellular biology **23**(8): 2800-2820.

Swanton, C. and N. Jones (2001). "Strategies in subversion: de-regulation of the mammalian cell cycle by viral gene products." International journal of experimental pathology **82**(1): 3.

Takata, M., M. S. Sasaki, E. Sonoda, C. Morrison, M. Hashimoto, H. Utsumi, Y. Yamaguchi-Iwai, A. Shinohara and S. Takeda (1998). "Homologous recombination and non-homologous end-joining pathways of DNA double-strand break repair have overlapping roles in the maintenance of chromosomal integrity in vertebrate cells." The EMBO journal **17**(18): 5497-5508.

Thangavel, S., M. Berti, M. Levikova, C. Pinto, S. Gomathinayagam, M. Vujanovic, R. Zellweger, H. Moore, E. H. Lee and E. A. Hendrickson (2015). "DNA2 drives processing and restart of reversed replication forks in human cells." J Cell Biol **208**(5): 545-562.

Thomas, A. (2013). The regulation of p53 transcriptional activity by hnRNPUL-1 and the DNA damage response induced by a novel chemotherapeutic agent, ALX, University of Birmingham.

Thornton, B. R. and D. P. Toczyski (2003). "Securin and B-cyclin/CDK are the only essential targets of the APC." Nature cell biology **5**(12): 1090.

Timmers, H. T. M. and L. Tora (2018). "Transcript buffering: a balancing act between mRNA synthesis and mRNA degradation." Molecular cell **72**(1): 10-17.

Toledo, L. I., M. Murga, R. Zur, R. Soria, A. Rodriguez, S. Martinez, J. Oyarzabal, J. Pastor, J. R. Bischoff and O. Fernandez-Capetillo (2011). "A cell-based screen identifies ATR inhibitors with synthetic lethal properties for cancer-associated mutations." Nature structural & molecular biology **18**(6): 721.

Tornaletti, S., L. S. Maeda, R. D. Kolodner and P. C. Hanawalt (2004). "Effect of 8-oxoguanine on transcription elongation by T7 RNA polymerase and mammalian RNA polymerase II." DNA repair **3**(5): 483-494.

Traven, A., A. Hammet, N. Tenis, C. L. Denis and J. Heierhorst (2005). "Ccr4-not complex mRNA deadenylase activity contributes to DNA damage responses in Saccharomyces cerevisiae." Genetics **169**(1): 65-75.

Tucker, M., M. A. Valencia-Sanchez, R. R. Staples, J. Chen, C. L. Denis and R. Parker (2001). "The transcription factor associated Ccr4 and Caf1 proteins are components of the major cytoplasmic mRNA deadenylase in Saccharomyces cerevisiae." Cell **104**(3): 377-386.

Vaziri, H. and S. Benchimol (1998). "Reconstitution of telomerase activity in normal human cells leads to elongation of telomeres and extended replicative life span." Current Biology **8**(5): 279-282.

Velimezi, G., L. Robinson-Garcia, F. Muñoz-Martínez, W. W. Wiegant, J. F. da Silva, M. Owusu, M. Moder, M. Wiedner, S. B. Rosenthal and K. M. Fisch (2018). "Map of synthetic rescue interactions for the Fanconi anemia DNA repair pathway identifies USP48." Nature communications **9**(1): 2280.

Venters, B. J., S. Wachi, T. N. Mavrich, B. E. Andersen, P. Jena, A. J. Sinnamon, P. Jain, N. S. Rolleri, C. Jiang and C. Hemeryck-Walsh (2011). "A comprehensive genomic binding map of gene and chromatin regulatory proteins in Saccharomyces." Molecular cell **41**(4): 480-492.

Vicencio, J. M., L. Galluzzi, N. Tajeddine, C. Ortiz, A. Criollo, E. Tasdemir, E. Morselli, A. B. Younes, M. C. Maiuri and S. Lavandero (2008). "Senescence, apoptosis or autophagy?" Gerontology **54**(2): 92-99.

von Hippel, P. H. (1998). "An integrated model of the transcription complex in elongation, termination, and editing." Science **281**(5377): 660-665.

Vujanovic, M., J. Krietsch, M. C. Raso, N. Terraneo, R. Zellweger, J. A. Schmid, A. Taglialatela, J.-W. Huang, C. L. Holland and K. Zwicky (2017). "Replication fork slowing and reversal upon DNA damage require PCNA polyubiquitination and ZRANB3 DNA translocase activity." Molecular cell **67**(5): 882-890. e885.

Wada, T. and A. Becskei (2017). "Impact of Methods on the Measurement of mRNA Turnover." International journal of molecular sciences **18**(12): 2723.

Wahba, L., J. D. Amon, D. Koshland and M. Vuica-Ross (2011). "RNase H and multiple RNA biogenesis factors cooperate to prevent RNA: DNA hybrids from generating genome instability." Molecular cell **44**(6): 978-988.

Wang, C., G. Wang, X. Feng, P. Shepherd, J. Zhang, M. Tang, Z. Chen, M. Srivastava, M. E. McLaughlin and N. M. Navone (2018). "Genome-wide CRISPR screens reveal synthetic lethality of RNASEH2 deficiency and ATR inhibition." Oncogene: 1.

Wang, X. W., Q. Zhan, J. D. Coursen, M. A. Khan, H. U. Kontny, L. Yu, M. C. Hollander, P. M. O'Connor, A. J. Fornace and C. C. Harris (1999). "GADD45 induction of a G2/M cell cycle checkpoint." Proceedings of the National Academy of Sciences **96**(7): 3706-3711.

Waterworth, W. M., C. Altun, S. J. Armstrong, N. Roberts, P. J. Dean, K. Young, C. F. Weil, C. M. Bray and C. E. West (2007). "NBS1 is involved in DNA repair and plays a synergistic role with ATM in mediating meiotic homologous recombination in plants." The Plant Journal **52**(1): 41-52.

Westmoreland, T. J., J. R. Marks, J. A. Olson, E. M. Thompson, M. A. Resnick and C. B. Bennett (2004). "Cell cycle progression in G1 and S phases is CCR4 dependent following ionizing radiation or replication stress in Saccharomyces cerevisiae." Eukaryotic Cell **3**(2): 430-446.

Williams, J. S., A. R. Clausen, S. A. N. McElhinny, B. E. Watts, E. Johansson and T. A. Kunkel (2012). "Proofreading of ribonucleotides inserted into DNA by yeast DNA polymerase ε." DNA repair **11**(8): 649-656.

Williams, R. S., J. S. Williams and J. A. Tainer (2007). "Mre11-Rad50-Nbs1 is a keystone complex connecting DNA repair machinery, double-strand break signaling, and the chromatin template " Biochemistry and cell biology **85**(4): 509-520.

Wind, M. and D. Reines (2000). "Transcription elongation factor SII." Bioessays **22**(4): 327-336.

Winkler, G. S., K. W. Mulder, V. J. Bardwell, E. Kalkhoven and H. T. M. Timmers (2006). "Human Ccr4-Not complex is a ligand-dependent repressor of nuclear receptor-mediated transcription." The EMBO journal **25**(13): 3089-3099.

Wohlschlegel, J. A., B. T. Dwyer, S. K. Dhar, C. Cvetic, J. C. Walter and A. Dutta (2000). "Inhibition of eukaryotic DNA replication by geminin binding to Cdt1." Science **290**(5500): 2309-2312.

Xie, M., Y. Yen, T. K. Owonikoko, S. S. Ramalingam, F. R. Khuri, W. J. Curran, P. W. Doetsch and X. Deng (2014). "Bcl2 induces DNA replication stress by inhibiting ribonucleotide reductase." Cancer research **74**(1): 212-223.

Yamaguchi, T., T. Suzuki, T. Sato, A. Takahashi, H. Watanabe, A. Kadowaki, M. Natsui, H. Inagaki, S. Arakawa and S. Nakaoka (2018). "The CCR4-NOT deadenylase complex controls Atg7-dependent cell death and heart function." Sci. Signal. **11**(516): eaan3638.

Yang, L., J. Wang, Y. Lv, D. Hao, Y. Zuo, X. Li and W. Jiang (2014). "Characterization of TATA-containing genes and TATA-less genes in S. cerevisiae by network topologies and biological properties." Genomics **104**(6): 562-571.

Yang, X. H. and L. Zou (2009). "Dual functions of DNA replication forks in checkpoint signaling and PCNA ubiquitination." Cell Cycle **8**(2): 191-194.

Yankulov, K., K. Yamashita, R. Roy, J.-M. Egly and D. L. Bentley (1995). "The transcriptional elongation inhibitor 5, 6-dichloro-1-β-D-ribofuranosylbenzimidazole inhibits transcription factor IIH-associated protein kinase." Journal of Biological Chemistry **270**(41): 23922-23925.

Yu, H. (2002). "Regulation of APC–Cdc20 by the spindle checkpoint." Current opinion in cell biology **14**(6): 706-714.

Zafar, M. K., A. Ketkar, M. F. Lodeiro, C. E. Cameron and R. L. Eoff (2014). "Kinetic analysis of human PrimPol DNA polymerase activity reveals a generally error-prone enzyme capable of accurately bypassing 7, 8-dihydro-8-oxo-2'-deoxyguanosine." Biochemistry **53**(41): 6584-6594.

Zellweger, R., D. Dalcher, K. Mutreja, M. Berti, J. A. Schmid, R. Herrador, A. Vindigni and M. Lopes (2015). "Rad51-mediated replication fork reversal is a global response to genotoxic treatments in human cells." J Cell Biol **208**(5): 563-579.

Zhang, Y.-W., T. L. Jones, S. E. Martin, N. J. Caplen and Y. Pommier (2009). "Implication of checkpoint kinase-dependent up-regulation of ribonucleotide reductase R2 in DNA damage response." Journal of Biological Chemistry **284**(27): 18085-18095.

Zhao, J., X. Yuan, M. Frödin and I. Grummt (2003). "ERK-dependent phosphorylation of the transcription initiation factor TIF-IA is required for RNA polymerase I transcription and cell growth." Molecular cell **11**(2): 405-413.

Zhong, Y., T. Nellimoottil, J. M. Peace, S. R. Knott, S. K. Villwock, J. M. Yee, J. M. Jancuska, S. Rege, M. Tecklenburg and R. A. Sclafani (2013). "The level of origin firing inversely affects the rate of replication fork progression." J Cell Biol **201**(3): 373-383.

Zhu, Z., W.-H. Chung, E. Y. Shim, S. E. Lee and G. Ira (2008). "Sgs1 helicase and two nucleases Dna2 and Exo1 resect DNA double-strand break ends." Cell **134**(6): 981-994.

Zimmermann, M., O. Murina, M. A. Reijns, A. Agathanggelou, R. Challis, Ž. Tarnauskaitė, M. Muir, A. Fluteau, M. Aregger and A. McEwan (2018). "CRISPR screens identify genomic ribonucleotides as a source of PARP-trapping lesions." Nature **559**(7713): 285.

Zou, L.-H., Z.-F. Shang, W. Tan, X.-D. Liu, Q.-Z. Xu, M. Song, Y. Wang, H. Guan, S.-M. Zhang and L. Yu (2015). "TNKS1BP1 functions in DNA double-strand break repair though facilitating DNA-PKcs autophosphorylation dependent on PARP-1." Oncotarget **6**(9): 7011.

Zwartjes, C. G., S. Jayne, D. L. van den Berg and H. M. Timmers (2004). "Repression of promoter activity by CNOT2, a subunit of the transcription regulatory Ccr4-not complex." Journal of Biological Chemistry **279**(12): 10848-10854.